

N70-36981

Syracuse University Research Corporation, Merrill Lane, University Heights, Syracuse, New York 13210

# General Aviation Weather Avoidance Sensor Study

by George M. Kirkpatrick

CASE FILE  
COPY

Prepared Under  
Contract No. NAS 12-2032

June 1970



SURC

ERRATA SHEET  
FOR  
GENERAL AVIATION  
WEATHER AVOIDANCE SENSOR STUDY

<u>Page</u>	<u>Correction</u>
100	figures a) and b) are reversed
200	place brackets around the two term expression to the right of the inverse sine in equation (C. 12)
209	in the line above equation (E. 9) add .a, to the denominator of the equivalent of y



GENERAL AVIATION  
WEATHER AVOIDANCE SENSOR STUDY

By  
George M. Kirkpatrick

June 1970

Distribution of this report is provided in the interest of information exchange and should not be construed as endorsement by NASA of the material presented. Responsibility for the contents resides with the organization that prepared it.

Prepared Under  
Contract No. NAS 12-2032

By  
SYRACUSE UNIVERSITY RESEARCH CORPORATION  
SYRACUSE, NEW YORK 13210

For  
NATIONAL AERONAUTICS AND SPACE ADMINISTRATION



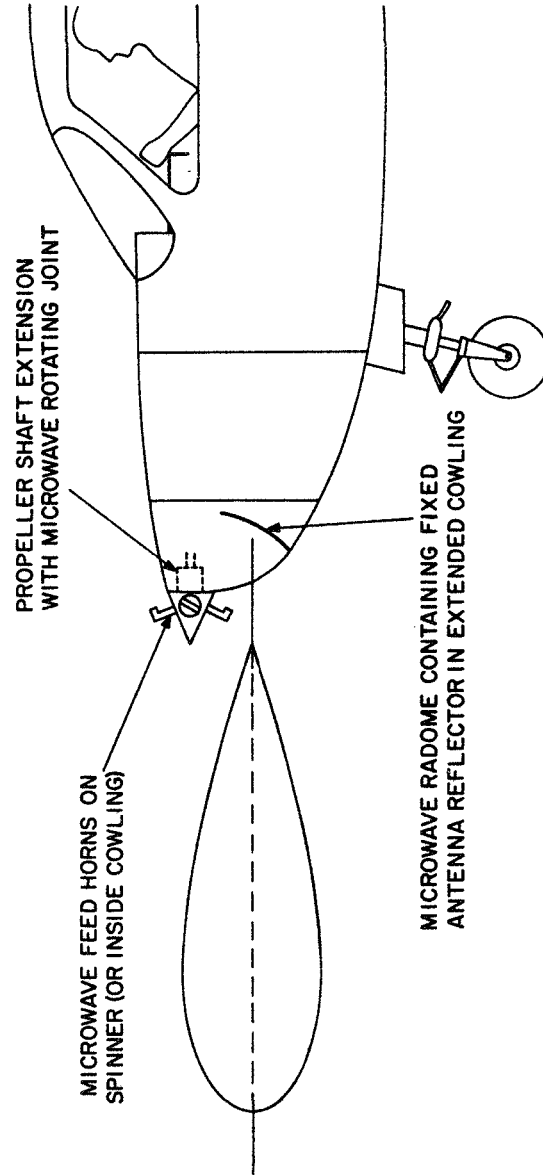


Janis Vilcans  
Technical Monitor  
NAS 12-2032  
Electronics Research Center  
575 Technology Square  
Cambridge, Massachusetts 02139

"Requests for copies of this report should be referred to:

NASA Scientific and Technical Information Facility  
PO Box 33, College Park, Maryland 20740."

AI1082



PROPOSED ANTENNA CONFIGURATION FOR LOW-COST WEATHER RADAR  
WITH ENGINE-DRIVEN SCANNER



# WEATHER AVOIDANCE SENSOR STUDY

By  
George M. Kirkpatrick

SYRACUSE UNIVERSITY RESEARCH CORPORATION  
Syracuse, New York

## SUMMARY

The objective of this study is to delineate the specifications of a general aviation weather avoidance sensor and to develop an approach to its design which will be suitable in view of cost, reliability, power, etc.; constraints typical of general aviation aircraft. A survey of new technology, primarily in the laboratories of Department of Defense contractors, revealed promising new components for electronic scanning. However, considerable investment in manufacturing facilities and/or major production runs ( $10^6$  units) will be required to meet the cost constraints of general aviation. The survey also served to emphasize that increased production is the primary route to a lower product cost.

The current generation of small airborne weather radars includes many solid-state components and adequately meets the needs of the light twin aircraft of the general aviation fleet. Single and dual in-line engine aircraft often operate in stormy weather and at present no airborne weather radars are available for this category of aircraft. Therefore, considerable emphasis in the study is placed on describing techniques which might enable a low-cost antenna development for the single and dual in-line engine aircraft. Success in such a development can meet an existing need and should result in lower weather radar prices because of increased production.

Major divisions of the report are (1) definition of the operational characteristics of on-board weather detection systems, (2) alternative techniques for weather sensing with particular stress on radar antenna techniques for single and dual in-line engine aircraft, (3) a survey of new system technology, particularly components for electronic scanning, and (4) several proposed system block diagrams with performance specifications and rough estimates on development and quantity production costs.

A sketch of a proposed antenna configuration for a low-cost weather radar with an engine-driven scanner is shown on the facing page. Laboratory measurements on the proposed antenna configuration are recommended for the first phase of a development program.

## TABLE OF CONTENTS

	<u>Page</u>
SUMMARY	v
1.0 INTRODUCTION	1
1. 1 Objective	1
1. 2 Background Information	1
1. 3 Acknowledgments	3
1. 4 Nomenclature	3
1. 5 Abbreviations and Acronyms	6
2.0 OPERATIONAL CHARACTERISTICS	9
2. 1 Introduction	9
2. 2 Operational Characteristics	12
2. 3 LIDAR Weather Model	16
2. 4 Precipitation Weather Model for Determining the Detection Range of Microwave Radar (No Attenuation From Intervening Rain)	18
2. 5 Precipitation Weather Model With Attenuation From Intervening Rain	20
2. 6 The Terrain Return Problem	23
2. 7 Elevation Plane Antenna Beam Tilt	30
2. 8 Sferic Weather Model	40
3.0 WEATHER RADAR TECHNIQUES	45
3. 1 Introduction	45
3. 2 Mechanical Scanning	47
3. 3 Frequency Scan	51
3. 4 Electronic Scan	52
3. 5 Slat/Wire Grating Reflector	59
3. 6 Test of Slat Reflector	60
3. 7 Aerodynamic Considerations	66
3. 8 Interference Drag Considerations	69
3. 9 Underwing Retractable Grating Antenna	71
3.10 Flush-Mounted Antenna Array in the Top of the Wing	71
3.11 Crossed-Beam Scanning Radar	74
3.12 Intra-Pulse Sampling in Multi-Beam Radar	77
3.13 Intra-Pulse Beam Scanning (MODSCAN)	79
3.14 Application of MODSCAN to Single Engine Aircraft	82
3.15 Non-Coherent MTI for Terrain Return Suppression	84



	<u>Page</u>
3.16 Monopulse Terrain Clutter Attenuation	87
3.17 Monopulse Beam Control for Terrain Return Suppression	98
3.18 Non-Coherent Monopulse Clutter Suppression	101
3.19 Random Noise Radar	102
4.0 NEW SYSTEM TECHNOLOGY	109
4. 1 Introduction	109
4. 2 Solid-State Phase Shifters for Electronic Scanning	109
4. 3 All Solid-State Microwave Radar	119
4. 4 Solid-State Display Panel	123
5.0 SYSTEM DESIGNS	125
5. 1 Introduction	125
5. 2 Minimum Cost Radar	128
5. 3 All Solid-State Radar	137
5. 4 Modulation-Scan Radar (MODSCAN)	152
5. 5 Laser Cloud Ranging	158
5. 6 Sferic Weather Detection	167
6.0 CONCLUSIONS AND RECOMMENDATIONS	175
6. 1 Conclusions	175
6. 2 Recommendations	176
BIBLIOGRAPHY	177
Appendix A Radar Storm Return	183
Appendix B Radar Range Calculations	190
Appendix C Derivation of Angles for Spherical Earth Model	198
Appendix D Analysis of Clutter Attenuation	201
Appendix E Monopulse Beam Tilt	208
Appendix F Laser Cloud Ranging	210
Appendix G New Technology	213

## LIST OF ILLUSTRATIONS

<u>Figure</u>	<u>Page</u>
2. 1    Visibility and Distance From Clouds for Visual Flight Rules (VFR) Minimums.	10
2. 2    Location of Ground Weather Radar Stations in the USA. FAA Flight Service Stations (FSS) Relay Weather Radar Information to Pilots.	11
2. 3    Relation Between Backscattering and Extinction Coefficient as Derived From Data by Barteneva <sup>10</sup>	19
2. 4    Model Complex Storm With Intervening Rain and In-Line Cells (Beam Assumed Filled).	21
2. 5    Frontal Storm Situation Which Might Trap Pilot Using Radar With Poor Penetration Capability.	22
2. 6    Effect of Rainfall Attenuation on Radar Storm Presentation for $\lambda = 1.8$ cms ( $K_u$ -Band).	24
2. 7    Effect of Rainfall Attenuation on Radar Storm Presentation for $\lambda = 3.2$ cms (X-Band).	25
2. 8    Effect of Rainfall Attenuation on Radar Storm Presentation for $\lambda = 5.6$ cms (C-Band).	26
2. 9    Average Radar Cross-Section per Unit Surface Area, $\sigma^0$ , for Small Grazing Angles, From Barrick <sup>15</sup> .	28
2.10    Photographs of Weather Radar PPI Display With Elevation Tilt Angles as Indicated and 10 Nautical Mile Range Marks.	29
2.11    Optimum Tilt Angles for Widebeam (14.5 degrees) Antenna for Near and Far Storm Detection and Analysis.	31
2.12    Terrain Return as a Function of Aircraft Height and Depression Angle.	33
2.13a    Antenna Pattern for Linear Aperture, Uniform Illumination.	34
2.13b    Antenna Pattern for Linear Aperture, Cosine Illumination.	35



<u>Figure</u>	<u>Page</u>
2.13c Antenna Pattern for Elliptical Aperture, Parabolic Illumination.	36
2.14 Sferic Count Rates on Two Thunderstorms as Measured by SPARSA (Heavy Line) Equipment.	41
3. 1 Radar Mounting Areas on Single-Engine Aircraft	46
3. 2 Cross-Section of Eagle Vane With Mechanical Scanning Linear Array.	48
3. 3 Proposed Antenna Configuration for Low-Cost Weather Radar With Engine-Driven Scanner.	49
3. 4 Schematic Diagram of Two Output Rotating Joint.	50
3. 5 Serpentine Waveguide for Frequency Scan Antenna	51
3. 6 Research Model of Flush-Mounted Frequency Scan Antenna in Top Surface of Aircraft Wing.	53
3. 7 $N^{\text{th}}$ Element Phase Shift Relative to Reference Point, 0.	55
3. 8 Analog Source of Phase Shifter Control Voltage.	56
3. 9 Graph of Phase Shifter Setting for Eleven- Element Array.	58
3.10 Grating of Edgewise Strips: Relation Between Strip Depth and Spacing for Constant Transmission.	60
3.11 Transmission Through a Grid of Parallel Wires.	61
3.12 Parabolic-Cylinder Slat Reflector and Twenty- Slot X-Band Waveguide Feed.	61
3.13 Parabolic-Cylinder Slat Reflector With X-Band Feed Mounted for Pattern Tests.	62
3.14 X-Band Azimuth Pattern of Slot Feed and Grating Reflector.	63
3.15 X-Band Elevation Primary Feed (Slotted Waveguide) Pattern.	64
3.16 X-Band Elevation Pattern of Slotted Waveguide Feed and Grating Reflector.	65
3.17 The Effect of Aperture Blocking: (a) Modified Aperture Distribution; (b) Secondary Pattern.	66

<u>Figure</u>		<u>Page</u>
3.18	Sea Level Horsepower Versus Aircraft Speed for Three $C_D A$ Products.	68
3.19	Effect of Side-by-Side Spacing on Interference Drag of Streamline Struts. Navy No. 1 Strut Section, Fineness Ratio 3, Air Speed 80 MPH.	70
3.20	Approximate Cross-Section of Piper Cherokee Wing With Offset Feed, Cylindrical Parabolic Grating Reflector Mounted Under the Wing.	72
3.21	Cross-Section of Wing With Flush Array.	73
3.22	Nearly Flush-Mounted Antenna in Top Surface of Aircraft Wing.	75
3.23	Diagram of Cross-Beam Scanning Antenna. One Antenna Generates Wide-Narrow Beam While the Other Narrow-Wide Beam Scans at Approximately Right Angles to it.	76
3.24	Sequential Scanning of Multiple Beam Outputs at Rate of $1/\tau$ .	78
3.25	MODSCAN Receiving Array.	81
3.26	MODSCAN Cross-Antenna for Weather Radar.	83
3.27	MODSCAN Transmitting Array.	83
3.28	Power Spectra of Various Clutter Targets.	85
3.29	Effect of Internal Fluctuations on Clutter Attenuation.	86
3.30	Depression Angle as a Function of Time for $h_1 = 500$ feet.	88
3.31	Omni-Directional Radar at Height $h_1$ Over Ground.	89
3.32	Spherical Wavefront Intersecting Plane Surface.	91
3.33	Incremental Area Illuminated on Ground.	92
3.34	Power Impulse Return From Clutter ( $\sigma^0/\sin \theta = \text{constant}$ ).	94
3.35	Assumed Symmetrical (Even) Power Pattern About Angle $\theta_1$ .	95
3.36	Approximate Effect of Vertical Antenna Pattern on Power Impulse Response.	95

<u>Figure</u>		<u>Page</u>
3.37	Two Intersecting Elevation Patterns, $k = 1$ .	96
3.38	Voltage Response for Difference Function, $ A  -  kB $ .	96
3.39	Clutter Return reduced With $k = f(t, \theta)$ .	97
3.40	Monopulse Equipment for Varying $k$ With Time so $ A /k - k B  \rightarrow 0$ .	97
3.41	Reflector and Array Monopulse Antennas.	99
3.42	Diagrams for Monopulse Dynamic Beam Tilt Control.	100
3.43	Elevation View With Radar Beam Filled With Rain Over Terrain and $\theta_{BW} \gg \delta\theta$ .	102
3.44	Experimental Spectrum Analysis Radar.	103
4. 1	Four-Bit, X-Band, Loaded Waveguide, Latching Ferrite Phase Shifter.	112
4. 2	Forty-Element Linear Array With Plated Wave- guide Feed and Four-Bit, X-Band, Latching Ferrite Phase Shifter.	113
4. 3	Four-Bit, X-Band, Transmission, Pin Diode Switch, Phase Shifter.	114
4. 4	Circuit Diagram of Four-Bit Transmission Phase Shifter of Figure 4.3.	114
4. 5	Four-Bit, X-Band, Reflective, Pin Diode Switch Phase Shifter With Logic and Driver Circuits at Left.	115
4. 6	Test Fixture and Assembled Unit of ESAM X-Band Analog, Reciprocal, Strip Transmission Line Phase Shifter.	116
4. 7	Rat-Race Feed Structure for ESAM 16-Element Linear Sub-Array.	117
4. 8	Block Diagram of MERA RF Module.	120
4. 9	MERA Module Showing, Left to Right, Dipole Antenna, X4 LO Multiplier, TX/RX Phase Shifters and Logic and S-Band Preamp and Duplexer.	121
4.10	MERA Module Showing, Left to Right, Dipole Antenna, X-Band Mixer/TR Switch and IF Preamp (Lower Left) X4/TX Multiplier and Pulsed Power Amplifier and Modulator.	122

<u>Figure</u>	<u>Page</u>
5. 1 Engine-Driven Mechanical Scan for Use on Single and Dual In-Line Engine Aircraft.	130
5. 2 Feed Horn Circle, Focal Line, and Reflector Relative Locations.	130
5. 3 Block Diagram of Minimum Radar With Proposed Engine-Driven Scanner.	133
5. 4 Transceiver System (Multi-Element Linear Array Module).	138
5. 5 Transceiver Module.	139
5. 6 360° Non-Reciprocal Latching Ferrite Phase Shifter.	143
5. 7 Phase Shift (Non-Reciprocal).	144
5. 8 Propagation Characteristics for Non-Reciprocal Phase Shifter.	145
5. 9 Eight-Element Linear Array With Printed Dipole Radiators (X-Band).	147
5.10 Boresight Pattern for Eight-Element Linear Array (Amplitude in dB).	149
5.11 Linear Plot of Steered Beams.	150
5.12 All Solid-State Weather Radar in Single or Dual In-Line Engine Aircraft.	151
5.13 Block Diagram of All Solid-State (SS) Weather Radar.	152
5.14 MODSCAN Receiving Array.	157
5.15 Block Diagram of Neodymium Rod Laser (1.06 Microns) Cloud Ranger for VFR Flight.	164
5.16 Block Diagram of Low Power Diode Laser for Cloud Ranging During Night VFR Flight.	165
5.17 Block Diagram of Instantaneous ADF for Sferic Detection and Use as Conventional ADF.	170
C-1 Geometric Relationships for Determining Depression Angle to Terrain and Storm, and Angle of Incidence on Terrain.	199

<u>Figure</u>		<u>Page</u>
D-1	Sketch Used to Derive $\delta \theta$ .	201
D-2	$\delta \theta$ as a Function of Depression Angle From Equation (D.2) for $(c\tau/2h_1) = 0.1$ .	203
D-3	Clutter Packet at Crossover of Elevation Beams.	204
D-4	Sketch for Clutter Attenuation Calculation.	205
D-5	Clutter Reduction as a Function of Depression Angle From Equation (D.7) for $(\lambda 2h_1/a_1 c\tau) = 1$ .	207

## LIST OF TABLES

<u>Table</u>	<u>Page</u>
2. 1 Primary Operational Characteristics	13
2. 2 Sample Radar Parameters	32
2. 3 Beam Tilt and Gain Loss for Various Antennas at Four Altitudes	38
2. 4 Classification of Storms by Flashing Rate	42
3. 1 Objectives of Technique and/or Design	47
4. 1 Comparison of X-Band Phase Shifter Techniques	110
4. 2 Characteristics of Ten Types of Ferrite Phase Shifters.	111
5. 1 Airborne Weather Radar Data	126
5. 2 Breakdown of Conventional Weather Radar Costs - 1969	128
5. 3 Transmitter Component Costs	131
5. 4 Operational Characteristics of Minimum Radar	134
5. 5 Estimated Cost of Minimum Radar	136
5. 6 Planar Ferrite Phase Shifter Performance	146
5. 7 Operational Characteristics (OC) of All Solid- State (SS) Weather Radar	153
5. 8 Estimated Costs on All Solid-State Radar	155
5. 9 Proposed MODSCAN Frequencies	158
5.10 Tentative Parameters and Operational Characteristics of MODSCAN	159
5.11 Estimated Cost of MODSCAN System (17-Element Array)	161
5.12 Estimated Costs on Pulsed Light Ranger	166
5.13 General Aviation ADF Equipment	168
5.14 Comparative Operational Characteristics and ADF/Sferic Detector Parameters	171
5.15 Estimated Cost of ADF/Sferic Detector	172

<u>Table</u>	<u>Page</u>
A-1 Two-Way Attenuation Factors, $K_2$ and $\gamma$	188
B-1 Conventional Weather Radar With 12-Inch Dish	192
B-2 Weather Radar With Electronic Scanning and Grating Reflector	193
B-3 Weather Radar With Intra-Pulse Scanning and Crossed-Beam Antenna	194
B-4 Range Estimation Form (Blank)	195
B-5 Range Estimation Form (Blank)	196

## 1.0 INTRODUCTION

### 1.1 Objective

The objective of this study report is to delineate the specifications of a general aviation weather avoidance sensor and to develop an approach to its design which will be suitable in view of cost, reliability, power, etc.; constraints typical of general aviation aircraft. The work carried out in performance of this contract is divided into the following items.

#### ITEM 1

A definition of the operational characteristics of weather detection systems suitable for on-board general aviation use.

#### ITEM 2

A study of alternative techniques which show promise of meeting the operational requirements in a suitably low-cost, low-power, reliable implementation which is useable by general aviation aircraft. Both passive and active systems have been considered in the study.

#### ITEM 3

Subsystems suitable for newly available technology are identified. Microwave integrated circuits, solid-state phase shifters, solid-state power sources, etc., are examples of such new technology.

#### ITEM 4

Several system design approaches are described in block diagram form, together with performance specifications.

### 1.2 Background Information

For those readers not familiar with the historical development and/or those seeking information on the current state-of-the-art of weather radar, the following books and articles are representative sources of information.

Hall, J. S., ed., "Radar Aids to Navigation," McGraw-Hill Book Company, New York, 1946. (This volume, No. 2, of the MIT Radiation Laboratory Series describes the AN/APS-10 navigation and weather radar on pp 171-185.)



- Kerr, D. E., ed., "Propagation of Short Radio Waves," McGraw-Hill Book Company, New York, 1947. (This volume, No. 13 of the MIT Radiation Laboratory Series devotes Chapter 7 to "Meteorological Echoes," pp 588-640.)
- Ayer, R. W., et al, "The Development of an Airborne Radar Method of Avoiding Severe Turbulence and Heavy Precipitation Areas of Thunderstorms and Line Squalls," Navy BuAer Contract N0a(s)-9006, ATI Document No. 65,395, 15 September 1949.
- Post, E. A., "The Operational Applications of Airborne Radar," IRE Transactions on Airborne and Navigational Electronics, September 1954, pp 15-23.
- Battan, L. J., "Radar Meteorology," The University of Chicago Press, 1959.
- Hansford, R. F., ed., "Radio Aids to Civil Aviation," Heywood and Company, Ltd., London, 1960, see Chapter 7, "Weather Radar," pp 425-478.
- RTCA Paper DO-105, "Minimum In-Flight Performance Standards - Airborne Weather and Ground Mapping Radar," Issued 1960, Published by Radio Technical Commission for Aeronautics, 2000 K Street, N. W., Washington, D. C. 20006.
- "ARINC Characteristic No. 564, Airborne Weather Radar," Prepared by Airlines Electronic Engineering Committee, dated 20 December 1968, Published by Aeronautical Radio, Inc., 2551 Riva Road, Annapolis, Maryland 21401.
- Skolnik, M. I., "Introduction to Radar Systems," McGraw-Hill Book Company, Inc., New York, 1962.
- "Airborne Weather Radar Data," Business and Commercial Aviation, Ziff-Davis Publishing Company, New York, April 1970.

Several manufacturers of general aviation weather radar publish informative pilot's handbooks and other brochures. Names and addresses of manufacturers are listed in annual buyer's guide issues of Business and Commercial Aviation, Flying, the AOPA Pilot, etc.

The proper understanding, interpretation and use of weather radar is essential for safe flight. A number of organizations conduct courses and/or have available training films for assisting pilots in obtaining and maintaining proficiency in the use of weather radar.

### 1.3 Acknowledgements

Initial work on the contract included visits and telephone conversations with individuals in representative laboratories to (1) review the state-of-the-art in weather detection and analysis, and (2) to determine the current and projected state-of-the-art in microwave phase-shifters and integrated circuits. The cooperation and helpful assistance, particularly in supplying reports, pictures, charts, etc., by the following organizations is gratefully acknowledged.

FAA Academy/ DOT	Oklahoma City, Oklahoma
Hughes Aircraft Company	Culver City, California
Ionospheric Telecommunications Laboratory/ESSA	Boulder, Colorado
Lincoln Laboratory/MIT	Bedford, Massachusetts
Microwave Associates	Burlington, Massachusetts
National Severe Storm Laboratory/ESSA	Norman, Oklahoma
NorthAmerican-Rockwell	Anaheim, California
Oklahoma State University Themis Project	Stillwater, Oklahoma
Radio Corporation of America	West Los Angeles, California
Raytheon Company	Waltham, Massachusetts
Stormy Weather Group/McGill University	Montreal, Quebec, Canada
Texas Instruments Company	Dallas, Texas
Westinghouse Corporation	Baltimore, Maryland

Although the views expressed here are those of the author, much credit is also due Mr. Janis Vilcans of NASA for encouragement and assistance in this study of a difficult subject.

### 1.4 Nomenclature

- a = Parameter dependent upon clutter, dimensionless.
- $a_0$  = Amplitude of antenna pattern without blanking.
- $a_1$  = Vertical aperture dimension.
- $a_2$  = Dimension of screen opening, units consistent with units for wavelength.

$\text{\AA}$	= Angstrom unit, $10^{-8}$ centimeters.
A	= Cross-sectional area, square feet.
$A_e$	= Effective receiving area of antenna, $Af_e$ .
$\alpha$	= Normalized elevation angle for continuous aperture.
$\beta$	= Receiver bandwidth, Hz.
c	= Velocity of light, $10^8$ meters/second.
C	= A constant; also with subscript.
C-Band	= Frequency range from 4,000 to 8,000 MHz.
$C_D$	= Drag coefficient.
d	= Interelement spacing in antenna array.
$D_i$	= Diameter of $i^{\text{th}}$ droplet, mm.
D	= Aerodynamic drag, in pounds.
$\delta$	= Round-trip attenuation, in decibels.
$\delta_a$	= Height of obstacle blanking aperture.
$\delta_s$	= Shift in MDS of terrain return, in decibels.
$\Delta$	= Round-trip antenna pattern with odd symmetry.
E	= Energy, Joules.
f	= Frequency, Hz.
$f_e$	= Antenna efficiency factor with a maximum value of one.
$f_n$	= Frequency at $n^{\text{th}}$ mixer, Hz.
$f_o$	= Local oscillator frequency, Hz.
$f_r$	= Pulse repetition frequency, pulse per second.
F or $F(t)$	= Fourier transform.
FOM	= Figure of merit, dB/360 degrees phase shift.
G	= Antenna gain.
$G(\theta)$	= Antenna gain at angle $\theta$ .
h	= Height above the surface.
$h_1$	= Height of aircraft above surface, NM.
$h_2$	= Height of storm above surface, NM.

$\theta$	= Far-field angle in elevation plane.
$\theta_{BW}$	= Elevation plane beamwidth.
$i_{180}$	= Backscatter parameter, for an incident plane wave; the back-scattering coefficient is $4\pi$ times the ratio of the reflected power per unit solid angle in the direction of the source divided by the power per unit area in the incident wave.
$I$	= Reflected radiance.
$I_b$	= Background flux density, photons/second/cm <sup>2</sup> .
K <sub>a</sub> -Band	= Frequency range from 26.5 to 40 GHz.
K <sub>u</sub> -Band	= Frequency range from 12.5 to 18 GHz.
$K$	= Antenna slope factor, volts/volt/degree.
$K_0$	= Minimum value of $K$ .
$l$	= Length of endfire array.
$L$	= Microwave loss factor, a ratio.
$\lambda$	= Wavelength.
$m$	= An integer, -2, -1, 0, 1, 2, etc.
$M$	= Pulse integration factor.
$N$	= Noise power in S/N ratio.
$N$	= Number of antenna elements in array, in horizontal dimension.
$\Omega$	= Solid angle, steradians.
$p$	= Sidelobe amplitude ratio.
$P$	= Power, in watts.
$q$	= Dynamic pressure, $1/2 \rho V^2$ , pound/feet <sup>2</sup> .
$r$	= Range-to-target, NM.
$r_{fill}$	= Maximum beam filling range.
$r_{max}$	= Maximum range of detection on standard target, NM.
$R$	= Rainfall rate in millimeters/hour.
$\rho$	= Density of air, slug/feet <sup>3</sup> .
$S$	= Signal power, watts.
$S_n$	= Distance from reference point to the $n^{th}$ array element.

$\sigma_a$	= Extinction coefficient; the power per unit area transmitted through the atmosphere decreases exponentially as the product of the extinction coefficient and the distance traversed, proportional to the inverse of the visibility, $V_a$ .
$\sigma$	= Target radar cross-section, meters <sup>2</sup> .
$\Sigma$	= Round-trip antenna pattern with even symmetry.
$t$	= Number of bits in digital phase shifter.
$T$	= Absolute temperature, degrees Kelvin.
$\tau$	= Pulse length, seconds.
$\phi_i$	= Scan angle between pulse transmissions, degrees.
$\phi_s$	= Antenna scan sector, degrees.
$\phi$	= Azimuth far-field angle, degrees.
$\phi_{BW}$	= Azimuth beamwidth, degrees.
$\psi_n$	= Electrical phase shift in radians of $n^{\text{th}}$ element.
$\Delta\psi$	= Smallest bit size in digital phase shifter in radians or degrees.
$V_a$	= Atmospheric visibility; that greatest distance toward the horizon at which an unaided normal eye can clearly distinguish prominent objects without aid of optical devices, proportional to the reciprocal of the extinction coefficient.
$V$	= Weather target volume, cubic meters.
$V_1$	= Velocity in feet/second.
$W(f)$	= Power spectrum, in watts/Hz.
X-Band	- Frequency range from 8,000 MHz to 12,500 MHz.
$Z$	= Weather parameter; $\Sigma D_i^6$ , in millimeters to the sixth power per cubic meter.

## 1.5 Abbreviations and Acronyms

For a more extensive listing of aviation abbreviations, the reader is referred to the Airman's Information Manual (AIM), a publication of the Federal Aviation Administration.

ADF	Automatic Direction Finder
ARSR	Air Route Surveillance Radar

AN/APQ-7	A World War II linear array for mapping radar with mechanical scan.
AN/APS-10	An early weather/navigation radar designed in 1944 at the MIT Radiation Laboratory.
ATC	Air Traffic Control
ATIS	Air Traffic Information Service
B-Scan	An X-Y, Range-Azimuth Display
CAVU	Ceiling and Visibility Unlimited
CRT	Cathode Ray Tube
dB	Decibel
FAA	Federal Aviation Administration
FOM	Figure of Merit
GA	General Aviation
HP	Horsepower
IFR	Instrument Flight Rules
IMPATT	Impact Avalanche Transit Time
LIDAR	Light Detection and Ranging
LOS	Line-of-Sight
LSA	Limited Space Charge Accumulation
MDS	Minimum Detectable Signal
MERA	Molecular Electronics for Radar Applications
MIC	Microwave Integrated Circuit
MIT	Massachusetts Institute of Technology
MO	Master Oscillator
MODSCAN	Modulating Scanning
MSL	Mean Sea Level
NACA	National Advisory Committee for Aeronautics (a predecessor of NASA)
NASA	National Aeronautics and Space Agency
NEP	Noise Effective Power
NF	Noise Figure

NM	Nautical Miles
NSSL	National Severe Storms Laboratory
OMNI/VOR	VHF Omni-Range, a short range navigation aid
PPI	Plan-Position Indicator
RADAR	Radio Detection and Ranging
RF	Radio Frequency
SCALO	Scanning Local Oscillator
SDF	Signal Degradation Factor
SEF	Signal Enhancement Factor
SFERIC	Contraction of Atmospheric
VFR	Visual Flight Rules
VOR/OMNI	VHF Omni-Range, a short range navigation aid
VSWR	Voltage Standing Wave Ratio
WSR-57	A 10 cm Wavelength Meteorological Radar

## 2.0 OPERATIONAL CHARACTERISTICS

### 2.1 Introduction

Two categories of weather are of operational interest to the General Aviation (GA) pilot. These are visual flight and instrument flight weather. Most GA flights are made under the Visual Flight Rules (VFR) of the Federal Aviation Administration (FAA) regulations. The VFR only pilot is restricted, for safety reasons, to flight in conditions where visibility is three miles\* or more and the ceiling is 1000 feet or higher (see Figure 2.1). The VFR pilot must also maintain a horizontal clearance from clouds of 2000 feet and a vertical clearance of 1000 feet above and 500 feet below clouds\*\*. Visibility and ceiling can change significantly over a distance of a few miles since weather forecasts and current meteorological reports provide the VFR pilot with the average conditions along a route. The fluctuations in visibility and ceiling which often occur along a route with deteriorating weather can lead the VFR pilot to estimate the weather as better than is actually subsequently encountered. Over optimism, in turn, may increase the risk of accident through disorientation of a VFR only pilot and through increased risk of collision with other aircraft, towers, mountains, etc. The safety of VFR flight operations, particularly night VFR, might be improved by a suitable low-cost weather sensor. This sensor should enable the VFR pilot to make quantitative measurements of visibility and horizontal and vertical distance to clouds. Radar and/or radiometer sensors operating at millimeter, IR or visual light wavelengths merit investigation for this application.

GA flight operations, with weather conditions such that visibility is less than VFR minimums, are in accord with the instrument flight rules (IFR) of the FAA. GA flights can be made under IFR in VFR conditions at the option of the pilot; however, an instrument rating is required when operating IFR. The instrument rated GA pilot is trained to maintain stable flight by reference to gyro instruments and without using an external reference such as the earth surface (horizon). During flight along the route of an IFR flight plan clearance, he may encounter and penetrate storm cells of varying intensity. He will receive some assistance in evaluating the strength and in avoiding these storms from Air Traffic Control (ATC); however, the enroute and terminal area radars are designed to minimize the weather return<sup>1</sup>.

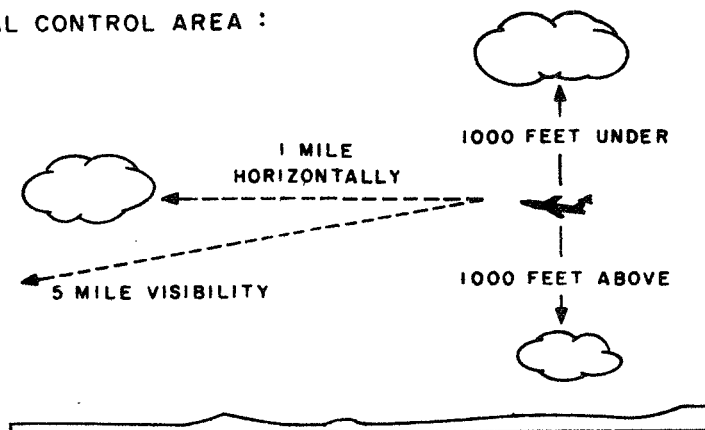
---

\*Outside controlled airspace the flight visibility must be one mile, also above 10,000 feet MSL the visibility must be at least five miles.

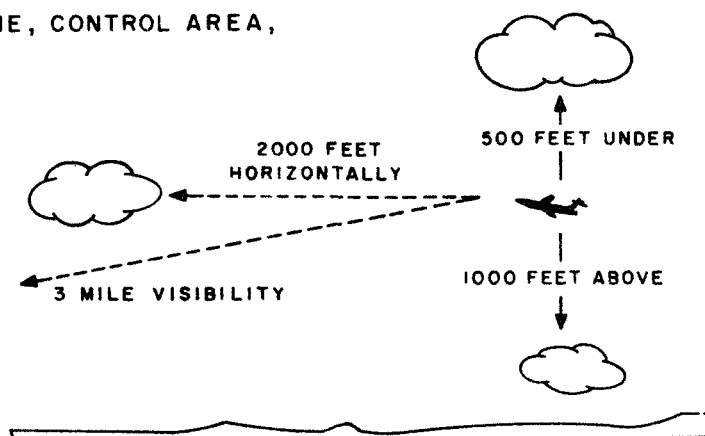
\*\*Outside controlled airspace and below 1200 feet above the surface to remain clear of the clouds, while above 10,000 feet MSL to maintain a distance of 1000 feet above and one mile horizontal.



WITHIN THE CONTINENTAL CONTROL AREA :



WITHIN A CONTROL ZONE, CONTROL AREA,  
OR TRANSITION AREA :



OUTSIDE CONTROLLED AIRSPACE :  
(FLIGHT ABOVE 1200 FEET ALTITUDE)

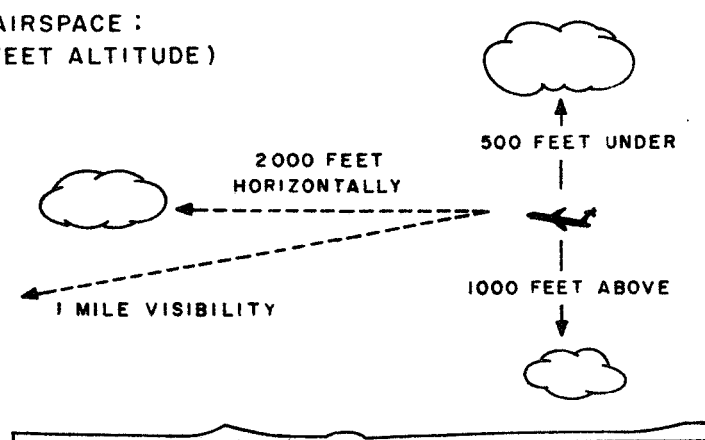


FIGURE 2.1. VISIBILITY AND DISTANCE FROM CLOUDS FOR  
VISUAL FLIGHT RULES (VFR) MINIMUMS

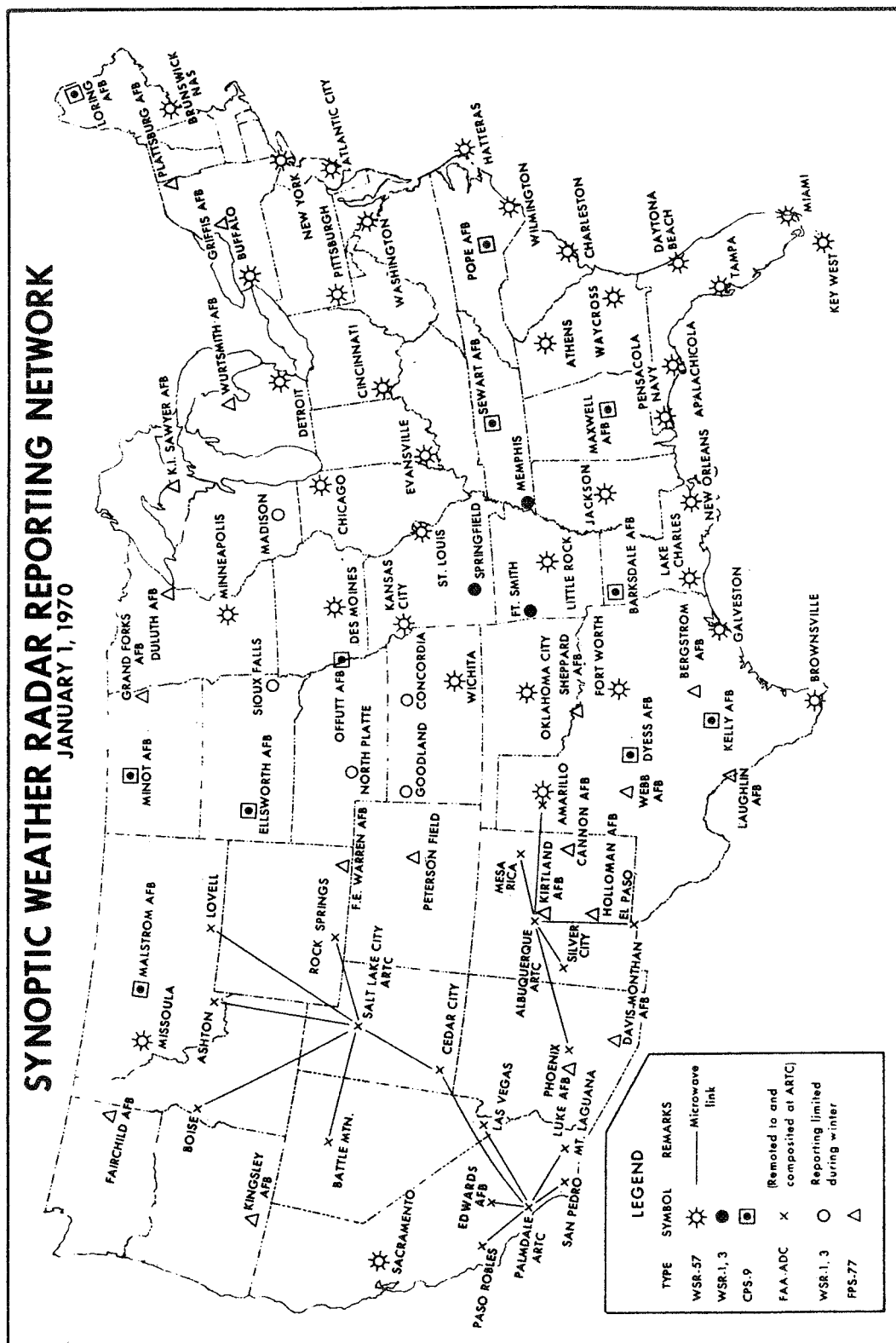


FIGURE 2.2 LOCATION OF GROUND WEATHER RADAR STATIONS IN USA  
(Chart Prepared by Environmental Science Services Administration)

The WSR-57, 10 cm wavelength, weather bureau radars (see Figure 2.2) delineate severe storm areas; however, at the present time the use of weather bureau radar information is often not coordinated with ATC. The need for improved coordination of ATC and weather information is recognized, and study, development and training effort is underway<sup>2,3,4</sup>. At the present time, the IFR pilot needs an airborne weather sensor to enable him to avoid severe storm areas and to penetrate only those areas of low storm intensity. In addition to avoiding the core area of severe storms, the quality of current radar weather sensors requires that the area immediately surrounding the severe storm also be avoided. FAA Advisory Circular, AC No. 00-24, dated 12 June 1968<sup>5</sup>, on Thunderstorms states in paragraph 3c on flight in and near thunderstorms the following:

"National Severe Storm Laboratory (NSSL) data indicate frequency and severity of turbulence encounters decrease slowly with distance from storm cores. Significantly, the data indicate that 20 miles from the center of severe storm cores, moderate to severe turbulence is encountered at any altitude about one-fifth as often as in the cores of severe storms whose radar reflectivity factor Z (see Appendix A) exceeds  $10^4$ . Further, the data indicate that moderate to severe turbulence is encountered at any altitude up to 10 miles from the center of less severe storm cores whose reflectivity factors Z lie between  $10^3$  and  $10^4$ ."

Weather radar, either ground or airborne, is capable of providing adequate estimates of rainfall rates and gradients though radar parameters such as transmitter wavelength and antenna beamwidth must be carefully selected. Because of the good correlation among radar measurements, instrumented flight tests and ground observations, radar is given primary consideration as an airborne weather sensor.

## 2.2 Operational Characteristics

The operational characteristics of the weather sensor must be compatible with the object of installation in single and dual in-line engine aircraft as well as twin engine aircraft and low-cost, light weight, etc. The primary characteristics are considered to be tilt angle sector, scanning sector, altitude, range, display, resolution, and scan rate. From the primary characteristics, a number of secondary characteristics can be derived such as transmitter frequency and power, beamwidth, antenna size, pulse length, pulse repetition rate, average power, etc. The primary characteristics are tabulated in Table 2.1, with separate characteristics for VFR and IFR weather sensors.

TABLE 2.1  
PRIMARY OPERATIONAL CHARACTERISTICS

I. VFR FLIGHT			
Characteristic	Desirable	Acceptable	Comments
1. Display	PPI	R Meter	Meter to measure range (r) to clouds and precipitation.
2. Scan Sector	Automatic $\pm 90^\circ$ Az.	Manual at Selected Angles	Used primarily along line of flight, but also to range in selected directions.
3. Tilt Sector	$\pm 90^\circ$ El.	$\pm 90^\circ$ El.	Discrete positions acceptable, possibly in five degree steps.
4. Altitude	Surface to 20,000 feet	Surface to 20,000 feet	Altitude range over which equipment is expected to operate.
5. Range	0 to 20 NM	3 NM	Use as radar altimeter possible if will work to nearly zero range.
6. Resolution	1 foot range $1/2^\circ$ angle	1/4 NM range $1^\circ$ angle	Use as landing altimeter, requires fine range resolution.
7. Target	Clouds, Fog, Rain, Terrain	Clouds	
8. Hours of Operation	Daylight and, Darkness	Night VFR only	Background skylight requires much stronger transmitter for daylight operation.

TABLE 2.1 (Cont'd.)

## PRIMARY OPERATIONAL CHARACTERISTICS

II. IFR WEATHER FLIGHT			
Characteristic	Desirable	Acceptable	Comments
1. Display Type	PPI	B-Scan	A-scope or meter to measure range might be of marginal value.
dynamic - range brightness	40 dB 50 to 100 foot lamberts	30 dB 10 to 25 foot lamberts	Limited by daylight on display. Light shield required for low brightness displays.
2. Scan Sector	$\pm 90$ degrees	$\pm 45$ degrees	Smaller scan sectors might be of limited value.
3. Tilt	$\pm 20$ degrees	$\pm 15$ degrees	To permit operation during climb and descent.
4. Scan Rate	Flicker-free display with one new picture/30 secs.	One frame one minute	Conventional radar scan rates are acceptable but either faster scan rates or better storage are preferred.
5. Altitude	Surface to 45,000 feet	Surface to 20,000 feet	Desirable to be able to operate when parked near the runway.
6. Range detection analysis penetration	100 NM 30 NM 5 NM	50 NM 20 NM Not defined	Standard 3 NM diameter storm just fills beam at analysis range. 50 mm/hour rainfall.

TABLE 2.1 (Cont'd.)  
PRIMARY OPERATIONAL CHARACTERISTICS

II. IFR WEATHER FLIGHT (Cont'd.)			
Characteristic	Desirable	Acceptable	Comments
7. Resolution angle range	6° Az. 1/4 NM	8.5° Az. 1 NM	
8. Target	Light to heavy rain. 5 mm/hour to 100 mm/hour	Moderate to heavy rain. 25 mm/hour to 100 mm/hour	
9. False Targets angle range	-50 dB > 100 NM	-40 dB > 60 NM	Sidelobes. Second-time echoes.

Many cross-country flights of a few hundred miles encounter marginal VFR weather over a portion of the flight route or at least require flight close to clouds. Currently, pilots make intuitive estimates of cloud clearances and visibilities along the flight route. If a low-cost device can be developed to measure cloud clearances and to give improved estimates on visibility, then the continuation of VFR flight into IFR conditions can be avoided, particularly at night. This statement is qualified since the device must have "pilot acceptance" as well as low initial cost. A pulsed light radar device (LIDAR) offers considerable promise for cloud ranging and a lesser capability for estimating visibility through backscatter measurements. The next section, Section 2.3, discusses some of the characteristics of clouds as viewed by a pulsed light ranging equipment (LIDAR).

Sections 2.4 and 2.5 describe weather models for use with microwave radar. These models supplement the primary operating characteristics and enable other radar parameters to be determined. The first model is a simple spherical rain target, while the second model includes attenuation from intervening rain. These sections are supplemented by information on the echo area of precipitation, Appendix A and charts for computation of radar range, Appendix B.

The next two sections, Sections 2.6 and 2.7, describe the effect of radar beamwidth and tilt angle on terrain return. First is a general description of the problem, followed by a method of synthesizing the lower edge of the elevation beam. The terrain return must be suppressed adequately or else the terrain return may be mistaken for storm returns on the radar display. This problem of suppression of terrain return is particularly critical for single and in-line engine aircraft where the nose section is not available for a conventional radome.

The final section, Section 2.8, discusses the characteristics of sferics, which might be used for a passive weather sensor. The use of airborne instantaneous direction finding (DF) on sferics to locate severe storm areas does not appear promising in comparison with airborne radar. Sferic DF indications do not adequately define either the location or intensity of severe storm areas.

### 2.3 LIDAR Weather Model

Light detection and ranging (LIDAR) equipment, is proposed as a VFR weather sensor. The LIDAR is used to range on clouds to enable the pilot to maintain legal cloud clearances and to enhance the safety of flight, particularly at night. A secondary role for the LIDAR is to assist the pilot in estimating forward visibility based upon the backscatter return. The need for a low-cost

cloud sensor for night VFR flight is well expressed by a private pilot, Mr. Archie Trammell, in Flying magazine. Quoting from his article<sup>6</sup> on night single-engine flight, "At least two dozen times at night, I've run into solid instrument weather that was neither forecast nor reported. Returning from New York one night, all stations along Victor 16, Charleston to Dallas, were reporting CAVU and forecast to remain so. Yet, directly over the Nashville Omni, I ran into gloom and had to descend 2,000 feet to get out of it.

"Another crystal-clear night, going into Baton Rouge, I had the airport visual 15 miles out. On a one-mile final and cleared to land, the runway lights suddenly disappeared - at the same time a breathless weather special was broadcast from the tower saying the field had just gone to 300 and one-half. What to do? Since I couldn't see the weather, a go-around or a 180 would likely have ended with me plunging into the muck. I asked for an approach and received the quickest clearance ever given.

"On yet another night, I was descending out of 3,000 from the north into Love Field, Dallas, listening to ATIS giving clear and eight miles. Suddenly, everything went so black I thought for an instant I'd been struck blind. I had, in a way, for I'd descended into haze just at the north end of Garza Little Elm Reservoir. I'd lost the visual horizon at the instant surface lights broke off at the water line."

The examples given by Mr. Trammell illustrate that restrictions to visibility are of a statistical nature. To the VFR only pilot, an unexpected restriction of visibility can be as serious as severe turbulence encountered by the IFR pilot in a thunderstorm. The statistical nature of the weather, particularly that aspect described by visibility, is currently recognized by the FAA requirement that new pilots have some experience in flying by reference to instruments. Pilots who were licensed prior to the current requirement are encouraged to update their qualifications by the "blue seal" program. While minimum instrument flight training can supplement warnings to VFR pilots concerning the statistical nature of weather, a probe is needed to sense the visibility along the projected flight path. Just as the IFR pilot uses weather radar to inspect storms for severity, the VFR pilot needs a visibility probe for marginal conditions.

Detection and ranging of clouds can be accomplished using an infrared laser (LIDAR equipment). Because of the much shorter wavelength of the pulsed light device, there is considerable backscattering by clouds. The clouds may be considered as perfectly diffused reflectors with reflectivity ranging from one to sixty percent. Hovis and Tobin<sup>7</sup> have reported on a spectral measurement of energy from clouds during a series of flights in NASA's Convair 990 jet aircraft. The wavelength region of 1.6 to 5.4 microns



was scanned with an instrument with a spectral resolving power of  $\lambda/\Delta\lambda = 100$ . For the best signal-to-noise ratio, a wavelength of about three microns should be used since the solar spectrum and the spectral radiance of the clear sky are lower at this wavelength. According to Hovis, et al, this is somewhat counterbalanced by the lower reflectance of clouds at the longer wavelengths. For example, 60 to 65% reflectance is measured at 1.6 microns and only 4.5%, both on stratus clouds at 3.7 microns. A fairly dense layer of cirrus clouds, as viewed from above, had a reflectance of only 1% at 3.4 to 4.2 microns. The transmitter power required for cloud ranging is estimated in Appendix D.

The measurement of the visual range (or visibility  $V_a$ ) from the backscatter from a monochromatic (laser) or white light source has been investigated by Fenn<sup>8</sup> and others. One investigation<sup>9</sup> concluded that there exists a relation, although not a unique one, between atmospheric backscattering and the extinction coefficient, and that this correlation is better for white than for monochromatic light. A major difficulty arises because of the variability of particle size for a constant liquid water content. The increase of visual range with a shift to larger particles for a constant total mass is well known from the relation holding for fog or cloud droplets, according to which the visual range is proportional to the droplet size, but inversely proportional to the liquid water content of the cloud. An extensive series of scattering measurements has been reported by Barteneva<sup>10</sup>. Her report includes 624 measurements of the scattering function in various locations. Her plot of backscattering intensity,  $i_{180}$ , is reproduced as Figure 2.3, and is a function of extinction coefficient and visibility.

In view of the results obtained by Barteneva, the conclusions given by Fenn seem valid, which are that no general relation exists between the atmospheric extinction coefficient and the backscattering property,  $i_{180}$ . The various processes involved in the formation and decay of the natural aerosol (like coagulation, increase or decrease in particle number, etc.) result in different relations between backscattering and extinction. The use of white light instead of monochromatic light will reduce considerably the uncertainty in the relation between backscattering and visibility.

#### 2.4 Precipitation Weather Model for Determining the Detection Range of Microwave Radar (No Attenuation From Intervening Rain)

The precipitating cumulonimbus can be represented by an equivalent target of uniform rainfall. For example, a nominal target for determining detection range is a 3 NM diameter sphere filled with a uniform precipitation of 50 mm per hour<sup>11</sup>. For the simple model, the two-way atmospheric attenuation from intervening precipitation is not considered.

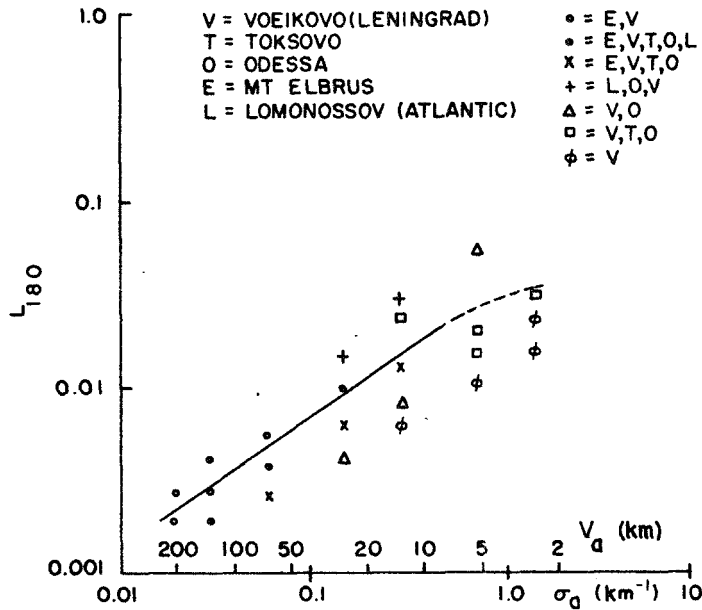


FIGURE 2.3. RELATION BETWEEN BACKSCATTERING  
AND EXTINCTION COEFFICIENT  
AS DERIVED FROM DATA BY BARTENEVA<sup>10</sup>

This 3 NM diameter target will just fill a circular radar beam at a range

$$r_{\text{fill}} = 172/\theta_{BW} \quad (2.1)$$

where  $r_{\text{fill}}$  = Maximum beam filling range, NM

$\theta_{BW}$  = Antenna beamwidth, degrees.

For ranges greater than  $r_{\text{fill}}$  the beam will not be filled by the 3 NM diameter storm model and the radar return becomes a less accurate measure of the rain fall rate.

Another parameter that must be specified on the model storm is the height above the earth surface of the center of the equivalent spherical target. Inspection of storm returns, as displayed by height-finding radar, indicates that the core region is generally elliptical rather than spherical with the major axis aligned vertically. After reviewing several photographs of height-finding displays of storms, a nominal height of 2 NM is assumed for the center of the

3 NM diameter spherical core. This is a conservative target in that severe storm cores will likely extend to 5 NM height instead of the assumed 3.5 NM.

## 2.5 Precipitation Weather Model With Attenuation From Intervening Rain

The spherical storm model described in the previous section is adequate when considering storms with isolated thunderstorm cells. If more complex storms are to be modeled, then consideration must be given to intervening precipitation and multiple in-line cells. This introduces the effect of the wavelength of the microwave signal both upon the attenuation of the signal and the antenna beamwidth. A shorter wavelength transmitter produces a narrower beamwidth for a particular antenna dish size but also results in more attenuation in the intervening rain between cells and particularly in the heavy rain within cells. From the packaging viewpoint, the use of a very short wavelength such as K<sub>a</sub>-Band is highly advantageous as the antenna requires a minimum of frontal area. A six-inch diameter K<sub>a</sub>-Band antenna can be contained within a small plastic tip-tank or in the wing leading edge of a single-engine aircraft. However, as will be shown by the use of a more complex weather model, the K<sub>a</sub>-Band radar has little ability to penetrate rain and is inadequate to define cells.

Marshall, et al,<sup>12,13</sup> of the Stormy Weather Group at McGill University have developed radar weather models which include intervening rain. In considering the effect of wavelength they have used rainfall rates as measured in actual storms near Montreal, Quebec, Canada. A simplified model of the actual storms measured by Marshall is used in this report to demonstrate wavelength effects. This model has a strong cell at 20 NM, with intervening rain and a second cell at 30 NM. The 20 NM distance is chosen as the minimum approach distance to the center of a storm cell until it has been categorized as weak, moderate, or severe. The model complex storm is sketched in Figure 2.4, assuming that the rainfall is uniform in the radial and vertical directions.

This model complex storm simulates the situation along the line-of-sight (LOS) in Figure 2.5, where lack of knowledge of the second storm might lead the pilot to select a flight path dangerously close to a severe storm.

Referring to Appendix A for a beam filling case, the expression for the average signal return power is

$$\overline{P_r} = \frac{CZ}{r^2} \quad (2.2)$$

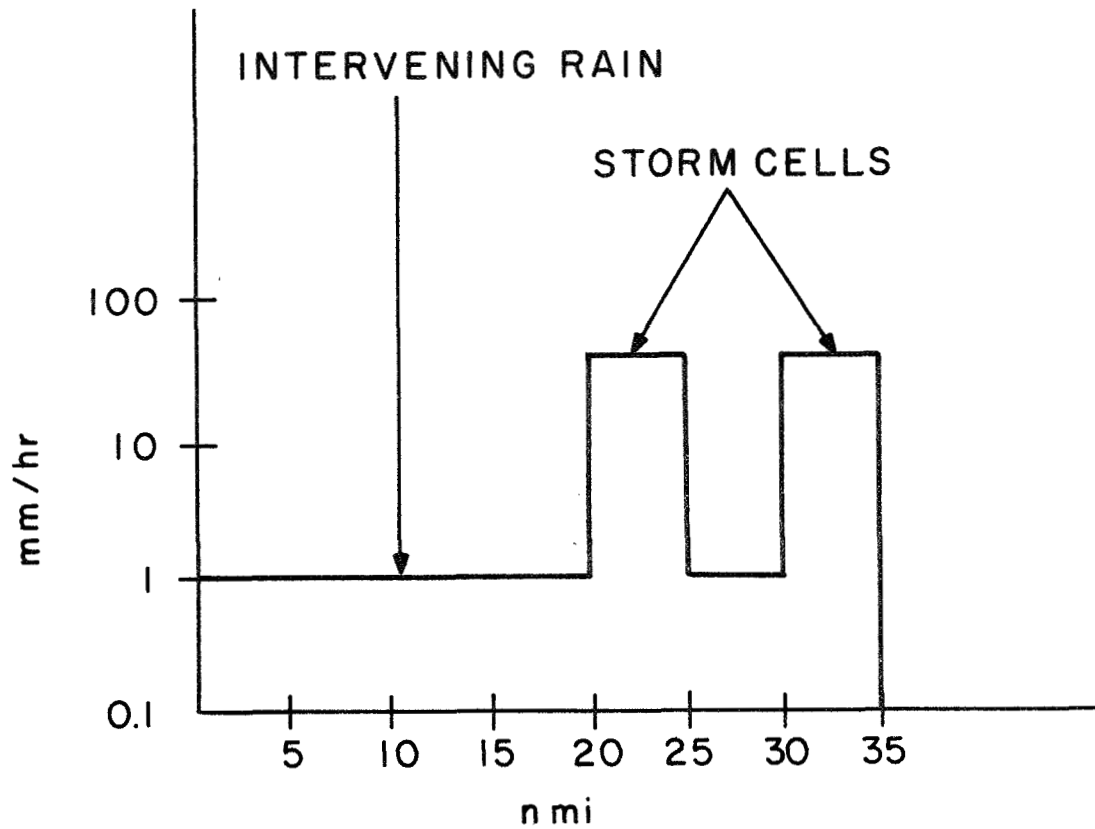


FIGURE 2.4. MODEL COMPLEX STORM  
WITH INTERVENING RAIN AND IN-LINE CELLS

where  $\overline{P_r}$  = Mean received power, watts

$C$  = A constant determined by radar parameters

$Z$  =  $\sum D_i^6$  in  $\text{mm}^6/\text{meter}^3$ , a measure of precipitation radar cross-section

$D_i$  = Diameter of  $i^{\text{th}}$  precipitation particle in the unit volume, mm

$r$  = Radar range in nautical miles (NM)

If there is attenuation, then the return power will be decreased and the equivalent  $Z$  corresponding to the lower return can be determined.

$$10 \log_{10} \frac{\overline{P_{r2}}}{\overline{P_{r1}}} = -\delta \text{ dB} = 10 \log_{10} \frac{Z_2}{Z_1} \quad (2.3)$$

where  $\delta$  = Roundtrip attenuation in dB.

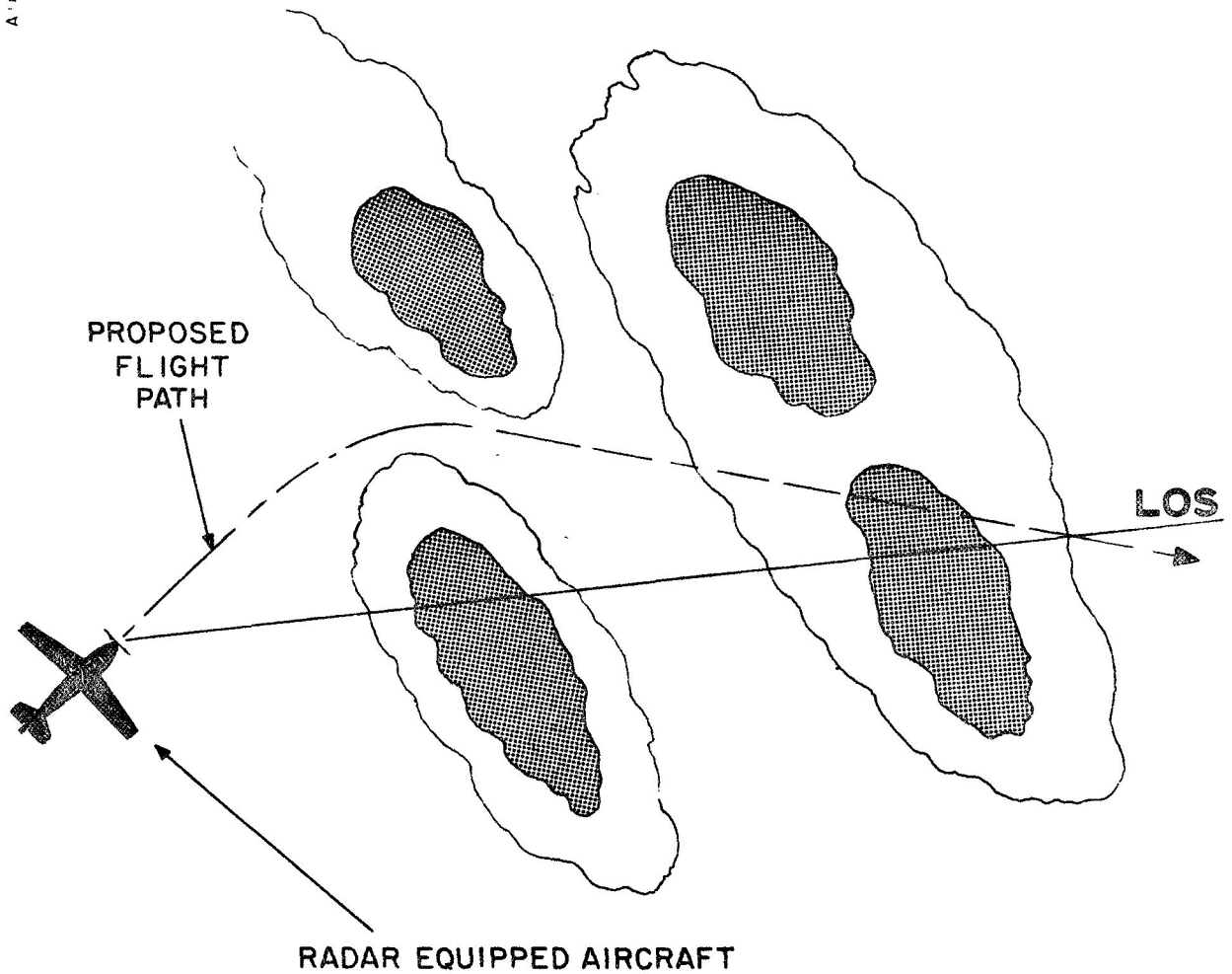


FIGURE 2.5. FRONTAL STORM SITUATION WHICH MIGHT TRAP PILOT USING RADAR WITH POOR PENETRATION CAPABILITY

Using the relation between  $Z$  and rainfall rate from Appendix A,

$$Z = 200 R^{1.6} \quad (2.4)$$

Where  $Z$  is as previously defined and  $R$  = rainfall rate in mm/hour, and substituting the expression for  $Z$  from Equation (2.4) into Equation (2.3), we obtain

$$10 \log_{10} R_2 = -\frac{\delta}{1.6} + 10 \log_{10} R_1. \quad (2.5)$$

Equation (2.5) shows that the equivalent rainfall rate,  $R_a$ , to give the same return at range,  $r$ , as the rainfall rate,  $R_1$  with intervening attenuation, is the initial rate expressed in dB, referred to 1 mm/hour, decreased by the attenuation in dB divided by 1.6. Since the attenuation increases linearly, in dB with range, a simulated display is plotted on semi-log graph paper. Further, it is assumed that the power gain of the receiver increases as the square of the range so that the inverse range squared term in Equation (2.2) is cancelled by the gain change. If there is no precipitation attenuation then the presentation intensity changes with range in accord with the rainfall rate, as in the model, Figure 2.4. Figures 2.6, 2.7, and 2.8 illustrate the effect of attenuation at three wavelengths, 1.8, 3.2, and 5.6 cms. The rainfall rates were selected as representative of severe storms after examination of actual storm cross-sections, as given by Marshall, and the 50 mm/hour rate is also the same as used for the model isolated storm, Section 2.4.

An examination of the graph, Figure 2.6, for 1.8 cm ( $K_u$ -Band) shows that the attenuation is very high within the storm cells and that a radar using such a short wavelength will not enable a pilot to make an accurate analysis of the assumed model storm. 3.2 cms (X-Band) represents a distinct improvement, but is marginal for severe storm analysis. A further increase of wavelength to 5.6 cms (C-Band) provides additional information. Ground-based weather radars usually operate at 10 cms (S-Band) where the precipitation attenuation is quite small; however, such long wavelengths require large antennas which are usually considered impractical for airborne use. (The modulation scanning technique described in Section 3.13 might enable a C-Band radar to be used on a single-engine aircraft.)

A recent NSSL report<sup>14</sup> compares PPI observations of severe thunderstorms by a WSR-57 ground weather radar and PPI displays obtained simultaneously with X-, C-, and  $K_a$ -Band airborne radars and with the ARSR-1D air traffic control radar used by the FAA. The results of this experimental study confirm the viewpoint that the attenuation is excessive above X-Band. Quoting from the abstract, "The data indicate that precipitation attenuation of C- and X-Band signals should not prevent their use for storm avoidance. Attenuation at  $K_a$ -Band is excessive, and use of this band is not advisable at middle and low flight altitudes."

## 2.6 The Terrain Return Problem

The weather model described in Section 2.4 requires that the antenna beamwidth be less than 8.6 degrees if the spherical model storm is to fill the beam at a range of 20 NM. A smaller beamwidth is desirable to better define the storm cell and to extend the range at which quantitative measurements of precipitation can be made. Also, vertical plane directivity in the antenna

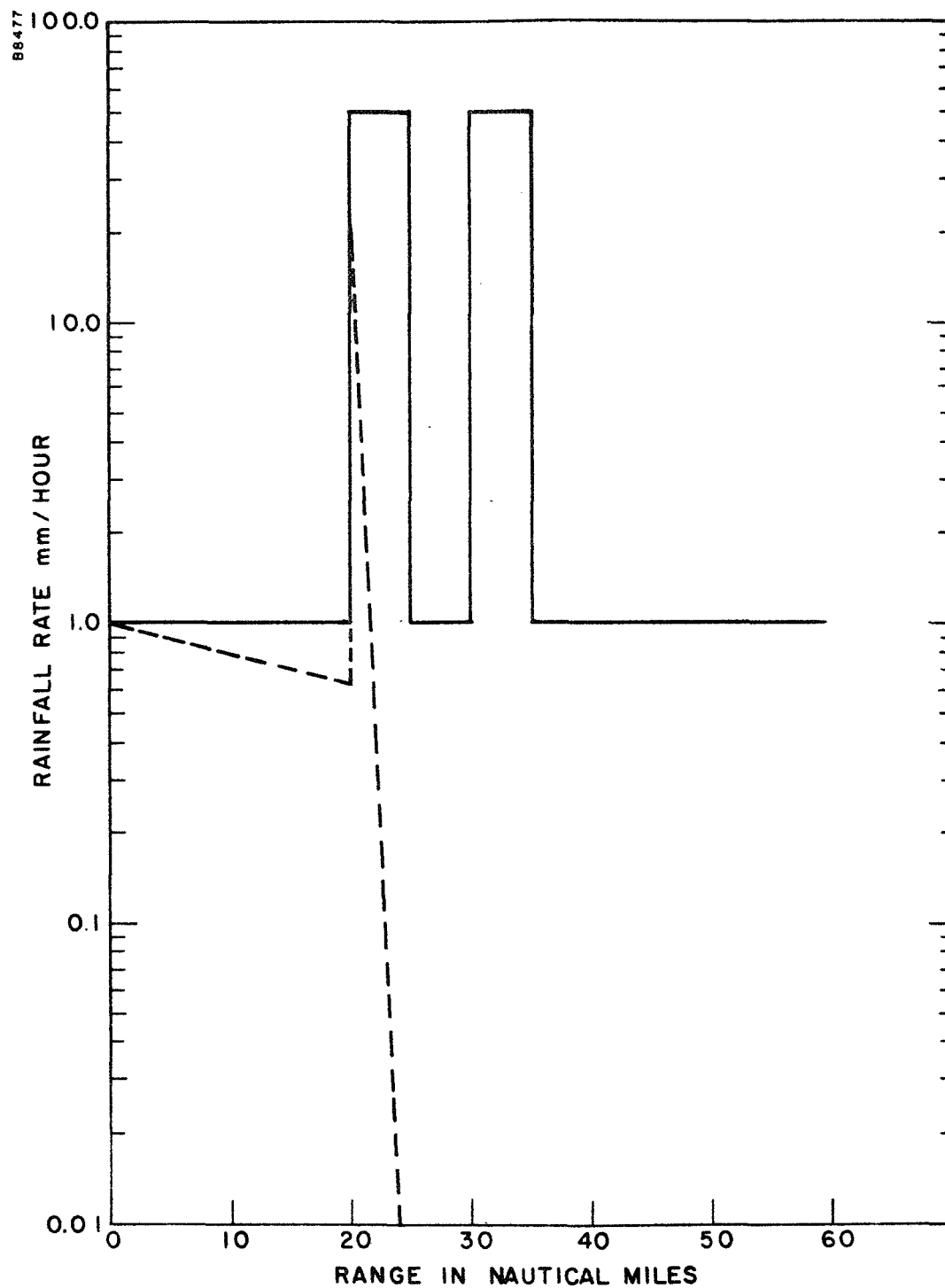


FIGURE 2.6. EFFECT OF RAINFALL ATTENUATION ON  
 RADAR STORM PRESENTATION FOR  $\lambda = 1.8$  cm ( $K_u$ -Band)  
 (Solid Line - No Attenuation; Dash Line - With Rainfall Attenuation)

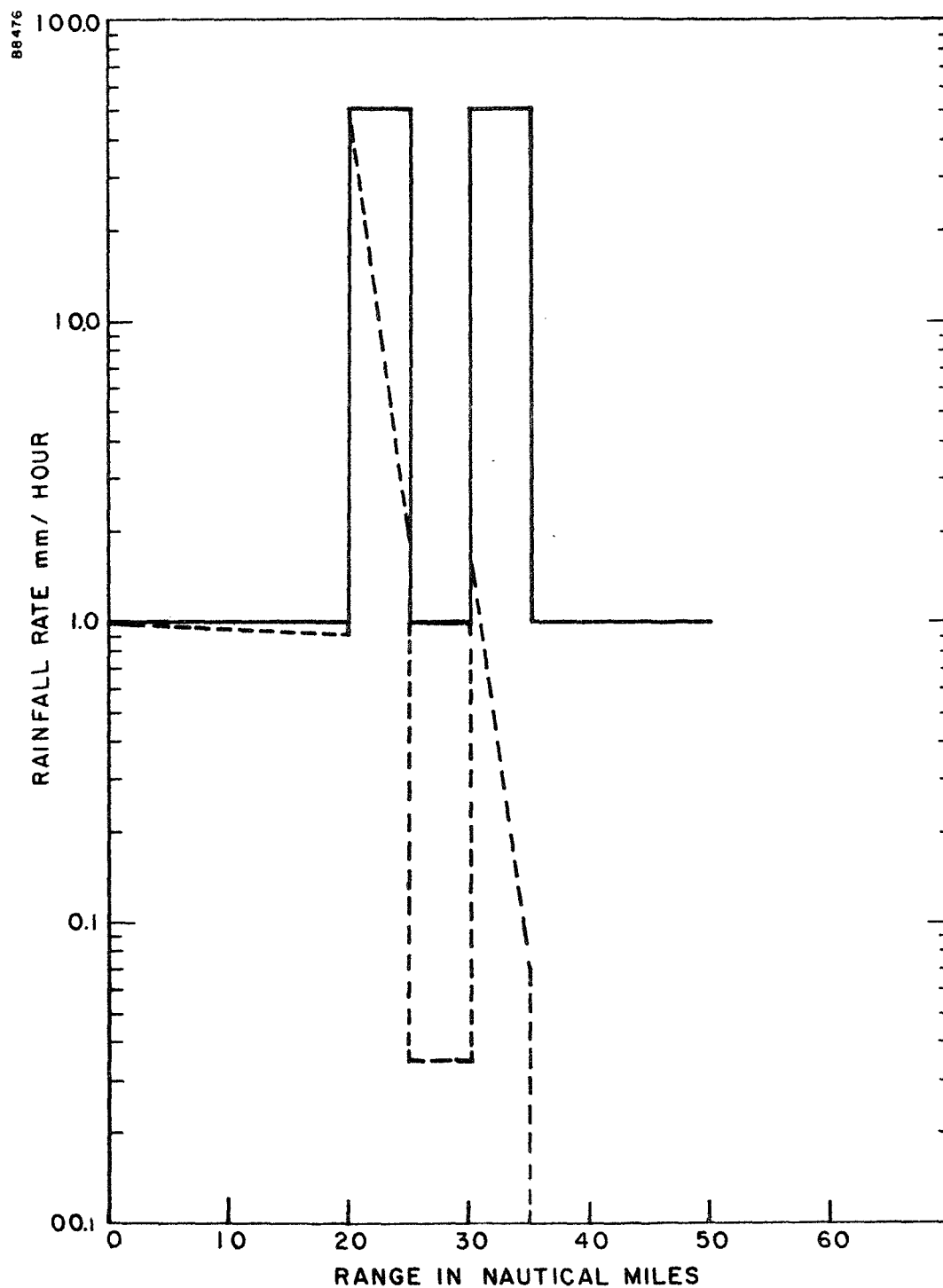


FIGURE 2.7. EFFECT OF RAINFALL ATTENUATION ON  
 RADAR STORM PRESENTATION FOR  $\lambda = 3.2$  cm (X-Band)  
 (Solid Line - No Attenuation; Dash Line - With Rainfall Attenuation)



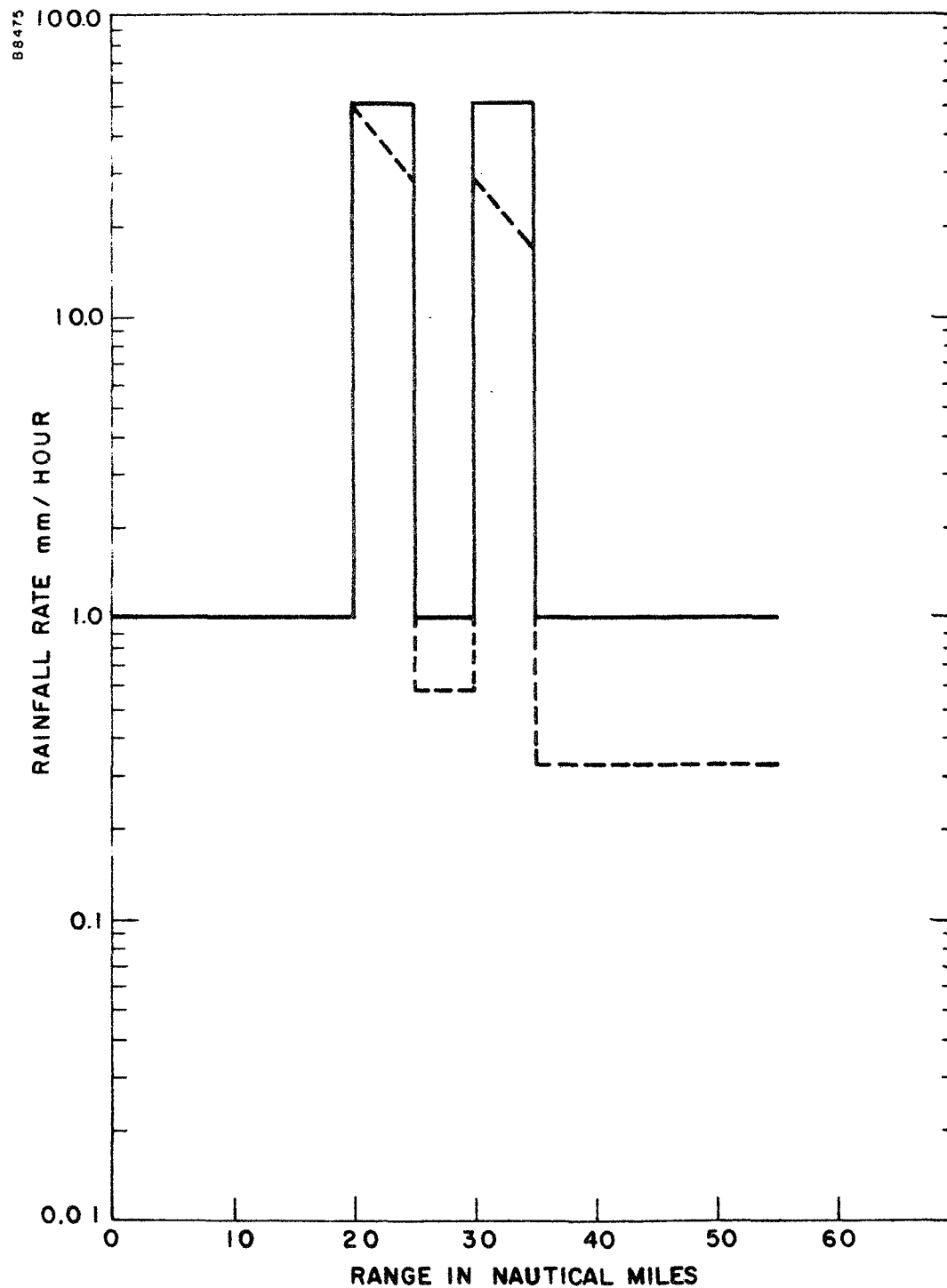


FIGURE 2.8. EFFECT OF RAINFALL ATTENUATION ON  
 RADAR STORM PRESENTATION FOR  $\lambda = 5.6$  cm (C-Band)  
 (Solid Line - No Attenuation; Dash Line - With Rainfall Attenuation)

pattern is necessary to provide adequate antenna gain and to suppress undesired terrain return. Terrain return often has more sharply defined edges than weather echoes, as viewed on a plan position indicator (PPI) display, though the presence of both can lead to confusion or at least to the obscuring of weather echoes. The complete elimination of terrain return from a weather radar display is difficult as a narrow vertical antenna beam and low vertical plane sidelobes are required as will be shown in the next section.

The radar cross-section of terrain can be expressed as a function of the parameters of pulse length, beamwidth, grazing angle and a terrain factor,  $\sigma^\circ$ , as in Equation (2.6).

$$\sigma_c = \sigma^\circ r \frac{c\tau}{2} \phi_{BW} \sec \theta_g \quad (2.6)$$

where  $\sigma_c$  = Radar cross-section, meters<sup>2</sup>  
 $\sigma^\circ$  = Average scattering cross-section per unit area illuminated by the radar, a ratio  
 $r$  = Range, meters  
 $c$  = Velocity of propagation, meters/second  
 $\tau$  = Pulse length, seconds  
 $\phi_{BW}$  = Azimuth beamwidth, radians  
 $\theta_g$  = Grazing angle, degrees

Unfortunately, there is little data on  $\sigma^\circ$  for the grazing angles of interest from 0 to approximately 15 degrees. Barrick<sup>15</sup>, in his Table 9-2, gives values for  $\sigma^\circ$  for X-Band which range from -12 dB at 10 degrees to -24 dB at 0-1 degree for cities and for the same angles, -20 to -36 dB for cultivated land. For further analysis, the ratio  $\sigma^\circ/\sin \theta_g$  is assumed constant at 0.1. (The ratio  $\sigma^\circ/\sin \theta_g$  has been designated  $\gamma$  by Cosgriff, et al,<sup>16</sup>.) The data points from Barrick, along with the assumed variation of  $\sigma^\circ$  with grazing angle, are plotted on Figure 2-9. The assumed curve for  $\sigma^\circ$  falls between the data points for cities and cultivated land. Barrick also footnotes his Table 9.2 with the comment that the radar cross-sections of cities have been observed to vary over several orders of magnitude as a function of street directions and plane of incidence. The values in his Table 9.2 represent, in general, the maximum reliable observed cross-section per unit area. Terrain returns, as observed on a small weather radar (12-inch dish, 10 KW and X-Band) are shown for four tilt angles in Figures 2.10a through d. In Figure 2.10a, the antenna is tilted down slightly and the strong terrain return out to 25 NM outlines Oneida Lake near Syracuse, New York, at approximately 12 NM range. From the 1 NM aircraft height, the peak of the antenna

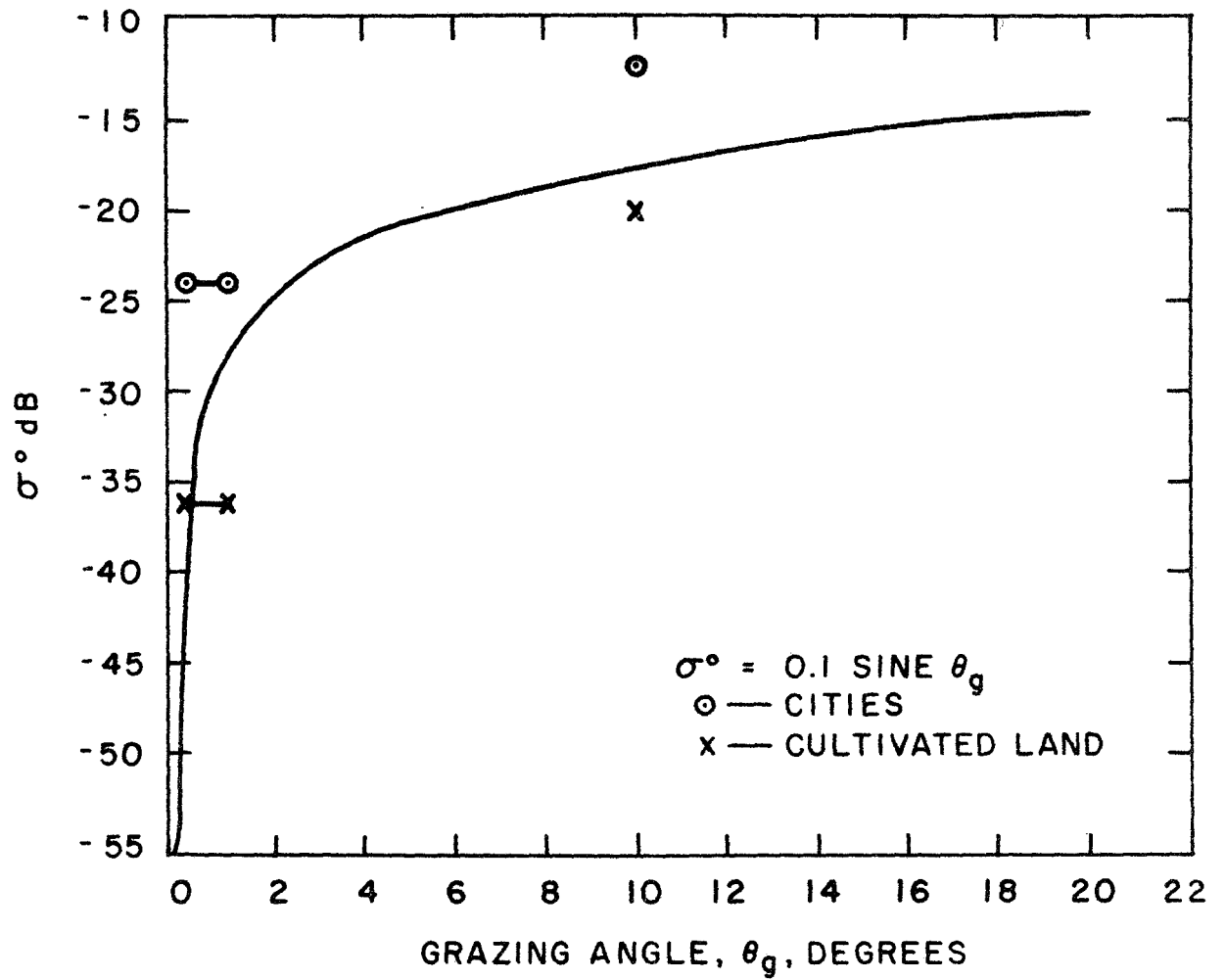
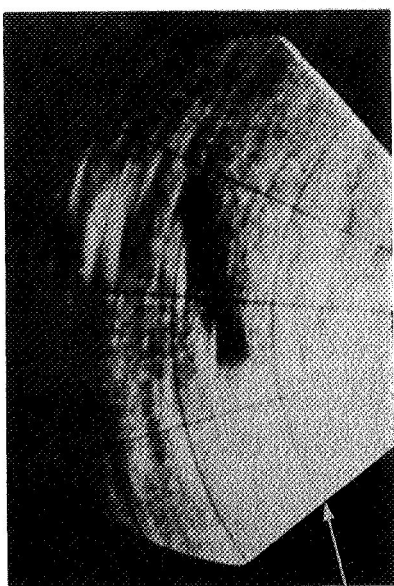
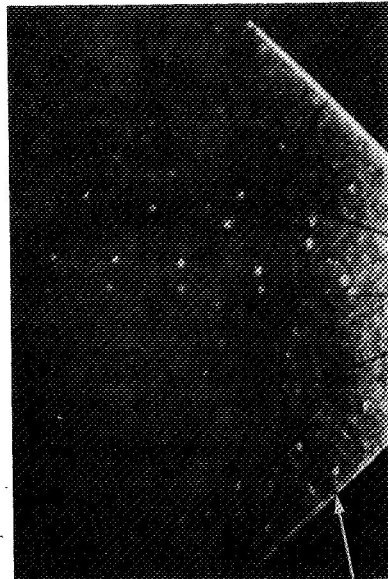


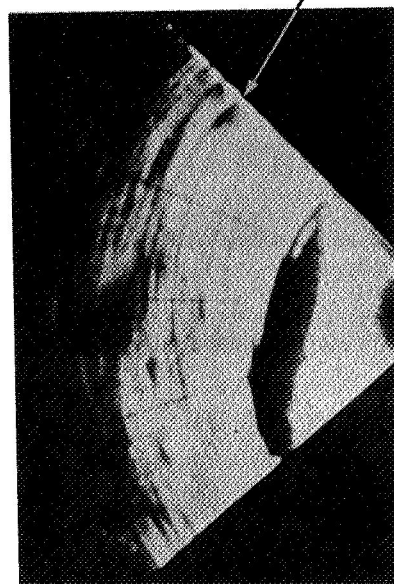
FIGURE 2.9. AVERAGE RADAR CROSS-SECTION PER UNIT SURFACE AREA,  $\sigma^\circ$ , FOR SMALL GRAZING ANGLES, FROM BARRICK<sup>16</sup>



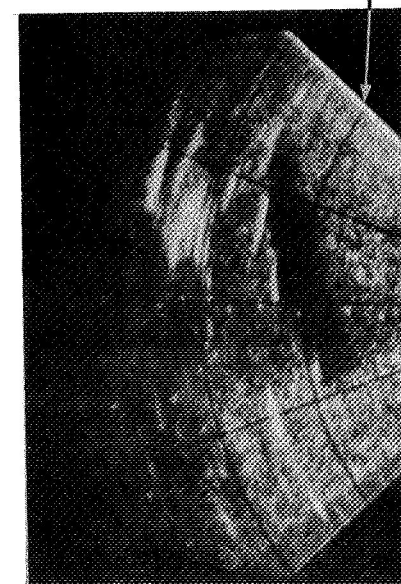
a. -3 Degrees



b. 0 Degrees



c. +3 Degrees



d. +6 Degrees

FIGURE 2.10 PHOTOGRAPHS OF WEATHER RADAR PPI DISPLAY WITH ELEVATION TILT ANGLES AS INDICATED AND 10 NAUTICAL MILE RANGE MARKS  
(X-Band, 12 Inch Dish and 10 KW,  $h_1 \approx 1$  NM)

beam intersects the ground at approximately 20 NM range, so terrain return beyond 25 NM does not paint. When the tilt angle is changed to zero degrees, Figure 2.10b, the ground clutter paints out to 40 NM with the City of Syracuse just beyond Oneida Lake giving a particularly strong return at 40 NM. When the tilt angle is increased to plus three degrees, much of the terrain return disappears, Figure 2.10c, though the City of Syracuse still paints strongly between 30 and 40 NM. When the tilt is increased to plus six degrees, Figure 2.10d, the terrain return essentially disappears and radar interference is revealed in the absence of terrain return.

## 2.7 Elevation Plane Antenna Beam Tilt

When an aircraft using a small weather radar is at a low altitude (under 10,000 feet) the pilot adjusts the antenna tilt control to a compromise position. Raising the beam gives some loss in detectability on distant storms but reduces the nearby terrain returns, as illustrated in Figures 2.10a - d. In this section, a quantitative estimate is made of the gain loss resulting from uptilt of the antenna. In Figure 2.11, a scale drawing illustrates the desired beam positions, assuming a flat earth. The up-tilted beam (solid line) is directed over the top of the model storm. Assuming the terrain cross-section  $\sigma^0 / \sin \theta_g$  a constant, the terrain return power is inversely proportional to  $h^3 \csc^4 \theta_g \cos \theta_g$  for an omni-directional antenna pattern. If radar terrain mapping is desired, then the well-known (one-way) antenna pattern shape of  $h^{3/2} \csc^2 \theta_g \sqrt{\cos \theta_g}$ <sup>17</sup> will result in an approximate uniform terrain return. For a weather radar, the antenna beam should be made as narrow and high gain in elevation as is compatible with the available vertical aperture and side-lobe specifications. Beam shaping, such as  $h^{3/2} \csc^2 \theta_g \sqrt{\cos \theta_g}$  (or to decrease sidelobes), decreases the gain so the use of special beam shaping for ground mapping should be avoided in a basic weather radar design.

Since the desired range of detection on large storms is 50 to 100 NM, the beam tilt loss calculation is made using a spherical earth model\*. In Appendix C, the corresponding depression and grazing angles (unequal for a spherical earth) along a particular line of sight are derived. The use of the spherical earth model alters the terrain return power as a function of depression angle so the inverse  $h^3 \csc^4 \theta_g \cos \theta_g$  relationship no longer applies. The spherical storm cell, 3 NM in diameter and centered at an altitude of 2 NM, is used as the storm model. While propagation effects are unpredictable, particularly at low angles, the presence of vertical plane refraction is

---

\*Levine<sup>18</sup> gives the criterion that when the ground range exceeds  $22 h$  NM, where the aircraft altitude,  $h$ , also is in units of nautical miles, the antenna pattern must be modified to conform to the spherical earth.

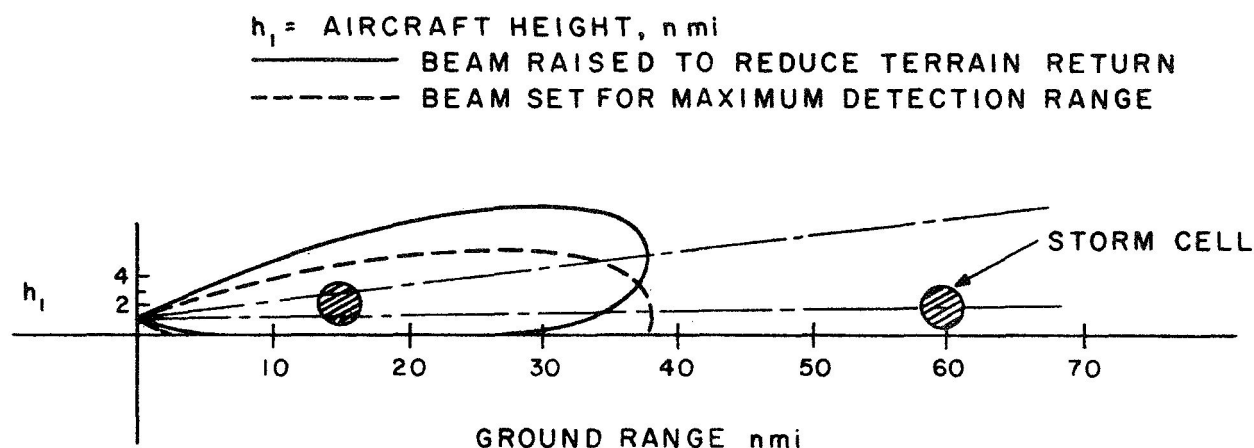


FIGURE 2.11. OPTIMUM TILT ANGLES FOR  
 WIDEBEAM (14.5 degrees) ANTENNA FOR NEAR AND FAR  
 STORM DETECTION AND ANALYSIS  
 (Sketch Approximately to Scale)

approximated by using a 4/3 earth radius. According to Bean and Dutton<sup>19</sup>, the correction will be too small over the altitudes at which most GA operations occur (i.e., under 10,000 feet).

Parameter values, considered representative for current small X-Band dish radars and listed in Table 2.2, are used in the radar equation to calculate the detection range of the assumed radar on the model storm. Reference should be made to Appendices A and B for sample calculations. The detection range on the 3 NM diameter precipitation target is approximately 65 NM.

Also using 1) the Table 2.2 parameter values, 2) Equation (2.6) for the terrain scattering cross-section, and 3) assuming a constant antenna gain (i.e., that the beam is pointed at the terrain at each range) the terrain signal-to-noise ratio was computed. The terrain signal-to-noise ratio is plotted as a function of depression angle, measured from horizontal at the aircraft, in Figure 2.12. The clutter signal-to-noise curves for various aircraft altitudes are similar to the inverse  $h^3 \csc^4 \theta_g \cos \theta_g$  gain functions as expected. The clutter S/N curves are concave to the left whereas the lower side of optimum gain antenna patterns are concave to the right when plotted on the same scales.

The opposite curvatures suggest that a graphical solution can be obtained for the smallest up-tilt which will prevent terrain clutter from exceeding the minimum detectable signal level (MDA). Transparencies of certain round-trip antenna patterns, plotted to the same scales as used on Figure 2.12, can be made from Figures 2.13a, b, and c. The transparencies can be overlaid on the terrain return curve and sliding the transparency to the right or left corresponds to changing the tilt angle of the antenna beam.

TABLE 2.2  
SAMPLE RADAR PARAMETERS

$P_t$	= Transmitted power in watts; 10,000
$\sigma$	= Echo area in square feet, assuming $\sigma^0/\sin \theta_g = 0.1$
$\lambda$	= Wavelength in centimeters; 3.2
$\phi_{BW}$	= Azimuth beamwidth, 8 degrees
$L$	= Microwave loss factor, 3 dB
$\beta$	= Receiver bandwidth, Hz; $10^6$
NF	= Receiver noise figure (NF), 10 dB
$G_t$	= $G_r$ = Antenna gain, 26.5 dB, circular 1 foot aperture
$M$	= Integration gain, 7.2 dB
MDS	= Minimum detectable signal, 10 dB single pulse

Sliding the transparency vertically corresponds to changing the system sensitivity. Since the MDS is at plus 10, the horizontal 0 dB axis of the transparent antenna pattern should coincide with the MDS dotted line. If the antenna pattern is tilted (slid to the right or left) so as to just touch the clutter signal curve then the terrain return will not exceed MDS. That is, the round-trip antenna pattern will introduce enough or more attenuation at each angle to reduce the terrain return to MDS if the terrain scattering cross-section does not exceed a  $\sigma^0$  of  $0.1 \sin \theta_g$ . For an example, the antenna pattern for the one foot diameter circular aperture, Figure 2.13c, must be shifted (up-tilted) 2.4 degrees to the left of zero (horizontal) to avoid crossing the clutter signal curve for an aircraft altitude of 1 NM. If a greater margin of attenuation of terrain return is desired, for example, no return above 10 dB below MDS, the up-tilt must be increased to 4.1 degrees. The observed results with a comparable radar, Figures 2.10c and d, show that the up-tilt must be between 3 and 6 degrees to essentially eliminate terrain return from the display.

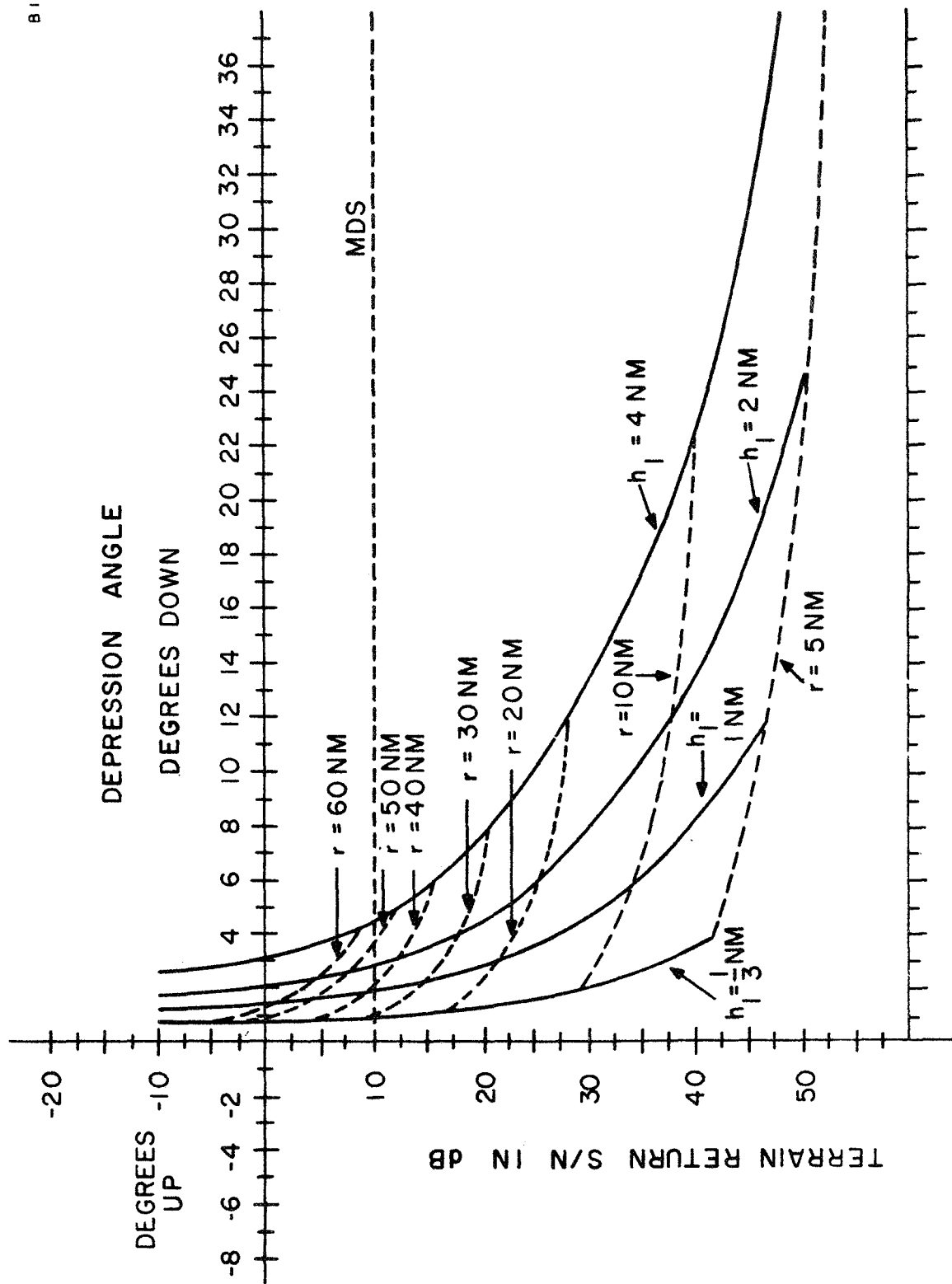


FIGURE 2.12 TERRAIN RETURN AS A FUNCTION OF AIRCRAFT HEIGHT AND DEPRESSION ANGLE

(See Table 2.2 for Radar Parameters and Text for Assumed Terrain Scattering Cross-Section)



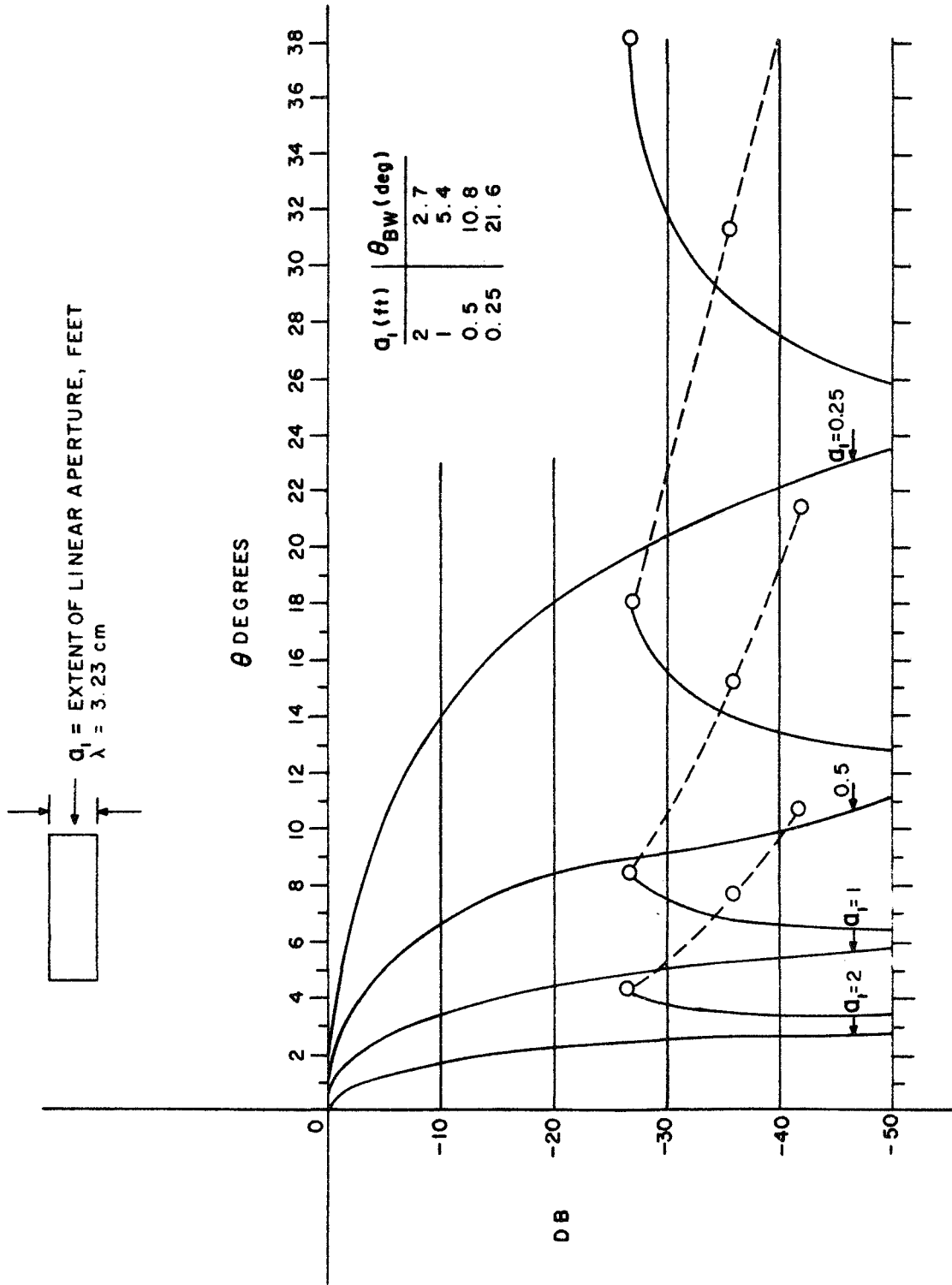


FIGURE 2.13a ANTENNA PATTERN FOR LINEAR APERTURE, UNIFORM ILLUMINATION  
(Round-Trip Pattern for use with Figure 2.12)

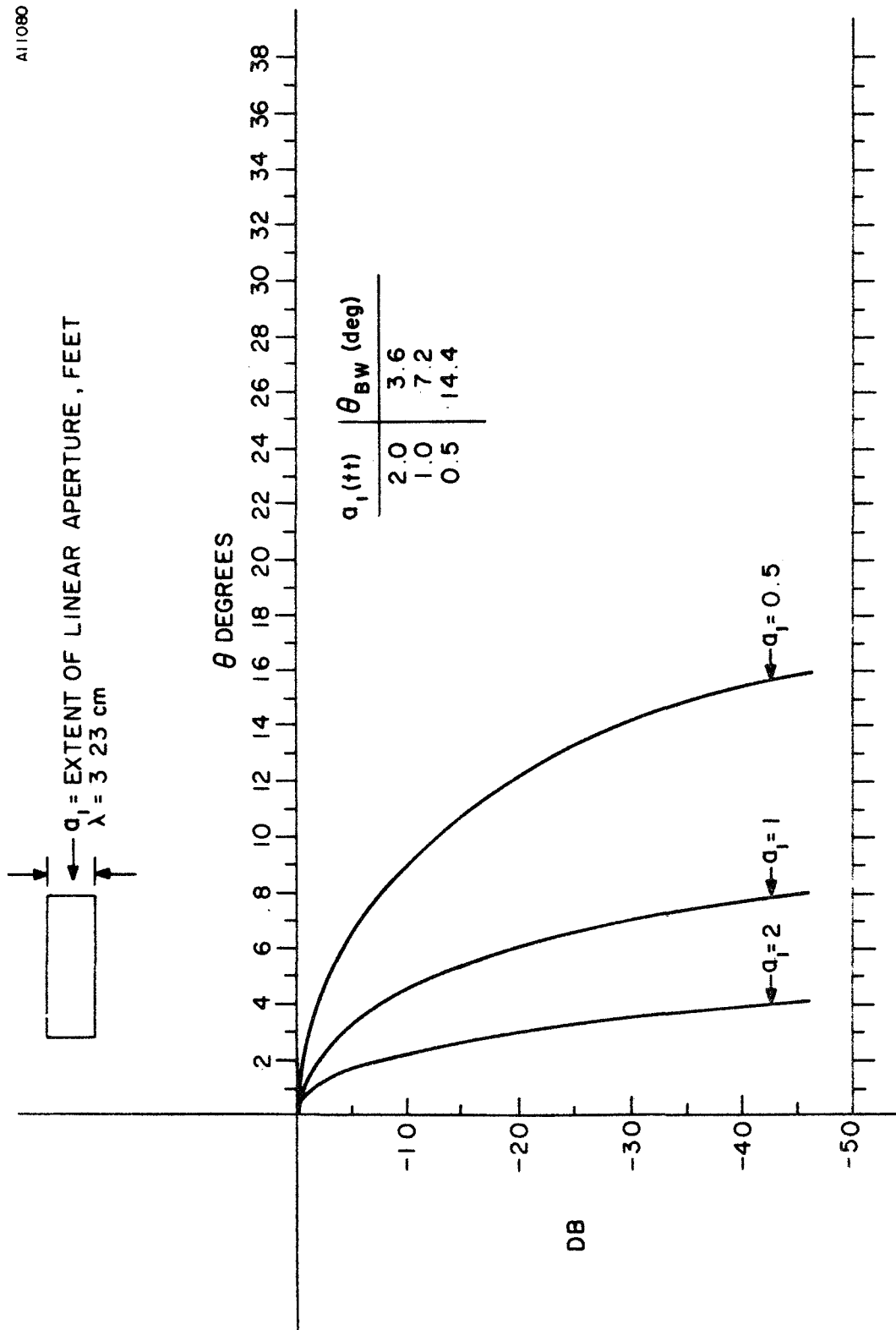


FIGURE 2.13b ANTENNA PATTERN FOR LINEAR APERTURE, COSINE ILLUMINATION  
 (Round-Trip Pattern for use with Figure 2.12)

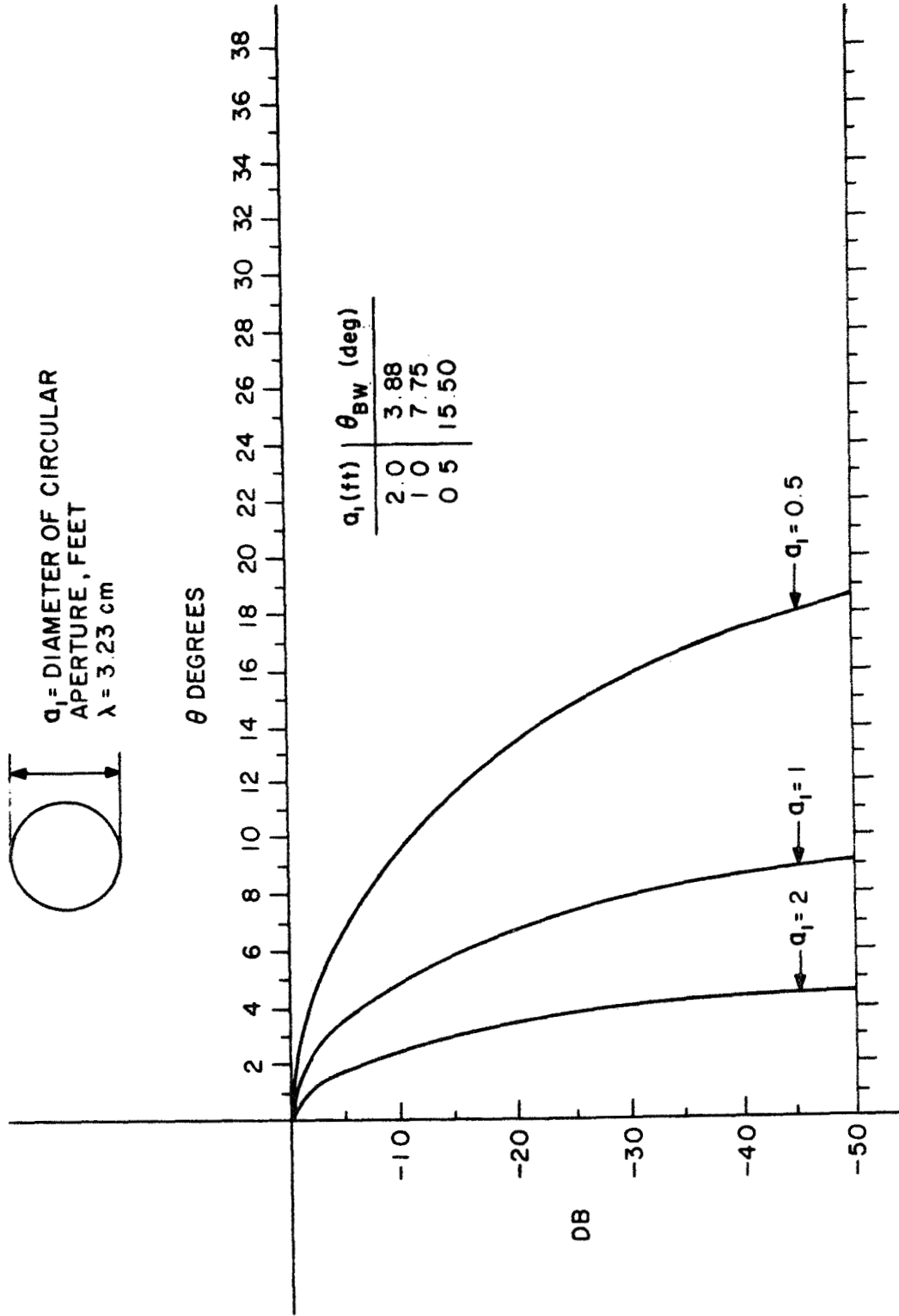


FIGURE 2.13c ANTENNA PATTERN FOR ELLIPTICAL APERTURE,  
PARABOLIC ILLUMINATION  
(Round-Trip Pattern for use with Figure 2.12)

In using Figure 2.12, if the sensitivity of the radar is changed, the zero reference of the dB scale of the transparent antenna patterns, Figures 2.13a - c, when laid on the terrain return curve, Figure 2.12, must be shifted vertically an amount corresponding to the change in sensitivity. For example, if the antenna aperture is decreased to one-half size, maintaining the azimuth beamwidth, then the radar sensitivity is reduced by 6 dB and the zero reference should be shifted to 16 dB for estimating the up-tilt. For the example used previously, a one foot circular aperture, the required up-tilt is reduced to 1.2 degrees from 2.4 degrees if the radar sensitivity is reduced by 6 dB. An expression which gives the required vertical scale shift in dB for a change in transmitter power, a change in antenna gain, and a change in azimuth beamwidth is

$$\delta_s = -10 [\log_{10} P_t + 2 \log_{10} G + \log_{10} \phi_{BW}] + 102 \quad (2.7)$$

where  $\delta_s$  = dB by which the MDS is shifted on Figure 2.12

$P_t$  = Peak transmitter power in watts

$G$  = Antenna power gain, one-way

$\phi_{BW}$  = Azimuth beam width in degrees

Assuming that the MDS on Figure 2.12 is maintained at 10 dB, by adjusting transmitter power, the tilt angles required to keep the clutter return at MDS or lower for various vertical apertures are tabulated in Table 2-3. While tilting the beam upward suppresses the terrain return it may result in some attenuation of the desired storm return because the antenna beam will be directed over the top of the storm (see Figure 2.11). The tilt angles that reduce terrain return to MDS or lower are tabulated in Table 2.3, along with the loss in gain on the model storm, which is located at a range of 60 NM. In Appendix C, the angle between the center of the model storm and the terrain sector is shown to be nearly constant at  $h_s/r$  radians (where  $h_s$  is the altitude of the storm center, 2 NM, over the terrain sector at range  $r$ ) for all aircraft altitudes. In this example the angle between storm and terrain is 0.0334 radians (1.91 degrees).

Actual storms will extend, in some cases, to greater heights than the assumed 3.5 NM (3 NM spherical target centered at 2 NM) and the effect of tilt in decreasing the useful gain will be decreased. Only terrain return which might "penetrate" the main beam and only ranges beyond 5 NM are considered in Table 2.3. As noted on Table 2.3, there are some cases where sidelobe responses extend beyond 5 NM and these will not be suppressed by the indicated tilt angles.

TABLE 2.3

## BEAM TILT AND GAIN LOSS FOR VARIOUS ANTENNAS AT FOUR ALTITUDES

(Assumes "no loss" target detectability maintained constant  
by changing transmitter power)

## A. Linear Aperture, Uniform Illumination (Figures 2.12 and 2.13a.)

Aperture $h_1$ (NM)	→ 0.25 ft.		0.5 ft.		1.0 ft.		2 ft.	
	Tilt Deg.	Loss dB	Tilt Deg.	Loss dB	Tilt Deg.	Loss dB	Tilt Deg.	Loss dB
1/3	17.0	14.0	6.4	5.5	2.5	1.0	1.2*	0.0
1	13.4	8.5	4.2*	2.0	0.7*	0.0	0.4	0.0
2	10.6*	5.5	2.2*	1.0	-0.5	0.0	-0.5	0.0
4	6.8*	3.2	-0.7*	0.5	-2.2	0.0	-2.4	0.0

## B. Linear Aperture, Cosine Illumination (Figures 2.12 and 2.13b.)

Aperture $h_1$ (NM)	→ 0.25 ft.		0.5 ft.		1.0 ft.		2 ft.	
	Tilt Deg.	Loss dB	Tilt Deg.	Loss dB	Tilt Deg.	Loss dB	Tilt Deg.	Loss dB
1/3	Not Measured		11.3	12.2	4.2	4.0	1.2	0.0
1	Not Measured		7.8	6.3	2.0	1.5	0.5	0.0
2	Not Measured		5.0	3.0	0.0	0.5	-0.4	0.0
4	Not Measured		1.5	1.5	-2.4	0.0	-2.4	0.0

TABLE 2.3 (Cont'd.)  
C. Elliptical Aperture, Parabolic Illumination (Figures 2.12 and 2.13c.)

Aperture $h_1$ (NM)	→ 0.25 ft.		0.5 ft.		1.0 ft.		2 ft.	
	Tilt Deg.	Loss dB	Tilt Deg.	Loss dB	Tilt Deg.	Loss dB	Tilt Deg.	Loss dB
1/3	Not Measured		12.2	13.0	4.8	4.7	1.4	0.0
1	Not Measured		8.6	7.4	2.4	1.7	0.4	0.0
2	Not Measured		5.8	4.0	0.4	0.5	-0.4	0.0
4	Not Measured		2.2	2.1	-2.2	0.0	-2.4	0.3

The effect of mountainous terrain was not considered in selecting the tilt angles in Table 2.3.

## 2.8 Sferic Weather Model

The use of sferic detectors for storm warning is based upon the relationship between atmospheric electricity and turbulence producing up and down drafts. Many studies have been made to define the relationship between the observable characteristics of sferics and the severity of the generating storms. Some of the characteristics of sferics which have been examined closely are, flashing rate (sferic strokes per unit of time), recorded sferic waveform, sferic frequency spectrum, and angular distribution. Jones<sup>20</sup>, Dickson<sup>21</sup>, and Shackford<sup>22</sup>, have attempted to set up a criteria of flashing rate as a measure of storm severity, as shown in Table 2.4. This classification has been modified to a more detailed breakdown and a qualification that long sferic bursts be separated into individual strokes for determining counting rate.

The GA pilot traversing a storm area needs to know the location of regions of severe turbulence and electrical activity. The National Severe Storms Laboratory (NSSL) at Norman, Oklahoma, has investigated the relationship between turbulence and lightning reported by pilots in controlled aircraft and the flashing rate in storms traversed by the aircraft. A commercial DF equipment, the SPARSA\*, which receives at 500 KHz, was used in the NSSL tests. A WSR-57 weather radar was used to direct the aircraft to selected storm areas. Ward, et al,<sup>23</sup> prepared a report on the observations made during the NSSL test of the sferics detector. In the report, the data are analyzed in various ways, including a presentation of SPARSA counts superimposed on a map outlining Z contours (see Appendix A for definition of Z) as measured by the WSR-57 weather radar. The maximum Z factors are well correlated with the directions of maximum flashing rate, Figure 2.14; however, note that the nearby storm with a Z exponent of 5.0 produces a significantly lower flashing rate than the more distant storm with a lower A exponent of 4.3. In the aircraft flights through the storm areas the pilot reported moderate to heavy turbulence in the lower count region northeast of the station and light turbulence in the high count region (dotted flight path) to the southeast of the station. This flight, with other examples, suggests that the SPARSA response is not regularly identified with turbulence and other severe storm manifestations. During the investigation of sferics, a total of 53 in-storm flights were made for which aircraft and SPARSA data can be compared. The correlation coefficient between normalized sferics and

---

\*Sferics Pulse Amplitude Rate Spectrum Analyzer, available from Litton Systems, Inc., Applied Science Division.

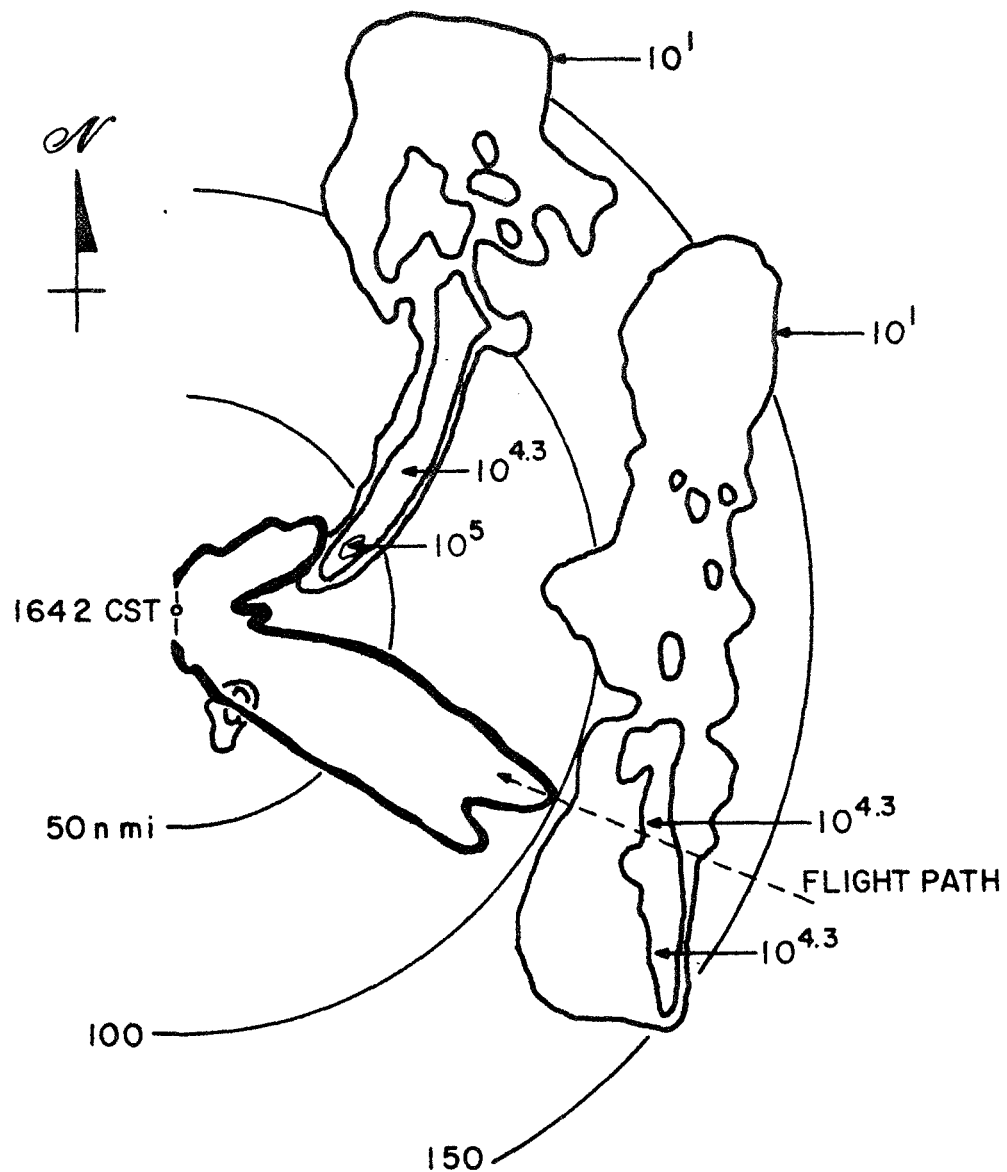


FIGURE 2.14 SFERIC COUNT RATES ON TWO THUNDERSTORMS  
AS MEASURED BY SPARSA (HEAVY LINE) EQUIPMENT  
(Note that the directions of intense activity  
are well correlated with the SPARSA (heavy line) (from [23]).)



turbulence based on pilot comments is + 0.52. The weather radar information was used on an operational basis to steer the aircraft into the storms and also to avoid areas of possible hail which might damage the aircraft. In three cases, severe turbulence was recorded with little or no SPARSA response.

TABLE 2.4  
CLASSIFICATION OF STORMS BY FLASHING RATE

Class of Storm	Type of Storm	Flashing Rate (Sferic Strokes Per Second)	Sferic Frequency
I	Low Level Cumulo Nimbus	1 S/s	Low
II	Squall Lines and Cumulo Nimbus	2 S/s	Low and High
III	Hail Storms	~ 10 S/s	Mostly High
IV	Hail Storms and Tornados	> 10 S/s	Mostly High

Except for informal pilot observations with ADF equipment, no information on in-flight directional measurements of sferics is available. Pilots have often reported obtaining useful indications on thunderstorm cells with ADF equipment; however, the NSSL results seem to indicate that equipment of the SPARSA type is not adequate to judge storm severity. In flight, cross-bearing DF information on storm cell sferics might be used to supplement area weather forecasts. The area forecasts, obtained by ground weather radar, would be used to judge the general severity of storms and the airborne instantaneous DF bearings on sferics would indicate to a pilot areas to be avoided. Lightning strikes present a hazard<sup>24</sup> to aircraft operating in a storm area, and information on sferic activity represents a desirable supplement to airborne weather radar displays. Oetzel and Pierce<sup>25</sup> have proposed a VHF technique for locating lightning, which might be adapted to aircraft.

#### REFERENCES

1. Wilk, K. E., et al, "Weather Detection by ARSR-1D, ASR-4, and WSR-57 Radars: A Comparative Study," Technical Memo No. 1, National Severe Storms Laboratory (NSSL), Norman, Oklahoma, March 1965.
2. McFann, H. L., "Outlining Radar Weather Clutter in Digital Processing Systems," Federal Aviation Agency paper presented at Aviation Electronics Symposium, U. S. Army Electronics Command, Fort Monmouth, New Jersey, March 5-7, 1968.

3. Blake, N. A., "NAS Design Concepts and System Configuration," a presentation at the Third International Aviation R&D Symposium, Automation in Air Traffic Control, Session II, page 6.
4. Air Traffic Training Proficiency Series, "Airborne Weather Radar" Publication S-10, FAA Aeronautical Center, Oklahoma City, Oklahoma, March 1, 1968.
5. Rudolph, J. F., "Thunderstorms," FAA Advisory Circular, AC No. :00-24, June 12, 1968.
6. Trammell, A., "Night Single-Engine, Yes or No," Flying, Ziff-Davis Publishing Company, September 1969, pp 40-44.
7. Hovis, W. A. Jr., and Tobin, M., "Spectral Measurements From 1.6 Microns to 5.4 Microns of Natural Surfaces and Clouds," Applied Optics, Vol. 6, No. 8, August 1967, pp 1399-1402.
8. Fenn, R. W., "Correlation Between Atmospheric Backscattering and Meteorological Visual Range," Applied Optics, Vol. 5, No. 2, February 1966, pp 293-295.
9. Towmey, S., and Howell, H. B., Applied Optics, Vol. 4, 1965, p 501.
10. Barteneva, D. D., Bulletin of Academy of Sciences, USSR, No. 12, 1960, p 852.
11. ARINC Weather Radar Characteristic, No. 564.
12. Hamilton, P. M., and Marshall, J. S., "Weather-Radar Attenuation Estimates From Raingauge Statistics," Scientific Report MW-32, Under Contract AF 19(604)-2065, January 1961, McGill University.
13. Marshall, J. S., et al, "Parameters for Airborne Weather Radar," Scientific Report MW-48 (ANTC Report No. 109) May 1965, McGill University.
14. Wilk, K. E., et al, "Detection and Presentation of Severe Thunderstorms by Airborne and Ground-Based Radars: A Comparative Study," Technical Memorandum ERLTM-NSSL 43, National Severe Storms Laboratory, Norman, Oklahoma, February 1969.
15. Ruck, G. E., ed., "Radar Cross-Section Handbook," Plenum Press, New York, 1970, Vol. II, Chapter 9.
16. Cosgriff, R. L., et al; "Terrain Scattering Properties for Sensor System Design (Terrain Handbook II)," Bulletin 181, Engineering Experiment Station Bulletin, The Ohio State University, May 1960, 118 pages.

17. Skolnik, M. I., "Introduction to Radar Systems," McGraw-Hill Book Company, New York, 1962, pp 522-527.
18. Levine, D., "Radargrammetry," McGraw-Hill Book Company, New York, 1960.
19. Bean, B. R., and Dutton, E. J., "Radio Meteorology," Dover Publications, Inc., New York, 1968.
20. Jones, H. L., "Recent Advances in Atmospheric Electricity," Pergamon Press, New York, 1958, pp 543-556.
21. Dickson, E., "Analysis of Sferics and its Relation to Severe Thunderstorm Phenomena," Proc of 5th Weather Radar Conference, 1955, SCEL, Fort Monmouth, New Jersey.
22. Shackford, C. R., "The Relation Between Precipitation and Electrical Activity in New England Thunderstorms," 1958 Proc. 7th Weather Conference, Miami Beach, Florida, pp C-9 and C-15.
23. Ward, N. B., et al, "Sferics Reception at 500 KHz, Radar Echoes and Severe Weather," National Severe Storms Laboratory, Norman, Oklahoma, Report RD-65-24, March 1965.
24. Robb, J. D., and Newman, N. M., "Lightning Strikes to Plastic Components of Light Aircraft," Society of Automotive Engineers, March 1970, Paper No. 700220.
25. Oetzel, G. N., and Pierce, E. T., "VHF Technique for Locating Lightning," Radio Science, Vol. 4, No. 3, March 1969, pp 199-202.

### 3.0 WEATHER RADAR TECHNIQUES

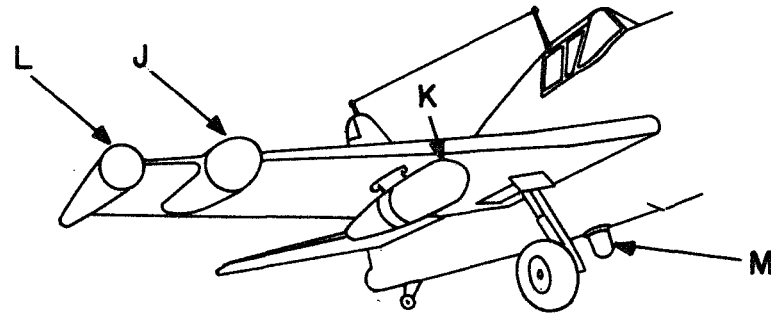
#### 3.1 Introduction

A need exists for radar techniques which can extend the use of airborne radar to single and dual in-line engines as well as multi-engine aircraft. With the exception of military application, the use of airborne radar has been restricted to multi-engine aircraft. Early methods of mounting streamline pods for radar on single-engine aircraft (propeller driven) are described in Volume 26, "Radar Scanners and Radomes," of the MIT Radiation Laboratory Series<sup>1</sup>. While the pod arrangements shown in Figure 3.1a are attractive for rapid installation and removal of radar equipment, integral mounting of radar in the regions shown in the dotted lines of Figure 3.1b is desirable to minimize cost and aerodynamic drag. The viewpoint taken in this report is that the majority of GA aircraft will continue to use a single nose-mounted engine and propeller. If the single-engine and propeller are located above the wing or in the rear of the aircraft, then the nose area is available for radar mounting as in multi-engine aircraft. Also, the use of jet propulsion leaves the nose area for radar use if the air intakes for a single rear-mounted jet are on the sides of the aircraft. These alternative methods of providing frontal area for a radar antenna should be considered in new aircraft designs, but the trade-offs, etc., in front versus rear engine mounting are not studied or reported.

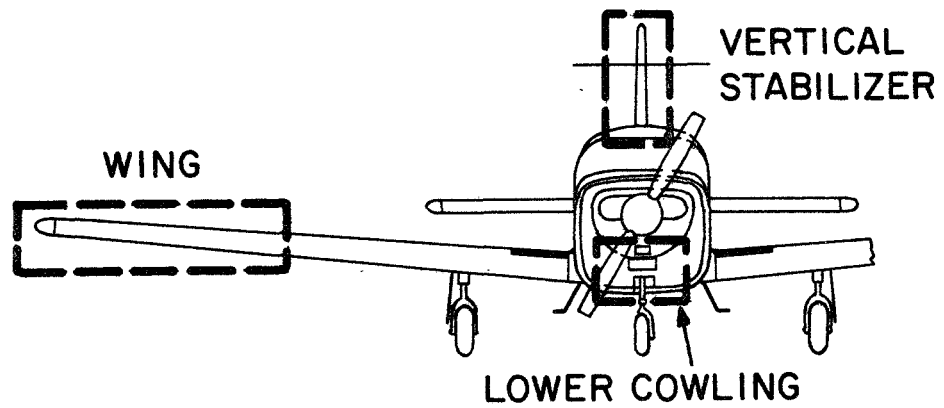
It may be feasible to use the aircraft engine to rotate a small feed horn for scanning an antenna located on the front cowling, Figure 3.1b. The radar beam must "fire" through the propeller and a flicker at the propeller blade rate is expected. Typically, this flicker is at an 80 Hz rate (2400 rpm and two-bladed prop), and might be no more disturbing than looking through the spinning propeller. The transmitter is turned off during the passage of the blade in front of the reflector to prevent operation with a distorted antenna beam. A thin solid-state scanning array might be mounted on the front cowling (perhaps conformally), below the propeller hub on a single-engine aircraft. This would take advantage of the thin package possible with solid-state design. The antenna scan rate is synchronized with the engine rpm to eliminate beating effects at a low difference frequency. Vibration effects are at a maximum so the array must be very rugged. Provision for tilt can be made electronically or mechanically within the radome. The same solid-state antenna can be readily used on a multi-engine aircraft in a nose location.

The radar techniques described in this section, together with the predicted improvement in radar characteristic, are listed in Table 3.1. When demonstrated as feasible, these techniques will give the radar designer more options in meeting design requirements.

A11666



(a) Pod Installations, Circa 1944, From<sup>1</sup>



(b) Frontal Areas on Current Single-Engine Aircraft

FIGURE 3.1 RADAR MOUNTING AREAS ON SINGLE-ENGINE AIRCRAFT

TABLE 3.1  
OBJECTIVES OF TECHNIQUE AND/OR DESIGN

Technique and/or Design	Reduce Cost	Decrease Drag	Reduce Terrain Return	Increase Transmitter Wavelength
a. Engine Driven Scanner	1	2		
b. Grating Reflector/ Electronic Scanning		1		
c. Surface Wave Antenna/Frequency Scanning		1		
d. Crossed-Beams Antenna (MODSCAN)		1		2
e. Non-Coherent MTI		2	1	
f. Monopulse Terrain Clutter Attenuation			1	2
g. Monopulse Beam Control			1	2
h. Non-Coherent Monopulse Terrain Clutter Suppression			1	2
i. Random Noise Radar	1			

### 3.2 Mechanical Scanning

During World War II, a mechanically scanned linear array, the AN/APQ-7 (Eagle), was developed to be fitted into the wing leading edge or for mounting in a streamlined auxiliary vane carried transversely below the fuselage. A sketch of the cross-section of the 250 dipole, X-Band array, taken from Volume 26 of the MIT Radiation Laboratory Series, is shown in Figure 3.2. The Eagle scanner was designed for use as a ground mapping radar and, consequently, a relatively small (a few inches) vertical aperture was adequate for the vertical plane beam shaping. In a weather radar, the terrain return should not be detectable to avoid confusing ground return echoes for weather echoes. More recently, the Sperry-Rand Corporation designed a

flush-mounted antenna for collision avoidance and mapping<sup>2</sup>. A mechanical drive is used to rotate the beam forming dielectric lens.

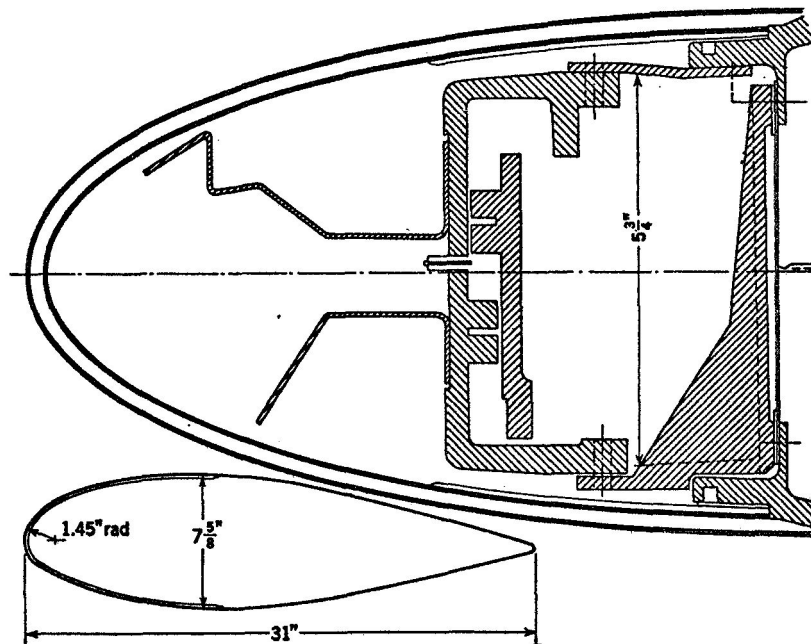


FIGURE 3.2 CROSS-SECTION OF EAGLE VANE  
WITH MECHANICAL SCANNING LINEAR ARRAY  
(From Volume 26, MIT Radiation Laboratory Series)

The feasibility of using the aircraft engine to mechanically rotate small feed horns for antenna scanning should be investigated. The feed horns are to be mounted on the propeller hub-spinner and the rotation will carry the feed horn through the focal region of an off-set parabolic reflector antenna. The parabolic reflector is mounted below and behind the hub of the propeller and on the front cowling of the aircraft, as shown in the side view in Figure 3.3. It may be necessary to use an extension to move the propeller out from the unmodified cowling and to provide space for the around-

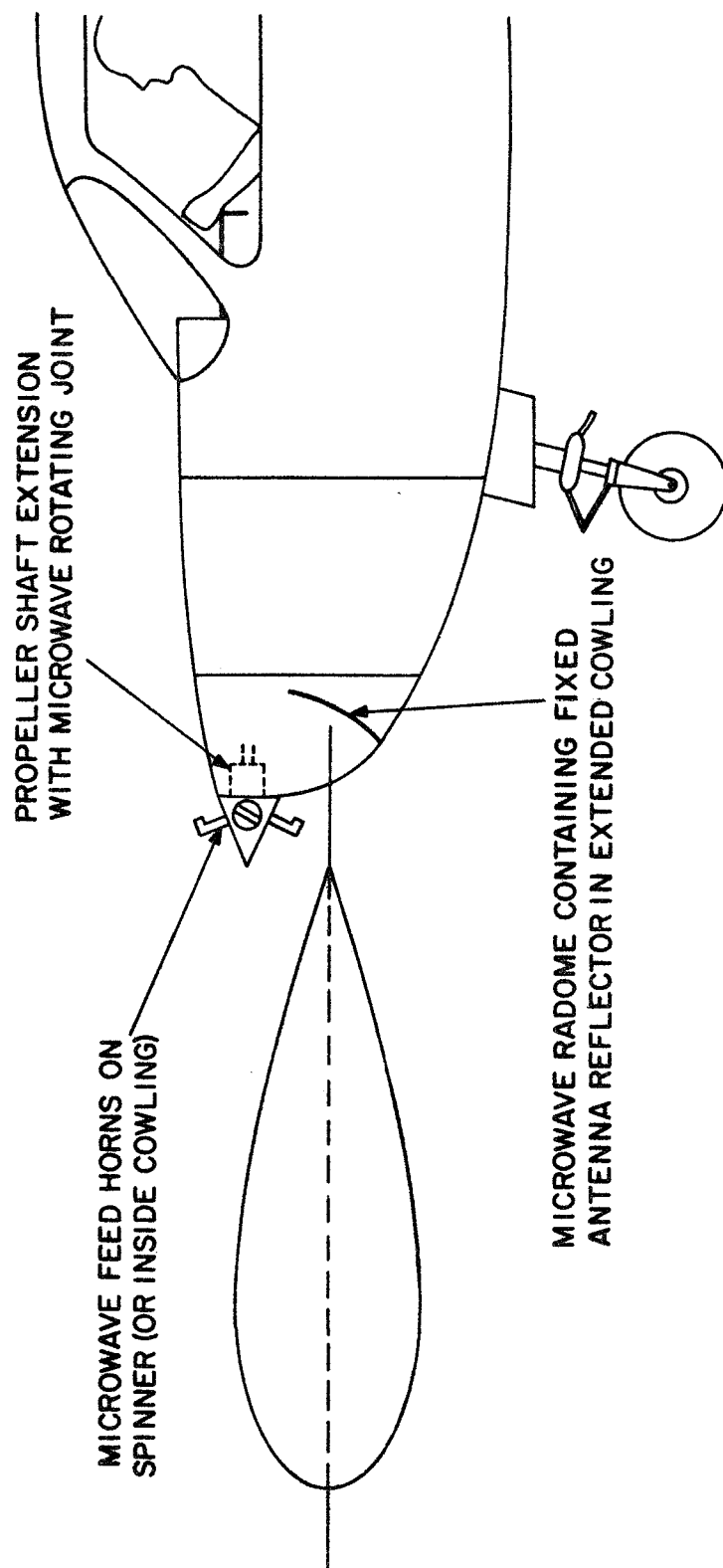


FIGURE 3.3 PROPOSED ANTENNA CONFIGURATION  
FOR LOW-COST WEATHER RADAR WITH ENGINE-DRIVEN SCANNER



the -shaft rotating joint. A schematic diagram of a two output waveguide rotating joint is shown in Figure 3.4, adapted from a design by Boronski<sup>3</sup>. The joint consists of three waveguide rings of equal diameter mounted around a shaft, with the narrow walls in contact. The middle ring is cut along the line of zero radial current to allow rotation. Three zero dB directional couplers provide for power transfer to one of the two feed horns, with the power shifting from one horn to the other horn with shaft rotation. Matched load terminations are incorporated in the other ring.

A11696

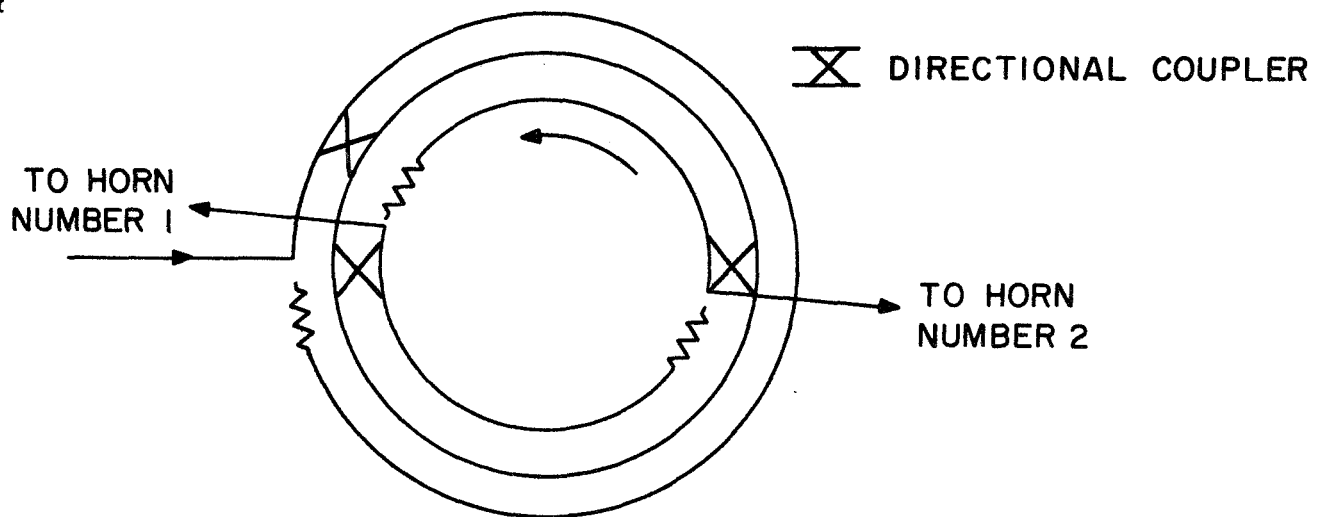


FIGURE 3.4 SCHEMATIC DIAGRAM OF TWO OUTPUT ROTATING JOINT

A pick-off (magnetic, electric or electromagnetic) is used to synchronize the pulse transmissions with the rotation of the engine to avoid transmission when the propeller is in front of the antenna reflector. An alternate design includes a propeller which is transparent to microwave radiation at the frequency of the radar transmitter. The portion of the propeller which intercepts the reflector might be hollow with transmissive surfaces, etc. In addition to triggering the transmitter to avoid the propeller, a mechanical take-off on the tachometer can be used to directly drive a PPI sweep coil in synchronism with the antenna beam scanning action to avoid the need for synchros.

### 3.3 Frequency Scan

Much attention in recent years has been given to electronic scanning techniques. One method of electronic scanning which has been thoroughly investigated is frequency scan<sup>4</sup>. The frequency shift, usually 5 to 10 percent of the frequency of a special transmitter, is converted into an angular antenna beam shift by a special feed structure. The feed structure usually takes the form of a serpentine line with the antenna elements fed by equally spaced turns of the serpentine (see sketch, Figure 3.5).

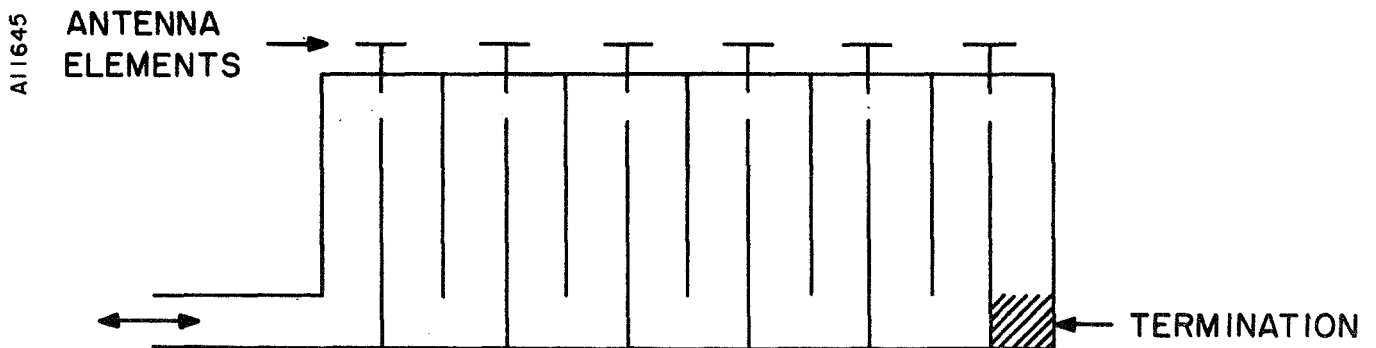


FIGURE 3.5 SERPENTINE WAVEGUIDE FOR FREQUENCY SCAN ANTENNA

The principal drawback of the frequency scan, linear array, is the high loss that is encountered in the long serpentine waveguide and in the end termination. Attempts to shorten the waveguide by using highly dispersive structures results in increased losses in the dispersive structure unless the size is increased excessively. The surface wave antenna, shown in Figure 3.6, uses frequency scan for azimuth scanning. In summary, frequency scan:

1. Requires a wide frequency band.
2. Requires a special frequency sweep transmitter, likely to be high cost.
3. Requires a long serpentine waveguide with possibly excessive losses.

### 3.4 Electronic Scan

Electronic scanning is currently used only with discrete element arrays. The desired phase shift of the signal of any element in the array is introduced by either an analog or digitally controlled phasor. In the case of digital control, the phase shifters can be set with an error which is always one-half or less of the least phase bit size. If there are N elements in one dimension of an array, and M in the other, the total number of elements is NM or N<sup>2</sup> in a square array. If N is 20, a two-dimensional square array requires 400 elements, and if each element, including driver, costs \$50.00, the total cost is \$20,000 for components only. Even with array thinning techniques, the cost of a two-dimension array is prohibitive for general aviation, so only one-dimensional linear arrays of N elements are considered in this study. The scanning is electronic in azimuth and the tilt control is assumed to be mechanical, as in present dish antennas. The electronic scanning rate, though not limited by inertia, is limited by the time required for pulse energy to travel to the most distant target and return. With the pulse repetition rate selected for the desired maximum range, the scan rate is:

$$\text{Scans/second} = \frac{f_r \phi_i}{\phi_s} \quad (3.1)$$

where  $\phi_i$  = Scan angle between pulses, degrees.

$f_r$  = Pulse repetition frequency, pulses per second

$\phi_s$  = Antenna scan sector, degrees.

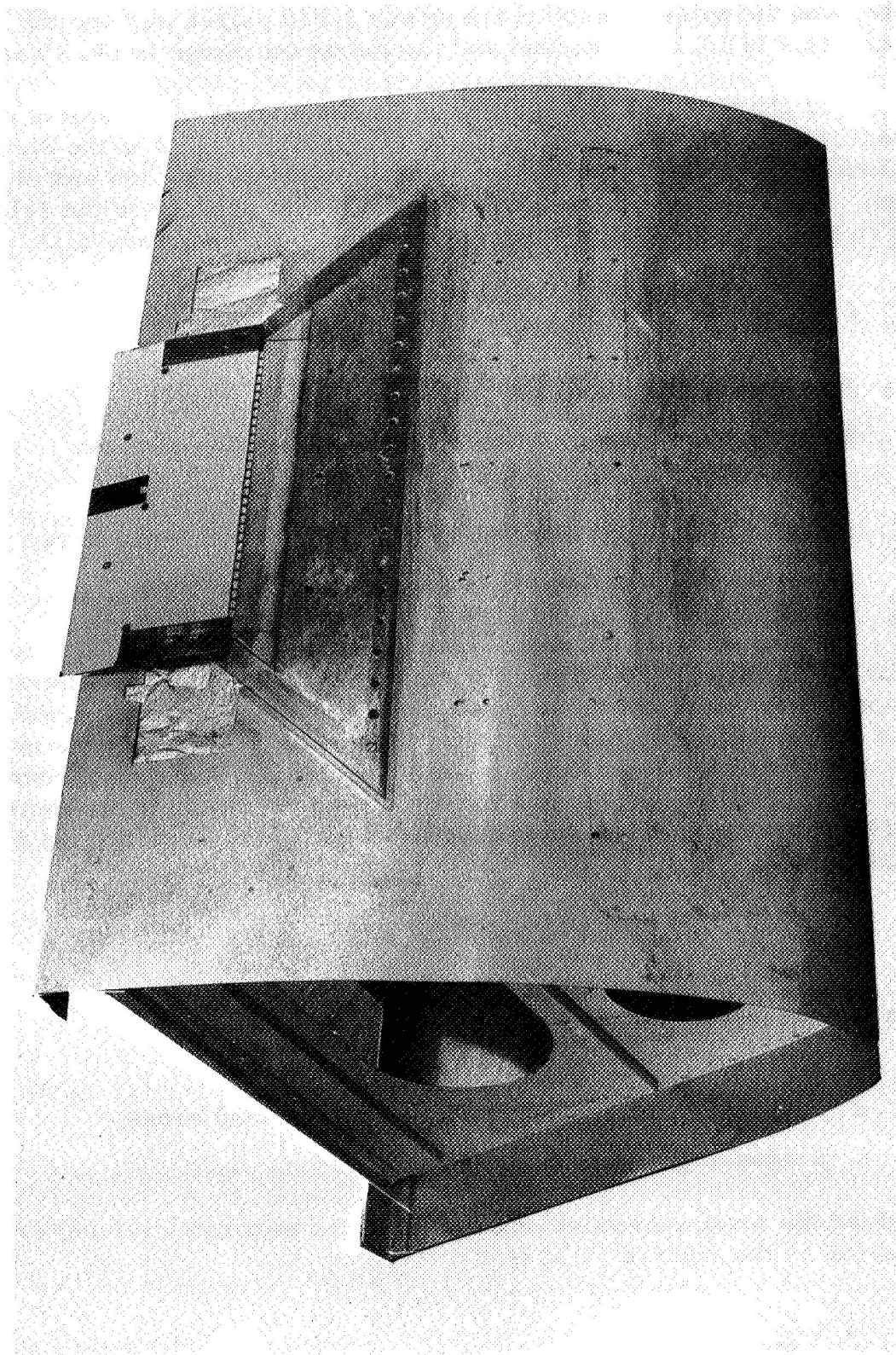


FIGURE 3.6 RESEARCH MODEL OF FLUSH-MOUNTED  
FREQUENCY SCAN ANTENNA IN TOP SURFACE OF AIRCRAFT WING  
(Courtesy of Autonetics, A Division of North American Rockwell Corporation)

If the scan sector is 90 degrees, the scan angle between pulses one degree, and the pulse repetition frequency 1,200 pulses per second, then the scan rate is 13.3 per second and the maximum range is 69.5 NM.

For phase shift beam steering, the phase shift of the signal at each element for a particular steering angle is linearly related to the distance of the element from a reference point (usually the center or one end of the array). The required phase shift of each element relative to the selected point on the array to steer the beam by the angle  $\phi$  from normal is:

$$\psi_n = \frac{2\pi S_n \sin \phi}{\lambda} \quad (3.2)$$

where  $\psi_n$  = electrical phase shift in radians of nth element

$S_n$  = distance from reference point to nth array element

$\lambda$  = wavelength

$\phi$  = far-field angle measured from the normal to the array

$n$  = array element number counted from reference.

With the element phasing proportional to the distance,  $S_n$ , except that for narrowband systems integer multiples  $m$  of  $2\pi$  can be subtracted, the array will form at least one wavefront. With  $N$  elements periodically spaced at a distance,  $d$ , more than one wavefront may form if the inter-element spacing is greater than one-half wavelength. The conditional equation for predicting the formation of undesired grating lobes can be obtained by rearranging the terms in Equation (3.2) after subtracting  $m 2\pi$  radians from  $\psi$ .

$$\sin \phi = \frac{\psi \lambda}{2\pi d} - m \frac{\lambda}{d} \quad (3.3)$$

where  $\psi$  = electrical phase shift

$m$  = integer -2, -1, 0, 1, 2, etc.

$d$  = interelement spacing for uniformly spaced array

$\lambda$  = wavelength

and, since the maximum value of  $\phi$  is  $\pm \pi/2$ , the permitted values for the expression on the right of (3.3) is

$$-1 \leq \frac{\psi \lambda}{2\pi d} - m \frac{\lambda}{d} \leq 1 \quad (3.4)$$

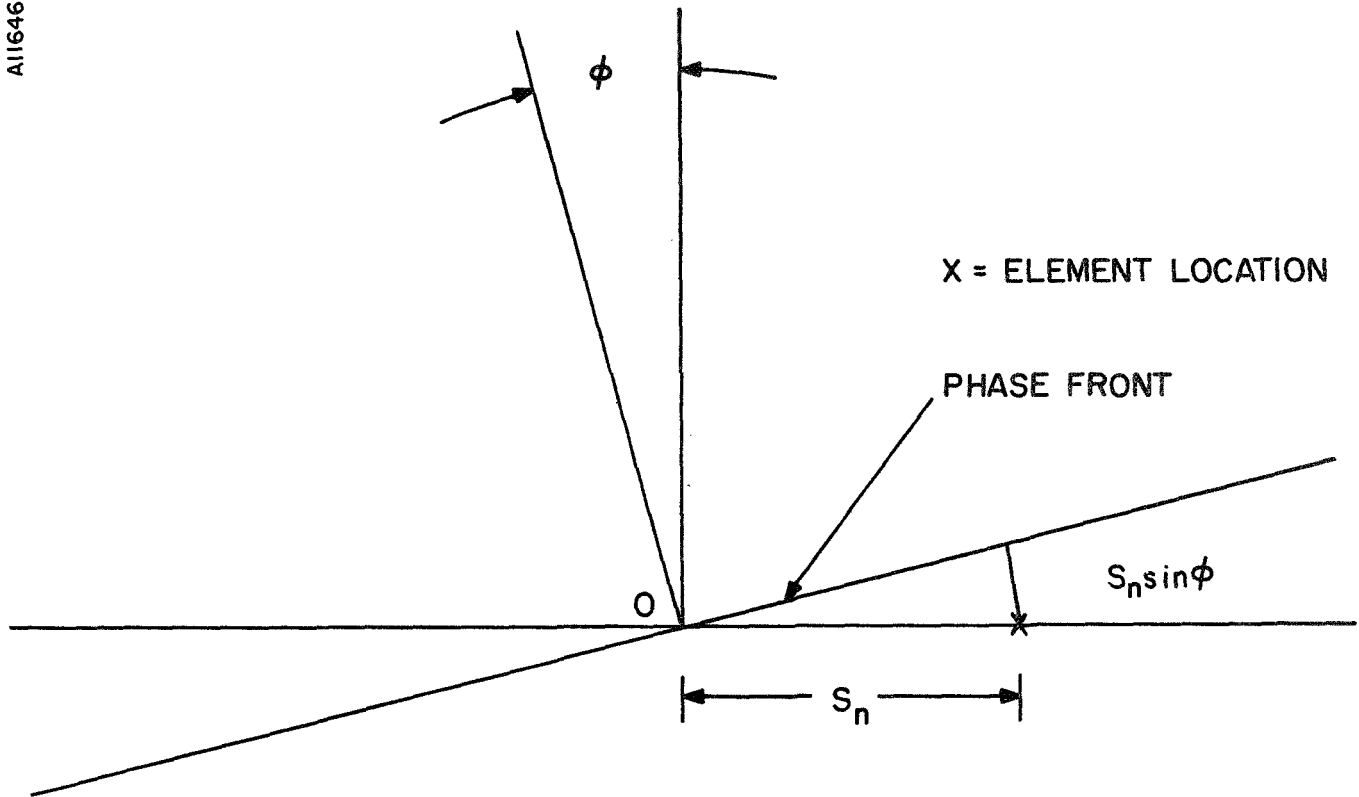


FIGURE 3.7 NTH ELEMENT PHASE SHIFT  
RELATIVE TO REFERENCE POINT, 0

The maximum value of  $\psi$  when inserted in (3.4) gives

$$-1 \leq \sin \phi_{\max} - m \frac{\lambda}{d} \leq 1 \quad (3.5)$$

To illustrate with an example, consider the beam steered to a maximum angle of  $\pm 60$  degrees so  $\sin \phi_{\max} = \pm 0.866$ , and assume  $d = 0.6 \lambda$ . Using these parameter values, the inequality (3.5) becomes:

$$-1 \leq \pm 0.866 - m 1.67 \leq 1. \quad (3.6)$$

From inequality (3.6), it is apparent that a grating beam will exist since  $m = \pm 1$  satisfies the inequality. Either the scan angle or the inter-element spacing must be reduced (or both) to prevent the grating lobe from appearing when the scan angle is greater than  $\pm 42$  degrees. The grating

lobe can be prevented by keeping the interelement spacing small enough (approximately  $\lambda/2$ ) that the inequality (3.5) is not satisfied for the maximum scan angle of interest except for  $m = 0$ , the main beam.

One method of determining the phase shift settings for either analog or digital phase shifters is to use a tapped voltage divider. The voltage at each tap is made proportional to the distance of each array element from the reference point. The voltage applied to the end of the resistor is varied, proportional to  $\sin \phi$ , to determine the setting of each phase shifter for scanning (see Figure 3.8).

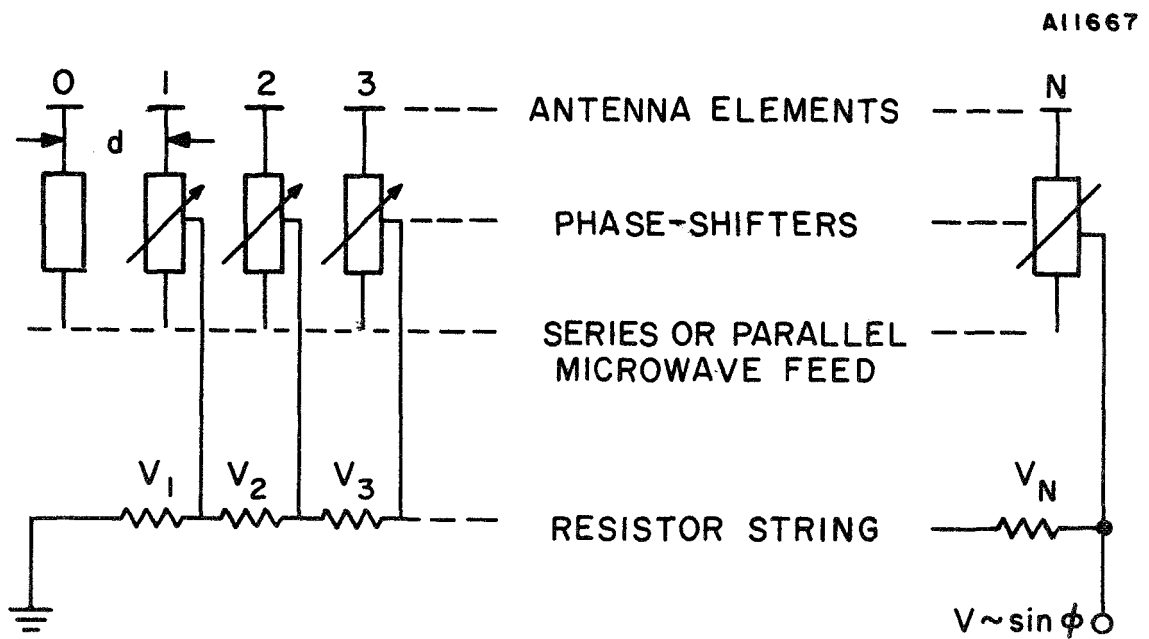


FIGURE 3.8 ANALOG SOURCE OF  
PHASE SHIFTER CONTROL VOLTAGE

The analog voltages can be converted by an analog-to-digital converter to control digital phase shifters or used directly to control analog settings. If the required phase shift exceeds  $2\pi$  radians, then multiples of  $2\pi$  must be subtracted either digitally or by step voltages for analog phase shifters. Direct computations of the digital settings can be handled by pulse counters, particularly for a simple linear scan.

For the linear scan, digital system, a binary pulse counter is connected to each binary phase shifter. The bit sizes of the phase shifter are designed to be multiples of  $2\pi/2^t$ , where  $t$  is the number of bits in the phase shifter. For a 4-bit phase shifter,  $t$  is 4 and the least bit is  $\pi/8$  (22.5 degrees), the next bit is 45, the next 90, and the largest 180 degrees. The least significant bit (LSB) of the counter is connected to the 22.5 degree phase shifter, the next bit beyond the LSB to the 45 degree phase shifter, etc. Pulses are fed to each counter with the average number of pulses proportional to the distance of each antenna element from the reference point. If an array has  $N$  elements (odd numbers) then the smallest change in the far field angle will be approximately, from Equation (3.2),

$$\Delta\phi = \frac{\lambda \Delta\psi}{\pi Nd} \quad (3.7)$$

where  $\Delta\phi$  = smallest change in scan angle

$\Delta\psi$  = smallest bit in digital phase shifter (LSB)

$N$  = number of elements in linear array.

The settings of the various phase shifters can be visualized from a graph which has element location as the abscissa and phase steps as the ordinate (Figure 3.9).

Only the integer multiples of  $\Delta\psi$  are permitted values for the phase shifters, and the counter output/phase shifter settings corresponding to a particular element are shown on the right. The far-field angle approximated by a particular line on the graph must be determined from Equation (3.2). The lines on the graph can have any slope; however, only a finite number of phase shifter settings are available to approximate a particular slope line, thus the angular change that corresponds to a change of  $\Delta\psi/2$  in the element farthest from the center is about the smallest significant beam shift. Smaller beam shifts can be produced by using only the inner phase shifters (nearer the 0 reference); however, the resulting phase errors may increase the antenna pattern sidelobes. Errors in the element phasing result in additional power in the sidelobes which can be significant if too few bits are used in the phase shifters. Assuming a worst case where the error



in each phase shifter is  $\pm \Delta\psi/2$ , then the one-way loss in gain in dB is:

$$\text{dB} = 10 \log_{10} \left( \frac{\sin \Delta\psi/2}{\Delta\psi/2} \right)^2 \quad (3.8)$$

where  $\Delta\psi$  = least bit size ( $2\pi/2^t$ ), and for 1 through 4 bits, the loss is:

No. of Bits, $t$	$\Delta\psi$	Maximum Loss dB (One-Way)
1	$\pi$	3.9 (Beam Splits)
2	$\pi/2$	0.9
3	$\pi/4$	0.24
4	$\pi/8$	0.06

The loss is quite small for three or more bit digital phase shifters. By randomizing the phase errors the periodic nature of the errors can be altered and the peak sidelobes decreased.

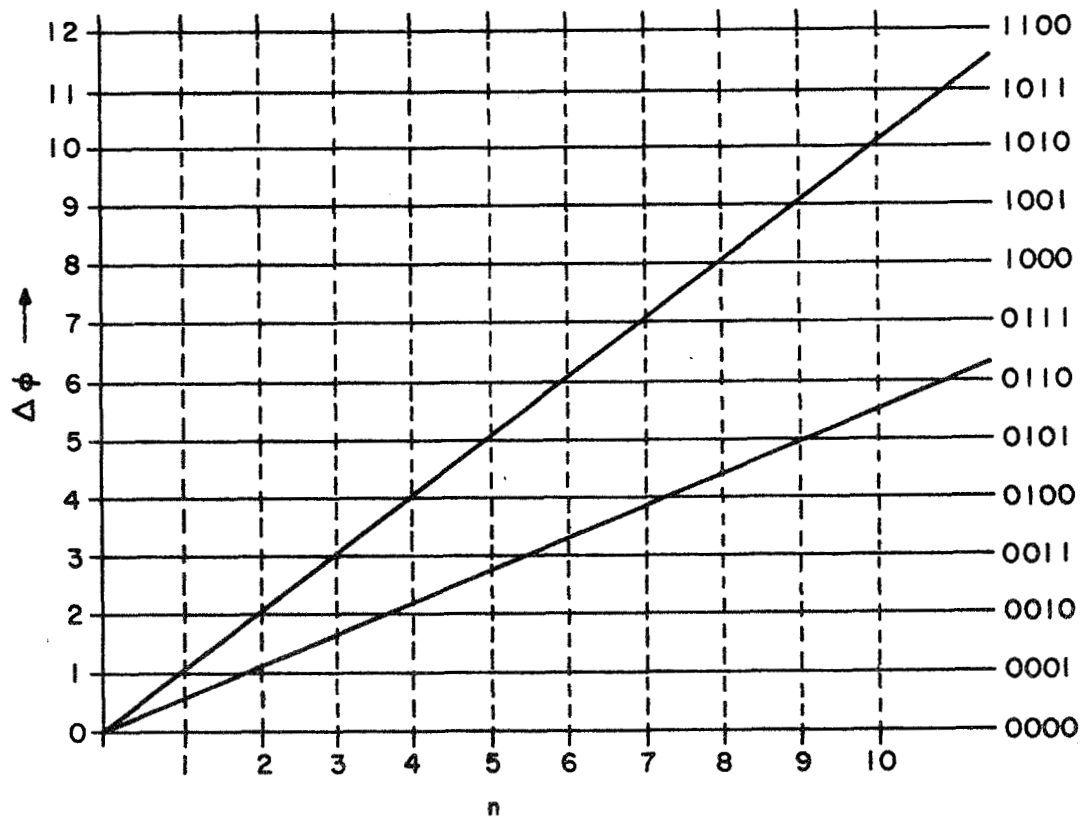


FIGURE 3.9 GRAPH OF PHASE SHIFTER SETTINGS  
FOR 11 ELEMENT ARRAY

### 3.5 Slat/Wire Grating Reflectors

It is proposed that reflectors consisting of either thin streamline slats or closely spaced wires be used to extend the vertical antenna aperture to the extent necessary to reduce the vertical beamwidth and control the sidelobes. The slats/wires must be closely spaced to prevent excessive microwave leakage; however, the spacing between slats must be large enough for free air flow. If the spacing is too small, the air flow is restricted and the resulting interference effects will increase the drag to excessive (flat plate) values. There are two major electrical restrictions that apply to all gratings:

1. The electric vector of the incident wave must be in the plane determined by the incident ray and the axis of the grating element.
2. The center-to-center spacing of the slats must be less than  $\lambda/(1 + \sin \phi)$ , where  $\phi$  is the angle between the incident ray and the normal to the axis of the grating element. Larger spacings cause the appearance of undesirable higher-order lobes in the secondary pattern. If the microwave leakage through the reflector is to be kept to the necessary low value, this requirement will be easily met.

The transmission through parallel strip gratings has been computed and the results, as presented on page 450 of Volume 12<sup>5</sup>, "Microwave Antenna Theory and Design," are reproduced in Figure 3.10.

The 1% transmission curve represents a loss of only 0.04 dB through the grating at normal incidence. The transmission must be kept low enough to prevent significant backlobes from forming. The spacing of the grating bars should be made as large as possible to minimize the aerodynamic drag. However, for a given width of bar, the bar must have greater depth as the spacing approaches a half-wavelength.

Wire reflectors are a possible alternate to the grating bars. Either a wire screen with square openings or parallel wires can be used. If the reflector is a wire screen with square openings, the edge length,  $a_2$ , of the openings must be such that

$$a_2 < \lambda/2.$$

This is the condition for cut-off in a square waveguide. Wire reflectors made from parallel wires require closer spacing than the above cut-off

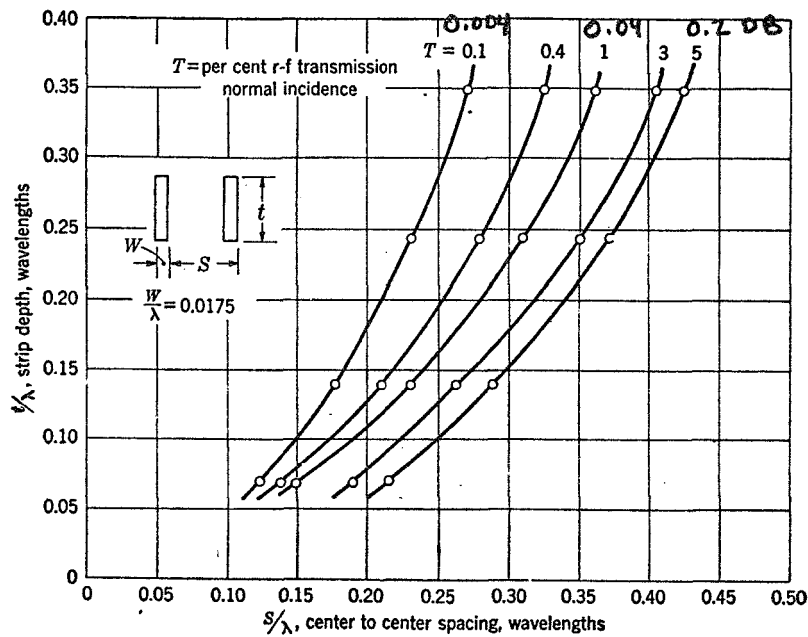


FIGURE 3.10 GRATING OF EDGEWISE STRIPS: RELATION BETWEEN STRIP DEPTH AND SPACING FOR CONSTANT TRANSMISSION (From Volume 12, Page 450, MIT Radiation Laboratory Series)

condition. Mumford has prepared a convenient nomograph relating power loss, wire spacing, and wire diameter (see Figure 3.11).

The accuracy of the nomograph, reproduced in Figure 3.11, has been established by experimental checks to be slightly better than  $\pm 1$  dB. Wire reflectors, either square mesh or parallel wires, require supports which can be metallic or dielectric. Since the reflector will normally be operating with air speeds in excess of 100 Knots, the supports must maintain the reflector shape with deformations less than  $\lambda/8$  from a cylindrical parabola.

### 3.6 Test of Slat Reflector

The beam forming capability of a parabolic cylinder slat reflector was investigated briefly. The reflector and a 20 slot X-Band waveguide feed are shown disassembled in Figure 3.12 and assembled for pattern tests in Figure 3.13. It is assumed that such a reflector would be partially concealed within the wing structure or used with a retractable mount. The antenna patterns for azimuth, Figure 3.14, and elevation, Figure 3.16, have maximum side-lobes of approximately -13 dB. The high sidelobes are accounted for by the uniform illumination in the azimuth plane and the aperture blocking by the

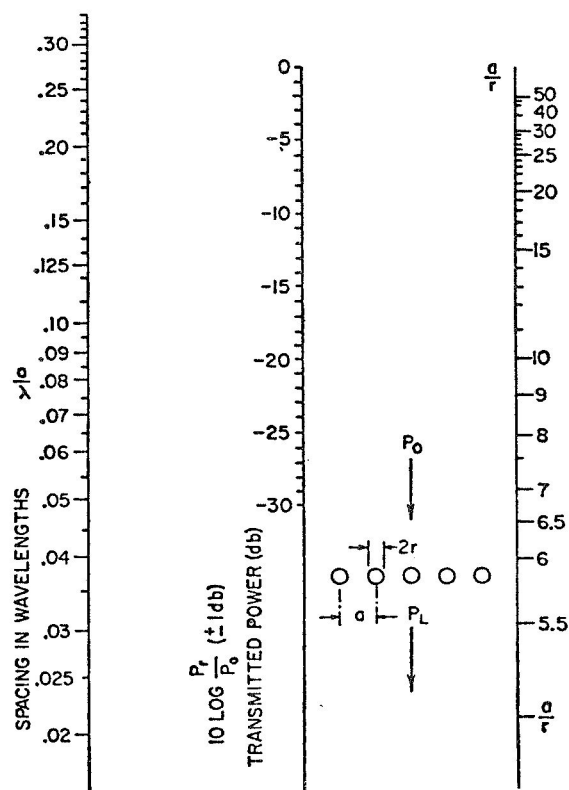


FIGURE 3.11 TRANSMISSION THROUGH A GRID OF PARALLEL WIRES

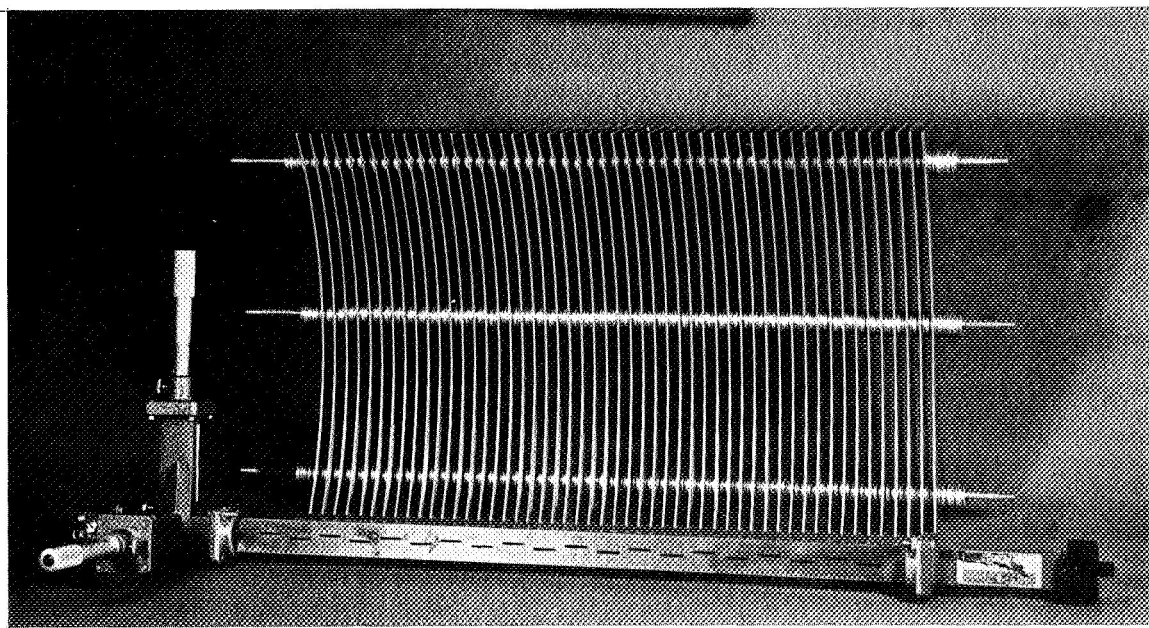


FIGURE 3.12 PARABOLIC-CYLINDER SLAT REFLECTOR  
 AND 20 SLOT X-BAND WAVEGUIDE FEED

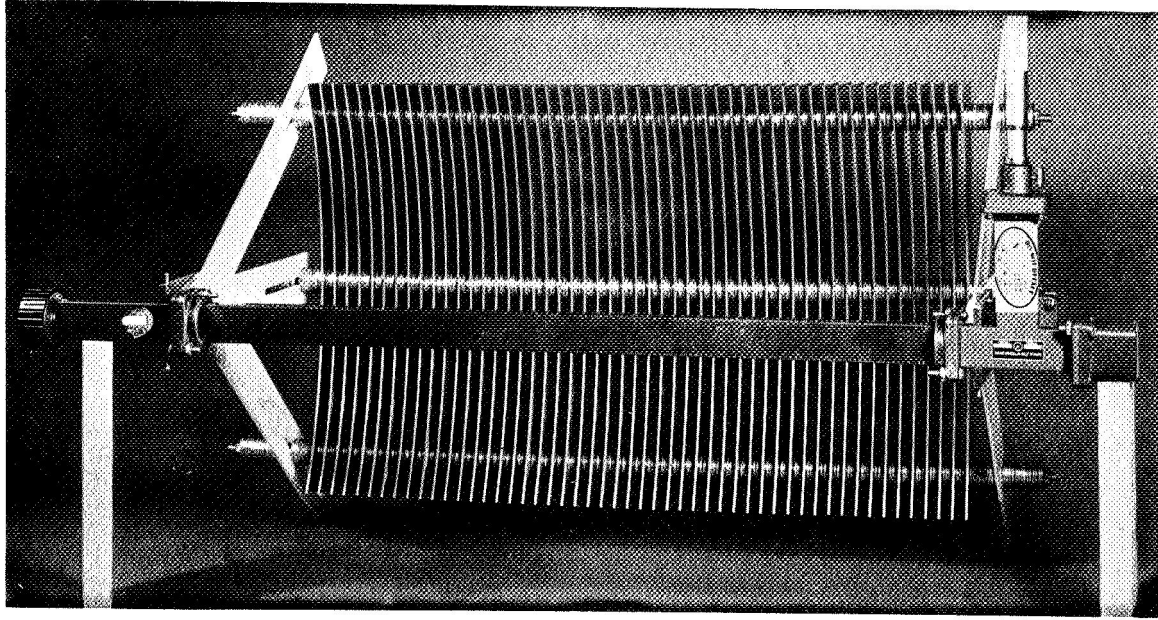


FIGURE 3.13 PARABOLIC-CYLINDER SLAT REFLECTOR  
WITH X-BAND FEED MOUNTED FOR PATTERN TESTS

line feed in the elevation plane. While the primary pattern, Figure 3.15, has about 6 dB of taper in the elevation plane, an appreciable part of the vertical aperture is blocked by the feed structure. The obstacle can be considered as an out-of-phase field superimposed on the original distribution, Figure 3.17a, and, since the width of the obstacle is small compared with the aperture width, the pattern produced by the former will be very broad compared with that of the full aperture, Figure 3.17b, from<sup>5</sup>.

The intensity of the first sidelobe, with aperture blocking relative to the peak is

$$p' = \frac{p + \frac{2\delta_a}{a_0}}{1 - \frac{2\delta_a}{a_0}}$$

- where  $p'$  = sidelobe amplitude ratio with blocking  
 $p$  = sidelobe amplitude ratio without blocking  
 $a_0$  = amplitude of pattern without blocking  
 $2\delta_a$  = height of blocking obstacle

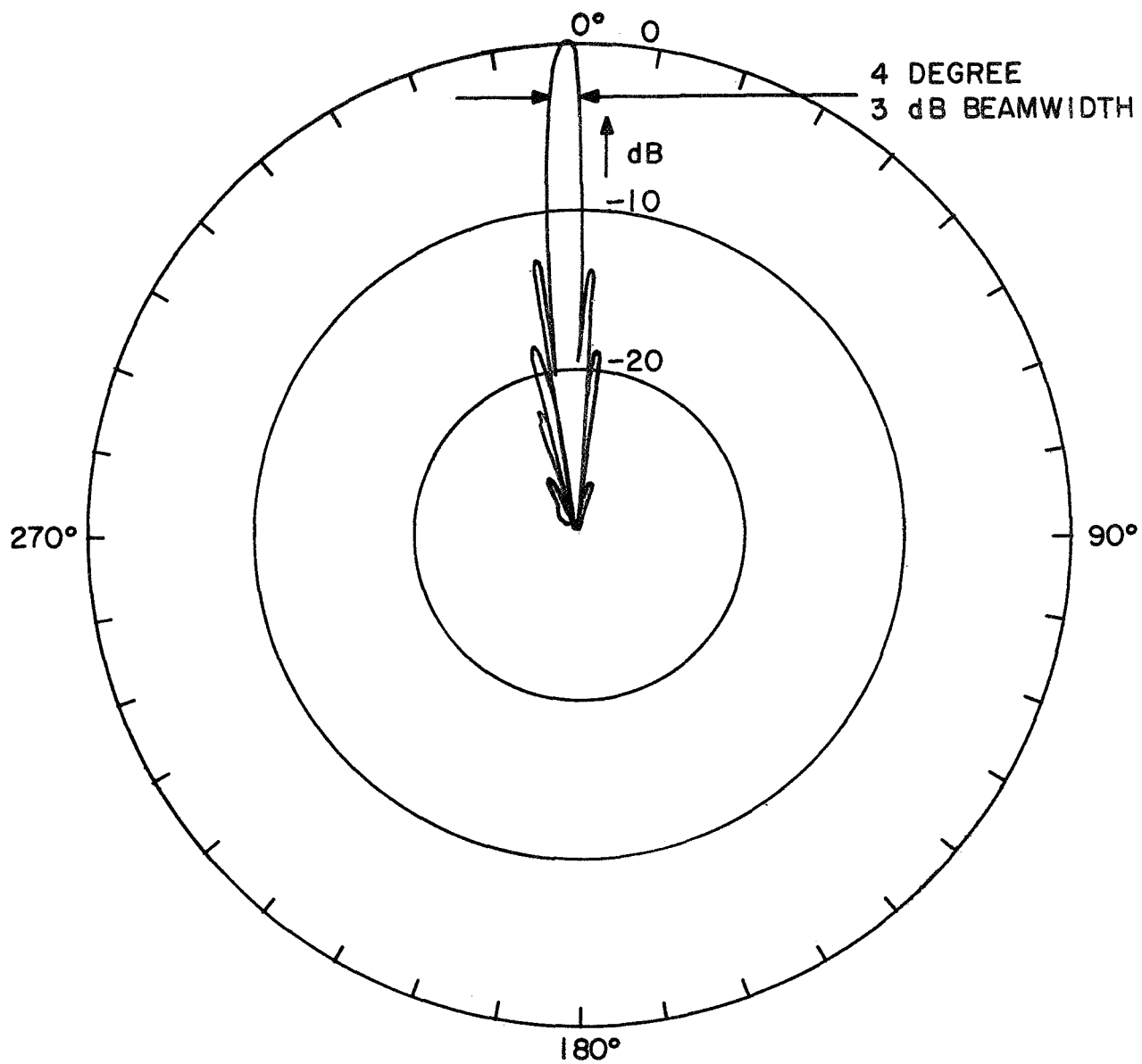


FIGURE 3.14 X-BAND AZIMUTH PATTERN  
OF SLOT FEED AND GRATING REFLECTOR

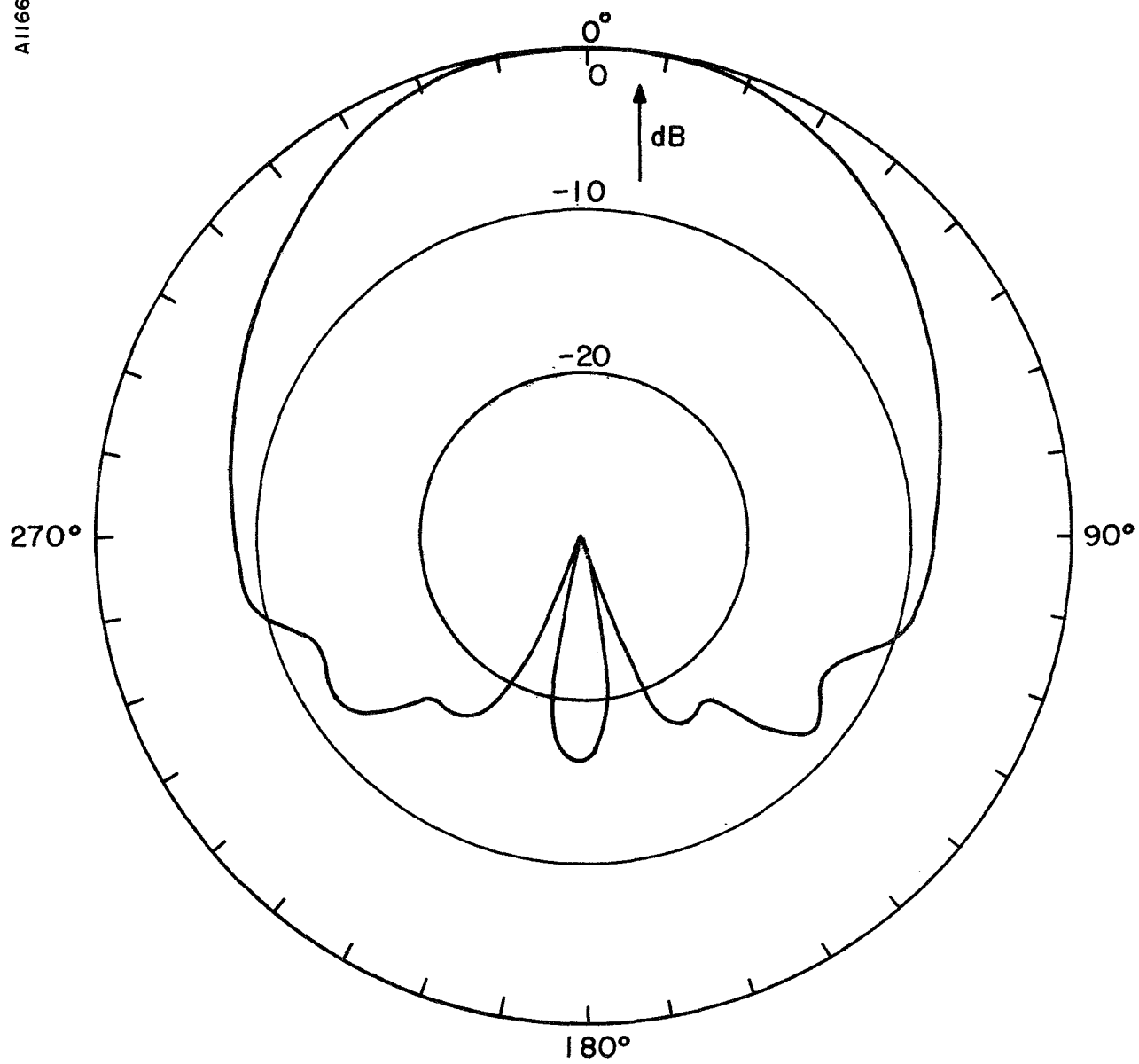


FIGURE 3.15 X-BAND ELEVATION PRIMARY  
FEED (SLOTTED WAVEGUIDE) PATTERN

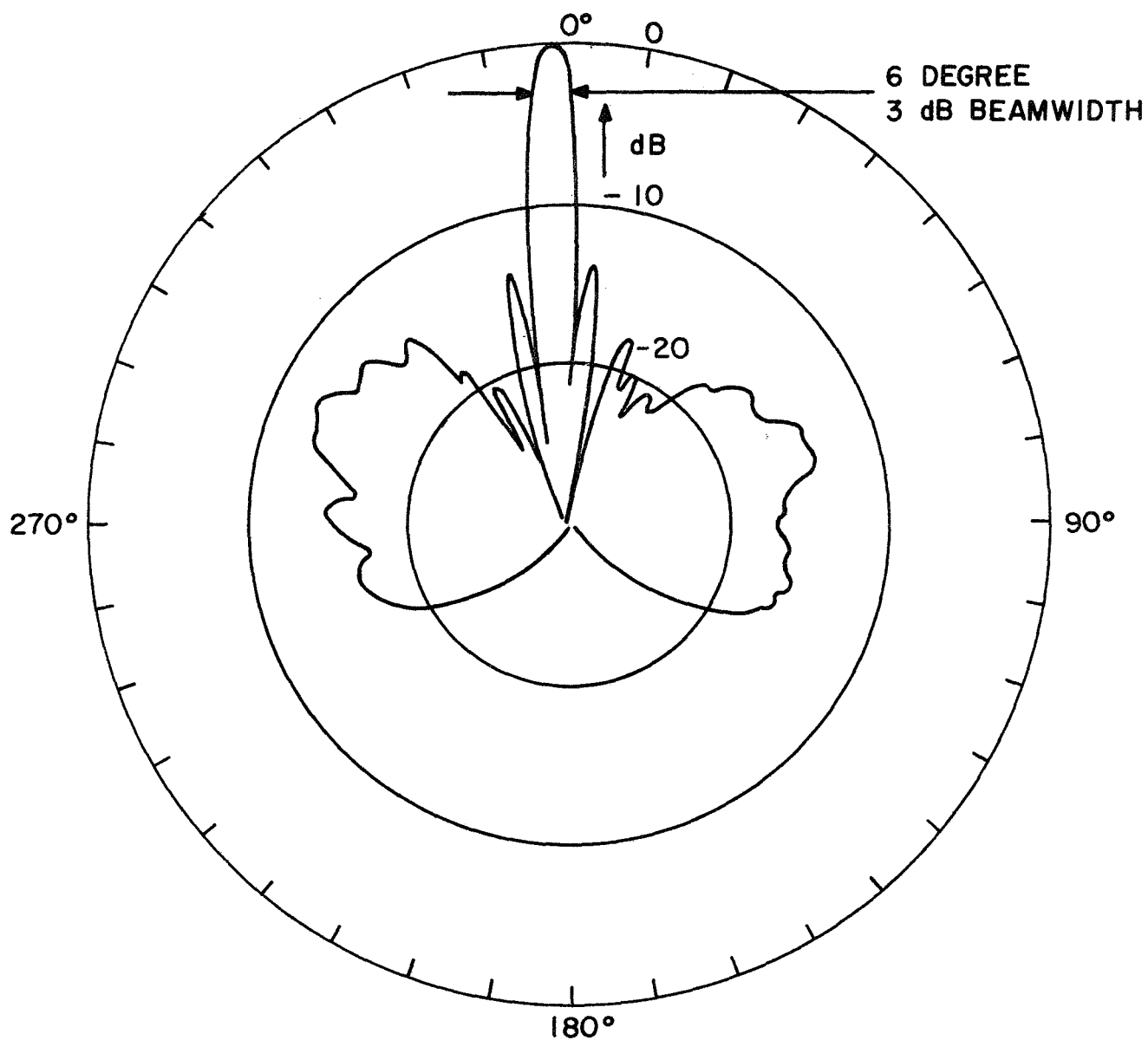


FIGURE 3.16 X-BAND ELEVATION PATTERN OF  
SLOTTED WAVEGUIDE FEED AND GRATING REFLECTOR



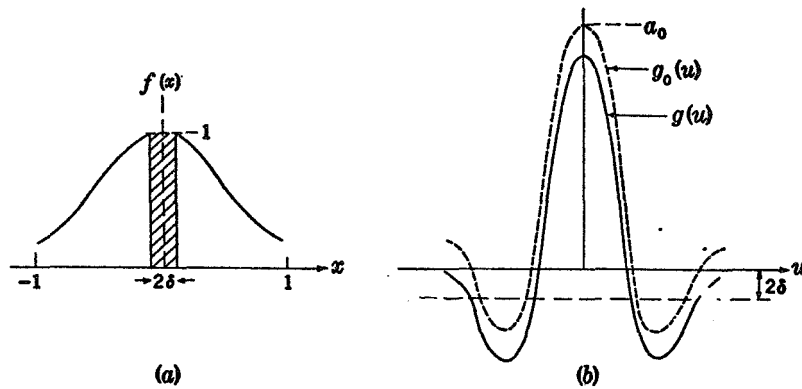


FIGURE 3.17 THE EFFECT OF APERTURE BLOCKING:  
 (a) MODIFIED APERTURE DISTRIBUTION;  
 (b) SECONDARY PATTERN  
 (From Volume 12, MIT Radiation Laboratory Series)

If the initial sidelobe ratio is 23 dB (a voltage amplitude ratio of 1/14), assuming cosine illumination, then a one-half wavelength obstacle in a 10 wavelength aperture will reduce the ratio to 18.7 dB. The experiments show that an obstacle width of nearer one wavelength is necessary to shape the primary pattern. With one wavelength of aperture blocking the sidelobe ratio would change from the initial 23 dB to 15.8 dB, which is nearly in accord with the observed test results (the taper was less than cosine so this is a rough approximation). Thus, the use of slats to extend a vertical reflector out of the wing and into the airstream does enable the vertical beam to be narrowed with a minimum increase of drag; however, the sidelobe control is not entirely satisfactory.

### 3.7 Aerodynamic Considerations

The aircraft designer/manufacturer/owner considers any drag producing protuberance a detriment to efficient flight. If the aircraft owner considers that radar is necessary to the safe and comfortable conduct of flight operations, then some compromise must be effected. One compromise

might be to eliminate all projections by using a very short radar transmitter wavelength such as K<sub>a</sub>-Band. The compromise in this case would be to accept the poorer performance (and higher cost) of K-Band over a longer wavelength such as X- or C-Band. Another compromise would be to accept a noticeable increase of drag from wing-tip projections only during operation of the radar and to include provision for partially retracting the reflector during periods when the radar is not in use. If the reflector can be at least partially retracted during inactive periods, then this type of radar would have an advantage over a mechanically scanned dish enclosed in a tear drop radome (refer back to Figure 3.1). With the radome, the drag will be constant regardless of whether the radar is operated. Also, since icing and thunderstorms are generally separate phenomena, the retractable reflector can avoid ice collection. (Flight in and near the tops of thunderstorms, above the icing level, can result in ice accumulation and provision must be made for deicing.)

At velocities below 300 mph, the effects of compressibility can be neglected and the drag computation problem can be considered as one of incompressible flow. For this type of flow, the expression for the drag of a body has the form:

$$D = C_d qA \quad (3.9)$$

where  $D$  = drag in pounds

$C_d$  = drag coefficient, dimensionless

$q$  = dynamic pressure,  $1/2 \rho V_1^2$ , pound/feet<sup>2</sup>

where  $\rho$  = 0.00238 slug/feet<sup>3</sup>. (This value is always used when the velocity,  $V_1$ , is indicated air speed, regardless of altitude of flight.)

$V_1$  = velocity in feet/second

$A$  = cross-sectional area, normal to the incident airflow, feet<sup>2</sup>.

The engine horsepower required to overcome the drag can be determined by multiplying the drag by the aircraft velocity to determine the work done and dividing by the appropriate constant. A plot of horsepower versus aircraft speed is shown on Figure 3.18 for three  $C_D A$  products. As an example of a drag computation, assume an X-Band reflector for a wavelength of 0.1 feet and vertical and horizontal effective apertures of one foot partially contained in a 0.5 foot thick wing. The reflector is assumed to be two feet long, to permit scanning at angles of plus and minus 45 degrees, and the grating bars are 0.005 feet thick and are spaced one-half wavelength apart. The external (outside the wing) portion of the 40 slats will

have a cross-section area, normal to the airflow, of 0.1 square feet. Assuming a conservative drag coefficient of 0.1 and an interference drag coefficient of 0.1, the sum of the drag coefficients multiplied by the area is 0.02. Using the chart, Figure 3.18, the horsepower required to overcome the drag at 150 knots is 0.7 and at 200 knots is 1.5. The ratio of drag horsepower to the total available horsepower is more significant, and assuming the 150 knot aircraft has a 180 horsepower engine, the antenna drag will require about 0.4% of the available power. The 0.4% drag power reduction will not be a significant factor in normal cruise, and as will be indicated later, the slats could be partially retracted when the radar is not in use or when icing conditions are encountered.

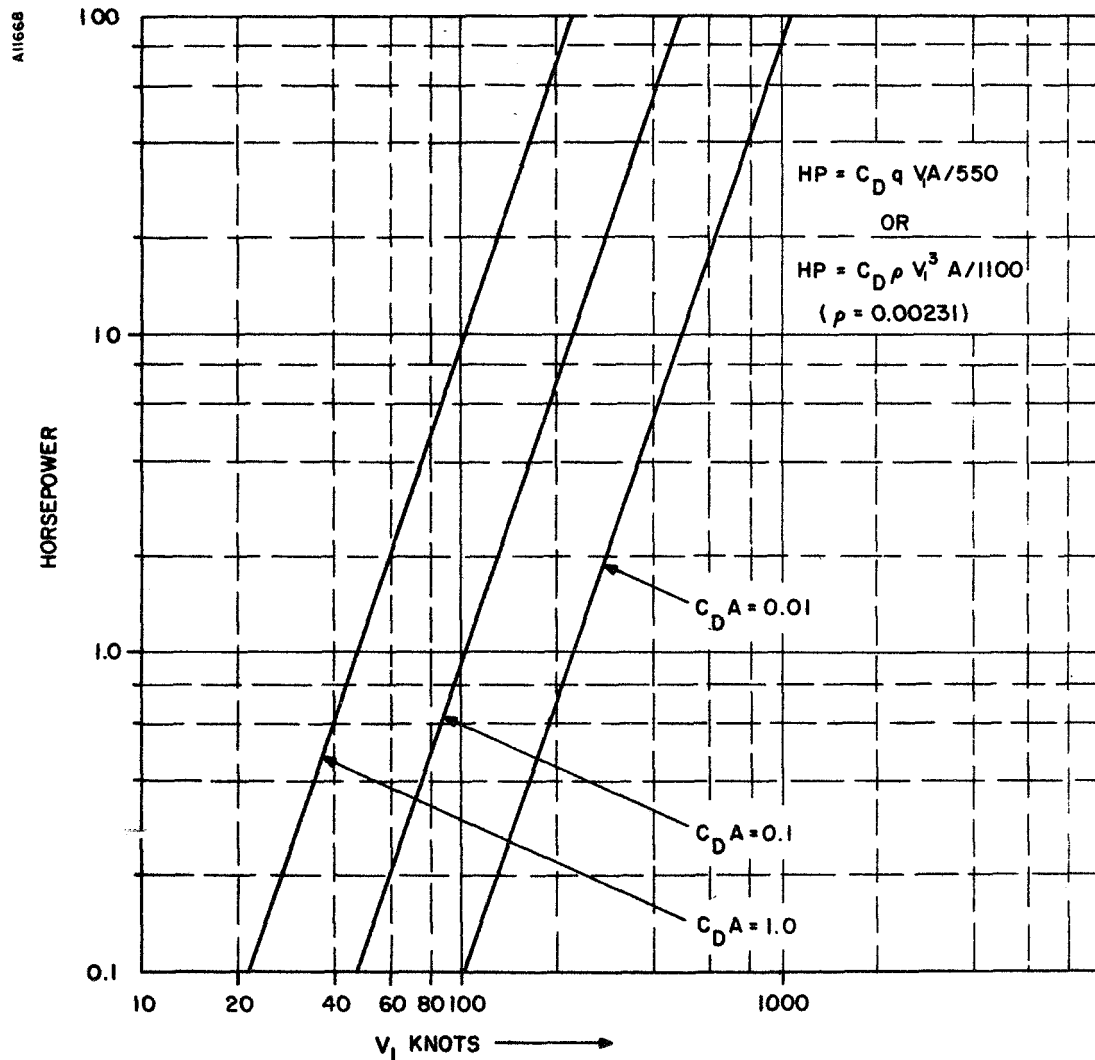


FIGURE 3.18 PLOT OF HORSEPOWER VERSUS AIRCRAFT SPEED FOR THREE  $C_D A$  PRODUCTS

As a second example, wires with circular cross-section can be used for the reflector with suitable supports for the wires. The wires must be closer together to prevent microwave leakage and would likely be horizontal and parallel to the wing surface. If the wires are assumed to be spaced 0.1 wavelength apart at X-Band and wires of 0.01 wavelength diameter are used with an assumed unity drag coefficient, the  $C_D A$  product for estimating the horsepower on Figure 3.18 is 0.1. In this case, the horsepower is 3.5 at 150 knots and is higher because of the higher drag coefficient for round wires. If the wires can be made smaller in diameter without encountering vibration problems or a requirement for too many vertical supports, the drag can be reduced. Reflectors made of thin wires might be electrically heated for deicing.

### 3.8 Interference Drag Considerations

The use of a streamline slat or wire reflector is intended to effect a reduction in drag over a tear drop radome by significantly reducing the frontal area obstructing the air flow. The reduction in frontal area can only be realized if the interference effect of one slat on the airflow over another slat is kept to a very low value. The importance of interference effects is illustrated by the World War II experience in mounting the AN/APQ-7 Eagle scanner under the fuselage of a B-29 aircraft. With the streamline radome, Figure 3.2, mounted adjacent to or slightly under the B-29 fuselage, the drag was very high from the interference effects. Since the Eagle radome could not be mounted far enough below the B-29 fuselage to eliminate interference effects, the radome was mounted adjacent to the fuselage and the gaps filled in to eliminate airflow between the radome and fuselage.

In NACA Report No. 468<sup>6</sup>, the interference between struts in various combinations is given. In this 1933 report, the airspeed was low, about 80 mph, and the struts under test were fairly large, 1 inch to 2 1/2 inches diameter. Keeping these limitations in mind, the report states, "Streamline struts spaced side-by-side, six diameters or more, have little or no interference effect (Figure 3.19). For smaller spacings, the interference drag increases gradually with decreases in spacing down to a spacing of about 2.5 diameters. For spacing of less than 2.5 diameters, the interference increases rapidly with reduction in spacing to a maximum value not determined in these tests because of excessive vibration. The magnitude of the interference drag may be ten or more times the drag of a single strut. Another significant fact is that each size strut defines a separate curve,

suggesting a Reynolds Number\* effect; but with the exception of struts spaced very close together, the drag coefficient is constant for all air speeds for each strut size, indicating the reason for the difference is elsewhere."

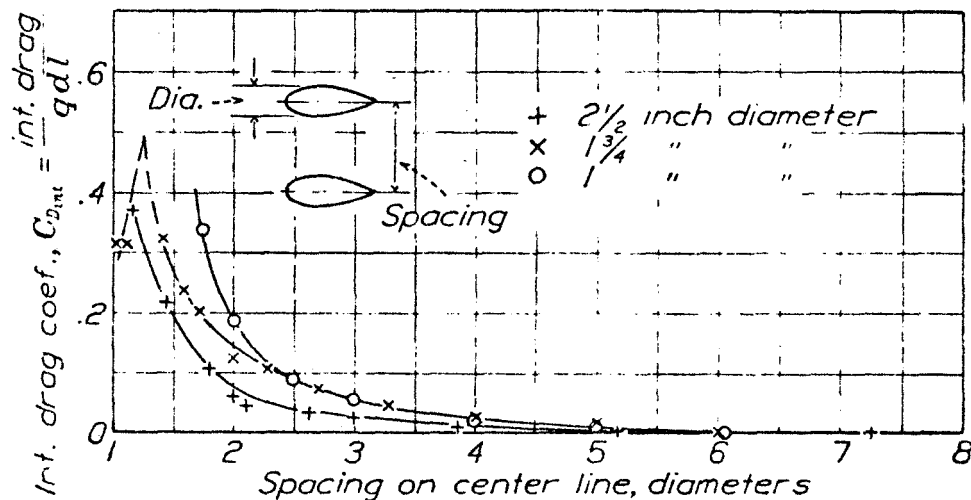


FIGURE 3.19 EFFECT OF SIDE-BY-SIDE SPACING ON INTERFERENCE DRAG OF STREAMLINE STRUTS.

Navy No. 1 Strut Section, Fineness Ratio, 3, Air Speed, 80 mph.

(From NACA Report No. 468)

The streamline slats for a reflector are about 1/10 or less of the diameter of the struts tested by NACA and reported in No. 468. However, the velocities are somewhat higher by a factor of two to five, so the Reynolds Number might still fall within the range of the NACA test. The results of work on smaller struts and higher velocities is needed to verify the conclusions of NACA Report No. 468.

\*The Reynolds Number of a flow is defined as the product of a scale velocity and a scale length divided by the kinematic viscosity of the fluid.

An alternate to the use of grating bars is the use of a porous mesh of round wires or simply parallel wires in the plane of the electric vector. Siao<sup>7</sup> shows that the drag coefficient rises from the isolated cylinder value of 1.2 to 2.0, because of interference effects, as the solidity ratio increases from 0 to 0.5.

### 3.9 Underwing Retractable Grating Antenna

The cylindrical parabolic grating antenna with offset feed mounted under the wing, overcomes some of the limitations of a symmetrical parabola (Figure 3.13). When not in use, the grating can be retracted either flush with the under surface of the wing or partially into the wing. The same mechanism as is used for the retraction might also provide the tilt. The offset feed, transmitter and control circuits can be contained inside the wing. No radome is required and with a secure mounting plate an installation could be made on any existing aircraft without complete rebuilding of the wing. If the predictions on interference drag effects in NACA Report No. 468 can be confirmed, then even in the extended position the drag from a grating reflector would be less than from a tear drop radome. With retraction initiated by the landing gear switch, the antenna reflector would be retracted when the aircraft is taxiing or parked on the ground. A cross-section sketch of an underwing antenna is shown on Figure 3.20.

### 3.10 Flush Mounted Antenna Array in the Top of the Wing

A linear array can be mounted in the top of the wing, with the array parallel to the long axis of the wing. The launcher is followed by a dielectric coating to give essentially endfire directivity to the beam in the vertical plane (Figure 3.21).

Theoretical and experimental work has been carried out on surface wave antennas and is reported in the literature. For example, Hanratty and Wheeler<sup>8</sup> describe the development of a slot antenna for missile and aircraft applications. Their X-Band antenna has a vertical beamwidth of between 10 and 15 degrees; however, the peak of the beam is approximately six degrees above the horizontal. The use of a dielectric coating on a downward curving surface to bring the nose of the beam down to the horizontal is described by Plummer<sup>9</sup>. He also worked with an X-Band model and demonstrated that with a dielectric coating on a flat surface the beam is elevated to an angle of 14 degrees, while with a dielectric coating on a spherical surface, the beam is lowered by 18 degrees to 4 degrees below the horizontal. Endfire antennas are not very efficient in elevation beam forming as the beamwidth is proportional to the square root of the ratio of  $\lambda/\ell$ , where  $\ell$  is the effective antenna length.

A11670

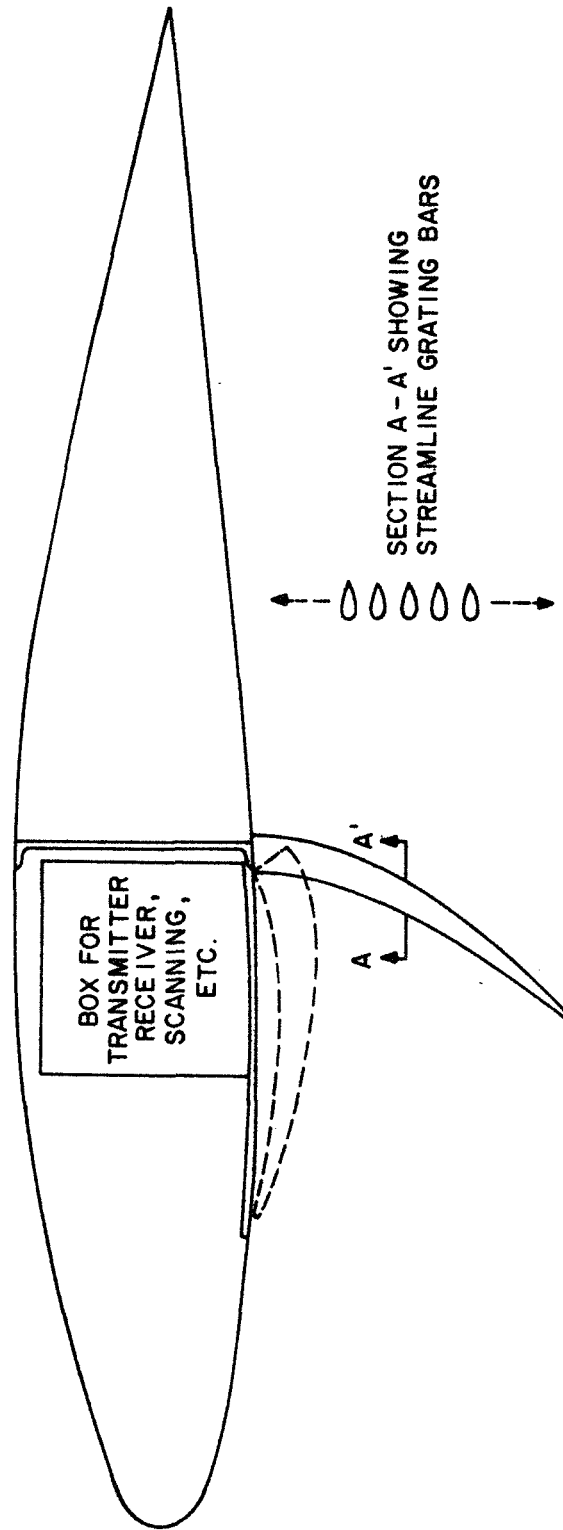


FIGURE 3.20 APPROXIMATE CROSS-SECTION OF PIPER CHEROKEE WING  
WITH OFFSET FEED, CYLINDRICAL PARABOLIC GRATING REFLECTOR  
MOUNTED UNDER THE WING  
(Dotted Lines Show Partial Retracted Position)

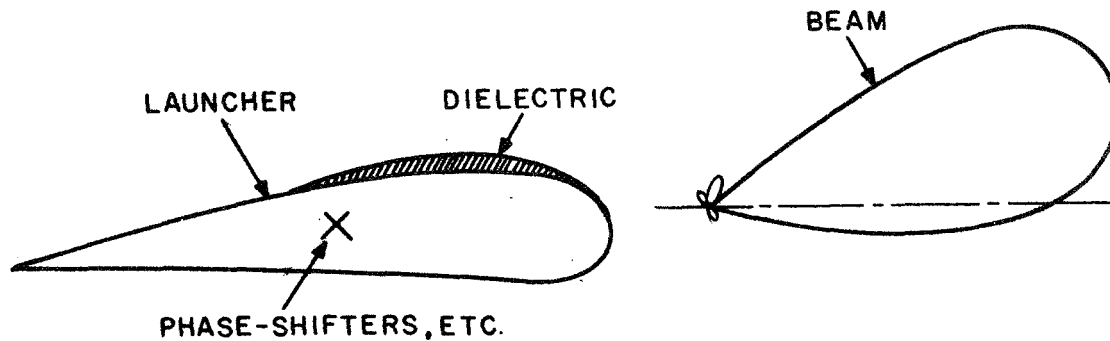


FIGURE 3.21 CROSS-SECTION OF WING WITH FLUSH ARRAY

$$\theta_{BW} = 55 \left[ \frac{\lambda}{\ell} \right]^{\frac{1}{2}} \text{ degrees (endfire)} \quad (3.10)$$

$$\theta_{BW} = 69 \lambda / a_1 \text{ degrees (sidefire)} \quad (3.11)$$

where  $\theta_{BW}$  = elevation beamwidth, degrees

$\lambda$  = wavelength, feet

$\ell$  = effective length of endfire antenna, feet

$a_1$  = height of sidefire antenna, feet

Therefore, a rather wide vertical beam is expected from a surface wave antenna; for example, a 25 wavelength section would give a beam of 11 degrees, according to (3.10). However, Equating (3.11) and (3.12) and solving for the endfire antenna length, it is apparent that if protrusions (slats) are not permitted that a surface wave antenna will produce a narrower vertical beam for



$$l > \frac{[(a_1)_W]^2}{1.2 \lambda} \quad (3.12)$$

where  $(a_1)_W$  = wing thickness.

Therefore, surface wave antennas appear to offer the only approach to a flush antenna in a thin wing. Figure 3.22 illustrates how an antenna can be mounted in the top surface of a wing with a small extension into the air-stream. This antenna is designed to illuminate the ground and is, therefore, mounted near the leading edge of the wing (also see Figure 3.6). A radar antenna would be positioned farther back from the leading edge by approximately 25 wavelengths. In-flight control of vertical tilt may be difficult.

McFarland<sup>10</sup> has designed and evaluated a flush mounted antenna for producing a glide-slope pattern at a low angle. The peak of the beam occurs at an angle of about 10 degrees above the horizontal and might be lowered by the aforementioned technique of using a dielectric coating on the downward curving leading edge of the wing. While there is little prospect of producing a long range weather radar design with a flush mounted antenna, a wide beam, short range radar appears feasible.

### 3.11 Crossed Beam Scanning Radar

In the search for radar techniques which can give acceptable angular resolution with a small frontal (drag) area the crossed beam arrangement has appealed to earlier investigators. A diagram (Figure 3.23) from Reference 11 illustrates how antenna beams which are broad in one angular dimension and narrow in the other can be combined to produce a narrow effective beamwidth in both dimensions.

If one wide-narrow beam is used for transmitting and the other narrow-wide beam is used for receiving, then the received power is proportional to the product of the two gain functions for radar operation. The transmitting and receiving arrays are essentially linear arrays mounted at 90 degrees, as shown on the left hand side of Figure 3.23. Quoting from Reference 11, "The antennas can be placed in various configurations; i.e., in the shape of a cross, a tee, an L, or an X. Since they have length, but little width or depth, they can be installed conveniently within the horizontal and vertical dimensions of an aircraft." And, another quotation, "As another example, for the case of a light fixed-wing aircraft, the antennas could be placed in the wing struts." The latter approach is not currently useful as most general aviation aircraft no longer use wing struts.

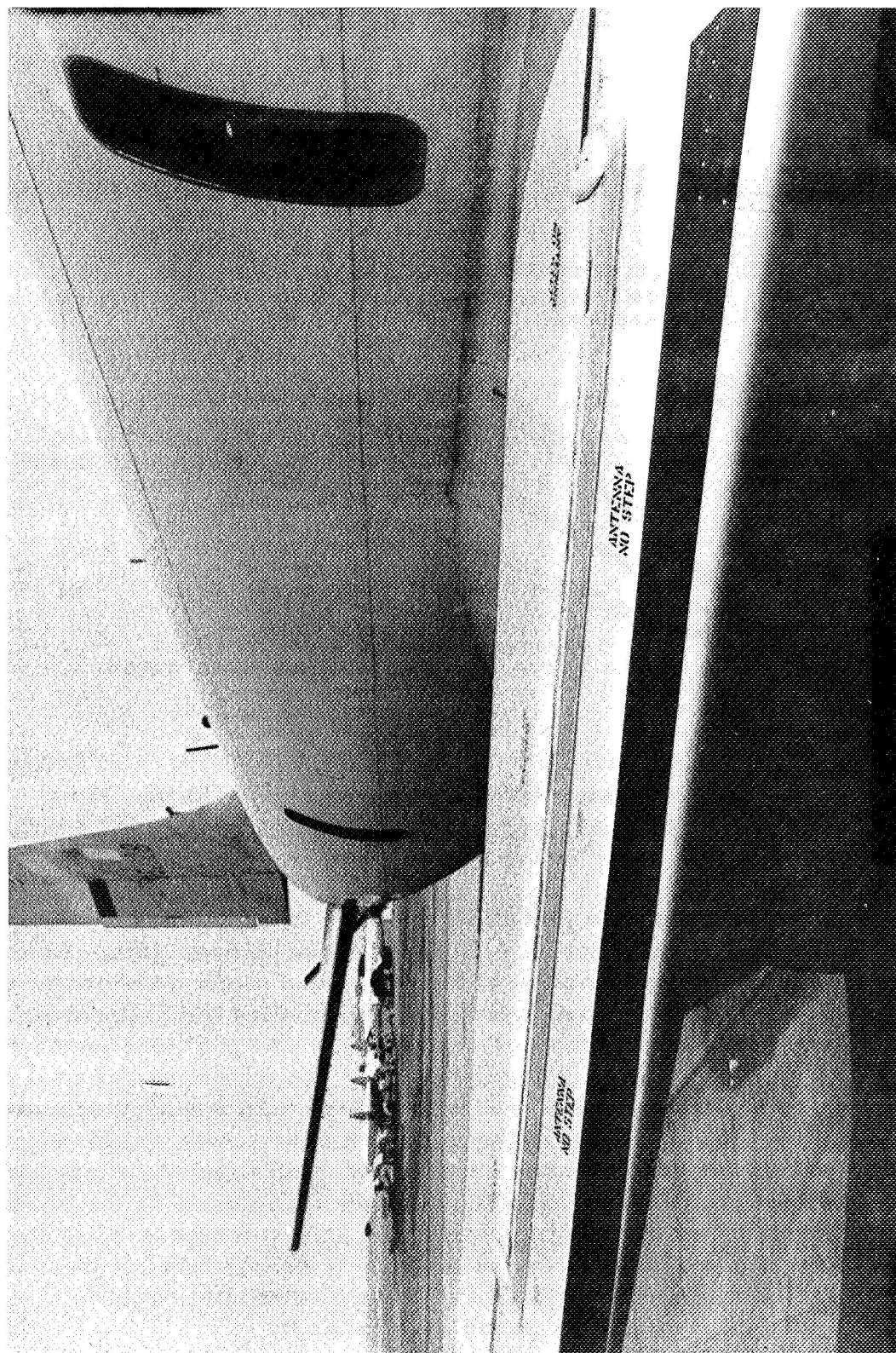


FIGURE 3.22 FLUSH MOUNTED ANTENNA IN TOP SURFACE OF AIRCRAFT WING  
(Courtesy of Autonetics, A Division of North American Rockwell Corporation)

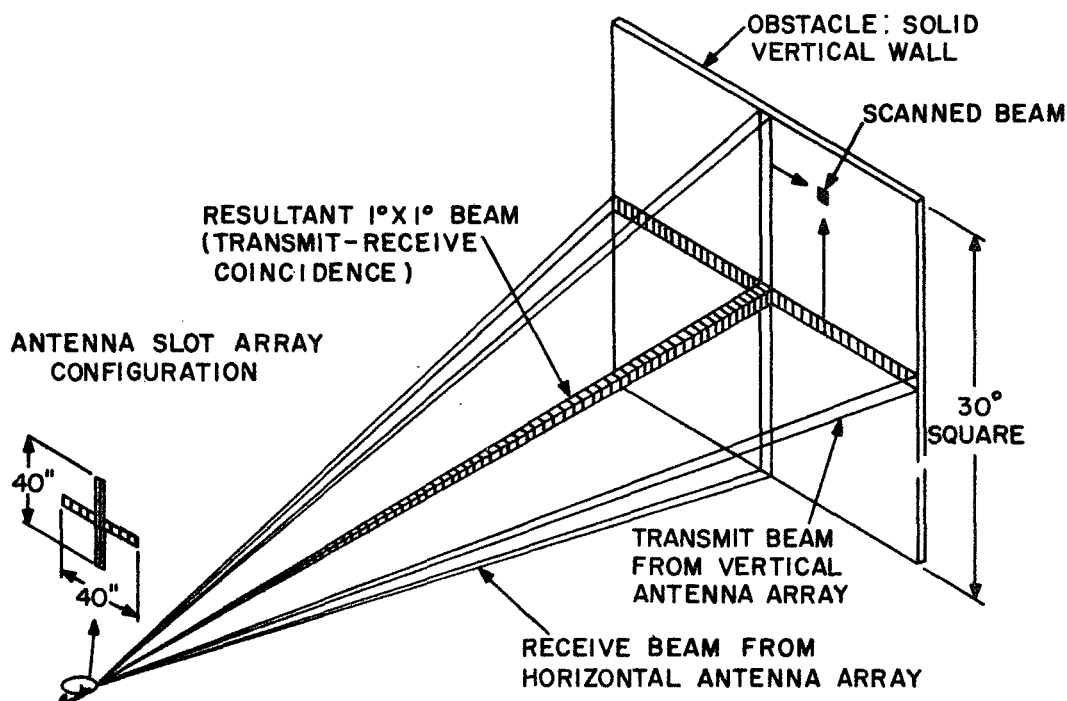


FIGURE 3.23 DIAGRAM OF CROSS-BEAM SCANNING ANTENNA.

One Antenna Generates Wide-Narrow Beam While the Other Narrow-Wide Beam Scans at Approximately Right Angles to it (From 11).

The major limitation that has prevented the application of the cross-beam antenna to general aviation radar is the low antenna gain. Again quoting from [11], "Only a portion of the generated microwave power is useful - actually only 1/30 of that radiated. This makes the cross-beam approach very inefficient compared with a large 40 by 40 inch parabolic antenna that produces a 1 by 1 degree beam." An experimental crossed-beam array detected targets up to 2 miles range with a peak transmitter power of 1 KW. A 12 dB increase in transmitter power would only double this range for point targets so the experiment confirmed the short range capability of the crossed-beam radar. Another limitation of the cross-beam antenna is the poor sidelobe characteristic. The sidelobe level of the product pattern is determined by the one-way sidelobe level of the individual patterns, for example, the sidelobes of the experimental equipment were only 16 dB below the maximum round-trip gain.

In Reference 11, the crossed-beam antenna gain limitation is not considered a limitation to the application of the principle to helicopter radars since the relatively low speed of a helicopter would enable a short-range high-resolution radar to be used for low altitude terrain clearance. Subsequent articles<sup>12,13</sup> have described the development of a linear array for installation in a helicopter blade and tests of crossed-beam antennas using a linear array in a helicopter blade. The motion of the helicopter blade provides the scanning action.

A method which enables a part of the low gain of the crossed-beam antenna to be overcome is described in the next section.

### 3.12 Intra-Pulse Sampling in Multi-Beam Radar

The crossed-beam antenna uses one antenna (the vertical array) to floodlight the azimuth sector of interest. The other horizontal array then scans the azimuth sector with a narrow azimuth beam. Only the crossed-beam intersection, Figure 3.23, produces a useful output at any instant. If the horizontal linear array is designed to produce simultaneous, overlapping receive beams in azimuth, Figure 3.24, then part of the loss of gain can be overcome as the multiple beam outputs can be examined sequentially with a scanning switch. If the beam outputs are sampled by switching at a rate of  $1/\tau$ , where  $\tau$  is the transmitter pulse length, then no information will be lost. If there are N receivers on the N overlapping beams, the duration of sampling at each will be  $\tau/N$  and the bandwidth  $N/\tau$  will be required in the sampling circuit. However, and this is important, the signal-to-noise ratio is established before sampling by the receiver bandwidth  $1/\tau$ . Since each beam provides an output on each transmitted pulse, the number of pulses available for integration is increased over a conventional slow scan by the ratio of the scanned sector to the beamwidth. If coherent integration of the pulses from each beam is assumed, the antenna gain loss resulting from the use of a narrow vertical transmitting array is partially overcome. The floodlighting of an azimuth sector by the transmitting beam reduces the transmit gain by the factor

$$G_t = G \frac{\phi_{BW}}{\phi_s} \quad (3.13)$$

where  $G_t$  = gain of linear transmitting array

$G$  = gain of square array

$\phi_{BW}$  = azimuth beamwidth, degrees

$\phi_s$  = azimuth sector illuminated, degrees.

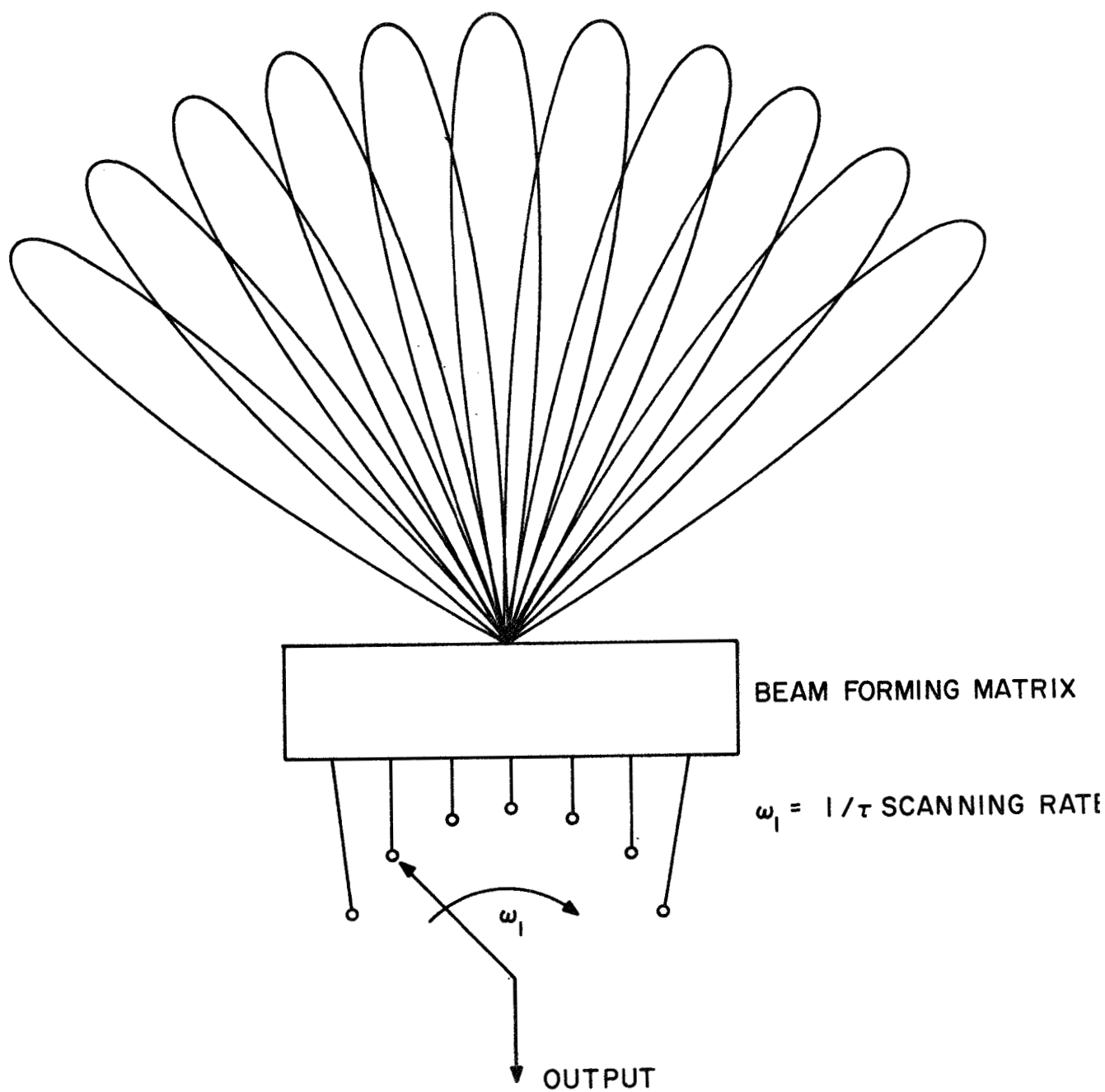


FIGURE 3.24 SEQUENTIAL SCANNING OF  
MULTIPLE BEAM OUTPUTS AT RATE OF  $1/\tau$

If a horizontal receiving array is assumed to have the same beam forming characteristics as the transmitting array, the receive gain will be the same as given by Equation (3.13). However, the postulated rapid scan in azimuth will increase the number of pulses available for integration by the ratio  $\phi_s/\phi_{BW}$ . The power gain from integration, assuming coherent integration of the additional pulses, will partially overcome the lack of a full aperture.

$$G_t G_r M_i = \left[ G \left( \frac{\phi_{BW}}{\phi_s} \right) \right]^2 \frac{\phi_s}{\phi_{BW}} = G^2 \frac{\phi_{BW}}{\phi_s} \quad (3.14)$$

where symbols are as defined for (3.13) except

$G_r$  = gain of receiving array

$M_i$  = coherent integration gain in power signal-to-noise ratio

The gain product, Equation (3.14), is lower than the gain product of a square array; however, it is higher by the integration gain than the gain product of a conventional crossed-beam array, as described in Section 3.11. Some additional gain in the receiving array may be possible by the use of a small vertical aperture to decrease the vertical beamwidth of the received beam. On weak targets the integration gain will be lower than  $M_i$  and might be estimated as the square root of  $M_i$  for non-coherent integration. Round-trip sidelobe levels of -40 to -50 dB are desirable (Table 2.1); however, these low sidelobe levels are difficult to achieve on the one-way patterns in the cross antenna. Low aerodynamic drag and a very high picture repetition rate (a complete picture for each pulse transmitted) are the desirable features of the intra-pulse sampling radar.

### 3.13 Intra-Pulse Beam Scanning (MODSCAN)

While a multiple beam forming matrix, such as was assumed in the last section, can be constructed, the loss may be excessive at microwave frequencies. It is also possible to produce the same effect by the use of a single fast scanning beam which samples all the beam directions in azimuth at a sampling rate of  $1/\tau$ . There are a number of methods of producing the high scanning rates required for intra-pulse scanning. Davies and Killick<sup>14</sup> describe several methods, one of which seems particularly suitable for application to general aviation equipment. This technique, which will be referred to as MODSCAN, for modulation scanning, mixes the signals from multiple receiving dipoles onto a selected sequence of frequencies. By appropriately selecting the frequencies used in each mixer the phase shifts on the local oscillator signals are transferred to the incoming signals and

the beam is caused to scan rapidly. The rate of scanning is determined by the difference in frequency between the local oscillator signals applied to adjacent mixers but must be at least at the rate  $1/\tau$  to sample all signals in the azimuth sector of interest within each pulse length,  $\tau$ . A block diagram of the MODSCAN receiving array is shown in Figure 3.25. The signals received on the  $N + 1$  dipoles are mixed in individual mixers with local oscillator signals generated by the SCALO. The local oscillator signal frequency for a particular mixer,  $n$ , is determined by the expression:

$$f_n = f_o + n \Delta f \quad (3.15)$$

where  $f_n$  = local oscillator frequency at  $n$ th mixer, Hz

$f_o$  = unmodulated local oscillator frequency, Hz

$\Delta f$  = sector scanning rate (approximately  $1/\tau$ ), Hz

$n$  = an integer 0, 1, 2, 3, etc.

The differential phase shift of the  $n$ th mixer output relative to the first mixer is:

$$\Delta\psi = n 2\pi (\Delta f) t \quad (3.16)$$

The differential phase shift,  $\Delta\psi$ , is linearly proportional to the element number (an integer) and time. This is the differential phase shift required for linear scanning in  $\sin \theta$  space since

$$\Delta\psi' = \frac{2\pi nd}{\lambda} \sin \phi \quad (3.17)$$

where  $\Delta\psi'$  = phase of signal on element  $n$  relative to the first element

$\phi$  = angle relative to normal of wave direction

$d$  = interelement spacing, cm

$\lambda$  = transmitter wavelength, cm

Solving (3.17) for  $\phi$

$$\phi = \sin^{-1} \frac{\lambda \Delta\psi'}{[2\pi nd]} \quad (3.18)$$

and replacing  $\Delta\psi'$  by  $\Delta\psi$  the transferred phase shift from Equation (3.16).

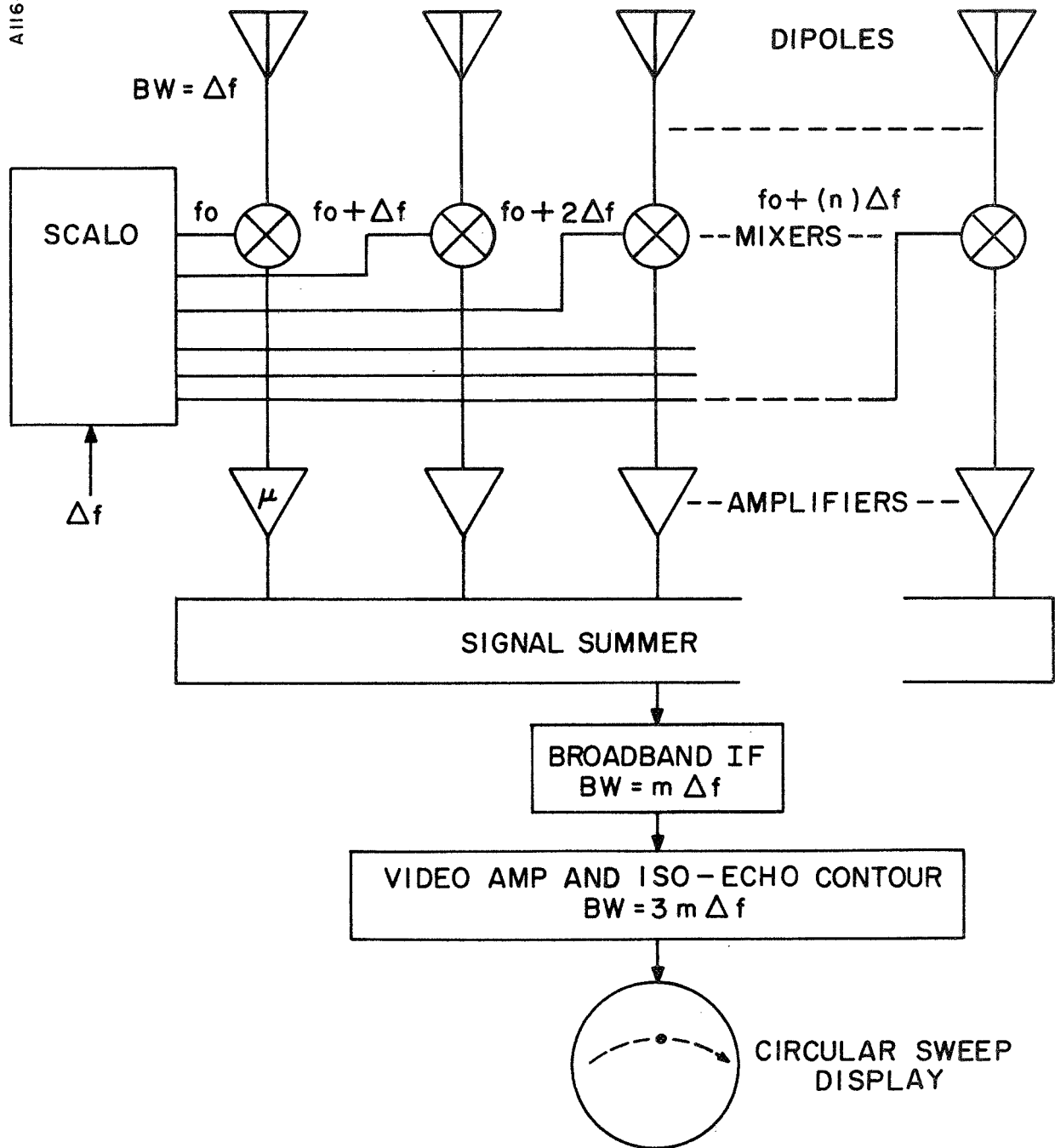


FIGURE 3.25 MODSCAN RECEIVING ARRAY



$$\phi = \sin^{-1} \frac{[\lambda (\Delta f) t]}{d} \quad (t = 0 \text{ at center of sector}) \quad (3.19)$$

The above expression for the scan angle,  $\phi$ , as a function of time is linear in  $\sin \phi$  and nearly linear with  $\phi$  across the center of the scan sector. Since the antenna beamwidth increases at angles off the normal, the scanning rate is nearly constant if expressed in beamwidths/second. The SCALO block of Figure 3.25 can be synthesized by using a narrow pulse at a repetition frequency of  $\Delta f$  to modulate the local oscillator (LO) signal. If a very short pulse is used to modulate the LO signal then the spectrum will be essentially flat out to  $N\Delta f$  from the carrier frequency. The individual lines of the comb spectrum are selected by filters to give the mixer signals, as shown on Figure 3.25. The design of the filters to select the mixer signals presents some difficulties since the lines of the spectrum will be separated by only 1 to 2 MHz at a carrier frequency of perhaps 9 GHz. One alternative is to convert the microwave received signals to an intermediate frequency of perhaps 500 MHz, another is to generate the SCALO at a low frequency and then convert to the proper microwave frequency. The success of the MODSCAN will depend considerably upon the ability to construct the SCALO and mixers at a low cost.

In addition to overcoming most of the gain loss encountered with the conventional crossed-beam system, Figure 3.23, the MODSCAN also has a very high display rate. A complete display frame is generated for each transmitted pulse which will result in a bright display with considerable dynamic range. Second time echoes are not a problem since a pulse repetition frequency of 400 Hz gives an unambiguous range of over 200 NM. The limitation of one-way antenna sidelobes of the crossed-beam radar is also present in the MODSCAN. By proper weighting of the received dipole signals and careful handling of signal phases, the sidelobes level can be as much as 35 dB below the main beam maximum gain. If a rainfall of 100 mm/hour is considered the strongest target of interest, then reference to Appendix A shows that a signal 35 dB below that from the 100 mm/hour rain corresponds to a rain of 0.65 mm/hour, usually classified as a light rain.

### 3.14 Application of MODSCAN to Single-Engine Aircraft

A possible implementation of the MODSCAN crossed-beam, intrapulse scanning radar on a single-engine aircraft is shown schematically in Figure 3.26. A vertical linear array mounted on top of the cabin is used for transmission and a horizontal linear array is contained in the wing leading edge and is used for receiving.

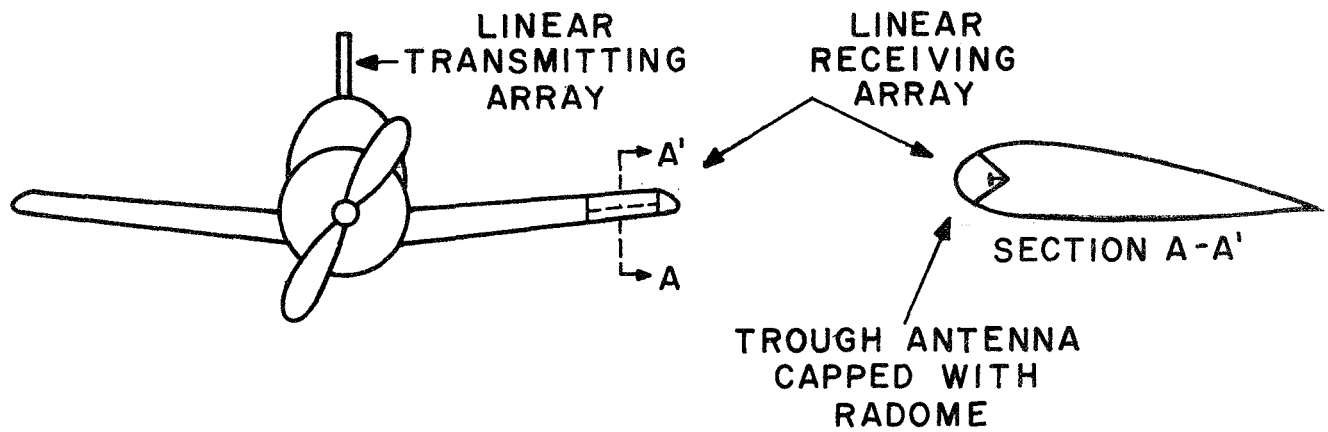


FIGURE 3.26 MODSCAN CROSS-ANTENNA FOR WEATHER RADAR

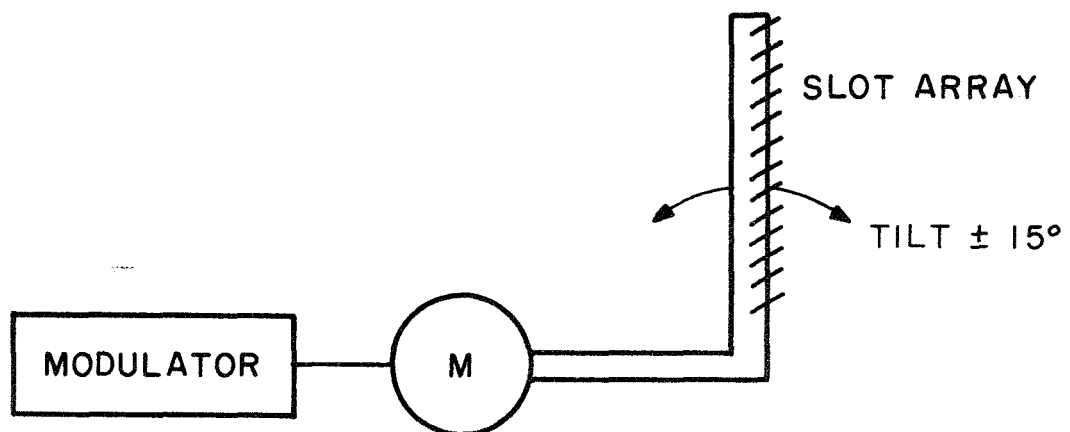


FIGURE 3.27 MODSCAN TRANSMITTING ARRAY

The linear transmitting array must be capable of tilting the transmitting beam perhaps plus and minus 15 degrees to enable the radar to function in climbs and descents. The near-field of the array must clear the propeller arc in all tilt positions to avoid periodic modulation of the display. Except for the tilt requirement it might be possible to put the vertical array in the vertical stabilizer. With the array in the vertical stabilizer, radar operation would likely be restricted to normal cruise attitudes. With the linear array on top of the cabin, the relatively heavy modulator and magnetron, Figure 3.27, can be placed near the center of gravity of the aircraft.

The receiving array in the wing, Figure 3.26, is designed to have as much vertical directivity as feasible within the cross-section of the aircraft wing. The sidelobes in the vertical plane are primarily determined by the transmitting array; however, the narrower the vertical pattern of the receiving array can be made, the lower the gain loss. A 90 degree trough antenna will provide some gain and also a low construction cost. The receiving array may require provision for tilt in synchronism with the transmitting array.

### 3.15 Non-Coherent MTI for Terrain Return Suppression

The grating antenna and MODSCAN attempt to eliminate terrain clutter by using an antenna beam which is narrow in elevation so that the desired weather target can be separated from the terrain clutter. A somewhat different method of reducing terrain clutter is to cancel the undesired terrain signal by placing a null (zero) response at the location (frequency, angle, or time) of the undesired signal. This technique is useful if the separation of the desired and undesired signal locations can be made large enough.

Terrain clutter targets such as buildings, water towers, bare hills, or mountains produce echo signals that are constant in both phase and amplitude as a function of time; however, there are many types of clutter that cannot be considered as stationary. Echoes from trees, vegetation, sea, chaff, and particularly rain, fluctuate with time. The greater fluctuation of the return from rain can be observed as a broadening of the spectra of the backscatter. Barlow<sup>15</sup> has determined representative power spectra for various types of clutter targets (see Figure 3.28). These data apply at a frequency of 1,000 MHz; however, the experimentally measured power spectra of clutter signals may be approximated by

$$W(f) = [F(t)]^2 = [g_0]^2 \exp \left[ -a \left( \frac{f}{f_0} \right)^2 \right] \quad (3.20)$$

where  $W(f)$  = clutter power spectrum as a function of frequency, watts/cycle  
 $F(t)$  = Fourier transform of input waveform (clutter echo)  
 $f_0$  = radar carrier frequency, Hz  
 $a$  = a parameter dependent upon clutter (see Figure 3.28)

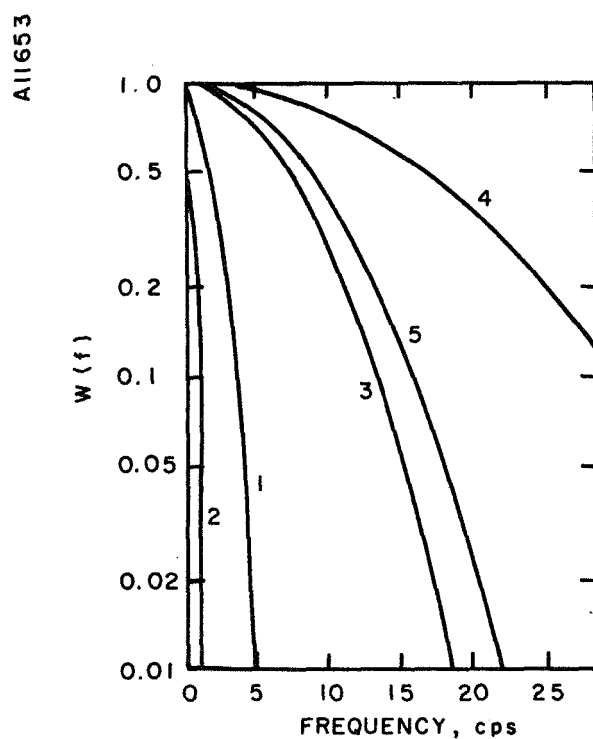


FIGURE 3.28 POWER SPECTRA OF VARIOUS CLUTTER TARGETS

(1) Heavily Wooded Hills, 20 mph Wind Blowing ( $a = 2.3 \times 10^{17}$ )

(2) Sparsely Wooded Hills, Calm Day ( $a = 3.9 \times 10^{19}$ )

(3) Sea Echo, Windy Day ( $a = 1.41 \times 10^{16}$ )

(4) Rain Clouds ( $a = 2.8 \times 10^{15}$ )

(5) Chaff ( $a = 1 \times 10^{16}$ )

(From Barlow<sup>15</sup>, Proceedings IRE)

The "a" parameter is a measure of the width of the clutter spectrum and the ratio of rain ( $a = 2.8 \times 10^{16}$ ) to heavily wooded hills with 20 mph ( $a = 2.3 \times 10^{17}$ ) is 82. If a moving target indicator (MTI)<sup>16</sup> (Chapter 4), is used to cancel the clutter then considerable reduction of the undesired terrain return can be obtained with little reduction in return from rain. Grisetti, Santa and Kirkpatrick<sup>17</sup> have shown that a graph can be constructed of the relative clutter attenuation for an ideal single cancellation MTI. This graph is reproduced as Figure 3.29 and shows that about 19 dB of terrain clutter reduction can be obtained with very little attenuation of rain return for the parameters,  $f_o = 10,000$  MHz and  $f_r = 1,000$  Hz, which are suitable parameters for a weather radar.

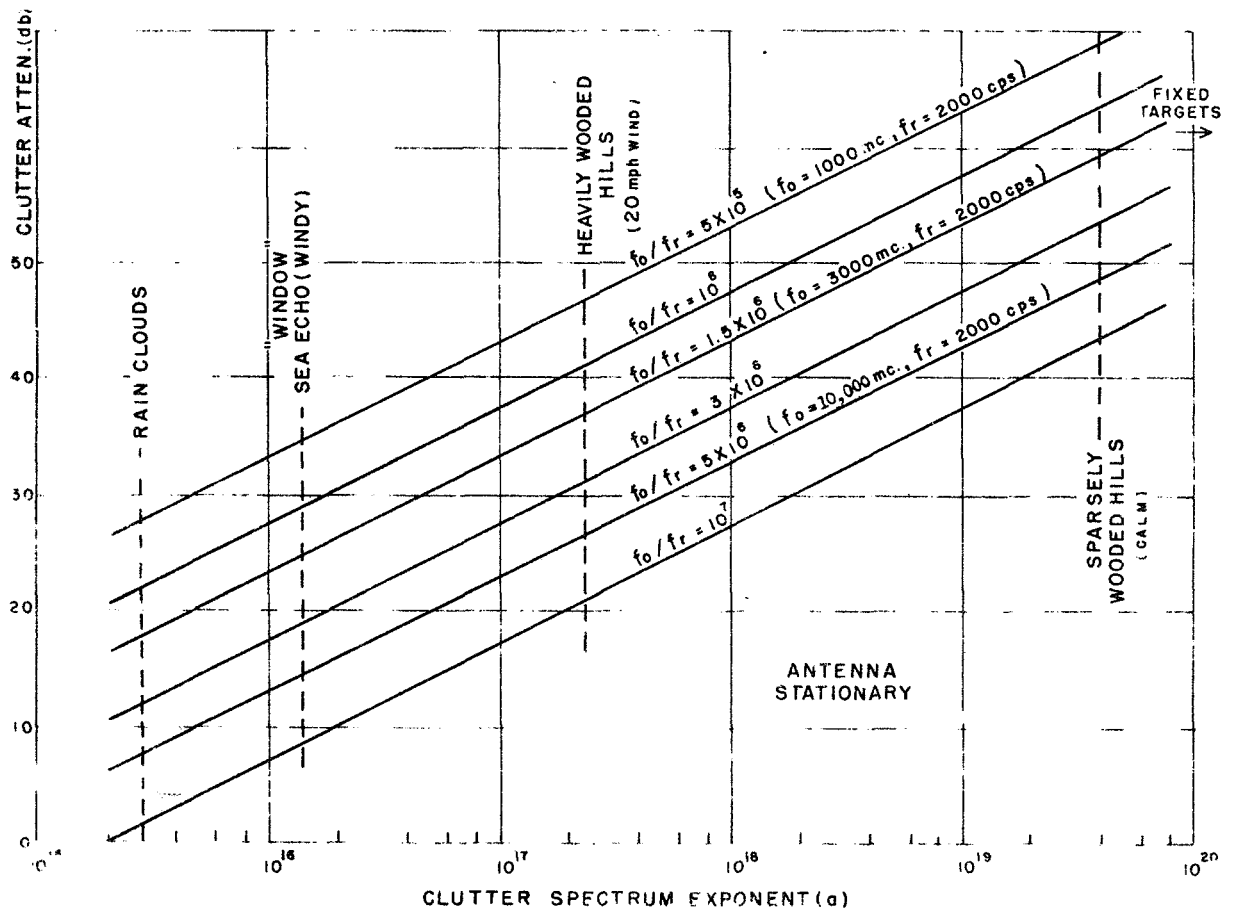


FIGURE 3.29 EFFECT OF INTERNAL FLUCTUATIONS  
ON CLUTTER ATTENUATION  
(From Grisetti, Santa and Kirkpatrick<sup>17</sup>)

To keep expense to a minimum, the MTI is implemented as a non-coherent single cancellation unit. The delay unit for the MTI (requires a delay of  $1/f_r$ ) is currently costly (several thousand dollars) though it may be possible to effect a significant reduction in cost by a judicious choice of specifications.

### 3.16 Monopulse Terrain Clutter Attenuation

The last section, Section 3.15, describes the use of MTI to reduce undesired terrain clutter by cancellation. The use of a narrow vertical antenna pattern to reduce terrain clutter was also described in previous sections. A more efficient reduction of clutter might result from an antenna pattern cancellation technique. By means of monopulse antenna tracking<sup>18,19</sup> a null would be constantly directed toward the instantaneous angle of arrival of terrain signals. Kirkpatrick<sup>20</sup> has described RF or IF circuits to cause the monopulse null to track the instantaneous angle of arrival of the return from clutter elements. Since the transmitted pulse scans the ground clutter with the velocity of propagation in the medium (approximately the velocity of light) the null in the elevation pattern must scan in angle at a rate so as to match the changing clutter source angle. The angle of arrival as a function of the dimensionless ratio  $2h/ct$  is shown on Figure 3.30 for an assumed flat earth. In MTI radar there must be an appreciable separation of the rain target and terrain clutter spectrums in the frequency domain; with the monopulse technique there must be an appreciable separation of a target and a terrain clutter patch in elevation angle. Because of the finite pulse length of the radar and the random nature of the clutter there will be some error in tracking of the clutter return and incomplete cancellation of the clutter.

This section considers the clutter power return from an impulse radiated by an elevated omni-directional antenna. A flat earth, covered with random clutter, is assumed for the initial model. The qualitative effect of using a single lobe pattern in elevation is considered next. This leads to the discussion of a two-lobe elevation pattern (monopulse) with ability to track the instantaneous angle of arrival of clutter signals. This largely qualitative discussion is followed in Appendix D by a preliminary calculation of the clutter reduction with the difference pattern formed from two overlapping elevation patterns. While the results are dependent upon pulse length, height, beamwidth and depression angle, for the assumed conditions, clutter reductions ranging from 10 dB for large depression angles to 60 dB at angles near the horizon are indicated. In the presence of clutter from other than a single depression angle, the cancellation is incomplete and a target return is indicated. If both a ground target and a diffuse rain target are present, or if only a diffuse rain cloud is in the antenna beam, the cancellation will be incomplete and a target output is generated. Thus, the monopulse circuit

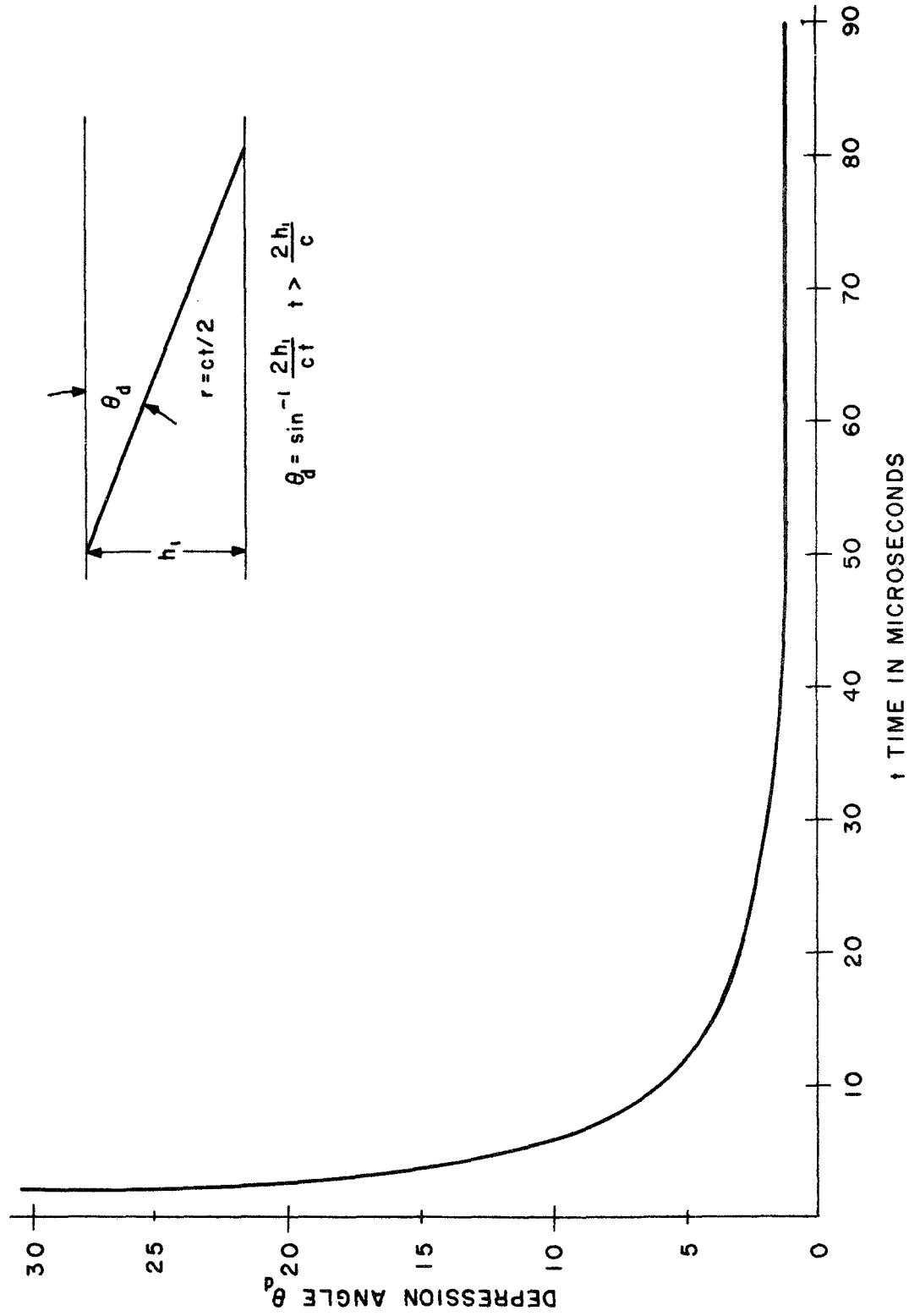


FIGURE 3.30 DEPRESSION ANGLE AS A FUNCTION OF TIME FOR  $h_1 = 500$  FEET

will attenuate undesired ground clutter but will permit desired rain clutter return to be displayed on the indicator. The only function of vertical beam shaping when using the monopulse technique is to enhance the antenna gain. The characteristics of terrain clutter return, as viewed by an airborne radar, will be considered in some detail.

First, consider the radar to radiate pulsed microwave energy omnidirectionally over a flat earth. A coordinate set is defined by Figure 3.31

AI1655

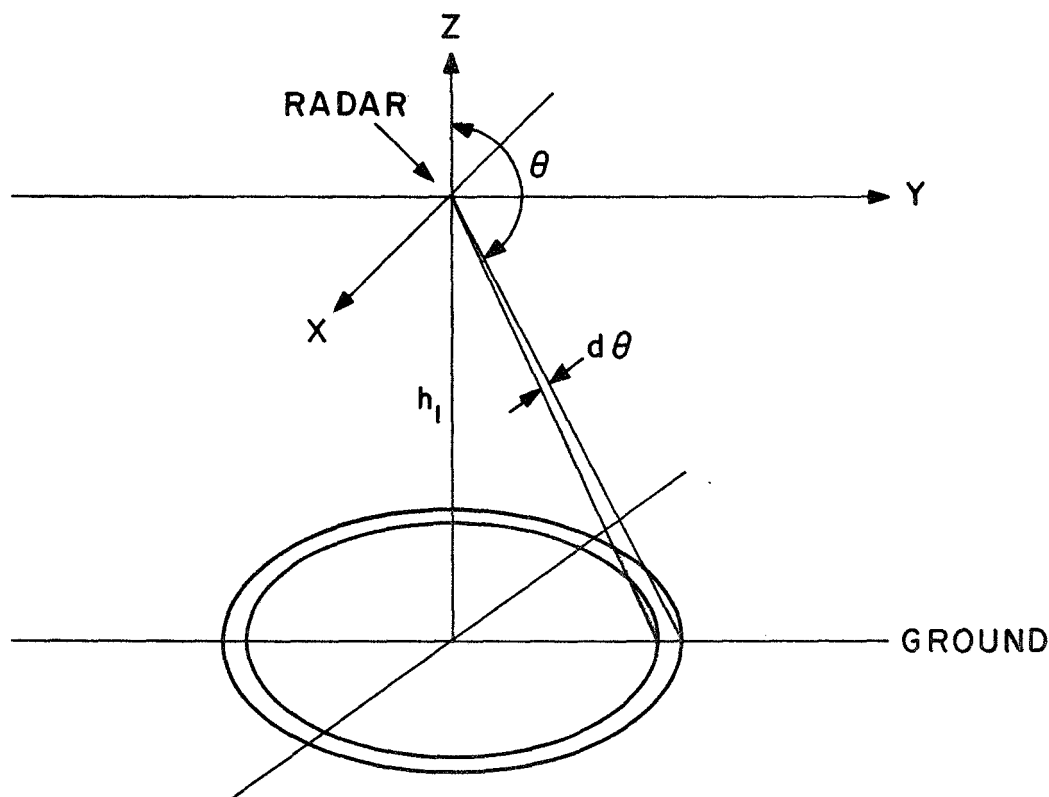


FIGURE 3.31 OMNI-DIRECTIONAL RADAR AT HEIGHT  $h_1$  OVER GROUND



The radar is assumed to radiate an impulse. Power is defined as the time rate of change of energy:

$$P = \frac{dE}{dt} \quad (3.21)$$

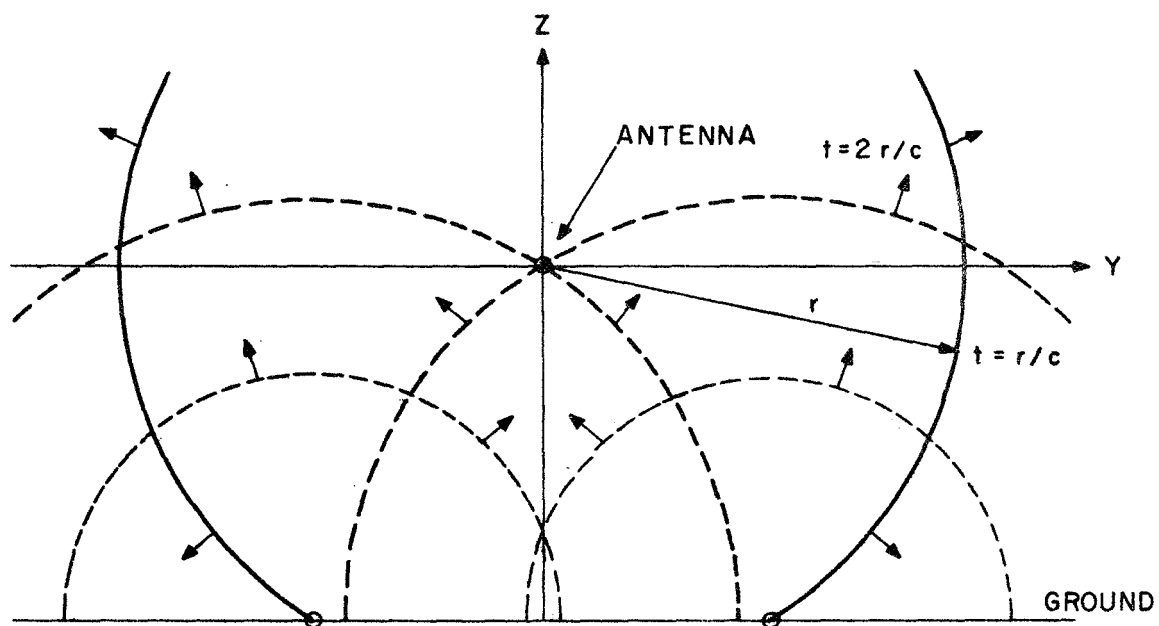
and for a unit impulse of energy

$$E = \int_{-\infty}^{\infty} P \, dt = 1 \quad (3.22)$$

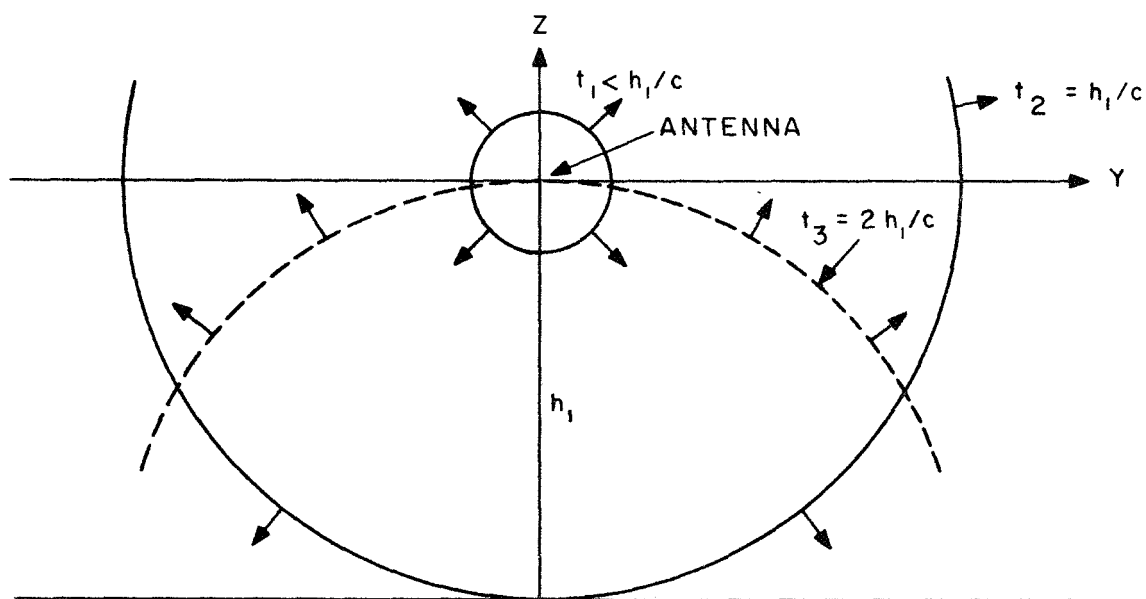
The impulse response will be determined by transmitting one unit of energy and noting the response as a function of time. The one unit of energy can be considered as a spherical wavefront, emanating from the antenna, intercepting the ground, and returning without any multi-path effects. The wavefront will strike the ground initially directly below the antenna after a time  $t = h_1/c$ , where  $c$  is the velocity of propagation in the medium. After a total elapsed time of  $2h_1/c$ , the reflection from the ground immediately under the antenna will be received at the radar. At a slightly later time, the wavefront will have expanded further and the intersection with the ground becomes an expanding circle. A cross-section through the  $yz$  plane is sketched in Figure 3.32a and 3.32b for two instances after the impulse is radiated.

An important thing to note in Figures 3.32a and b is that even though an omni-directional antenna is used, only an annular region on the ground reflects the spherical wavefront at a particular instant of time. Thus, the clutter return is from a ring  $d\theta$  in width and  $2\pi(R^2 - h_1^2)^{\frac{1}{2}}$  in circumference at any particular instant. Thus, there is angular resolution in the  $\theta$  direction without using a narrow antenna beam in the  $\theta$  direction. It is this principle which is used in terrain avoidance radars to enable an antenna with a broad elevation beam to return useful elevation angle data. The azimuthal angle must be restricted by providing a narrow beam in the azimuth direction ( $x, y$  plane) and the antenna gain can be enhanced by providing some directivity in the elevation plane ( $y, z$  plane). The actual earth's surface differs considerably from the assumed flat earth model since there are hills, large buildings, cliffs, etc., and these must be given consideration in practical problems.

The nature of the return energy as a function of time for the flat earth model can be determined by developing the radar equation. The energy per unit area of the expanding spherical wavefront is:



a.  $t \leq 2h_1/c$



b.  $t > 2h_1/c$

FIGURE 3.32 SPHERICAL WAVEFRONT INTERSECTING PLANE SURFACE

$$E_a = \frac{E}{4\pi r^2} \quad (3.23)$$

where  $r$  = radius of impulse wavefront.

The radar cross-section of the reflecting surface is a function of  $\theta_d$ , the depression angle, plus  $\pi/2$ . The echo area per unit area illuminated is designated  $\sigma^0$ . The area illuminated is indicated in Figure 3.33.

A11658

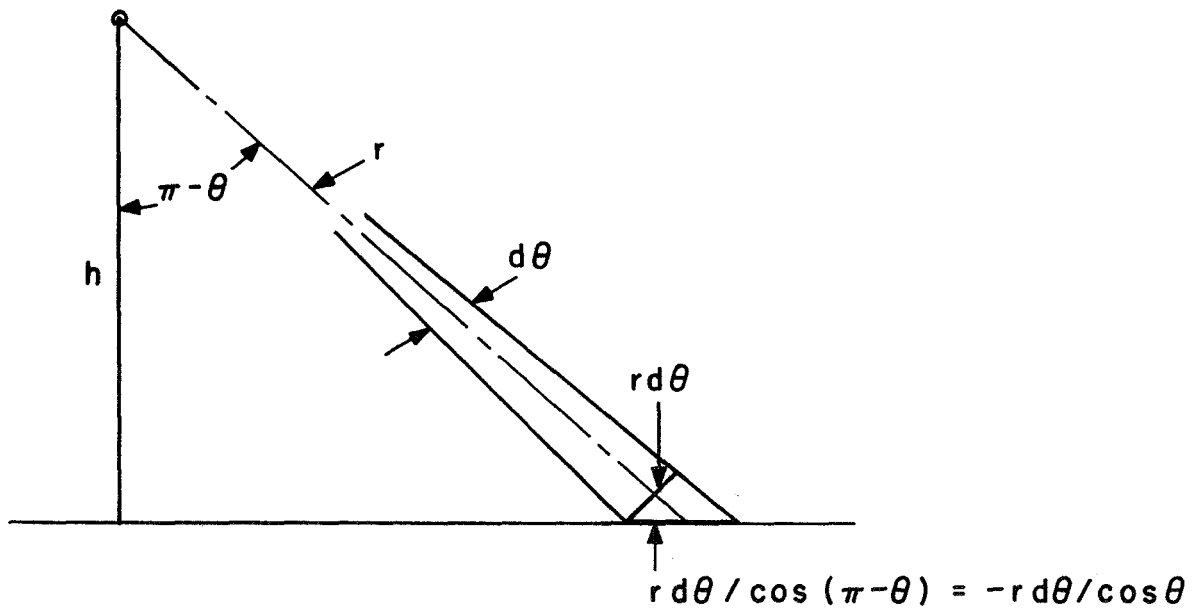


FIGURE 3.33 INCREMENTAL AREA ILLUMINATED ON GROUND

The energy received by the radar from a section of illuminated annular ring one unit long, assuming incoherent addition of the returns from the ring is:

$$dE_r = \frac{EA_r d\theta \sigma^0}{(4\pi r^2)^2 \cos \theta} \quad (3.24)$$

where  $A_r$  = receiving area of antenna (for the assumed omni-directional antenna  $A_r = \lambda^2/4\pi$ ).

To determine the power impulse response, the dependence of  $r$  and  $\theta$  upon time must be examined.

$$\cos \theta = h_1/r \quad (3.25)$$

$$r = h_1 + ct/2 \quad (3.26)$$

where  $h_1$  = height of antenna over assumed flat earth

$t = 0$  at  $2h_1/c$  seconds after impulse is transmitted.

Eliminating  $r$  by substitution:

$$\cos \theta = \frac{-h_1}{h_1 + ct/2} \quad (3.27)$$

Taking differentials and solving for  $d\theta$ :

$$d\theta = \frac{h_1 c dt}{2 \sin \theta (h_1 + ct/2)^2}$$

Substituting  $d\theta$  from the above expression into the energy received expression, the power impulse response is:

$$P = \frac{dE_r}{dt} = 0 \quad \text{for } t < 0 \quad (3.29)$$

$$P = \frac{dE_r}{dt} = \frac{A_r c (\sigma^0 / \sin \theta)}{(4\pi)^2 2 (h_1 + ct/2)^4} \quad \text{for } t > 0 \quad (3.30)$$

where  $\sigma^0 / \sin \theta$  is assumed constant over the region of interest, and  $E = 1$ , the transmitted energy.

The power impulse response for the assumed condition,  $\sigma^0 / \sin \theta =$  constant, the same as used in Section 2.6, is sketched in Figure 3.34.

A11659

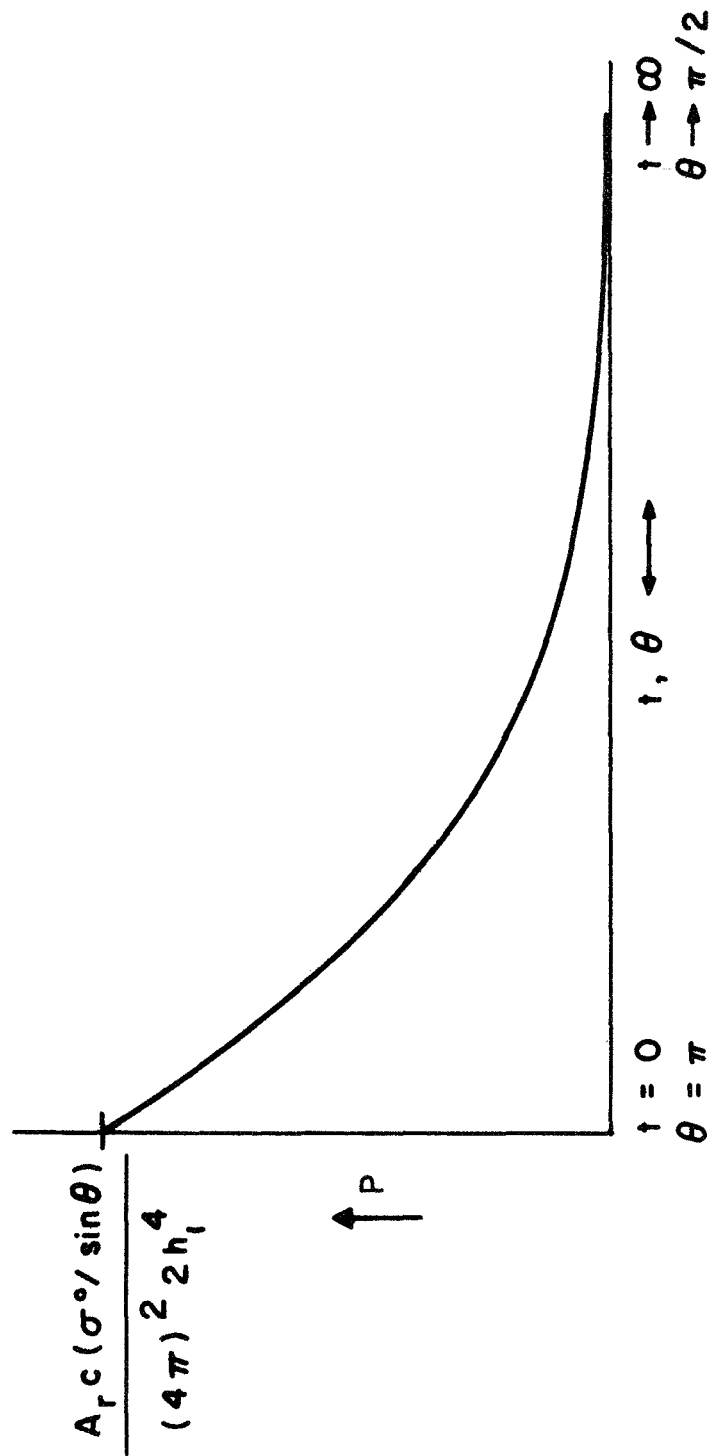


FIGURE 3.34 POWER IMPULSE RETURN FROM CLUTTER  
 $(\sigma^\circ / \sin \theta = \text{constant})$

The curve of Figure 3.34 represents the average power return from clutter, whereas the instantaneous return will fluctuate widely as a function of time. If, instead of omni-directional radiation, an antenna pattern, Figure 3.35, is assumed for the elevation plane, then the impulse response will be modified.

AI1639

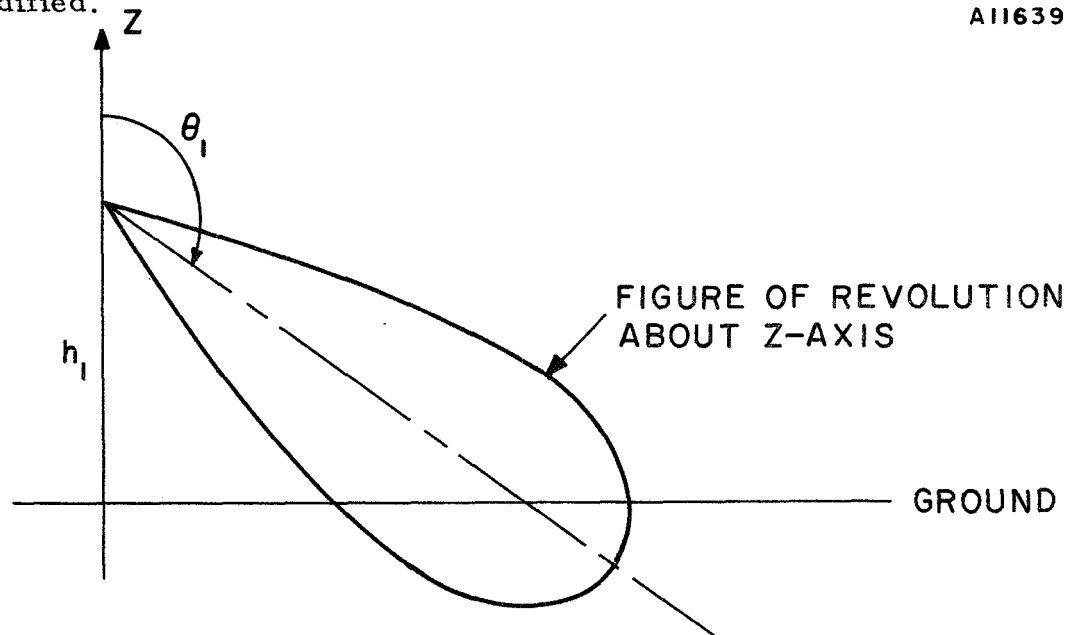


FIGURE 3.35 ASSUMED SYMMETRICAL (EVEN) POWER PATTERN ABOUT ANGLE  $\theta_1$

With an elevation pattern symmetrical about an angle  $\theta$ , the power impulse response might appear as sketched in Figure 3.36.

AI1640

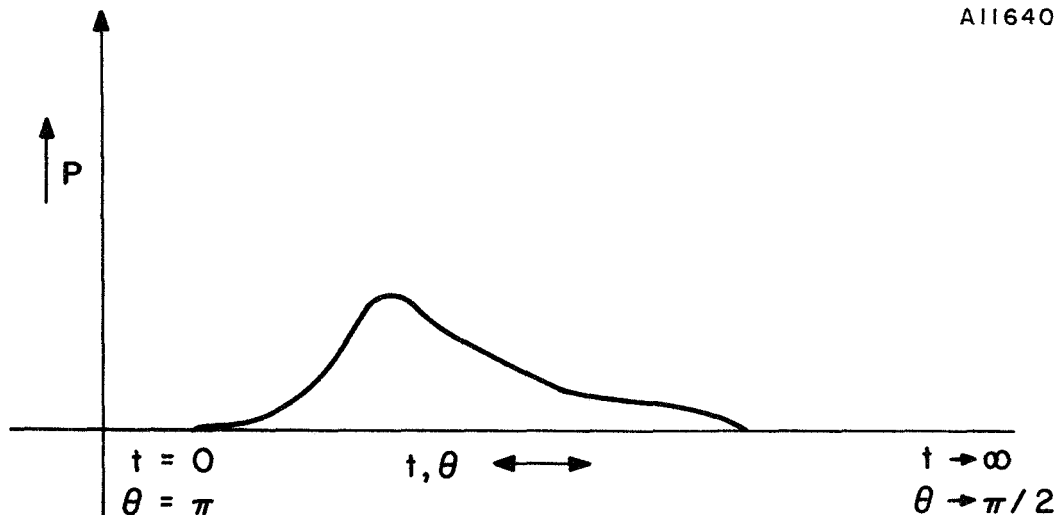


FIGURE 3.36 APPROXIMATE EFFECT OF VERTICAL ANTENNA PATTERN ON POWER IMPULSE RESPONSE

If, instead of a single power antenna pattern shown in the previous sketch, a pair of voltage patterns, A and B, are used, two linear functions of these patterns can be formed,  $|A| + |kB|$  and  $|A| - |kB|$ , where  $k$  is a constant multiplier factor. The voltage patterns, A and B, are assumed to be offset by angles plus and minus  $\Delta\theta$  from  $\theta_1$  (Figure 3.37).

A11641

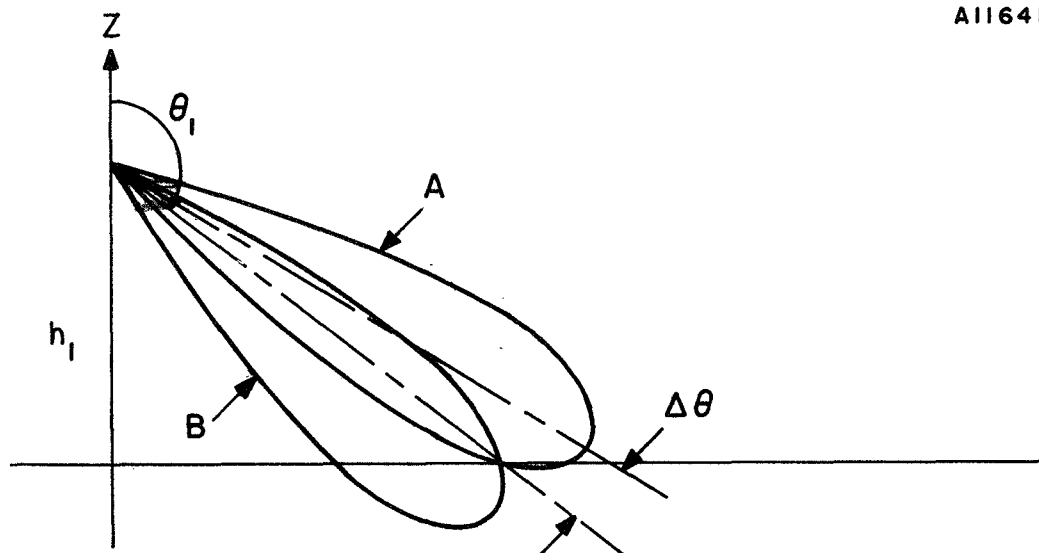


FIGURE 3.37 TWO INTERSECTING ELEVATION PATTERNS  $k = 1$

For the function  $|A| - |kB|$ , at the time (angle) where the function is zero, the difference signal reverses polarity. If  $k = 1$ , this angle is  $\theta$ , and for  $k < 1$ , the angle is greater than  $\theta$ , and for  $k > 1$ , the angle will be less than  $\theta$ . Representative voltage impulse responses for the difference functions  $|A| - |kB|$  are sketched in Figure 3.38 for three values of  $k$ .

A11642

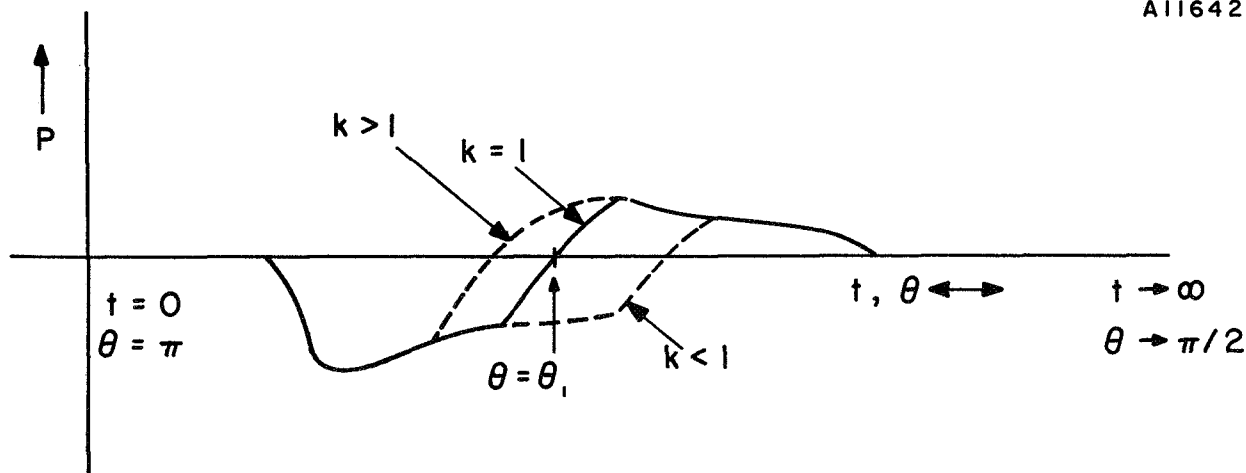


FIGURE 3.38 VOLTAGE RESPONSE  
FOR DIFFERENCE FUNCTION  $|A| - |kB|$

Figure 3.38 suggests that the clutter can be reduced significantly over an angular sector by continuously adjusting the  $k$  factor as a function of time in a difference function  $|A| - |kB|$ . For the assumed flat earth, the  $k$  factor can be computed as a function of the antenna patterns, time, and altitude. A feedback loop can be used to adjust for changing terrain features or feedback can be used as an adjunct to a computer. A typical voltage impulse response with feedback and/or computer control is shown in a sketch in Figure 3.39).

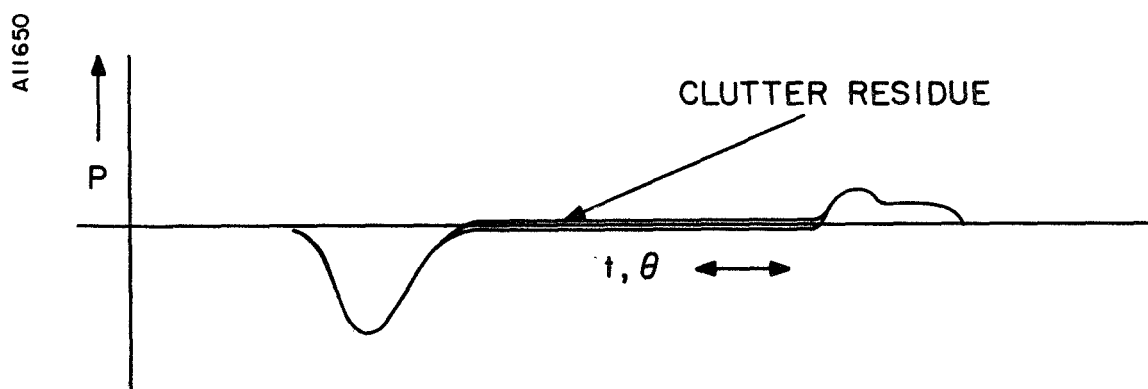


FIGURE 3.39 CLUTTER RETURN REDUCED WITH  $k = f(t, \theta)$

A block diagram of a proposed experimental equipment to observe clutter return on a difference function is shown in Figure 3.40.

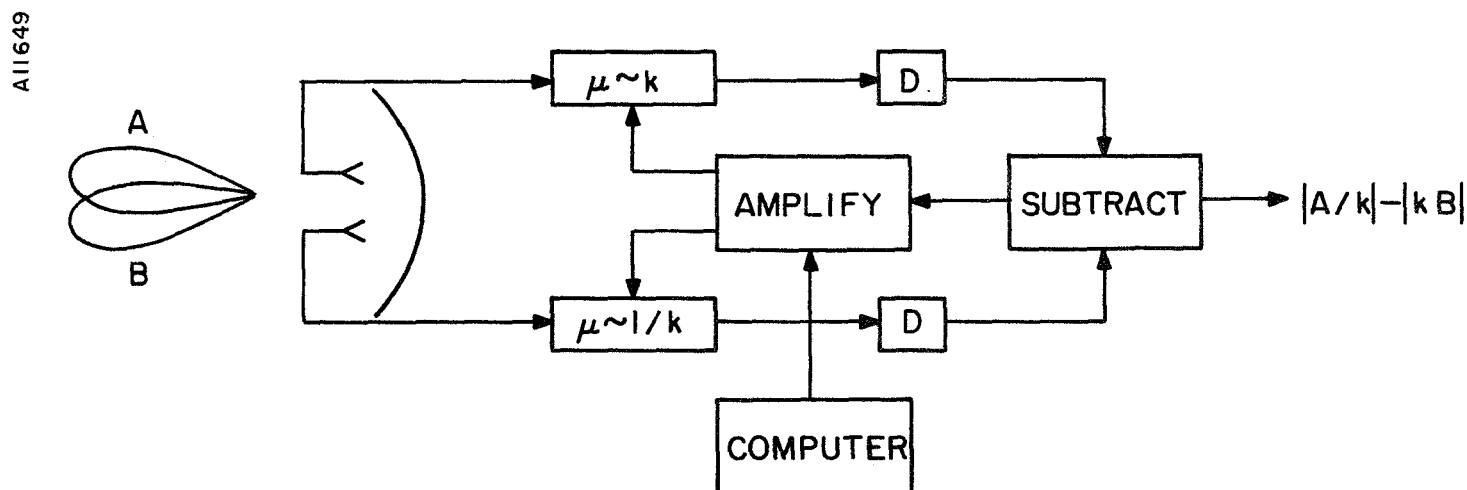


FIGURE 3.40 MONOPULSE EQUIPMENT FOR VARYING  $k$  WITH TIME SO  $|A|/k - k|B| \rightarrow 0$



Since  $k$  must be varied rapidly as a function of time, at the same rate as the spherical wavefront intersection with the ground expands, a wide frequency bandwidth is required for the feedback loop. An "and" gate must be included in the output to "and" the feedback circuit output with the sum signal from beams A and B. In the absence of a sum signal, the output is blocked.

An impulse was assumed for the transmitted pulse; however, the transmitted pulse is likely to be of a rectangular shape. Knowing the terrain impulse response, the rectangular (or other) pulse shape response can be determined by the superposition integral (i.e., the convolution integral), Equation (3.31).

$$P_p(t) = \int_0^t P_t(t - x) P_i(x) dx \text{ pulse response.} \quad (3.31)$$

where  $P_p(t)$  = power response to prescribed pulse shape

$P_t(t)$  = pulse shape as a function of time

$P_i(x)$  = power impulse response of terrain return

In Appendix D the expected cancellation of clutter for assumed perfect tracking of the instantaneous clutter return is investigated. The clutter reduction can be quite large but depends upon the pulse length, antenna patterns, and altitude.

### 3.17 Monopulse Beam Control for Terrain Return Suppression

In the section on vertical beam tilt, Section 2.7, it is shown that a conventional antenna with a small vertical aperture (one foot or less) is marginal for an X-Band radar weather sensor. The antenna must be tilted up to keep the main beam above the nearby clutter (5 to 25 NM) when flying at low altitudes and, as a consequence, the ability to detect storms at long range is reduced. For long range detection, the beam should be pointed near the horizon to keep the storm at the peak of the beam (see Figure 2.11). With a one-foot antenna reflector, it is possible to find a compromise tilt angle that minimizes nearby clutter and reduces the maximum detection range only slightly. If the antenna vertical dimension is reduced to 0.5 feet, then a compromise tilt angle is of marginal value and separate tilt settings must be used to observe weather at near, middle, and long ranges. When observing at long range with the beam on the horizon, it may be desirable to blank the scope from 0 to 25 NM to prevent confusing terrain return for weather echoes. With the beam tilted up, the display should show only short range return, perhaps 0 to 30 NM, to remind the pilot that the detection range is limited by the tilt.

A method to simultaneously improve operation at short and long range, suggested by the previous study of monopulse radar techniques, is to use dynamic control of the tilt angle of the antenna beam. When receiving signals at close range, the beam is tilted up electronically to minimize terrain return, and when the signals from long range arrive the beam is directed to the horizon. Electronic scanning techniques, such as are proposed for the azimuth scan, are too slow and expensive for the needed dynamic beam control in elevation (tilt). Instead, it is proposed to use a simple monopulse antenna arrangement together with a function generator to provide the required dynamic control of the receive beam. The transmitted energy is radiated over the usual even antenna pattern, designated the sum ( $\Sigma$ ) pattern, and reception is on both an even ( $\Sigma$ ) pattern and a delta ( $\Delta$ ) difference pattern. It is the presence of the  $\Delta$  pattern output that distinguishes the monopulse antenna from a conventional single output antenna. If an array antenna is used for vertical beam shaping, then the addition of a  $\Delta$  output is straightforward and not expensive. If a conventional mechanical scanning feed-reflector antenna is used, then a second feed must be added together with a second rotating joint to provide the  $\Delta$  output. Other arrangements, such as putting the receiver on the back of the reflector, can avoid the requirement for a second microwave rotating joint. The two types of antennas are shown schematically in Figure 3.41.

A11739

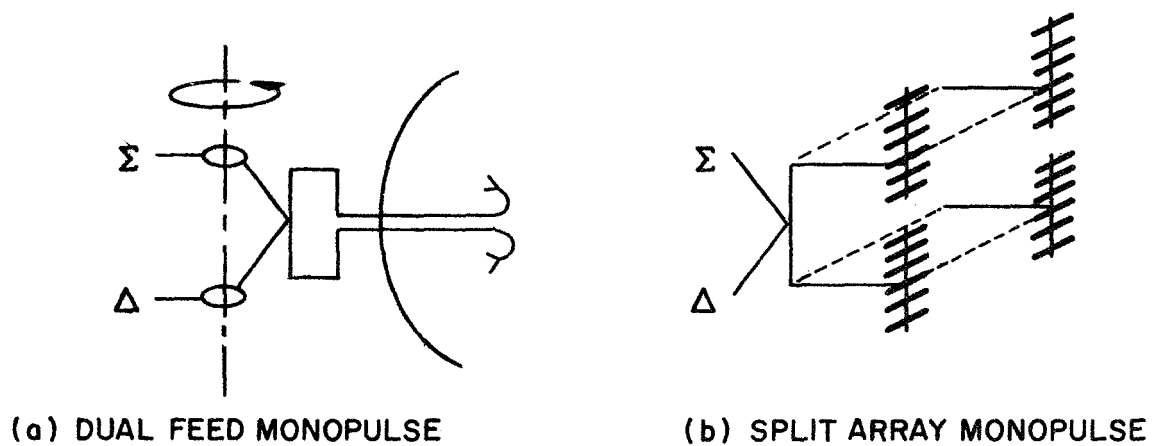
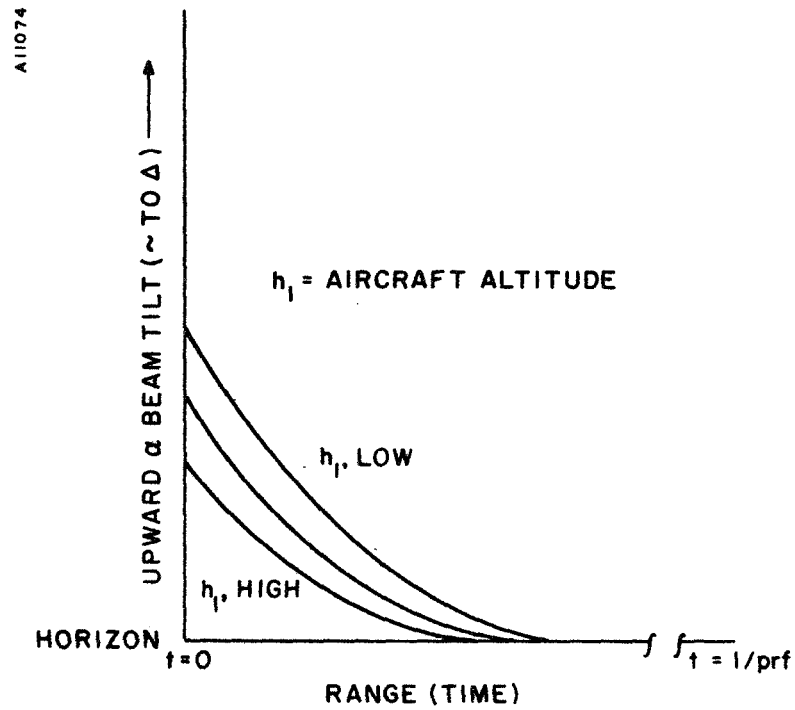
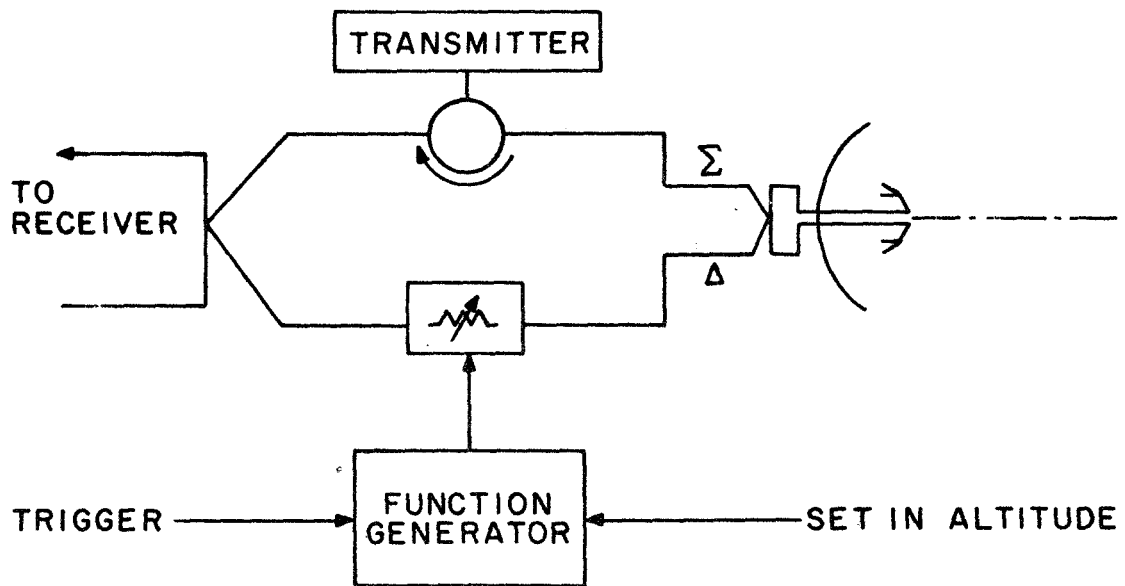


FIGURE 3.41 REFLECTOR AND ARRAY MONOPULSE ANTENNAS



a. Block Diagram of Microwave and Control Circuitry



b. Beam Position as a Function of Time

FIGURE 3.42 DIAGRAMS FOR MONOPULSE DYNAMIC BEAM TILT CONTROL

Using the signals from a suitable monopulse antenna, the  $\Delta$  signal phasor is added to the  $\Sigma$  signal in the amount necessary to steer the beam to the desired angle (within a range of approximately plus and minus one-half beamwidth). The amount of  $\Delta$  signal added to the sum signal is adjusted as a function of time within the pulse repetition frequency (PRF) interval, and also as a function of aircraft altitude. A block diagram of a complete dynamic beam steering arrangement is sketched in Figure 3.42, together with the approximate beam angle as a function of time and altitude. The beam steering process is analyzed in more detail in Appendix E.

The proposed monopulse technique is similar to the dual beam design currently used in ground radar for air route surveillance (ARSR). A "high" beam is used for close range reception to avoid terrain clutter and operation is automatically switched to a low beam for long range detection of aircraft.

### 3.18 Non-Coherent Monopulse Clutter Suppression

In Section 3.15, the spectral characteristics of rain and other clutter targets, as observed by radar, are described. It is suggested that the rapid pulse-to-pulse fluctuations of amplitude of rain return be used to separate rain and terrain return by airborne MTI circuits. The diffuse nature of rain as a radar target suggests another method whereby rain return can be detected in the presence of terrain signals. A typical situation might find the antenna beam "filled" with rain over terrain, as depicted in Figure 3.43.

Dickey<sup>21</sup> has suggested that elevated objects can be detected above terrain clutter by spacial sampling of the backscatter. If two point targets are widely separated in angle (perhaps at the upper and lower edge of the beam) but in the same range sector, then the scattered signals will create an interference pattern in the region of the radar. The resulting interference pattern will have very fine lobes in the region of the radar antenna. The resulting amplitude variation across the antenna can be detected by probes and indicates the presence of an extended target in the beam. A point target (in elevation) such as terrain will return a uniform amplitude across the radar antenna and can be arranged to cancel when no extended target such as rain is present in the same range increment. While rain extending throughout the elevation beam does not create the same interference effect as two point targets separated by a beamwidth, there will likely be useful interference patterns created. Amplitude probes, such as are suggested here, give the spacial derivative of the amplitude distribution of the backscatter field at the initial radar aperture (aircraft). Additional study and development are needed to fully evaluate this terrain suppression technique.

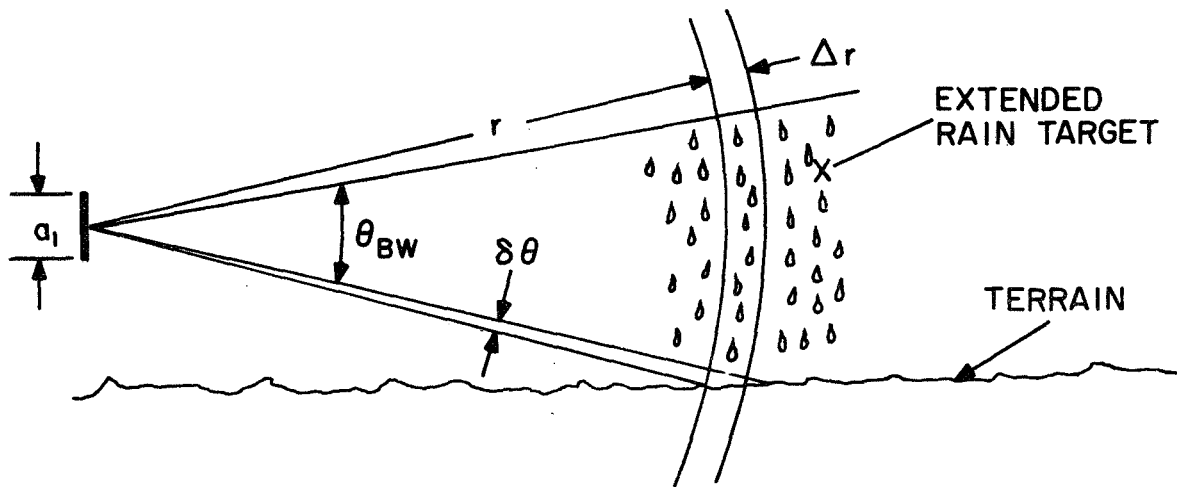


FIGURE 3.43 ELEVATION VIEW WITH RADAR BEAM FILLED WITH RAIN OVER TERRAIN AND  $\theta_{BW} \gg \delta\theta$

### 3.19 Random Noise Radar

Currently, the microwave solid-state transmit-receive modules under development by several companies [e.g., see 22] have a low peak power capability of perhaps one watt. In order to construct a weather radar from these units either some form of intrapulse modulation or a large number of modules, or both, must be used to obtain adequate pulse energy for storm detection. Some form of pulse compression, with a compression ratio of perhaps 100 to 1, can be used with the modules; however, a peak effective power of 10,000 watts still requires 100 of the modules with 100 to 1 pulse compression. Since the modules currently cost several thousand dollars and are projected to cost at least fifty dollars over the next five to ten year period, a drastic reduction in the number of modules required to construct a radar is desirable. Pulse compression ratios beyond 100 to 1 are expensive, as are conventional noise modulation techniques. Therefore,

an announcement in the 22 July 1968 issue of Electronics magazine<sup>23</sup> on a new continuous noise modulation radar at Air Force Cambridge Research Laboratories merited investigation. Quoting from the article, "Poirier sees a place for his radar in small boats or light planes and in a variety of military applications."

The radar concept has been demonstrated by Poirier<sup>24</sup> as capable of detecting single targets. A most attractive feature of the concept, in addition to the continuous transmission, is that no storage of the transmitted waveform is required. A block diagram of the basic equipment, from Reference 24, is shown in Figure 3.44.

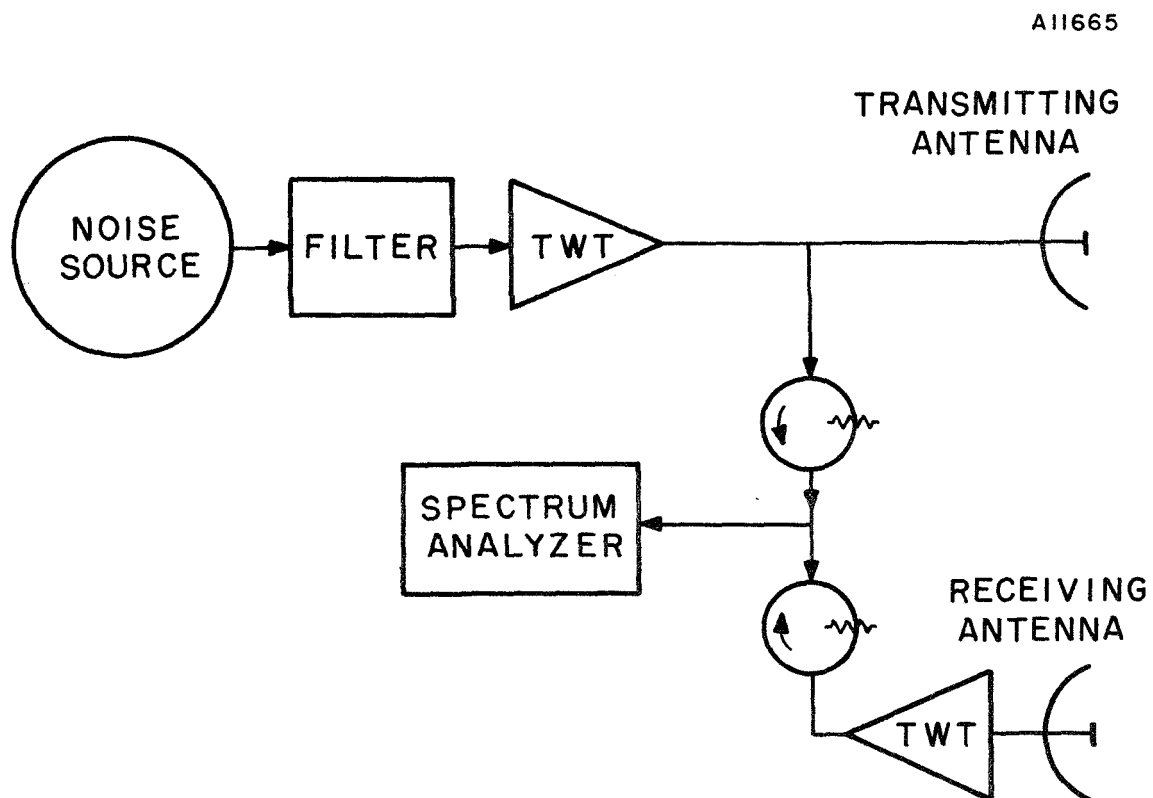


FIGURE 3.44 EXPERIMENTAL SPECTRUM ANALYSIS RADAR

A wideband noise source is amplified and radiated and the backscatter is received on a second antenna. Approximately equal signal from the transmitter is added to the received signal and a spectrum analyzer is used to determine the spectrum. A second spectrum analyzer (not shown in Figure 3.44) can be used to convert the output of the first spectrum analyzer to a plot of target range and amplitude on a linear time scale. The presence of two, possibly expensive, spectrum analyzers is a limitation on the application to general aviation.

Poirier has provided a theory of operation and points out that undesirable cross-product terms may be present. In order to directly compare the theory of the Poirier technique with conventional radar, we have made a brief independent analysis to further clarify the characteristics of the two methods.

#### A. Conventional Radar

If a radar transmits  $\text{Re} \{u(t) e^{j\omega_0 t}\}$  and receives  $\text{Re} \{v(t) e^{j\omega_0 t}\}$ , then it should try to form [see 16, Chapter 9]

$$g(\tau) = \int_{-\infty}^{\infty} v(t) u^*(t - \tau) dt = v(t) \otimes u(t) \quad (3.32)$$

or the equivalent

$$= \int_{-\infty}^{\infty} V(\omega) U^*(\omega) e^{j\omega\tau} d\omega \quad (3.33)$$

where  $V(\omega) = F[v(t)]$ , the received signal

$U^*(\omega) = F[u(t)]$ , the transmitted signal

\* denotes complex conjugate (superscript)

F denotes Fourier transform

$\otimes$  operation of convolution

and display  $|g(\tau)|$  on an A-scope. This is customarily done by matching the receiver to the transmitted waveform as nearly as possible (i.e., the impulse response of the receiver is the transmitted waveform). The received signal transform is

$$V(\omega) = U(\omega) T(\omega) \quad (3.34)$$

where  $T(\omega)$  = the filter function (impulse spectral response) of the targets in space.

Then, reuniting Equation (3.33) with the expression for  $V(\omega)$  substituted from Equation (3.34)

$$g(\tau) = \int_{-\infty}^{\infty} U(\omega)^2 T(\omega) e^{j\omega\tau} d\omega \quad (3.35)$$

Where  $|U(\omega)|^2$  is the spectrum of the autocorrelation function of the transmitted signal since multiplication in frequency  $F[U(\omega) U^*(\omega)]$  is equivalent to convolution (autocorrelation) in the time domain. Then the integral expression in Equation (3.35) is equivalent to the convolution of the autocorrelation function of the transmitted waveform with the impulse response (complex envelope for targets in space), or

$$g_c(\tau) = R(t) \otimes I(t) \quad (3.36)$$

where  $g_c(\tau)$  = conventional radar target response in time (A-scope)

$R(t)$  = autocorrelation of transmitted waveform

$I(t)$  = target impulse response

#### B. Poirier Noise Radar

Here, a fraction,  $(\alpha)$ , of the transmitted signal,  $u(t)$ , is added to the received signal,  $v(t)$ , forming a sum signal

$$s(t) = \alpha u(t) + v(t) \quad (3.37)$$

and the average power density spectrum of  $s(t)$  is estimated by a spectrum analyzer.

$$\overline{S(\omega)^2} = \overline{|\alpha U(\omega) + V(\omega)|^2} \quad (3.38)$$

$$\text{or} \quad = \overline{|\alpha U(\omega) + U(\omega) T(\omega)|^2} \quad (3.39)$$

The detector followed by the second spectrum analyzer will invert (take the Fourier transform) of the signal expression in Equation (3.39) to produce a target response in time (A-scope display). Performing this operation on the signal will enable comparison with the time response of a conventional radar, as given by Equation (3.36).



$$g_p(\tau) = \int_{-\infty}^{\infty} \overline{|S(\omega)|^2} e^{j\omega\tau} d\omega \quad (3.40)$$

where terms are as previously defined except

$g_p(\tau)$  = Poirier radar target response in time (A-scope).

Expanding the squared term in the signal expression Equation (3.39) obtains a modified form of Equation (3.40).

$$g_p(\tau) = \int_{-\infty}^{\infty} |U(\omega)|^2 \cdot [\alpha^2 + |T(\omega)|^2 + \alpha T^*(\omega) + \alpha T(\omega)] e^{j\omega\tau} d\omega \quad (3.41)$$

Rewriting the sum of Fourier transforms as a sum of convolutions obtains

$$g_p(\tau) = \alpha^2 R(t) + \quad (3.42)$$

$$R(t) \otimes [I(t) \otimes I^*(t)] + \quad (3.43)$$

$$\alpha R(t) \otimes I(-t) + \quad (3.44)$$

$$\alpha R(t) \otimes I(t) \quad (3.45)$$

Only the last convolution expression (3.45) corresponds to the output of a conventional radar, as given by Equation (3.36). The next expression (3.44) is similar but gives target images at ranges which are the negative of the true ranges and can be ignored. The next expression, Equation (3.43), produces ghosts of varying strengths at all possible range differences (including zero) between each pair of targets. According to the Poirier paper<sup>24</sup> the noise radar concept was tested with a point target. Since a rain cloud is a diffuse target, additional investigation is necessary before the noise radar technique can be applied to a GA weather radar. If further investigation can demonstrate that false targets can be eliminated and if low-cost spectrum analyzer techniques, perhaps based upon microsound components<sup>25</sup>, can be developed, then the ability to operate with low average power is attractive.

## REFERENCES

1. Cady, W. M, et al (editors), "Radar Scanners and Radomes," Vol. 26 MIT Radiation Laboratory Series, McGraw-Hill Book Company, New York, 1948.
2. "Flight Test Evaluation of Flush Mounted, Luneberg Lens Antenna for PWI/CAS System," FAA Contract BRD-190, Sperry Report No. CA-4283-0196, December 1961, or see Lorenzo, J. J., et al, "An Airborne Flush Mounted Scanning Antenna," Sperry Engineering Review, Winter 1963, pp 22-27.
3. Boronski, S., "A Multi-Channel Waveguide Rotating Joint," The Microwave Journal, June 1965, pp 102-105.
4. Hansen, R. C. (editor), "Microwave Scanning Antennas," Vol. III, Array Systems, Academic Press, 1966.
5. Silver, S (editor), "Microwave Antenna Theory and Design," Vol. 12, MIT Radiation Laboratory Series, McGraw-Hill Book Company, New York, 1947.
6. Biermann, C. and Herrenstein, W. H., Jr., NACA Report No. 468, "The Interference Between Struts in Various Combinations," describes interference drag effects, but the results are not directly applicable here.
7. Siao, T. T., Comments on Paper by Baines, W. D. and Peterson, E. G., "An Investigation of Flow-Through Screens," July 1951, Transactions of the ASME, pp 467-480.
8. Hanratty, R. J. and Wheeler, H. A., "An End-Fire X-Band Flush Antenna Based on the Branch-Waveguide Directional Coupler," IEEE Transactions on Antennas and Propagation, July 1963, pp 433-438.
9. Plummer, "Surface-Wave Beacon Antennas," IRE Transactions on Antennas and Propagation, January 1958, pp 108-112.
10. Baechle, J. R. and McFarland, R. H., "A Flush Mounted Runway Antenna for Use With the FAA Directional Glide-Path System," IRE Transactions on Aeronautical and Navigational Electronics, June 1960, pp 32-39.
11. Miller, B., "Multi-Mode Helicopter Radar Developed," Aviation Week and Space Technology, October 26, 1964, pp 88-91.
12. Klass, P. J., "Rotor Blade Radar Array to Undergo Test," Aviation Week and Space Technology, July 4, 1966, pp 67-69.

13. Miller, B., "Army Plans Rotor Blade Radar Test," Aviation Week and Space Technology, June 17, 1968, pp 66-73.
14. Blackband, W. T. (editor), "Radar Techniques for Detection, Tracking and Navigation," AGARDograph 100, Gordon and Breach, New York, 1966, pp 428-431.
15. Barlow, E. J., "Doppler Radar," Proc. of IRE, April 1949, pp 340-355.
16. Skolnik, M. I., "Introduction to Radar Systems," McGraw-Hill Book Company, New York, 1962.
17. Grisetti, R. S., Santa, M. M. and Kirkpatrick, G. M., "Effect of Internal Fluctuations and Scanning on Clutter Attenuation in MTI Radar," IRE Transactions on Aeronautical and Navigational Electronics, March 1955, pp 37-41.
18. Kirkpatrick, G. M., "Angular Accuracy Improvement," Final Engineering Report on Contract DA 36-039-sc-194, August 1, 1952, AD 46,849.
19. Rhodes, D. R., "Introduction to Monopulse," McGraw-Hill Book Company, Inc., New York, 1959.
20. Kirkpatrick, G. M., "Clutter Attenuation Radar," U. S. Patent 3,392,387, filed January 4, 1967, issued July 9, 1968.
21. Dickey, F. R. and Santa, M. M., "Report on Anti-Clutter Techniques," Final Report on Contract DA 36-039-sc-5446, March 1, 1953, pp 50-56.
22. Hyltin, T. M. and Pfeifer, L. R., "Annual Report on Molecular Electronics for Radar Applications," Contract AF33(615)-2525, Texas Instruments, Inc., December 1966, and subsequent reports.
23. "Random Radar," Electronics, McGraw-Hill Publication, July 22, 1968, pp 41-42.
24. Poirier, J. L., "Quasi-Monochromatic Scattering and Some Possible Radar Applications," Radio Science, September 1968, pp 881-886.
25. Stern, E., "Microsound Components, Circuits and Applications," MIT Lincoln Laboratory, Technical Note 1968-36, October 30, 1968.

## 4.0 NEW SYSTEM TECHNOLOGY

### 4.1 Introduction

Modern airborne weather radars make extensive use of solid-state components such as SCR modulator, transistorized receivers and video amplifiers, and microwave ferrite isolators and circulators. However, the general radar configuration of separate units consisting of:

1. Mechanically scanned antenna,
2. Tube-type transmitter and receiver,
3. CRT indicator,

has changed little since the AN/APS-10 of World War II (1944) design<sup>1</sup>. The AN/APS-10 included two additional units - the synchronizer, which also served as a control panel, and the synchronizer power supply; these two units have been eliminated as separate boxes in current weather radar designs. It appears feasible at this time to develop an all solid-state airborne weather radar consisting of two units: 1) an integrated microwave power generation and electronic scanned antenna unit, and 2) a solid-state display panel. The resulting radar would be too expensive to compete with current designs; however, this is likely to be the future trend; a further reduction in number of installed units from three to two, and toward universal designs that can be utilized on single-engine as well as twin-engine aircraft.

### 4.2 Solid-State Phase Shifters for Electronic Scanning

The use of phase shifters for antenna scanning is described in the radar techniques section of the report, Section 3.4. Much progress in microwave integrated circuits has been made in recent years through development work under Department of Defense sponsorship as well as on company-sponsored programs. Since a low cost phase shifter is a key to a low cost electronic scanning radar, a survey was made of several manufacturers during the winter of 1968-1969, to sample the status of phase shifter developments. The results of this survey are presented in abbreviated form in Table 4.1. Numerous articles have appeared in the technical/trade journals describing phase shifters and/or electronic scan arrays. The reader is referred to these journal articles<sup>2-9</sup>, each of which contains additional references, as well as to numerous microwave conference records. A chart, Table 4.2, is reproduced for ready reference to the numerous types of ferrite phase shifters. To assist in documenting the current state-of-the-art in phase shifters, photographs of representative types are reproduced on the following pages as Figures 4.1 through 4.7. Examination of a latching ferrite phase shifter, Figure 4.1, indicates that the device can be built for perhaps \$20.00


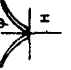


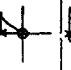

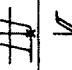
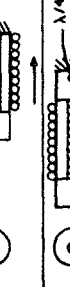







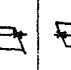

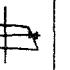
TABLE 4.1

## COMPARISON OF X-BAND PHASE SHIFTER TECHNIQUES





Phase Shifter	One-Way Loss	Peak Power	10,000 Unit Cost (4-bit) per Phase Shifter (E-Estimated)	10,000 Unit Driver Cost (4-bit) (E-Estimated)	Availability	Remarks
Ferrite in Waveguide	< 1 dB	Several Kilowatts	\$20.00 E	\$30.00 E	From several manufacturers at high unit cost.	Extensive development on DOD projects.
Ferrite With Stripline	< 2 dB	Approximately 10 watts	\$ 5.00 E	\$30.00 E	Research models only.	Requires further development including increase in power capability.
Ferrite With Microstrip	< 2.5 dB	Approximately 1 watt	\$ 3.00 E	\$30.00 E	Devices under test in laboratory.	Requires major increase in power capability.
Diode Switches in Waveguide	< 2 dB	> 1 KW	N/A	Approximately \$100.00	Available on special order.	Currently operating in multi-bit laboratory models.
Diode Switches in Microstrip	< 2.5 dB	1 KW or less	\$100.00	Included in phase shifter cost.	Available on firm quotation basis.	Transmission or reflection types available.

TABLE 4.2

CHARACTERISTICS OF 10 TYPES OF FERRITE PHASE SHIFTERS  
(From TR No. 2, Special Microwave Devices Operation, Raytheon Company)

DEVICE	TYPE		RECIPROCALITY		TRANSMISSION LINE		CONTROL		POLAR- IZATION	R.F. # PER- MEABILITY	PHASE SHIFT V CONTROL	FREQUENCY BAND
	NAME	DIGI- TAL	ANA- LOG	RECIPROCAL	NON- RECIPROCAL	WAVE- GUIDE	CO-AXIAL	STRIP				
	REGGIA SPENCER		✓	✓		✓			LINEAR ONE-HAND	$\mu'$		L-K
	E-PLANE		✓	✓		✓			LINEAR ONE-HAND	$\mu'$	AS ABOVE	L-K
	W/G RECIPROCAL LATCHING	✓		✓		✓			LINEAR ONE-HAND	$\mu'$		L-K
	W/G NON RECIPROCAL LATCHING	✓			✓	✓			LINEAR ONE-HAND	K		L-K
	B +		✓		✓	CIRCULAR			CIRCULAR LINEAR	K		L-K
	P.I.P.		✓	✓		CIRCULAR			ALL	$\mu'$		L-K <sub>u</sub>
	CO-AX BEAD	✓		✓			✓		LINEAR	$\mu'$		L-C
	TEM RECIPROCAL LATCHING	✓		✓				✓	LINEAR	$\mu'$	SWITCH BETWEEN $\mu'$ LONG AND $\mu'$ TRANS	L-C
	MICROSTRIP MEANDER LINE	✓		✓	✓			✓	LINEAR	$\mu'$		L-S
	HELICAL	✓			✓		HELIX		LINEAR	K		L-C

\* FOR DEFINITION OF SYMBOLS SEE SECTION 2.2.4

DIAGRAM SHOWS  
FERRITE   
MATCHING   
CONTROL   
DIRECTION  
OF MAGNETIC  
FIELD 

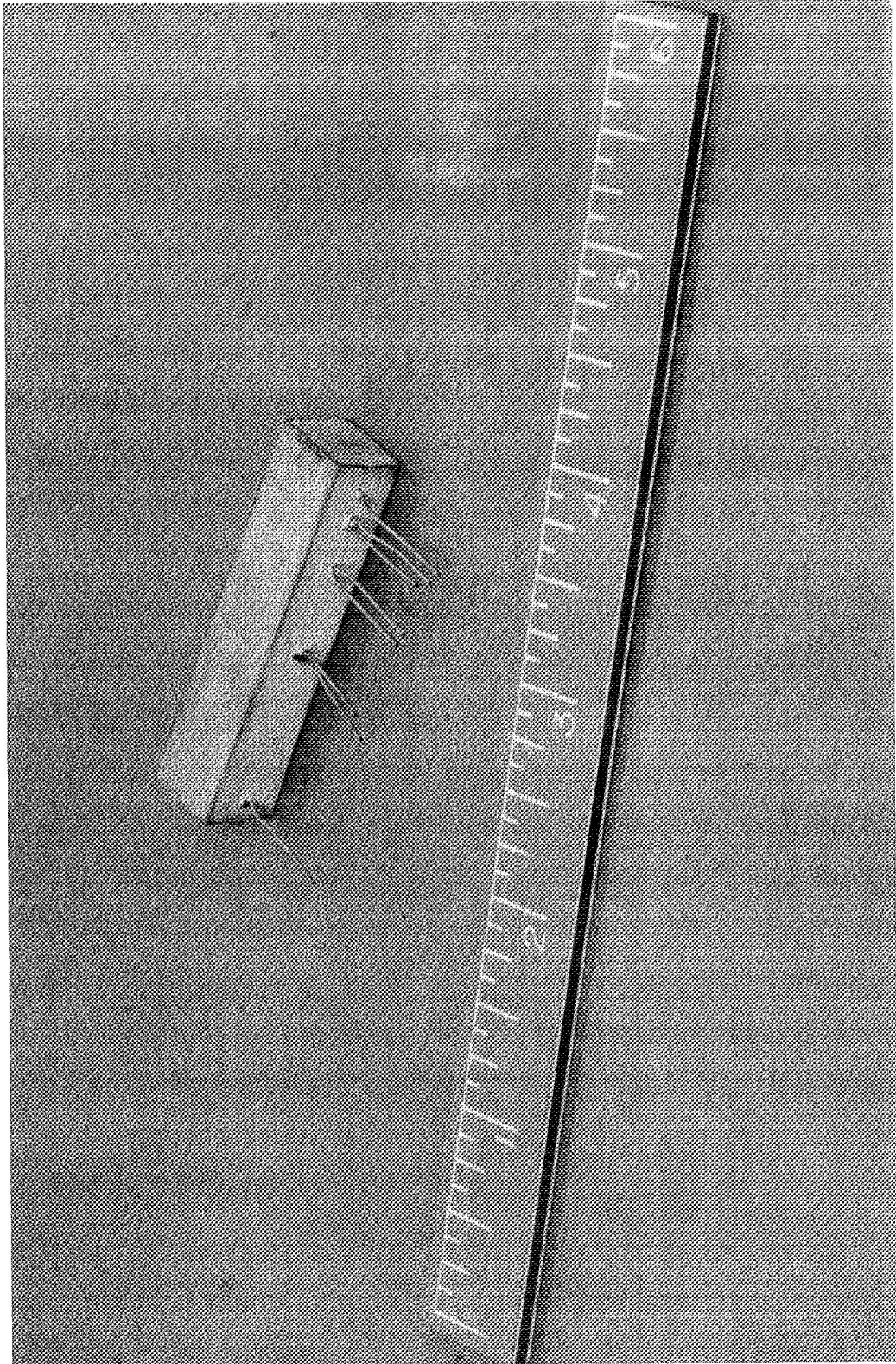


FIGURE 4.1 4-BIT, X-BAND, LOADED WAVEGUIDE,  
LATCHING FERRITE PHASE SHIFTER  
(Courtesy of Autonetics, A Division of North American Rockwell Corporation)



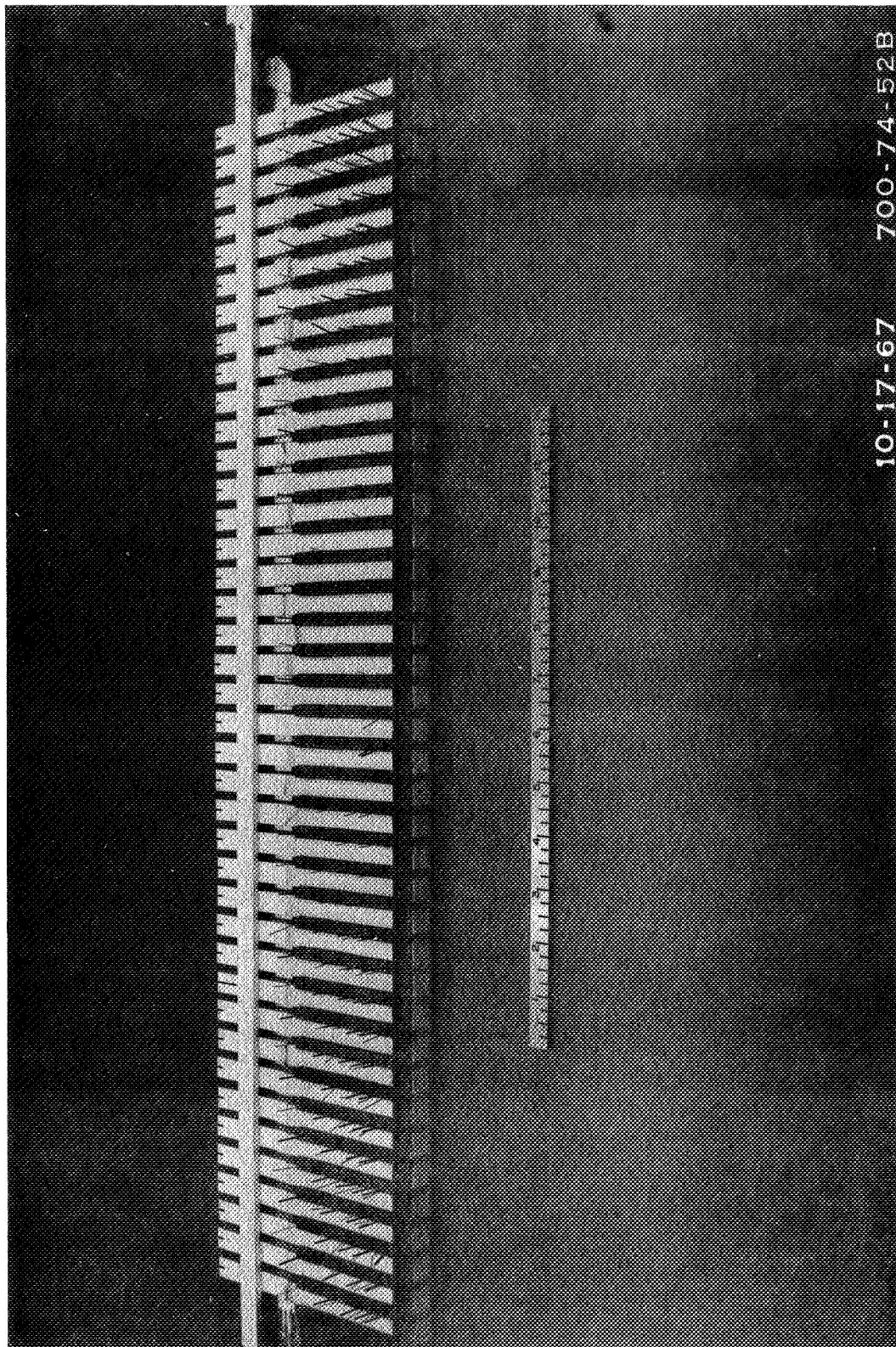


FIGURE 4.2 40 ELEMENT LINEAR ARRAY WITH PLATED WAVEGUIDE FEED  
AND 4-BIT X-BAND LATCHING FERRITE PHASE SHIFTER

(Courtesy of Autonetics, A Division of North American Rockwell Corporation)



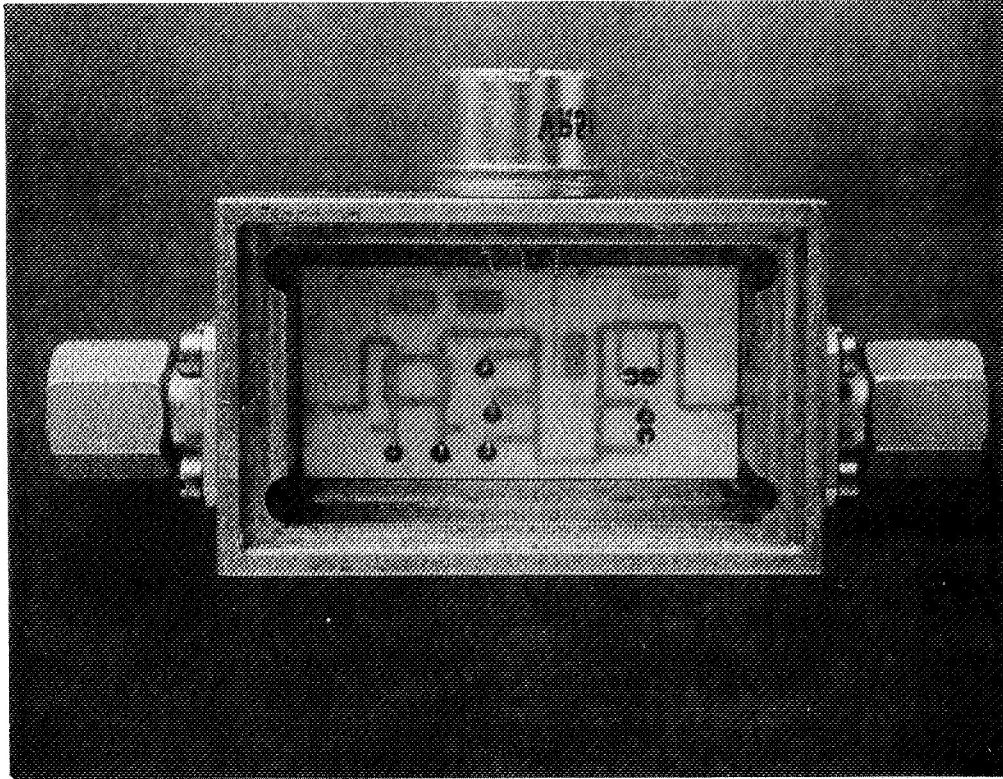


FIGURE 4.3 4-BIT, X-BAND, TRANSMISSION,  
PIN DIODE SWITCH, PHASE SHIFTER  
(Courtesy Microwave Associates)

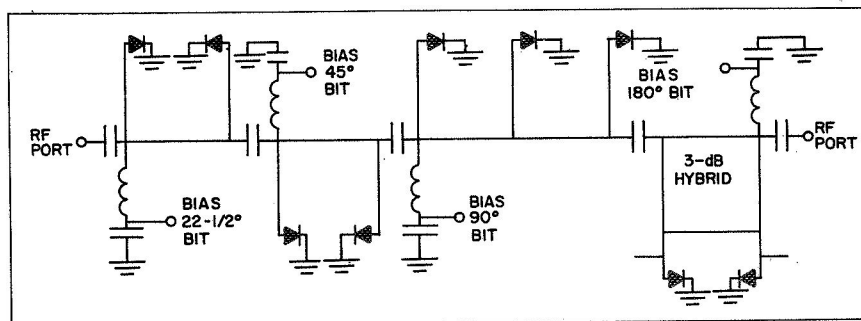


FIGURE 4.4 CIRCUIT DIAGRAM OF 4-BIT  
TRANSMISSION PHASE SHIFTER OF FIGURE 4.3  
(Courtesy Microwave Associates)

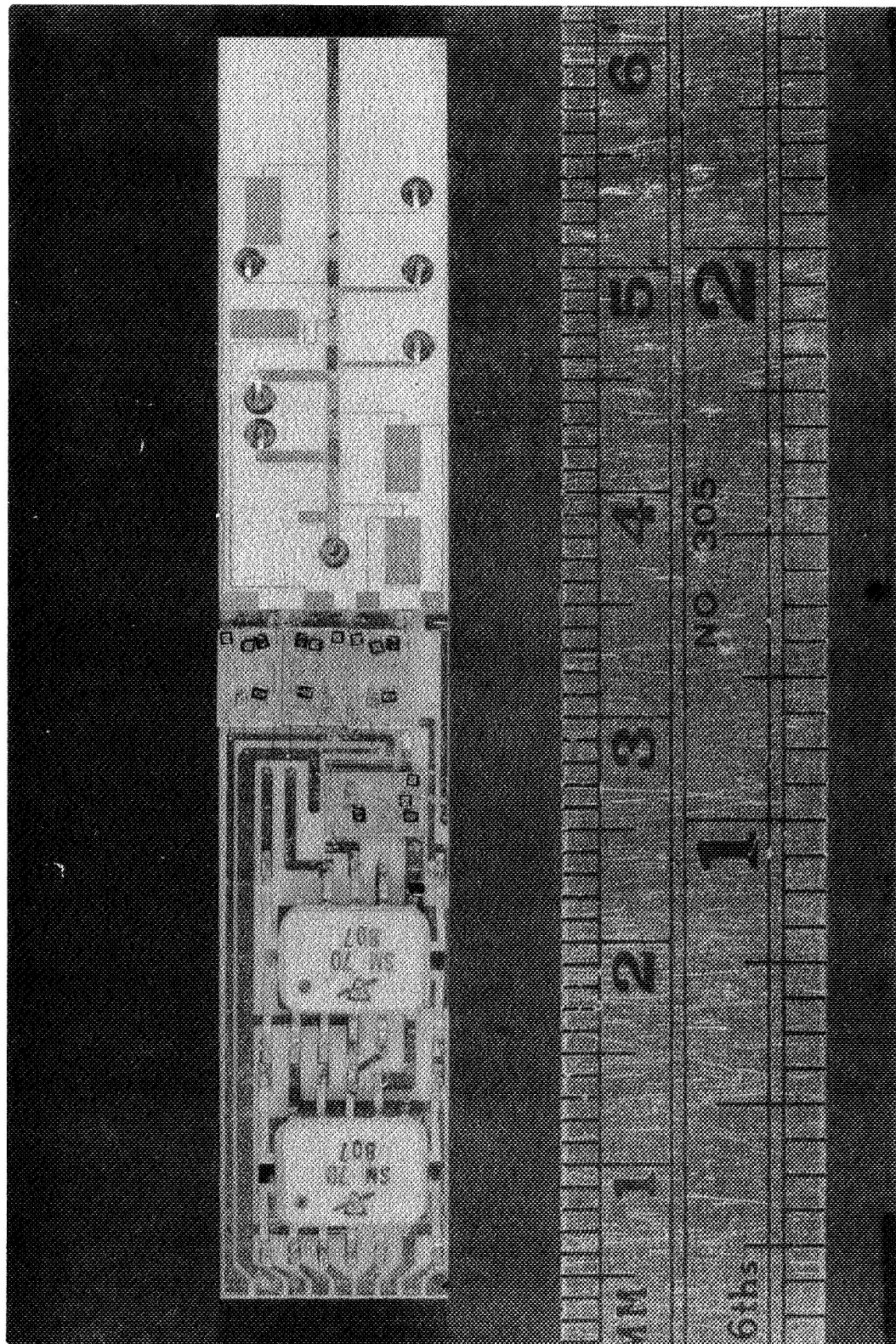


FIGURE 4.5 4-BIT, X-BAND, REFLECTIVE, PIN DIODE SWITCH  
PHASE SHIFTER WITH LOGIC AND DRIVER CIRCUITS AT LEFT  
(Courtesy of Microwave Associates)

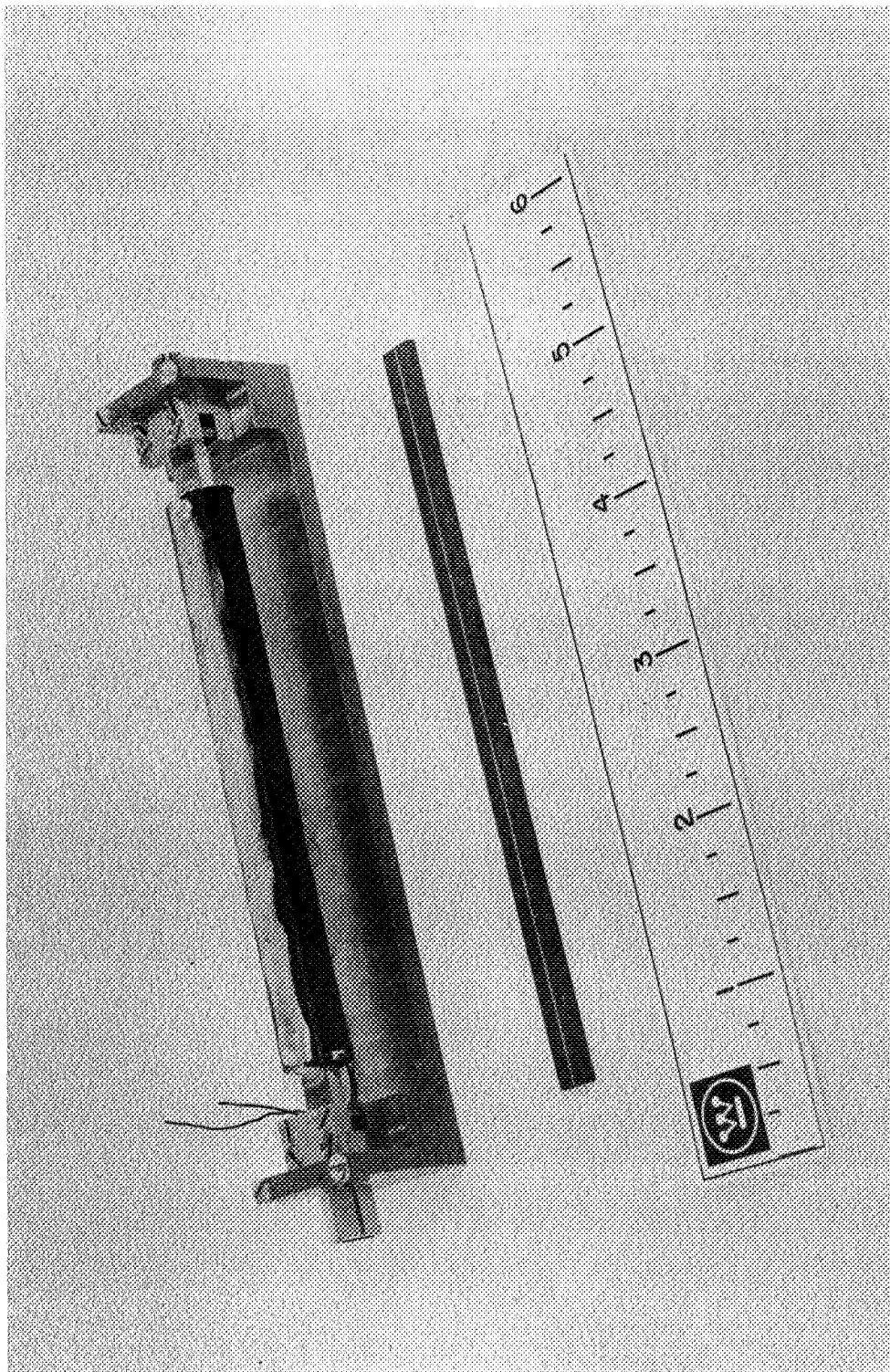


FIGURE 4.6 TEST FIXTURE AND ASSEMBLED UNIT OF ESAM X-BAND ANALOG,  
RECIPROCAL, STRIP TRANSMISSION LINE PHASE SHIFTER  
(Courtesy of Aerospace Division of Westinghouse Electric Corporation)



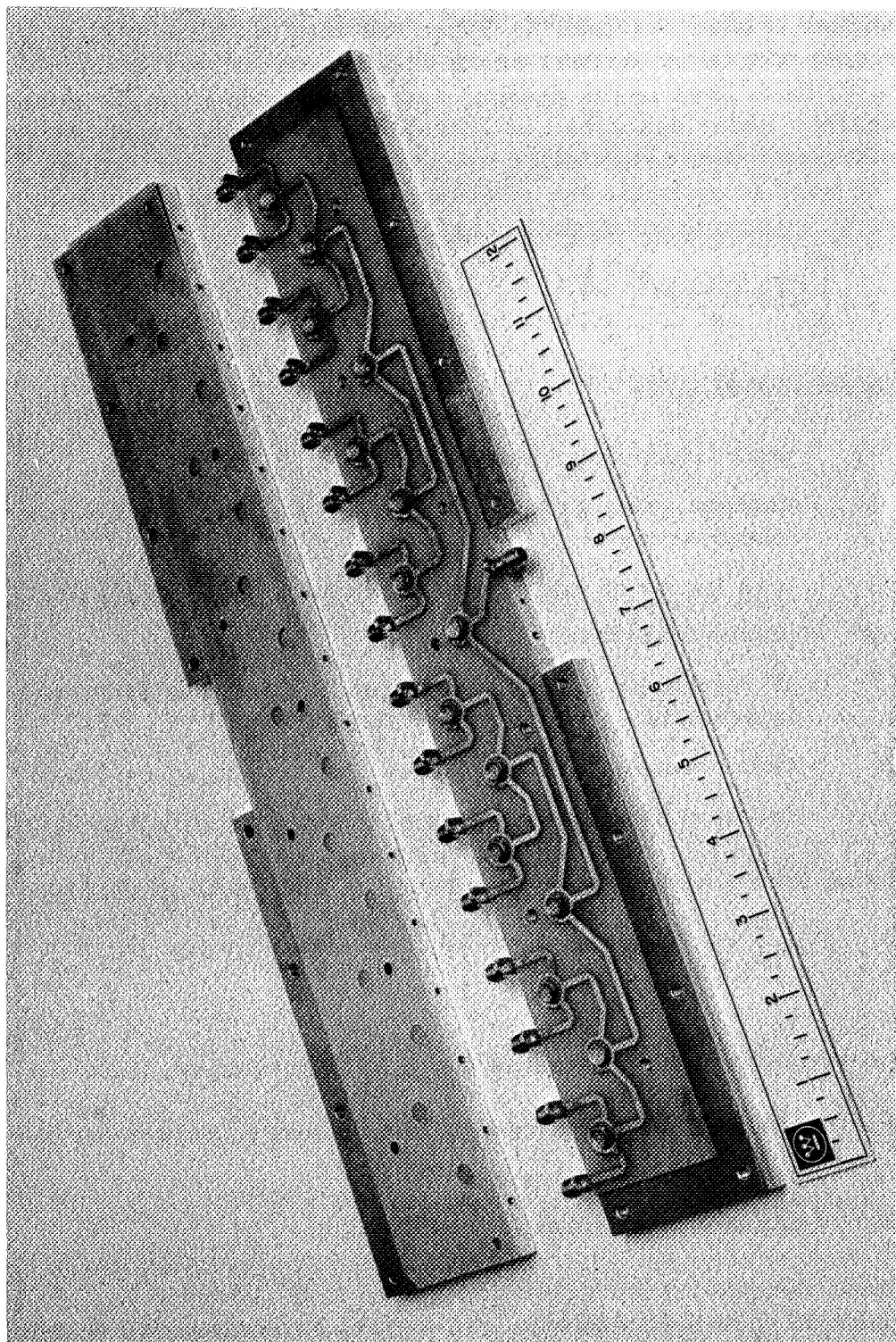


FIGURE 4.7 RAT-RACE FEED STRUCTURE  
FOR ESAM 16 ELEMENT LINEAR SUB-ARRAY  
(Courtesy of Aerospace Division of Westinghouse Electric Corporation)

in quantity; however, driver circuitry currently costing \$30.00 or more per phase shifter is also required<sup>10</sup>. From the data in Table 4.1, it is apparent that the cost of a large antenna array will depend primarily upon the number of phase shifters used in the design, and secondarily upon the antenna mount. If the weather radar described in Table 2.2 in Section 2, is considered to be a minimum useful radar capability, then the radar equation, (B-4), Appendix B, can be used to estimate the minimum number of phase shifters. For a point target (storm at maximum range):

$$r = \left[ \frac{C P_t G^2 L M^{\frac{1}{2}}}{\beta} \right]^{\frac{1}{4}} \quad (4.1)$$

where in consistent units

- $P_t$  = peak transmitter power, watts
- $G$  = antenna gain, proportional to  $N$ , the number of elements for a linear array
- $L$  = loss factor of microwave circuits
- $M$  = pulses integrated
- $\beta$  = IF bandwidth in Hz, proportional to inverse of pulse length,  $\tau$ , in seconds
- $r$  = radar range, meters
- $C$  = constant dependent upon storm size, receiver noise figure, etc.

Rearranging terms within the brackets on the right side of (4.1):

$$r = \left[ \frac{C (P_t \tau f_r) N^2 G_e^2 L M^{\frac{1}{2}}}{f_r} \right]^{\frac{1}{4}} \quad (4.2)$$

where the symbols are the same as given for Equation (4.1) except

- $f_r$  = transmitter pulse repetition frequency, pulses per second
- $G_e$  = gain of array element
- $N$  = number of elements in array

Until recently, the microwave losses in solid-state phase shifters has been as high as 4 or 5 dB one way. However, as indicated in Table 4.1, the losses are now 2 to 3 dB or even less for waveguide phase shifters. The gain-loss product for the conventional, circular, one-foot diameter antenna from

Table B.1 in Appendix B is 10 dB below the theoretical two-way antenna gain of 60 dB. The gain-loss product for the electronic scan-grating reflector, with a one-foot square aperture, from Table B.2 is 17 dB below the theoretical two-way gain of 62 dB. There is an additional two-way loss of 3 dB when scanning at an angle of 45 degrees from normal with the electronic scan antenna. Assuming an average two-way theoretical gain of 60 dB over isotropic for the electronic scanner, the gain-loss product is 7 dB lower than the conventional antenna which represents a 16% decrease in range. This loss can be overcome by increasing the transmitter average power (product of  $P_t \tau f_r$  in Equation (4.2)) or the antenna size. The approximate minimum number of phase shifters,  $N$ , required for a linear scan is the aperture length divided by one-half the transmitter wavelength. For example, for the one-foot aperture and a wavelength of 0.1 feet (X-Band), the number of phase shifters is 20. If the aperture is made longer to increase the antenna gain, then additional phase shifters are required.

Each phase shifter must handle approximately  $1/N$  of the peak transmitter power. If the illumination is tapered over the linear array, then the elements in the center of the array transmit more power than those at the ends. If the phase shifters will not handle  $1/N$  of the peak power, then the number of phase shifters must be increased to reduce the peak power per phase shifter.

If the cost of a phase shifter-driver combination is assumed to be \$50.00 and the number of antenna elements is 20, then the basic component cost per antenna is \$1,000.00. To this cost must be added the feed, the beam collimator, tilt mechanism, and mount to complete the antenna. The total cost of the electronically scanned antenna does not compare favorably with the cost of currently available mechanically scanned antennas at this time.

#### 4.3 All Solid-State Microwave Radar

The next step beyond the use of electronic scanning with a conventional tube transmitter is to develop an all solid-state radar with microwave integrated circuitry. Such radars are already operating in the laboratory and have been described in a variety of articles and reports<sup>11,12,13</sup>. In view of the extensive coverage given to these recent microwave integrated circuit developments, the reader is again referred to the literature for detailed discussion of current work.

The Molecular Electronics for Radar Applications (MERA) program<sup>11,13</sup> has developed techniques for production of a one-watt, X-Band module, Figures 4.8, 4.9, and 4.10, consisting of rf power amplifiers, IF amplifiers, mixers, frequency multipliers, phase shifters and switches. Each module is essentially a complete miniature radar set, and several modules are combined

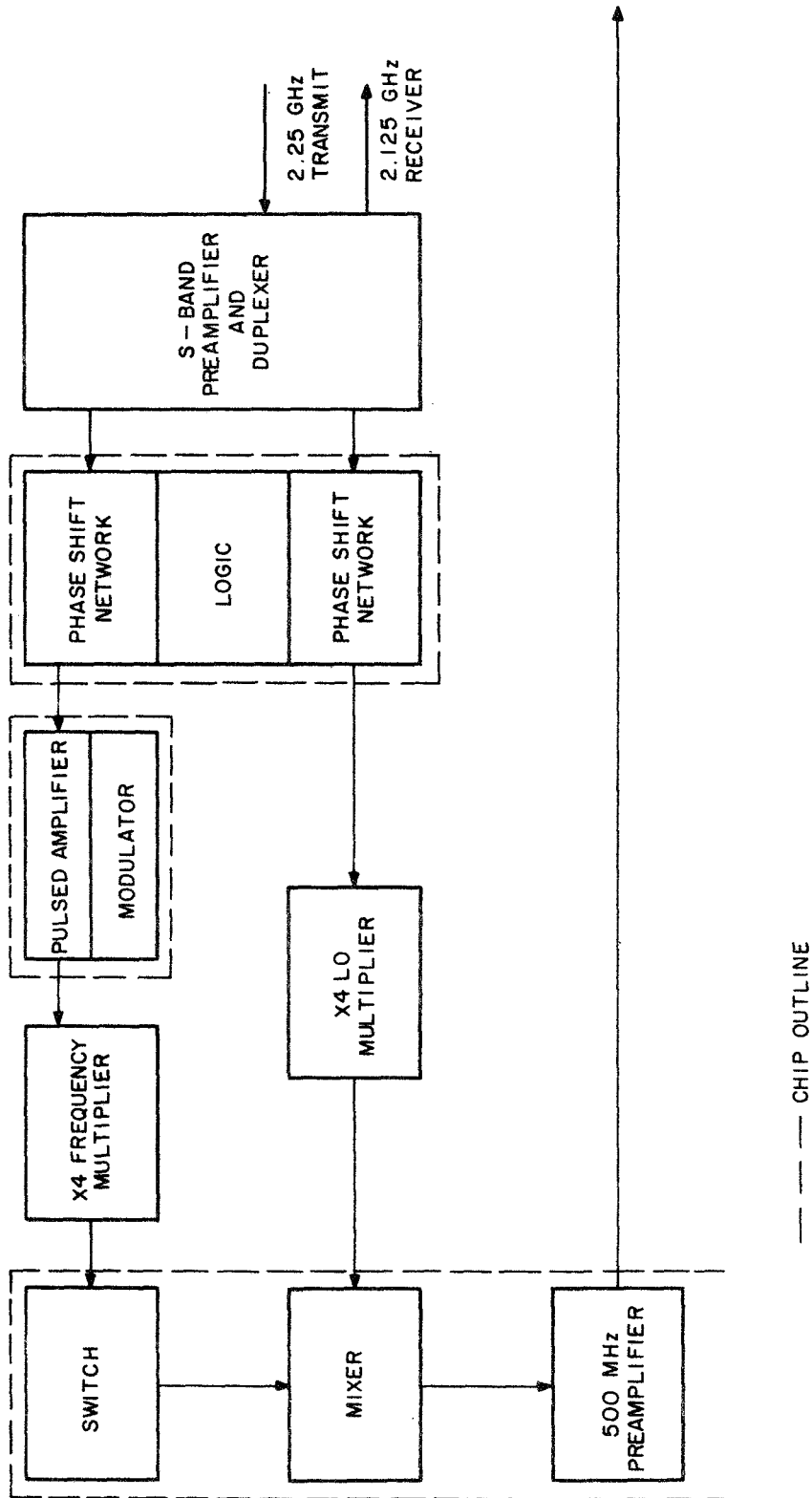


FIGURE 4.8 BLOCK DIAGRAM OF MERA RF MODULE

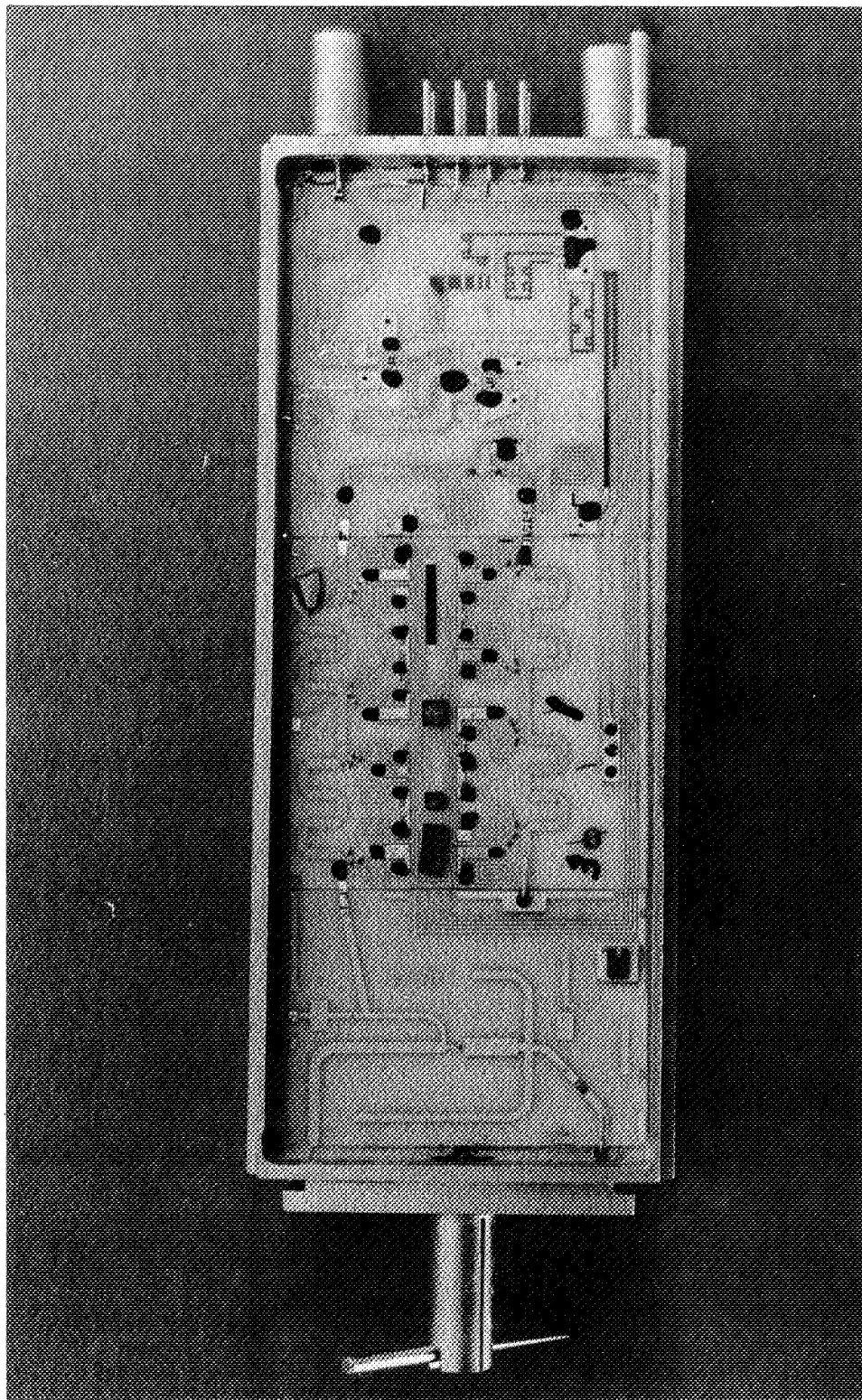
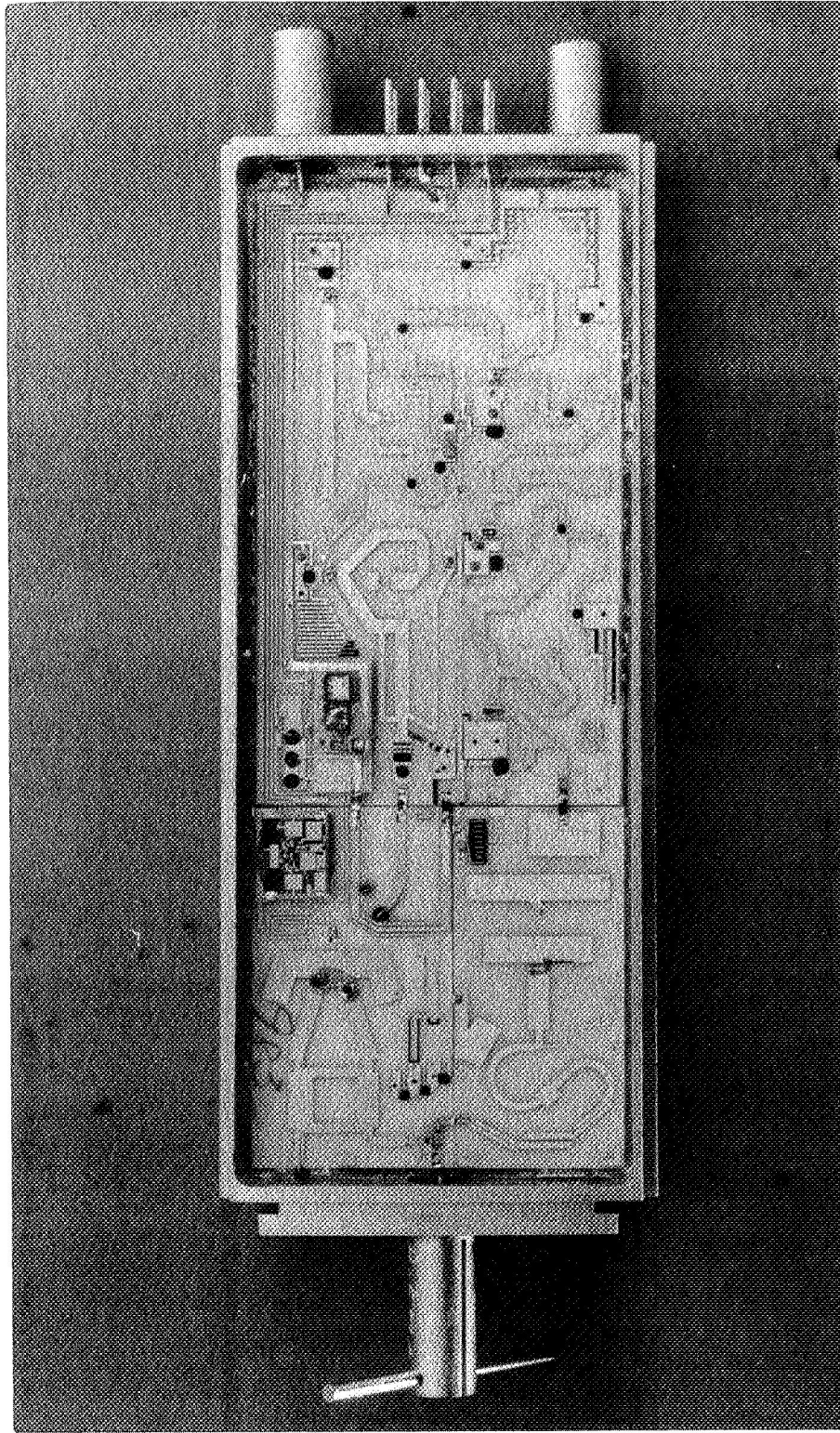


FIGURE 4.9 MERA MODULE SHOWING LEFT TO RIGHT, DIPOLE ANTENNA,  
X4 LO MULTIPLIER, TX/RX PHASE SHIFTERS AND LOGIC  
AND S-BAND PREAMP AND DUPLEXER  
(Courtesy of Texas Instruments, Inc.)





**FIGURE 4.10** MERA MODULE SHOWING LEFT TO RIGHT, DIPOLE ANTENNA,  
X-BAND MIXER/TR SWITCH AND IF PREAMP, (LOWER LEFT)  
X4 TX MULTIPLIER AND PULSED POWER AMPLIFIER AND MODULATOR  
(Courtesy of Texas Instruments, Inc.)

to increase the power and to provide for electronic beam scanning. The MERA module power output is too low and the cost too high for a simple linear array radar at the present time. If higher power modules are manufactured in very large quantities (greater than  $10^6$  modules), so extensive automation is justified, then the module costs per array will likely become competitive with conventional radar.

#### 4.4 Solid-State Display Panel

The cathode ray tube (CRT) has two principal drawbacks when used as a plan position radar indicator. These are size, particularly depth, and potential for catastrophic failure. Work directed at a solid-state replacement for the thermionic CRT has usually involved some form of thin panel, matrix display. A light emitting diode<sup>15</sup> or gaseous cell<sup>16</sup> is used at the intersection of the cross-bars of the matrix. Computer storage and logic circuitry is used to drive the matrix elements. Recently, displays with enough resolution for radar display in helicopters have been developed and described<sup>15</sup>. No estimate of the cost of solid-state displays is available at this time, but in approximately five years, sample display devices should be available for evaluation.

#### REFERENCES

1. Hall, J. S. (Editor), "Radar Aids to Navigation," McGraw-Hill Book Company, New York, 1946, pp 171-185.
2. Burns, R. W. and Stark, L., "PIN Diodes Advance High-Power Phase Shifting," Microwaves, November 1965, pp 38-48.
3. Whicker, L. R. and Jones, R. R., "Design Guide to Latching Phase Shifters," (Part I), Microwaves, November 1966, pp 31-39.
4. Whicker, L. R. and Jones, R. R., "Design Guide to Latching Phase Shifters," (Part II), Microwaves, December 1966, pp 43-47.
5. Frank, J., Kuck, J. H. and Shipley, C. A., "Latching Ferrite Phase Shifter for Phased Arrays," The Microwave Journal, March 1967, pp 97-102.
6. Rosenblatt, A., "Potential of Phased-Array Radar Spurs Increasing R and D Activity," Electronics, September 2, 1969, pp 94-103.
7. Schell, A. C., Sletten, C. J., Blacksmith, P., and Pankiewicz, C. J. "Electronic Scanning," Electro-Technology, November 1968, pp 29-41.
8. Turner, E. M., "Antenna in Perspective," The Microwave Journal, December 1968, pp 32-38.

9. Jones, R. R. and Whicker, L. R., "Now - Ferrite Microstrip Devices," Microwaves, January 1969, pp 32-38.
10. Odum, W. J., et al., "Selection of a Phased Array Antenna for Radar Applications," Supplement to IEEE Transactions on Aerospace and Electronic Systems, Vol. AES-3, No. 6, November 1967, pp 226-235.
11. Bandy, G. C., et al, "MERA Modules - How Good in an Array?" Microwaves, August 1969, pp 39-49.
12. Napoli, L. and Hughes, J., "Low-Noise Integrated X-Band Receiver," The Microwave Journal, July 1968, pp 37-42.
13. Hyltin, T. M., et al, "Molecular Electronics for Radar Applications (MERA)," Reports on Contract AF 33(615)-2525 by Texas Instruments, Inc., PO Box 5012, Dallas, Texas, 75222.
14. Cooke, H. F. and Stover, H., "Development of a Solid-State X-Band Power Source," Contract F33(615)-67-C-1909, Technical Report AFAL-TR-68-325, by Texas Instruments, Inc., PO Box 5012, Dallas, Texas, 75222.
15. Miller, B., "Moving Target Radar Test Planned," Subtitle, "Army to Evaluate Device Using Solid-State Display in Helicopter; Array Incorporates 2,500 Gallium Arsenide Light Emitting Diodes," Aviation Week and Space Technology, August 11, 1969.
16. "Flat Display Has Inherent Memory," Electronics, March 31, 1969, pp 133-136.

## 5.0 SYSTEM DESIGNS

### 5.1 Introduction

The final item of work on this study is the specification in block diagram form plus performance specifications on at least four proposed systems which are obtainable in the near future. Five representative systems are described in this division of the report, as follows:

1. Minimum-cost radar.
2. All solid-state radar.
3. Modulation-scan radar.
4. LIDAR (pulsed light cloud ranger).
5. Sferic detectors.

At least the following information is given on each system, and in some cases this minimum information is supplemented by additional details.

1. Range of operation/scanning approach.
2. Operating frequency/ies.
3. Description of the various modes of operation.
4. Primary, average, and peak power estimate.
5. Cost estimate: initial development and unit cost for large quantities.
6. Identification of the major components in the block diagram with alternatives, including proposed development for the components of marginal performance.

For ready reference to the current state-of-the-art, a chart on airborne weather radar, Table 5.1, from the April 1970 Business and Commercial Aviation magazine is reprinted. The chart shows that an excellent selection of small weather radars is available for light twin and larger aircraft; however, no radars are listed for single and dual in-line engine aircraft. In the systems described in this section, an attempt is made to provide universal designs though the emphasis is on single-engine aircraft equipments.

TABLE 5.1  
AIRBORNE WEATHER RADAR DATA  
(From Business and Commercial Aviation Magazine  
Ziff-Davis Publishing Company, April 1970)

MANUFACTURER	MODEL	FREQ (mc)	POWER OUTPUT (peak kw)	WT ALL UNITS (lb)	POWER INPUT	RANGES (mi)	DISH SIZE & BEAM WIDTH (in./deg)	SCAN (deg)
Bendix Avionics Div. Ft. Lauderdale, Fla. 33310	RDR-1E	9375 (X-band)	50	89.7 (30 in. ant)	28 V DC, 1 amp; 115 V 400 cps. 495 VA	30, 80, 180, 300	18/5 22/4.4 30/2.5	18" ant 120 sector 22" ant--360 30" ant--360
	RDR-1F	9375 (X-band)	75	118- (approx)	115 V AC 400 cps 640 VA	50, 150, 300	30/2.5	360
	RDR-10	15,500 (Ku-band)	10	19.8	28 V DC, 2 amp; 115 V, 400 cps, 100 VA	15, 30, 90 (9, 30, 90 optional for helicopters)	12/4.5	±45 sector
Collins Radio, Cedar Rapids, Iowa 52406	WXR-80	9345 (X-band)	30	57	115 V, 400 cps. 350 VA	30, 60 150, 300	12/7.3 18/4.8	±90 or ±60 sector
RCA, Aviation Equipment Dept. 11819 W. Olympic Blvd. Los Angeles, Calif. 90064	AVQ-10	5400 (C-band)	75	119	28 V DC, 1 amp; 115 V, 400 cps. 875 VA	25, 50, 150	20/7 34/4	360
	AVQ-20A	9375 (X-band)	20	45	28 V DC, 0.5 amp; 115 V, 400 cps, 250 VA	30, 90, 180	12/7.4 15/5.9 18/5.0 24/3.8 30/2.9	180 120
	AVQ-30-C	5400 (C-band)	75	128	115 V AC 400 cps, 650 VA	30, 100, 300	30/5.2	180
	AVQ-30-X	9345 (X-band)	65	116	115 V AC 400 cps, 650 VA	30, 100, 300	30/2.9	180
	AVQ-46	9375 (X-band)	8	25	28 V DC, 5 amp	20, 80	10/8.5 12/7.0	90
	AVQ-55	9375 (X-band)	15	43	28 V DC, 3 amp; 115 V, 400 cps, 200 VA	30, 60, 90	12/7.2 15/5.8 18/4.2	120

TABLE 5.1 (Cont'd.)

SCANS (per min)	ANT TILT (deg)	ANT BEAM (type)	STABLZTN (deg)	SCOPE SIZE (dia-in.)	PRICE (uninstalled)	REMARKS
18" ant 30 22" ant 15 rpm 30" ant 15 rpm	±15	pencil & CSC <sup>2</sup>	line of sight ±1 at zero deg tilt	5	\$19,027	180 mi range w 20° reserve gain; bright display avail; 5 units: cntrl, ind, ant, R/T, 1 ATR size; magnetron base TSO-C-63; cat B (R/T) cat B (ant)
20	±15	pencil & CSC <sup>2</sup> COS	roll and pitch ±25 deg	5	\$26,432	300 mi range, TV display capability, solid state except for magnetron and indicator tube, self test, split axis antenna, TSO-C-63a; Arinc 564
0-360 (0-6 per sec)	±12	pencil	no	5	\$7866	polarized filter built in; 4 units: R/T cntrl/ind, ant, shock mnt TSO-C-63a AAAAX CL3
22	±15	pencil	roll and pitch ±20	4 (bright display)	\$17,992	300 nmi weather radar, includes coax magnetron, solid-state modulator, increased pulse width (5.5 usec), options include complete in-line monitoring with self test, high- contrast, black faced display in hangar self-test 3 units: R/T (3/4 ATR short), antenna, indicator w/controls TSO-C-63a
15 rpm	+10 to 15	pencil	±35	5	\$20,759	bright display tube optional; 4 units: R/T (1 ATR size) accessory unit (1 ATR size) ind, ant, self test features TSO-C-63
20 rpm	±15	pencil & CSC <sup>2</sup>	±30 line of sight	5	\$16,099	bright display tube optional; 3 units: R/T (7 x 15 x 7 in.), ind, ant; TSO-C-63a, cat A (ant & R/T) cat B (ind)
30 rpm	±15	pencil	split-axis ±40 deg roll; ±20 deg pitch	5	on request	solid-state duplexer eliminates T/R tube, 360 nmi indicator available; 3 units, TSO-C-63a Env cat C/DB AAAX, class VI (R/T & ind) ABAAAX (ant) Arinc 564
30 rpm	±15	pencil & CSC <sup>2</sup>	split-axis ±40 deg roll, ±20 deg pitch	5	\$24,192	Same as above Env cat CBAAAX, class VI (R/T ind); ABAAAX (ant)
70 rpm	±12	pencil	no	5	\$6621	all controls on ind panel, full electronic tilt, no AC power required, 30,000 ft capability; TSO-C-63a cat B
60 rpm	±15	pencil	no	5	\$10,006	3 units: R/T ind & ant; bright display tube optional TSO-C-63; cat A (ant) cat B (R/T & ind)

## 5.2 Minimum-Cost Radar

### 5.2.1 Introduction

The lowest price airborne radar in Table 5.1 lists for approximately \$6,000 and to this must be added approximately \$1,500 for radome and installation in a light twin. A cost breakdown by units with approximate list prices is given in Table 5.2.

TABLE 5.2  
BREAKDOWN OF CONVENTIONAL WEATHER RADAR COSTS - 1969

Transmitter-Receiver Unit	\$3,000
Display	1,800
Antenna	1,200
Radome	1,000
Total Radar (Uninstalled)	\$7,000

Price reductions of airborne weather radar are likely to result from increased production and/or simplification of the radar. The feasibility of simplifying the radar is discussed first. There is a major redundancy in weather radar operation in that new pictures (scans) are generated at a much faster rate than the weather changes. One complete scan of the area ahead of the aircraft per minute or even every five minutes in slow aircraft would be adequate. A fast, small plane might travel 3 to 4 NM per minute, while the slower plane would have a 2 NM per minute velocity. The simplest radar which might take advantage of the available scan time ( 1 to 5 minutes) would have an antenna fixed to the aircraft and a simple A-scope presentation. The aircraft would turn at a standard rate (3 degrees per second) to provide the angular scan and the pilot would interpret and mentally "store" the A-scope display. When supplemented with ground weather reports received by radio, this simple radar is able to provide useful information on the range, direction, and intensity of storms. Unfortunately, the careful study of the A-scope by the pilot would conflict with the requirement to maintain a watch for other aircraft. If the A-scope is ruled out because of safety, a trade-off such as a slow antenna scan plus a graphic recorder might yield an intermediate performance to and less cost than a conventional radar. A rapid development camera photographing an oscilloscope, a dry paper facsimile machine, or a video tape recording with CRT playback can serve as the graphic recording medium. Any of these recording methods take advantage of the slowly changing nature of storm return. If the antenna is fixed to the aircraft, the pilot

(or autopilot) must hold a prescribed turn rate across a sector of interest. Since the requirement to hold a prescribed turn rate presents undesirable operational limitations for the general aviation pilot, another radar-antenna concept is proposed for the minimum-cost, minimum-performance radar.

### 5.2.2 Engine-Driven Antenna Scanner

In Section 3.2, the use of the aircraft engine to drive an antenna scanner is introduced. The feed horn (or pair of feed horns) are mounted on the propeller hub-spinner and the rotation carries the feed horn through the focal region of an off-set fed parabolic antenna. The parabolic antenna is mounted below and behind the hub of the propeller and on the front cowling of the aircraft. It may be necessary to use an extension to move the propeller out from the unmodified cowling, and the parabolic dish can be filled with a low-loss foam to create a satisfactory aerodynamic shape. A waveguide feeds, by non-contacting directional coupler action, Figure 3.4, the horn in the propeller spinner. This permits the transmitter-receiver to be mounted in the cockpit or on the firewall. The scan angle is limited to perhaps  $\pm 15$  degrees, by beam distortion, though additional development of a linear feed for the antenna might extend the scan to as much as  $\pm 25$  degrees. A sketch of the proposed square antenna arrangement is shown in Figure 5.1. The array can be used only when the feed horn is traversing the central region of the top of the reflector, and horns cannot be placed in the blade region. Viewing the feed horn circle from the front, a 12-inch diameter feed horn circle will intersect the top of the reflector, as shown in Figure 5.2. A short focal length reflector is desirable; however, the reflector may be too deep with a short focal length and intersect the propeller arc at the bottom. A longer focal length will permit a flatter reflector; however, the feed horn must be larger to properly illuminate the reflector. This method of scanning does not appear capable of meeting the minimum operational characteristic of  $\pm 45$  degrees and the scanning should be accompanied by small aircraft heading changes to cover an adequate field of view along the flight path. It must be emphasized that no experimental work has been carried out on this antenna concept and a feasibility study is necessary.

### 5.2.3 Transmitter-Receiver

Referring to Table 5.2, the largest single unit cost is the transmitter-receiver at \$3,000. Taking two significant components of the transmitter, the magnetron and the modulator, the cost trends with quantity are examined in Table 5.3.



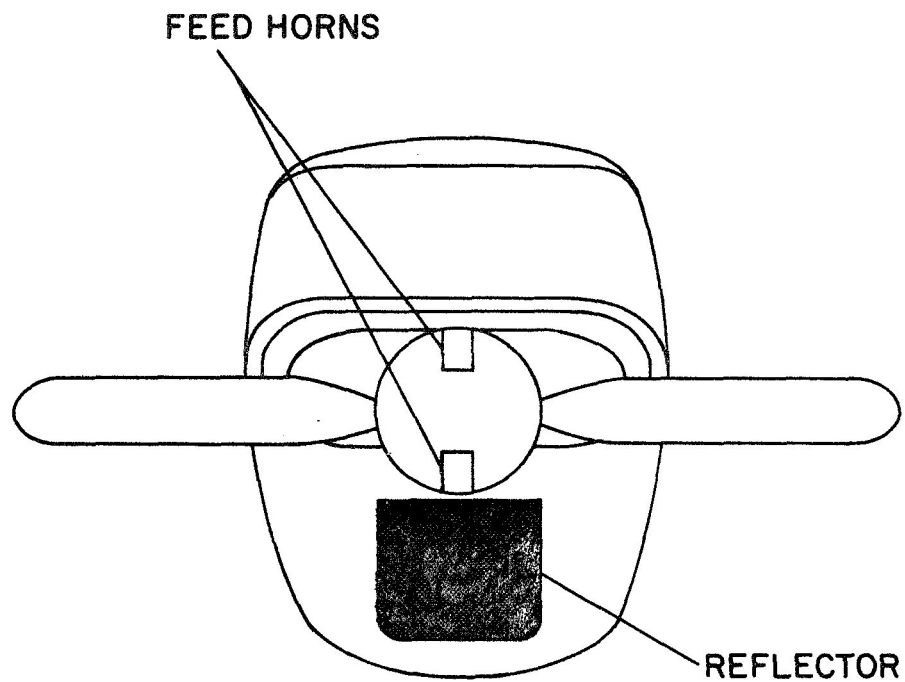


FIGURE 5.1 ENGINE-DRIVEN MECHANICAL SCAN  
FOR USE ON SINGLE AND DUAL IN-LINE ENGINE AIRCRAFT

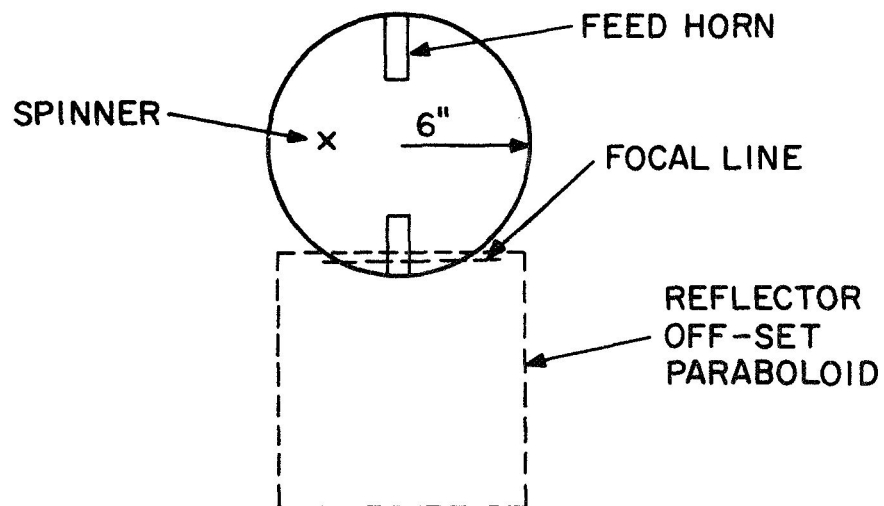


FIGURE 5.2 <sup>80</sup> FEED HORN CIRCLE, FOCAL LINE,  
AND REFLECTOR RELATIVE LOCATIONS

TABLE 5.3  
TRANSMITTER COMPONENT COSTS

Quantity	Magnetron (2J42)	Modulator	Total	X5
1	\$ 90.00 (Surplus)	\$2,700	\$2,790	N/A
100	\$100.00	\$ 250	\$ 350	\$1,750
1,000	\$ 75.00	\$ 160	\$ 235	\$1,175
10,000	\$ 65.00	\$ 100	\$ 165	\$ 825

The column headed X5 in Table 5.3 is an approximate factor by which a component cost is multiplied to arrive at the final cost of putting the component into an assembly. This factor might vary from 4 to 8 for various assemblies. The cost of the 2J42 magnetron is so low and the reliability so good that almost any low-cost radar must use this transmitter. The current production rates on the 2J42 are based upon use in small marine radars as well as airborne radar, and further cost reductions are unlikely unless the quantity becomes very large. At the present time, the modulator is manufactured by several suppliers to customer specifications and is quite expensive in small quantities, but sizeable reductions are expected with quantity production, as shown in Table 5.3. A further reduction in the modulator cost is related to the peak voltages and currents in the modulator, and while the range will be reduced by about 30% the performance reduction may be essential to gain a significant cost reduction. A small marine radar, which uses the 2J42 magnetron at a 5 KW peak power output has a list price of approximately \$2,500, including radome.

Other significant component costs for the transmitter-receiver are estimated in tabular form for 1000 unit quantity.

IF Amplifier	\$ 65.00 x 5	\$ 325
Automatic Frequency Control	\$ 50.00 x 5	\$ 325
Power Supply	\$110.00 x 5	\$ 550
Mixer Assembly	\$100.00 x 5	\$ 500
Miscellaneous Components, Cabinet, etc.		\$ 200
	<u>Sub-Total</u>	<u>\$1,825</u>
Adding Magnetron and Modulator		<u>\$1,175</u>
	<u>Transmitter-Receiver Total</u>	<u>\$3,000</u>

#### 5.2.4 Minimum Radar Display

A B-scope, storm range versus angle, display is proposed for the minimum radar. The transmitter will be synchronized to operate only when the feed horn is traversing the focal region of the offset parabolic reflector. The propeller of a typical general aviation aircraft turns at 2400 rpm or 40 rps.

If the propeller rotation per transmitted pulse is the same as the antenna beamwidth, which is assumed to be 7 degrees, then a beamwidth is scanned in 480 microseconds, which corresponds to a maximum radar range of 40 NM. Since at least two pulses per beamwidth are necessary for the display, two horns must be used, diametrically opposite on the propeller spinner. The display should be essentially flicker-free since the interlace with the two horns will yield an 80 fields per second rate with 40 complete pictures (frames) per second. The transmitter operation must be synchronized with the propeller rotation, perhaps by a toothed wheel and magnetic pickup on the tachometer shaft. A PPI display might use a direct mechanical drive of the rotating sweep coil from a tachometer shaft.

#### 5.2.5 Minimum Radar Block Diagram, Parameters, and Cost Estimates

Sections 5.2.1 through 5.2.4 have described how, with some sacrifice in performance characteristics, a low-cost radar may be marginally achievable (development and feasibility tests are necessary to verify the assumed antenna, etc.). A block diagram, Figure 5.3, gives the main components of the radar and the next chart, Table 5.4, gives the tentative parameters and operational characteristics of the minimum radar. In addition to reducing the transmitter peak power to 5 KW, the antenna gain is assumed to be 7 dB below theoretical aperture gain of 31 dB for a one foot square aperture and the losses at 3 dB are intended to include the rotary joint losses.

In the estimated costs, Table 5.5, the antenna cost is speculative since the antenna feasibility has not been demonstrated. The receiver-transmitter cost is based upon a lower performance unit than is currently found in state-of-the-art weather radar and the display is simpler (B-scope instead of PPI).

In the proposed development program, Item III of Table 5.5, the initial feasibility study should be made with simulated aircraft structures and relatively rough antenna models to verify analytical studies. The initial feasibility study and experiments should be followed by a development program to construct an operational/demonstration model of the radar.

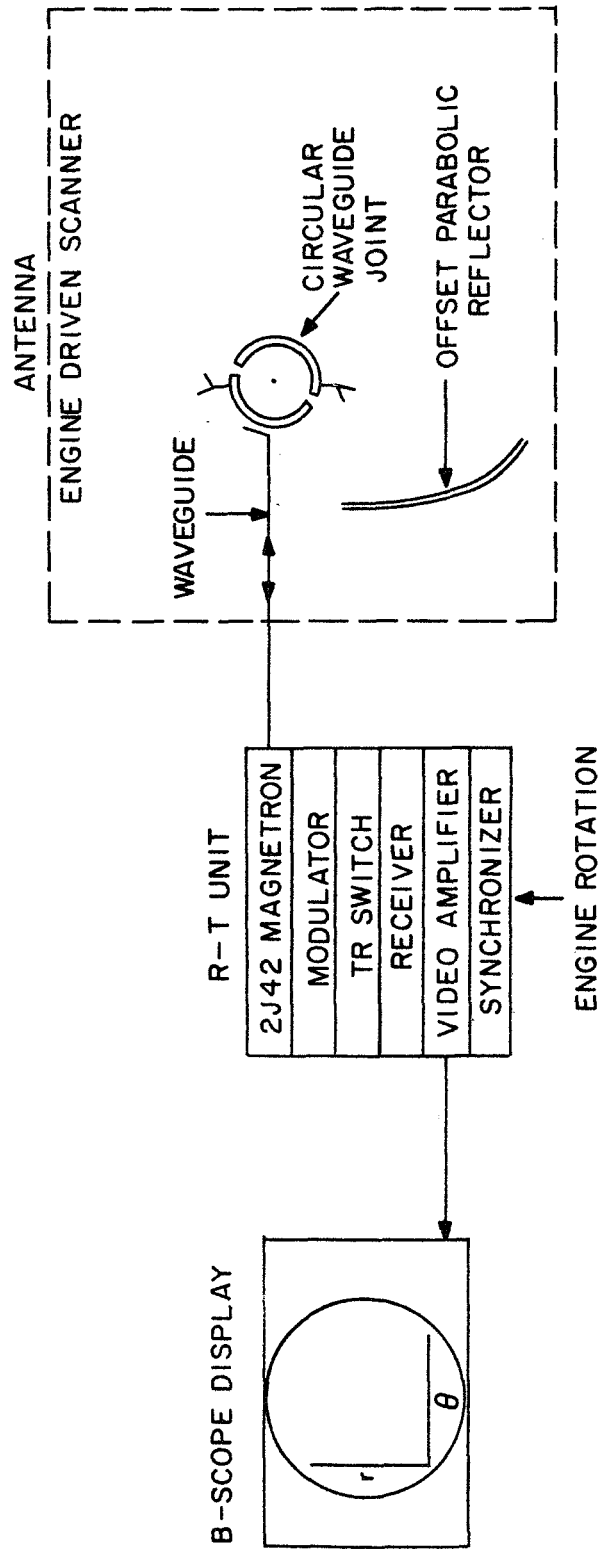


FIGURE 5.3 BLOCK DIAGRAM OF MINIMUM RADAR WITH PROPOSED ENGINE-DRIVEN SCANNER

TABLE 5.4  
OPERATIONAL CHARACTERISTICS OF MINIMUM RADAR

Characteristic	Acceptable	Minimum Radar
<u>Display</u>		
Type	B-Scan	B-Scan
Dynamic Range	40 dB	20 dB
<u>Scan</u>		
Sector	$\pm 45$ degrees	$\pm 15$ degrees
Tilt	$\pm 15$ degrees	$\pm 15$ degrees
Rate (Frame)	1 frame/minute	40/seconds Interlaced
<u>Altitude</u>	Surface to 20,000 feet	Surface to 20,000 feet
<u>Range</u>		
Detection	> 50 NM	40 NM
Analysis	> 20 NM	25 NM
<u>Resolution</u>	1 NM Range 8.5 deg. Az.	1/2 NM Range 7 deg. Az.
<u>Targets</u>		
Primary	Moderate to Heavy Rain	Moderate to Heavy Rain
False Angle	-40 dB Sidelobes	-30 dB Sidelobes
False Range	> 60 NM	> 40 NM

TABLE 5.4 (Cont'd)  
TENTATIVE PARAMETERS

Transmitter Peak Power	5 KW
Receiver/Transmitter Antenna Gain	24 dB
Receiver/Transmitter Vertical Beamwidth	7 degrees
Receiver/Transmitter Horizontal Beamwidth	7 degrees
Transmitter Wavelength	3.2 cm
Receiver Noise Figure	12 dB
Microwave Loss Factor	3 dB
Pulses Integrated	80 pulses/BW/second
Scan Sector	30 degrees
Scan Rate (Fields)	80/second Interlaced
Pulse Repetition Frequency	2000 pulses/second
Pulse Length	5 microseconds
Duty Factor	0.006
S/N for Detection on Single Hit	10 dB

TABLE 5.5  
ESTIMATED COST OF MINIMUM RADAR

<b>I.     <u>Estimated Cost (Present)</u></b>	
<u>100 Units</u>	
Antenna (Including Cowling* and Spinner)	\$ 1,500
Receiver-Transmitter (5 KW, X-Band)	2,000
Display (B-Scope)	<u>400</u>
<u>Total</u>	\$ 3,900
<u>10,000 Units</u>	
Antenna (Including Cowling and Spinner)	\$ 750
Receiver-Transmitter (5 KW, X-Band)	1,000
Display (B-Scope)	<u>300</u>
<u>Total</u>	\$ 2,050
*A representative fiberglass cowling lists for approximately \$300.	
<b>II.    <u>Estimated Cost (Future)</u></b>	
Except for decreased costs from circuit integration, the above costs are not expected to change significantly in the next five-year period.	
<b>III.   <u>Development Cost</u></b>	
(1 Year) Feasibility study of Antenna/Display (construction of models and antenna analysis).	\$100,000
(18 Months) Develop Operational Antenna, Modify Transmitter-Receiver and Develop B-Scan Display.	450,000
<u>Total</u>	<u>\$550,000</u>
Development Cost/Unit = \$55.00 for 10,000 Units	

### 5.3 All Solid-State Radar

Efficient utilization of airborne phased-array radars requires the development of quality microstrip microwave components which can be produced in large volume and at low cost. In order to achieve these goals, it may be necessary for the system designer to consider a mixture of components and technology in his systems concept. An example which is indicative of this approach is described in the following sections.

#### 5.3.1 A Hybrid Integrated System

There are many levels of sophistication that a solid-state radar might assume. However, if cost with reasonable performance is of prime importance, simple microwave integrated circuits must be considered first. A system which is representative of a functional general purpose MIC radar is schematically shown in Figure 5.4. It basically consists of individual transceiver modules at each radiating element, an appropriate corporate feed network, and a gated master oscillator for phase locking of the individual bulk effect sources.

Figure 5.5 describes the transceiver module in more detail. In the transmit mode, the gated master oscillator (MO) output is fed to each transceiver module by way of the corporate feed network to synchronize all of the source elements in phase. Beam steering is achieved by adjusting the relative phase of the synchronizing signal with a planar latching ferrite phasor. In the receive mode, the signal is coupled from the dipole element through C-3 (ferrite junction circulator) and into the receive amplifier module. A limiter is interposed for additional receiver isolation. This amplified signal is then coupled to the corporate feed for summation. The same beam forming phasor arrangement is used for receiving as was used for transmitting. Since there are a number of ferrite devices (4) required for each element, a significant cost saving should be possible if a common ferrite substrate is used for a multiple number of array elements (at least 8). This is possible since these passive ferrite devices can all be readily batch fabricated. Where semiconductors are used individual ceramic chips may be inserted into pre-formed voids in the large ferrite substrate. The RF source can be accommodated in microstrip form on the ferrite substrate.

In addition to the above features, this system design permits the utilization of a low power, control phasor for beam steering which simplifies the device construction considerably. Because of the phasor location, its characteristic insertion loss (typically  $< 2.5 \text{ dB}/360^\circ$ ) does not compromise the transmitter efficiency or deteriorate the receiver effective noise temperature.



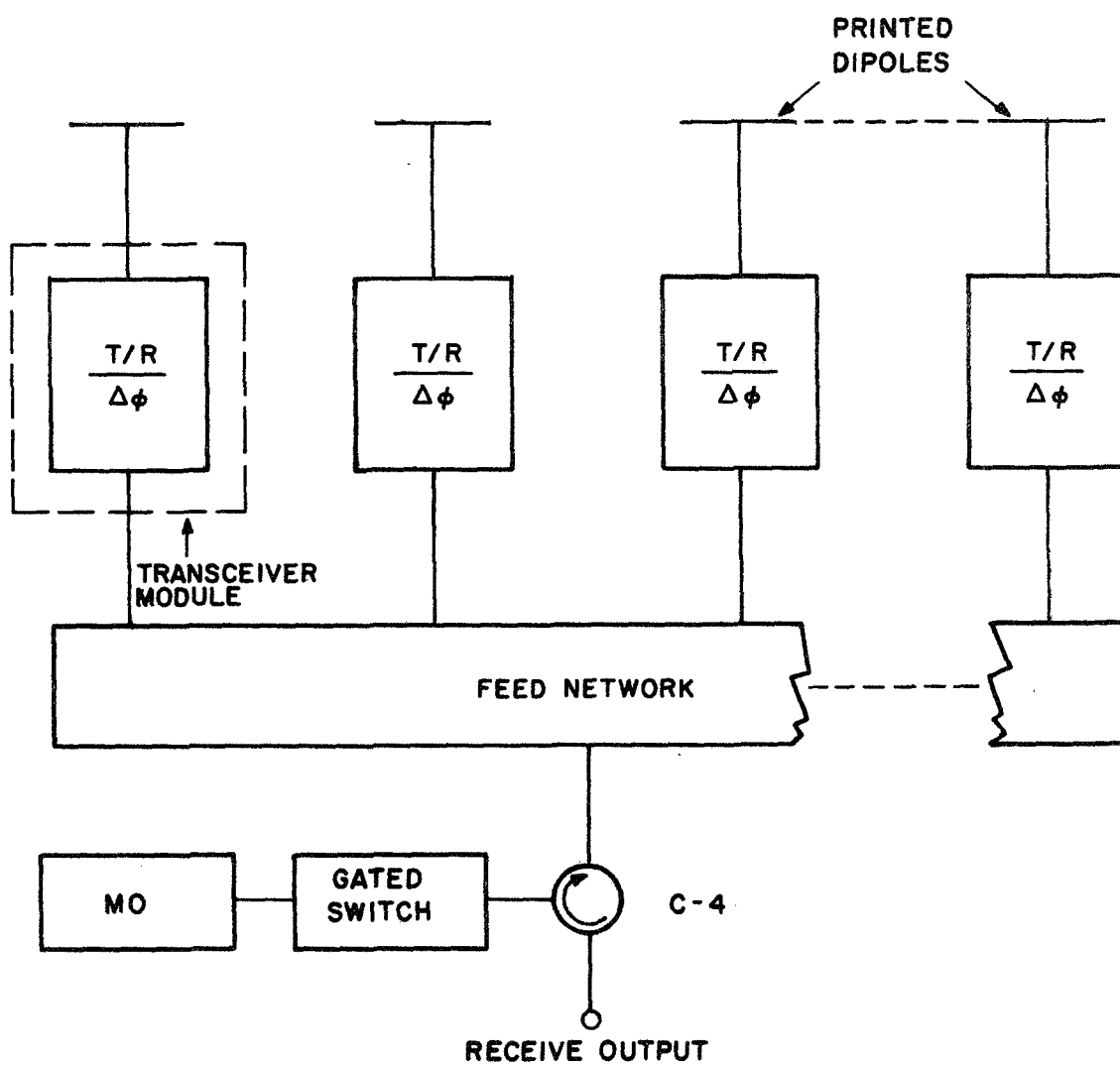


FIGURE 5.4 TRANSCEIVER SYSTEM  
(MULTI-ELEMENT LINEAR ARRAY MODULE)

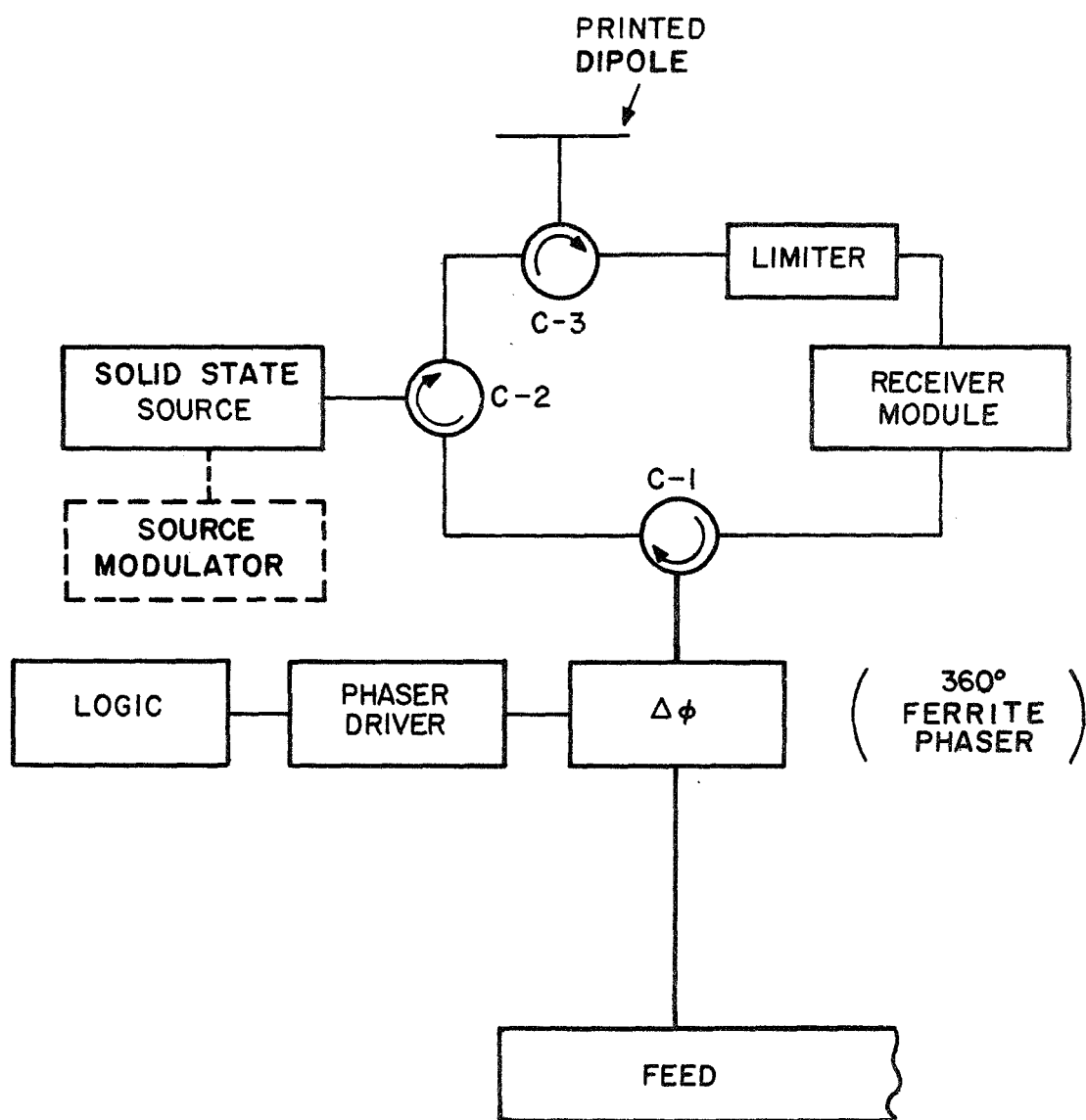


FIGURE 5.5 TRANSCEIVER MODULE

It appears that with the possible exception of the source modulator, every modular subsystem and discrete components could be contained in the same relative plane of the microstrip structure. Exception is made for the modulator since the efficiency and peak power requirement of the solid-state source which is used will determine whether or not it can be made in an integrated form factor consistent with the space available per element. If the modulator cannot be placed on the same common substrate level it can certainly be placed on a modulator sub-array above or below it.

### 5.3.2 Solid-State Sources

#### 5.3.2.1 Gunn Effect-Domain Mode

Pulse devices are now made on a commercial basis which consistently have 12 to 18 percent conversion efficiencies at low duty cycles (less than 1%). Output power levels of 4 to 9 watts peak are achieved in C- and X-Bands.

#### 5.3.2.2 Gunn Effect-LSA Mode

This mode of operation is capable of producing very large pulsed peak powers at lower frequencies, since its operating frequency may be larger than the transit-time frequency. Because a great deal more bias power can be supplied to a large volume device, more RF power can be generated provided the efficiency is not degraded. Typical of this mode of oscillation is a pulsed device working at 7.0 GHz with a peak power of 2000 watts and an efficiency of 5%.

There are several advantages of the LSA mode over the basic domain mode. First of all, one would expect a higher efficiency since the whole sample exhibits a negative resistance for a major portion of each RF cycle. This is in contrast to the domain mode where only a thin dipole layer of the sample is active. However, the potential efficiency advantage of the LSA mode has not been realized yet in a clear manner. The high efficiencies which have been reported are probably for the hybrid mode which will be considered in the next section. Another advantage of the LSA mode is that the fields within the sample never approach the peak fields within a domain, thus permitting very high bias and operating voltages before avalanche breakdown will occur. This, of course, permits higher input powers, as mentioned before.

#### 5.3.2.3 Gunn Effect-Hybrid Mode

This mode is intermediate between the LSA mode and the quenched domain operation of the domain mode. In some respects this mode claims

the advantages of the LSA and domain modes without some of their specific disadvantages. This mode is not as difficult to adjust as the LSA mode which could be critically important when large numbers of these components are considered for use. Drive circuit requirements may not be as severe to implement as with the LSA mode requirements.

#### 5.3.2.4 IMPATT

Unlike Gunn devices which are built with gallium arsenide, IMPATT diodes are being made from silicon and germanium, as well as gallium arsenide. This class of devices shows more promise as an item which can be more readily produced if gallium arsenide is not used since gallium arsenide is a material which is difficult to hold to specifications.

The attractive feature of IMPATT devices is the impressive conversion efficiencies which have been achieved. A pulsed germanium diode at 3 GHz has shown an efficiency of 40% with a 7.5 watt output (Bell Telephone Laboratory). There is already some theoretical indications that 100 to 200 watts may be possible within a few years.

#### 5.3.2.5 Conclusions

Whatever bulk-effect RF source is used in the subject system, it must be capable of being deployed in the microstrip environment efficiently. Most of the sources just mentioned have already shown adequate compatibility with contemporary microstrip circuit design.

The peak power output of the source must be consistent with the system requirement ( $\sim 500$  watts). In two years, hybrid mode devices may be capable of about 200 watts peak, with 10% efficiency and 1% duty cycle. The LSA mode should be capable of even higher power levels, but does present some control circuit problems which must be resolved to form compatible driver integrated circuits.

IMPATT diodes are making rapid gains in maximum power output and, more importantly, with improving conversion efficiencies. This particular feature could substantially reduce the cost of the array by simplifying the fabrication of the drive circuitry.

### 5.3.3 Ferrite Microstrip Developments

#### 5.3.3.1 A Latching 360° Control Phasor

Techniques have been developed under Contract AF 33(615)-3332<sup>6</sup> which could have a significant impact on the development of practical low-cost phased array radars. In particular, low-loss ferrite phasors have been constructed which could be used as control elements in the system shown in Figure 5.5. A photograph of this phasor is shown in Figure 5.6.

The differential phase shift characteristic for this device is shown in Figure 5.7. It demonstrates a  $\pm 2\%$  phase variation about  $370^\circ$  for a 10% frequency band.

Figure 5.8 shows the VSWR and loss characteristic of this same device. The minimum insertion loss is about 2.2 dB, which includes transition and lead in-line losses.

Efficient control of the phase shifter for multi-bit performance is accomplished through the use of an appropriate flux-driver (voltage-time generator).

#### 5.3.3.2 Comments on Performance

Table 5.6 is a summary of the pertinent device characteristics for a typical 360° non-reciprocal phase shifter. While some characteristics were measured in the range L-through K-Band, our main experimental emphasis has been at S- and X-Band.

At L-Band, the substrate material (ferrite or garnet) shows less promise and at K-Band the dimensions of the meander line begin to be more critical and difficult to work with. The beamwidth can be readily adjusted to any need depending on what sacrifices in FOM one is willing to tolerate. The specified phase shift ( $360^\circ \pm 2\%$ ) is easily achieved for a 10% bandwidth.

An item which could be of significant importance is the loss variation from a given phase state as an excursion of all intermediate bit-states is read out. Large variations could seriously compromise the quality of steered beams for a phased array. For diode phasors this may be as much as 1.0 dB. In the case of this ferrite device, it is less than 0.3 dB. Incidentally, this 0.3 dB variation is to the lower side of the 2.2 dB maximum loss figure given.

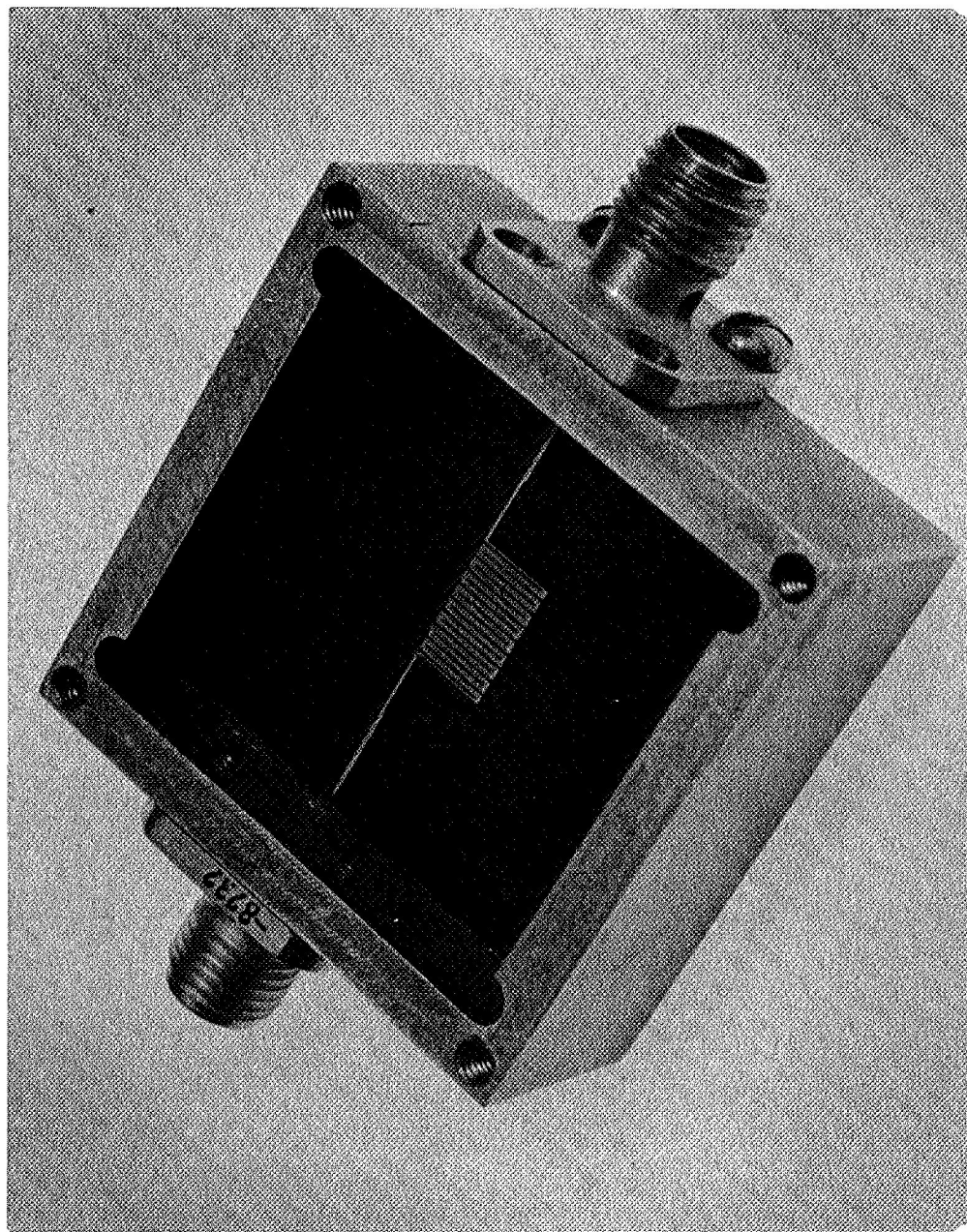


FIGURE 5. 6 360° NON-RECIPROCAL LATCHING FERRITE PHASE SHIFTER  
(Syracuse University Research Corporation Photograph)

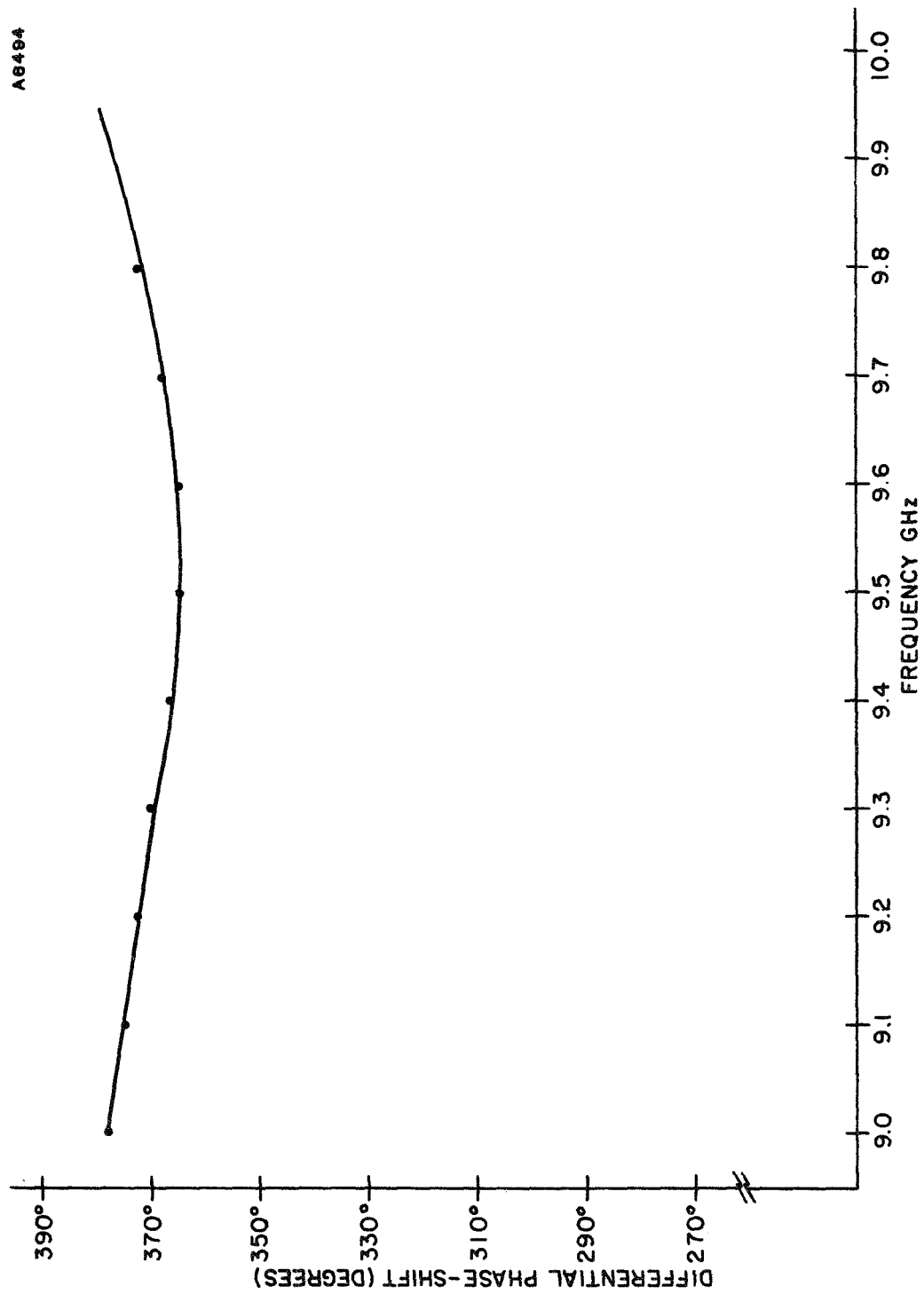


FIGURE 5.7 PHASE SHIFT (NON-RECIPROCAL)

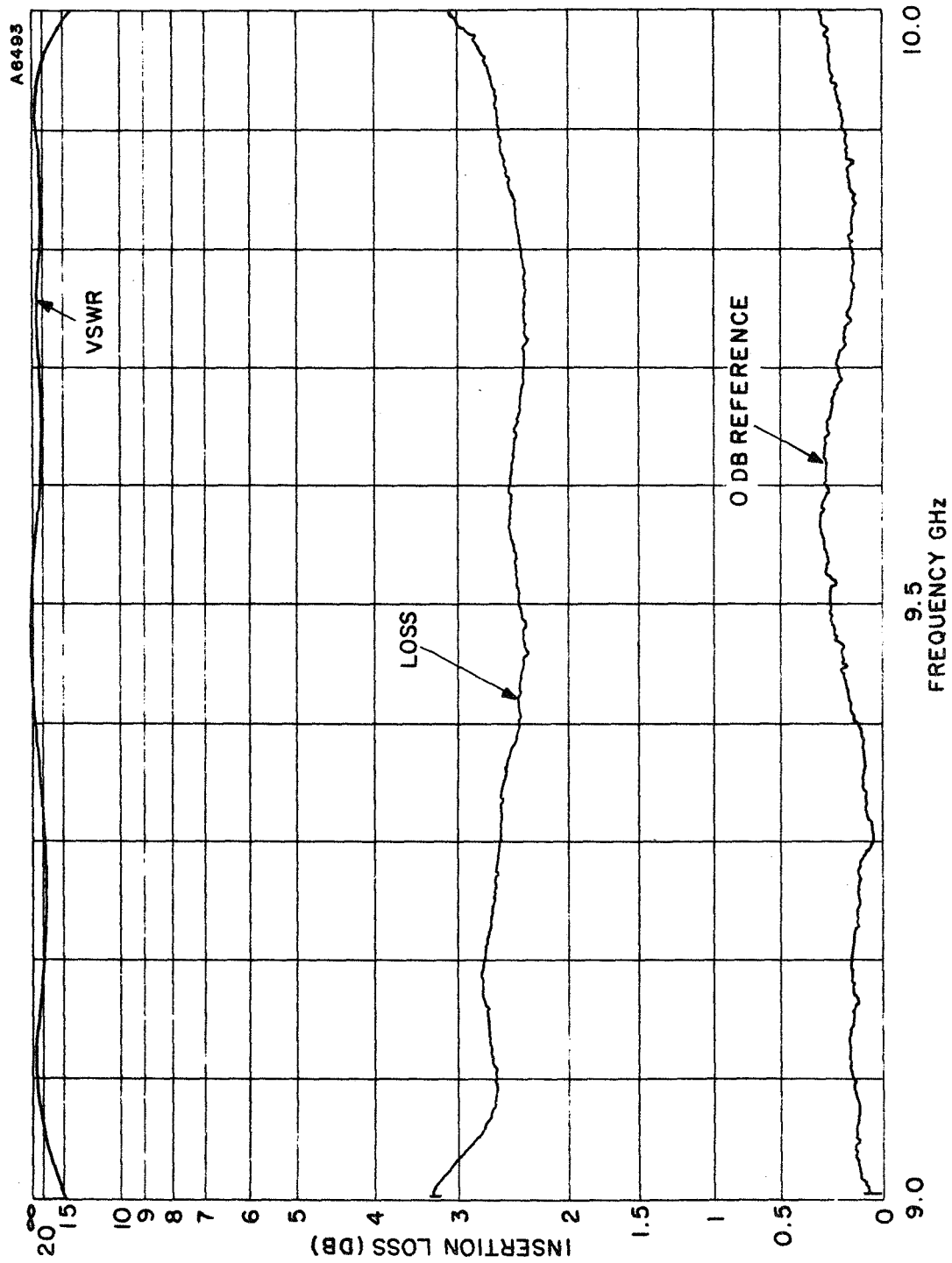


FIGURE 5.8 PROPAGATION CHARACTERISTICS  
FOR NON-RECIPROCAL PHASE SHIFTER



TABLE 5.6  
PLANAR FERRITE PHASE SHIFTER PERFORMANCE

Parameter	Range	Determining Factors
Frequency	L - K -	Intrinsic Material Properties
Bandwidth	10% (50%)	Inherent Material Dispersion
Phase Shift	$360^\circ \pm 2\%$	Network Design
Phase Control	$< \pm 1^\circ$ (Bit Setting)	Flux Drive Circuit
Insertion Phase	$6\lambda$	Degree of Interaction
Insertion Loss	1.9 dB to 2.2 dB	Usual Microstrip Losses
Loss Variation	0.3 dB	Insertion Length Variation
RF Power	10 w to 100 w Peak	Network and Material
VSWR	$< 1.3$	
Switching Speed	$\sim 1$ -3 Microsecond	Drive Circuit
Switching Energy	$\sim 10 \mu$ Joules	Material and Frequency
Size	Typically 1" x 1" x .020" at X-Band	
Weight	$< 1/2$ Ounce	
Reliability		Set by Driver

The switching speed is primarily limited by the type of drive circuit. The stated figures are for currently developed flux-drivers. The device can actually be switched by a current driver in tens of nanoseconds. There is obviously some trade-off in cost for switching speed.

#### 5.3.3.3 Linear Phased Array Antenna

A steerable array antenna can be easily fabricated by the integration of many ferrite control elements on a common ferrite substrate. Figure 5.9 shows an X-Band, eight-port corporate feed with non-reciprocal phase shifters. A partially switched (flux-driven)  $360^\circ$  single meander line element appears to be best suited to satisfy the requirements of multi-bit capability, minimum insertion loss, and minimum use of ferrite surface area.

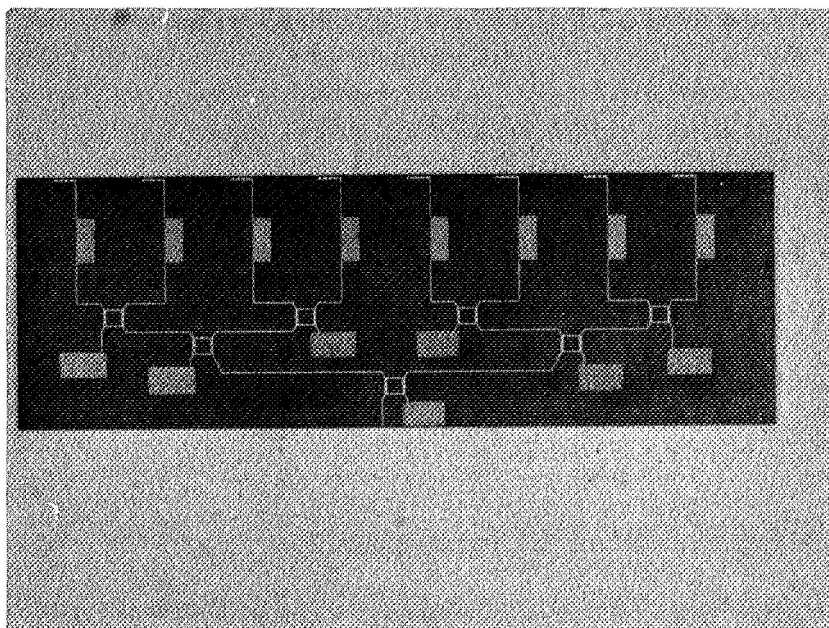


FIGURE 5.9 EIGHT-ELEMENT LINEAR ARRAY  
WITH PRINTED DIPOLE RADIATORS (X-BAND)

The corporate feed consists of appropriately placed 3 dB branch line couplers and short-phase compensating line lengths which provide a maximum relative phase variation of less than  $3^\circ$  between all eight output ports. Each hybrid in the corporate feed, including the prime input coupler, has a deposited chromium film termination. Reflections from this type of load are better than 20 dB down. The output ports are separated by a half-wavelength in air to facilitate the evaluation of antenna patterns. The substrate measured 2" x 6" x .020" and in Trans-Tech TTI-105 magnesium manganese ferrite. Twin switching holes in the substrate are used to control each phase shifter.

#### 5.3.3.4 Antenna Patterns

A typical antenna pattern is shown in Figure 5.10. The mainlobe has a 3 dB beamwidth of  $12^\circ$  with the first sidelobes down 13 dB. This is as expected with no amplitude weighting across the array. Some preliminary data on steered patterns were also taken. The main beam was steered off boresight by appropriate partial switch setting of each phase shifter. These results conformed quite well with the theory and are shown in Figure 5.11. These antenna patterns (linear plot) correspond to the conditions where the progressive increment in phase setting between adjacent elements was  $0^\circ$  (boresight)  $45^\circ$  and  $90^\circ$ .

#### 5.3.3.5 Conclusions

It appears that a ferrite substrate can be used as the basic modular building block which will provide inexpensive passive components such as phase-shifters and circulators, and also serve as a suitable transmission medium between the other semiconductor chip modules (receiver amplifier, limiter, etc.).

#### 5.3.4 All Solid-State Radar Installation

Ultimately, the all solid-state antenna can be constructed in a thin package. The front cowling, below the propeller, is the suggested location for such a package on a single or dual in-line engine aircraft. Since the transmitter will be integrated with the array, the radar should be readily adaptable as a modification or retrofit to aircraft not currently equipped with radar. While the propeller on single-engine aircraft will interfere with the operation, the transmitter can be turned off during blade passage. There will be a loss of 30 to 40% in potential operating time, but the operation should be satisfactory. If an all solid-state display panel can be developed with provision for storage, then the interference from the propeller will be minimized. A rough sketch of the proposed system is given in Figure 5.12.

A 3866

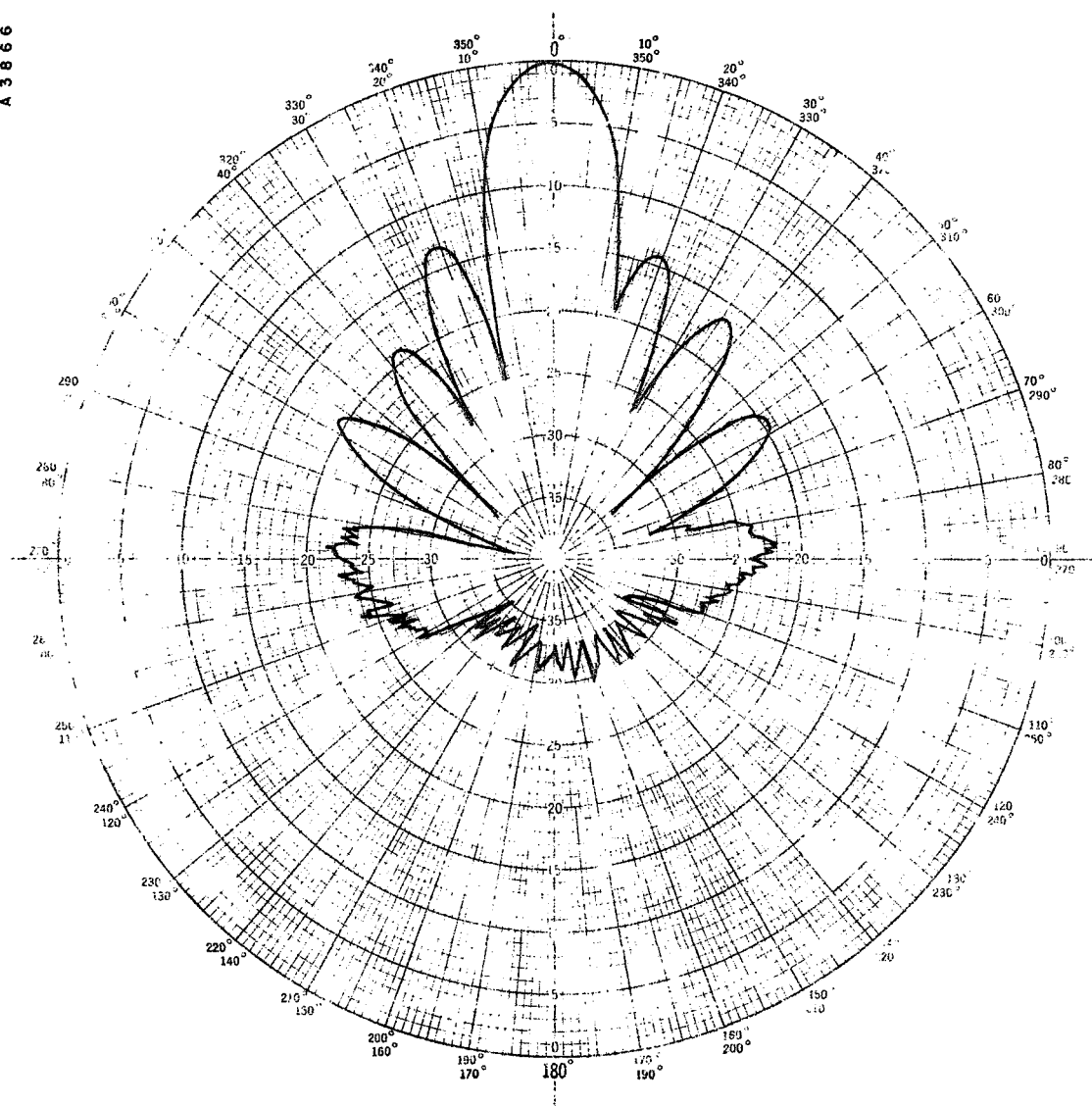


FIGURE 5.10 BORESIGHT PATTERN FOR EIGHT-ELEMENT  
LINEAR ARRAY (AMPLITUDE IN dB)

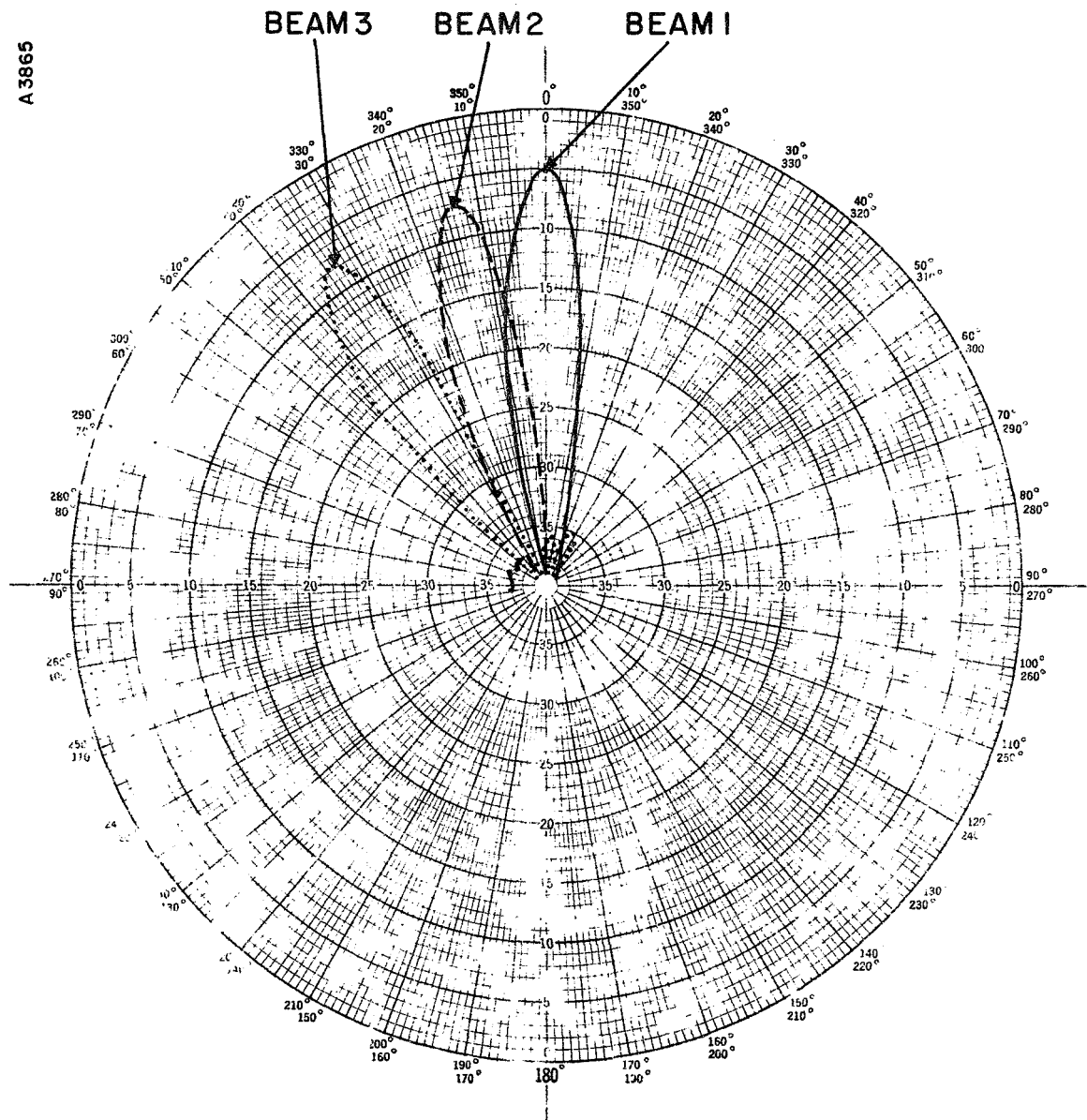


FIGURE 5. 11 LINEAR PLOT OF STEERED BEAMS

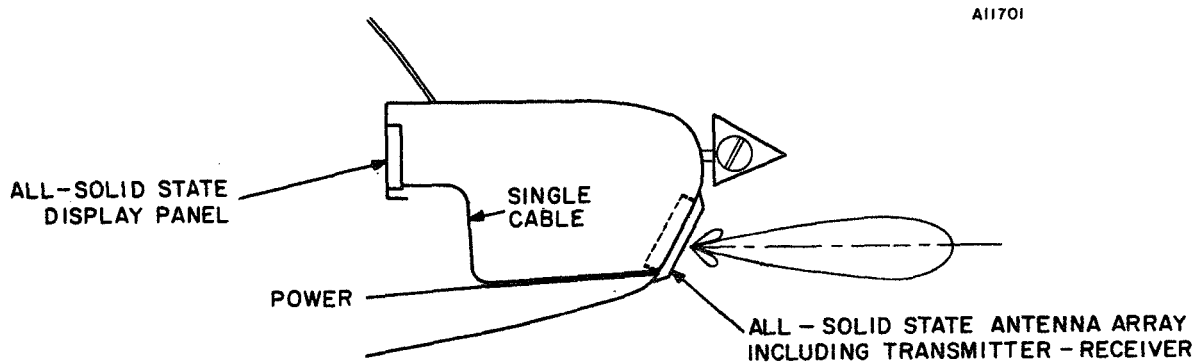


FIGURE 5.12 ALL SOLID-STATE WEATHER RADAR  
IN SINGLE OR DUAL IN-LINE ENGINE AIRCRAFT

#### 5.3.5 All Solid-State Radar Block Diagram, Parameters and Cost Estimates

Partial block diagrams of an all solid-state radar are given in Figures 5.4 and 5.5, and a conceptual diagram of the complete radar in Figure 5.13. A major asset of the all solid-state radar is the reduction to two units 1) a combined antenna-transmitter, and 2) the display. In view of the current low efficiency of solid-state microwave generators, a front cowling location, where the unit receives a flow of air from the propeller, should assist in keeping the unit cool during ground operation.

While all solid-state modules of the transistor-multiplier type (MERA modules) are currently in small production, the cost of the units is too high and the power output too low for a low-cost GA radar. Therefore, it is not practical to estimate the cost except on a very large quantity basis (greater than  $10^6$  modules). The status of other microwave solid-state sources, such as Gunn effect devices, is also too ambiguous to make reasonable cost estimates at this time. In view of the need for continuing development of solid-state

sources, integrated microwave circuitry and a high performance modulator, the development of a complete radar is estimated at 1 to 2 million dollars. It is assumed that a conventional CRT would be used for the display initially, though a solid-state display can be added when available.

AI1702

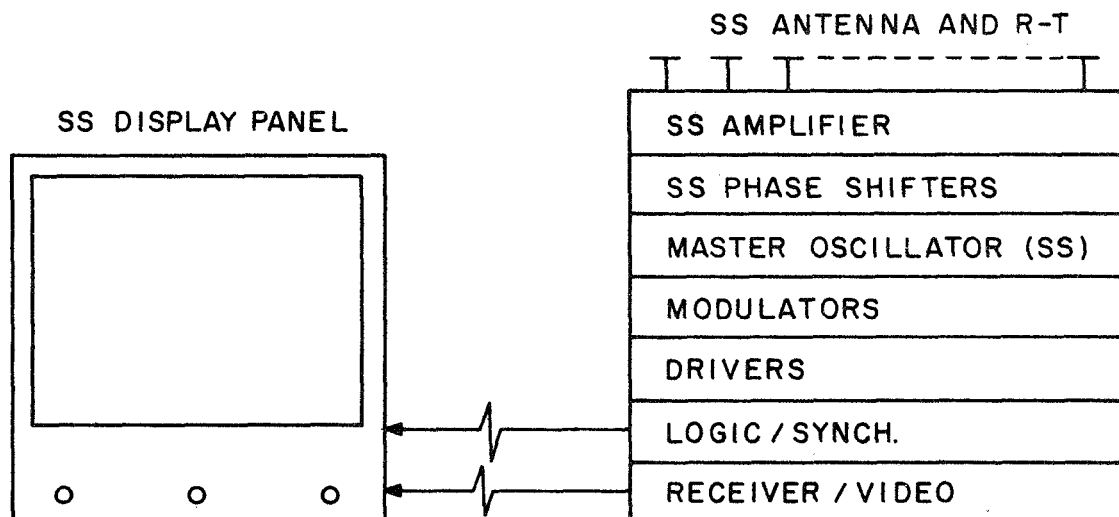


FIGURE 5.13 BLOCK DIAGRAM OF ALL SOLID-STATE (SS)  
WEATHER RADAR  
(Also See Figures 5.6 and 5.7 For Microwave Block Diagrams)

#### 5.4 Modulation-Scan Radar (MODSCAN)

##### 5.4.1 Introduction

In Section 3.13, the principle of intrapulse scanning using mixers and multiple frequencies is explained. The phase shifts on the multiple frequency oscillator signals are transferred to the incoming signals and the beam scans very rapidly. The whole azimuth sector is scanned repeatedly, with each scan requiring a time less than the radar pulse length (and, consequently called intrapulse scanning). A possible implementation of the MODSCAN radar on a single or dual in-line aircraft is described in Section 3.14. The receiving and transmitting linear arrays are at right angles. The transmitting

TABLE 5.7  
OPERATIONAL CHARACTERISTICS (OC)  
OF ALL SOLID-STATE (SS) WEATHER RADAR

Characteristic	Desired OC	All SS Radar OC
Display	PPI	PPI
Scan Sector	$\pm 90$ degrees	$\pm 45$ degrees
Tilt	$\pm 20$ degrees	$\pm 15$ degrees
Scan Rate	$> 30$ frames/second	40 frames/second
Altitude	Surface to 20,000 feet	Surface to 20,000 feet
Range		
Detection	100 NM	60 NM
Analysis	30 NM	25 NM
Resolution	1/4 NM range 6 degrees Az.	1/12 NM range 7 degrees Az.
Target	Light to Heavy Rain	Light to Heavy Rain
False Targets		
Angle	-50 dB sidelobes	-40 dB sidelobes
Range	$> 100$ NM	$> 50$ NM
Display Dynamic Range	40 dB	30 dB



TABLE 5.7 (Cont'd.)  
TENTATIVE PARAMETERS

Transmitter Peak Power	10 KW
Receiver/Transmitter Antenna Gain	28 dB
Receiver/Transmitter Beamwidth	7 degrees
Transmitter Wavelength	3.2 cm
Receiver Noise Figure	10 dB
Microwave Loss Factor (Amplifier -to-Antenna)	1 dB
Pulses Integrated	80
Scan Sector	90 degrees
Scan Rate	40 frames/second
Pulse Repetition Frequency	1600 pulses/second
Pulse Length	1 microsecond
Duty Factor	0.001
S/N, Single Pulse	10 dB

TABLE 5.8  
ESTIMATED COSTS ON ALL SOLID-STATE RADAR

I. <u>Estimated Cost (Present, Per Radar)</u>	
<u>One Unit (50 Modules)</u>	
50 One-Watt Modules at \$3,000	\$ 275,000
Plus Associated Circuitry for 200 to 1 Pulse Compression and Display	
<u>20,000 Units (10<sup>6</sup> Modules)</u>	
50 One-Watt Modules at \$50.00	\$ 25,000
Plus Associated Circuitry With 200 to 1 Pulse Compression and Display	
II. <u>Estimated Cost (Future)</u>	
<u>50,000 Units (20 Modules Each)</u>	
20 Ten-Watt Modules at \$50.00	\$ 8,000
Plus Associated Circuitry With 100 to 1 Pulse Compression <sup>9</sup> and Receiver	\$ 1,000
PPI Display	\$ 800
<u>Total</u>	\$ 9,800
III. <u>Development Cost of Integrated Circuit All Solid-State Radar</u>	
One Year Feasibility Study of Gunn Oscillators, Phase Shifters, Synchronization, etc., and Comparison with Transistors - Multipliers	\$ 100,000
Three Year Development of Demonstration Array for Dual In-Line Engine Aircraft	\$1,000,000
<u>Total</u>	\$1,100,000
Development Cost/Unit = \$110 for 10,000 Units	

antenna has a broad azimuth pattern and a narrow elevation pattern, while the scanning receive antenna has a narrow azimuth pattern. The elevation pattern of the receive antenna should be made as narrow as feasible to increase the system gain. A major advantage of the MODSCAN technique is that the complete azimuth sector, in range and angle, is scanned at the pulse repetition frequency (PRF) and many pulses from a single target are available for integration on the display. With the decorrelation time for rain about equal to the inverse of the PRF, the large number of pulses available for integration should give a smooth display. The primary disadvantage of the MODSCAN antenna arrangement, as with any cross-type antenna, is that the round-trip sidelobe level in azimuth is equal to the one-way sidelobe level of the receiving array. The round-trip sidelobes of the weather radar antenna should be -50 dB relative to the main beam to minimize the possibility of false targets. With the MODSCAN design, a relative sidelobe level of -30 to -35 dB round-trip may be feasible though additional investigation is needed. The phase and amplitude stability of all active and passive circuit elements in each channel of the receiver must be maintained to close tolerances. For example, for a random sidelobe level of -30 dB, the channel amplitude responses must be held to  $\pm 0.5$  dB, and the phase tolerance to  $\pm 3.6$  degrees.

#### 5.4.2 MODSCAN Block Diagram, Parameters and Cost Estimates

The block diagram shown in Section 3.13, Figure 3.25, requires the generation, in a scanning local oscillator (SCALO), of the narrowly separated frequencies for mixing with each incoming signal. Since the SCALO frequencies are separated by the intrapulse scanning rate, the multiple LO signals are easy to generate but difficult to isolate for use in the mixers. The SCALO signals can be generated by pulse modulating a conventional local oscillator at the scanning rate, which might be 2 MHz. The desired spectrum of SCALO signals, centered on the LO frequency, is generated by the pulse modulation, but the SCALO signals must be separated by filters before mixing. Q's of 10,000 with stable filters are necessary to isolate the desired spectral lines at X-Band. An alternate to ease the filtering problem is to perform an initial conversion from X-Band to perhaps 500 MHz, where the SCALO signals are easier to isolate. A double conversion block diagram is given in Figure 5.14. For a system with a one microsecond transmit pulse and a 16 element array, the frequencies listed in Table 5.9 are typical.

The transmitter block diagram is the same as given previously, Figure 3.27. The radar parameters are tabulated in Table 5.10. The SCALO filters are likely to be the critical cost items. For adequate stability and band separation, the use of AT cut crystals with a Q of 10,000 in the filters appears to be a satisfactory choice. The phase and amplitude stability requirement on the IF strips will likely make these amplifiers more costly than the usual

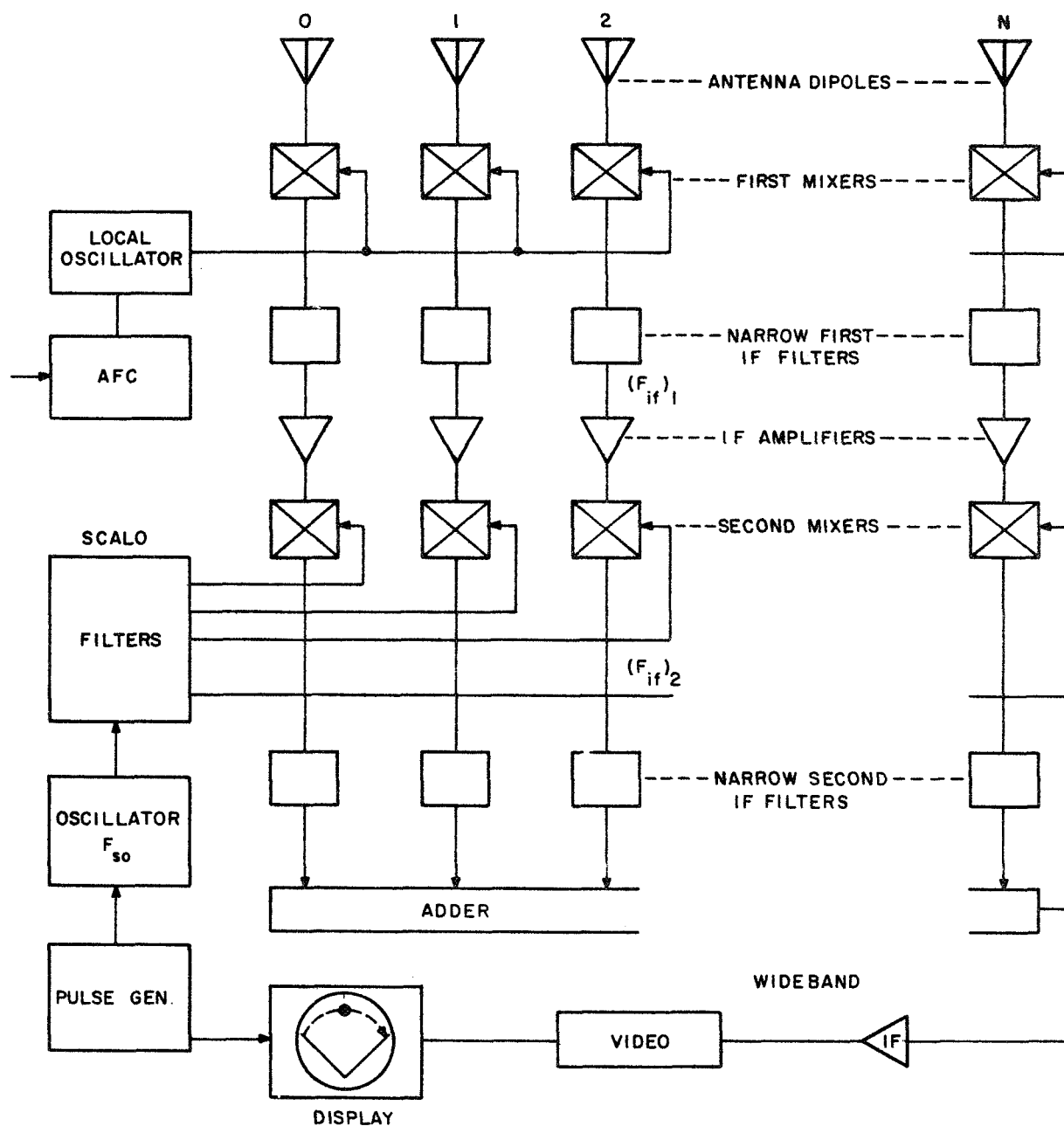


FIGURE 5.14 MODSCAN RECEIVING ARRAY

TABLE 5.9  
PROPOSED MODSCAN FREQUENCIES

$(F_{if})_1$	= 190 MHz	First IF
$(F_{if})_2$	= 94 MHz	Second IF
$F_{so}$	= 96 MHz	STALO Oscillator
$\Delta f$	= 2 MHz	Scan Frequency
$(\Delta\beta)_2$	= 2 MHz	Second IF Bandwidth

low-cost radar IF strips. The final IF amplifier and video detectors have bandwidths of 32 and 16 MHz, respectively, and the display must be designated for the wideband video signals. The display sweep can be obtained by off-setting a circular sweep at the scan rate (applying two quadrature 2 MHz signals to the vertical and horizontal deflection plus a dc offset). The amplitude of the circular sweep is modulated linearly by a normal range sweep. Thus, the display should not be more expensive than a conventional radar PPI except for the requirement for wideband video input. The detailed cost estimate is given in Table 5.11.

## 5.5 Laser Cloud Ranging

### 5.5.1 Introduction

Just prior to World War II, pulsed light ranging devices were developed to range on aircraft in order to supplement the large 100-inch searchlights used for aircraft detection and tracking. Spark gap discharges were used as incoherent light sources and the 100-inch searchlight mirrors served to collimate the beam for transmission and as efficient collectors on reception. However, these incoherent pulsed light devices could not penetrate clouds and had a very limited range in daylight, so were soon supplanted by microwave radar in World War II. The cloud detecting properties of the pulsed light equipment were noted, so a special cloud-height measuring set was developed. The wide-spread use of pulsed equipment for cloud-height measurement is limited by initial cost and maintenance. The vertical light beam scanned by a remotely located detector has continued to be the standard equipment at U. S. Weather Bureaus.

With the advent of the laser, a new narrowband pulsed light source became available for development of cloud-height measuring equipments and other applications<sup>1,2</sup>. When combined with solid-state circuitry, including

TABLE 5.10  
TENTATIVE PARAMETERS AND  
OPERATIONAL CHARACTERISTICS OF MODSCAN

Characteristic	Desirable	MODSCAN
Display	PPI	PPI
Scan Sector	$\pm 90$ degrees	$\pm 45$ degrees
Tilt	$\pm 20$ degrees	$\pm 15$ degrees
Scan Rate	$> 30$ frames/second	800 frames/second
Altitude	Surface to 45,000 feet	
Range		
Detection	100 NM	51 NM
Analysis	30 NM	20 NM
Resolution	1/4 NM 6 degrees Az.	1/12 NM 7 degrees Az.
Target	Light to Heavy Rain	Light to Heavy Rain
Display Dynamic Range	40 dB	35 dB
False Targets		
Angle	-50 dB sidelobes $> 100$ NM	-30 dB sidelobes $> 100$ NM

TABLE 5.10 (Cont'd.)

## PARAMETERS

Transmitter Peak Power	10 KW
Transmitter Antenna Gain	15.4 dB
Transmitter Antenna Beamwidth	3 degrees El. by 90 degrees Az.
Receiver Antenna Gain	23 dB
Receiver Antenna Beamwidth	15 degrees El. by 7 degrees Az.
Transmitter Wavelength	3.2 cm (X-Band)
Receiver Noise Figure	10 dB
Microwave Loss Factor	1 dB
Pulses Integrated	800
Pulse Repetition Frequency	800 pulses/second
Pulse Length	1 microsecond
Duty Factor	0.0008

TABLE 5. 11  
ESTIMATED COST OF MODSCAN SYSTEM  
(17 Element Array)

Component	Quantity		
	1	100	10, 000
I. <u>Cost Estimate</u> (Present, Per Radar)			
17 Element Antenna (136 Dipoles)	\$ 3, 400	\$ 2, 100	\$ 850
SS Oscillator 9.4 GHz	1, 300	750	520
1st Mixers	3, 800	1, 700	1, 200
Power Divider	3, 800	300	170
1st IF Filters	3, 000	1, 700	850
1st IF	8, 500	3, 000	1, 700
AFC	400	120	80
2nd Mixers	700	250	80
2nd IF Filters	2, 400	1, 200	680
Power Divider	800	250	100
Oscillator Xtal	700	400	250
Adder	800	250	100
Pulse Generator	1, 500	500	200
Wideband IF	1, 000	700	250
Video Amplifier	800	500	100
Display	3, 000	1, 700	400
<u>Receiver Total</u>	\$ 35, 900	\$15, 520	\$7, 530
Power Supply	1, 500	500	250
Modulator	2, 700	180	100
Magnetron	150	90	60
Antenna	5, 000	1, 000	300
<u>Transmitter Total</u>	\$ 9, 350	\$ 1, 770	\$ 710
<u>System Total</u>	\$ 45, 300	\$17, 290	\$8, 240



TABLE 5.11 (Cont'd.)

Component	Quantity		
	1	100	10,000
II. <u>Cost Estimate (Future)</u>			
<u>Quantity of 10,000 (Each)</u>			
Display			\$ 400
Receiver			5,200
Transmitter			<u>600</u>
<u>System Total</u>			\$6,200
III. <u>Development Cost</u>			
One-Year Feasibility Study and Construction of Discrete Circuit Radar.	\$250,000		
Two-Year Development of Microwave Integrated Circuit (MIC) Flyable Radar	\$500,000		
<u>Total</u>	<u>\$750,000</u>		
Development Cost/Unit = \$75.00 for 10,000 Units			

detectors, there exists the possibility of a small device suitable for use in cloud ranging from light aircraft.

#### 5.5.2 Laser Cloud Ranging Block Diagram, Parameters and Cost Estimates

The cost of lasers at the present time is too high for immediate application to GA aircraft. However, laser devices are already under investigation for a rear obstacle detector on motor vehicles<sup>7</sup>. Both semiconductors and prepared glass rods are promising sources of infrared laser light. A neodymium (Nd) glass rod is a promising laser material since an Nd rod can be purchased for approximately \$200.00 versus a cost of \$1,000 or more for a ruby rod or other material. The Nd rod operates at a wavelength of 1.06 microns\*. The use of gallium arsenide diodes (at 0.92 microns) also merits consideration, though the cost is currently high (perhaps \$250.00 per diode) and an array of diodes is required to obtain adequate output. The power requirements for pulse ranging on clouds with a laser are described in Appendix F.

The neodymium laser, with a very narrow bandwidth filter (20 angstroms\*), needs a power output of only one kilowatt peak to range on clouds at a distance of five miles. Since the laser power required is low, and operation can be outside the visible region, there should be no danger to people.

A preliminary evaluation of the ability of a laser to range on clouds from an aircraft can be done with commercial or military equipment, already developed. If the evaluation indicates that the safety and efficiency of VFR flight can be enhanced by more accurate measurements on cloud clearances, under both day and night conditions, then further evaluation with special equipment should be considered.

The range of a LIDAR is greater at night because of the lower background light level. It is desirable to give the night VFR pilot additional time to plan an alternate route before actually encountering clouds. A low powered diode laser, at a relatively low cost, may be feasible at the present time (see Table 5.12); however, the range will be appreciably less than desirable. Block diagrams are provided of a neodymium laser, Figure 5.15, and a diode laser, Figure 5.16, rangefinders.

---

\*A micron is  $10^{-4}$  cm, an angstrom unit is  $10^{-8}$  cm.

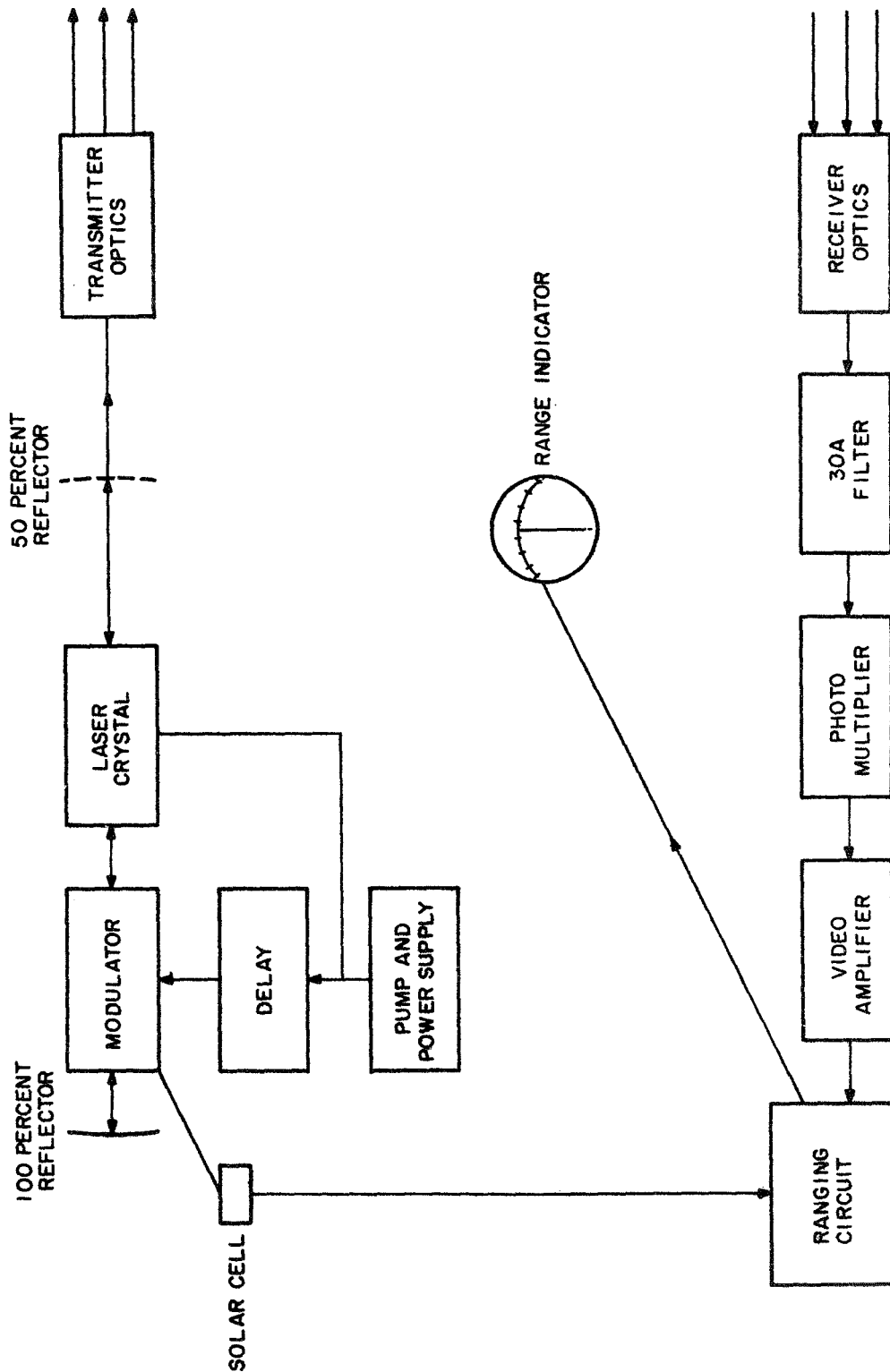


FIGURE 5.15 BLOCK DIAGRAM OF NEODYMIUM ROD LASER  
(1.06 MICRONS) CLOUD RANGER FOR VFR FLIGHT

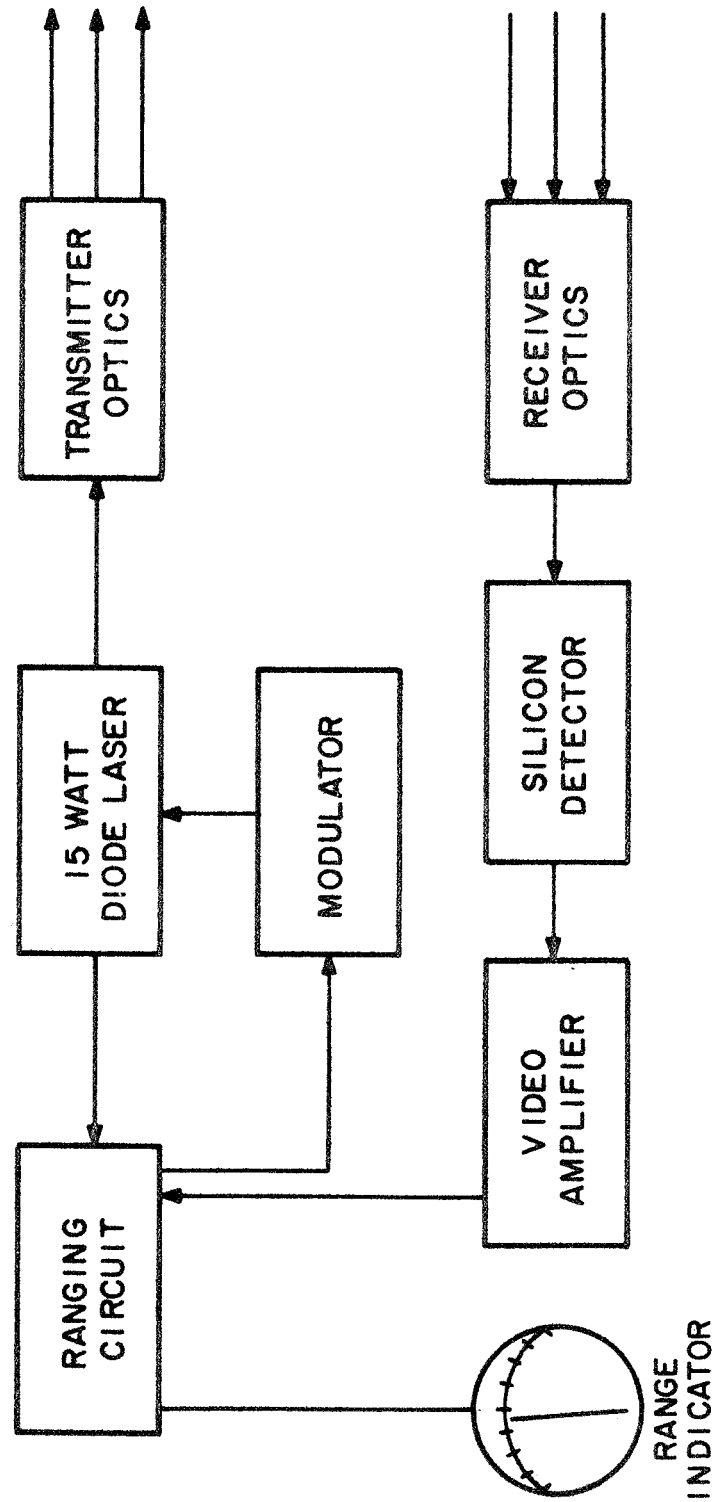


FIGURE 5.16 BLOCK DIAGRAM OF LOW POWER DIODE LASER  
FOR CLOUD RANGING DURING NIGHT VFR FLIGHT

TABLE 5.12  
ESTIMATED COSTS ON PULSED LIGHT RANGER

(Since there is no comparable device currently marketed for General Aviation, only the cost of assembling single units will be estimated.)		
IA. <u>Estimated Cost</u> (Neodymium Laser)		
Laser Rod	\$	250.00
Flash Tube and Container		2,000.00
Power Supply and Modulator		2,000.00
Receiver-Transmitter Optics and Steerable Mount		5,000.00
Receiver and Ranger Unit		<u>5,000.00</u>
<u>Total</u>		\$14,250.00
IB. <u>Estimated Cost</u> (Diode Laser)		
20-Watt Diode	\$	100.00
Modulator		500.00
Receiver, Optics and Steerable Mount		<u>5,600.00</u>
<u>Total</u>		\$ 5,600.00

## 5.6 Sferic Weather Detection

### 5.6.1 Introduction

Severe storms radiate energy over a wide spectrum of frequencies. The greatest intensity is usually in the region of 10 KHz and decreases rapidly beyond though "static" is present through and beyond the LF broadcast band of 540 KHz to 1.7 MHz. Automatic direction finder (ADF) equipment currently installed in numerous general aviation aircraft operates over the range 190 KHz to 1.75 MHz. A list of current ADF equipment taken from the April 1970 Business and Commercial Aviation magazine is shown in Table 5.13. The ADF will often indicate the approximate direction to isolated thunderstorms though the indication cannot be relied upon because of the inertia of the pointer. Instantaneous ADF techniques which utilize cathode ray tube (CRT) indicators have the rapid response needed to provide DF indications on the impulse-like signals generated by lightning discharges. While the instantaneous ADF can provide indications on the direction to storm cells, the pilot must interpret the sequential responses. If these indications can be integrated on a display, as the aircraft moves along a constant heading, then "fixes" can be obtained on storm cells to the side of the ground track. At the present time there is no equipment available to print the moving "fixes" for the benefit of a pilot. If the pilot flies a constant heading then the undeflected spot on the CRT display can be designed to move from the bottom of the display tube to the top. Instantaneous DF indication would be present on the moving spot and storm "fixes" will be obtained at right angles to the ground track. The only recording medium that is suitable for producing a graphic display is rapid development photographic film. The pilot would reset the mechanism by pulling the film clip when the electron beam reaches the top of the CRT tube. The requirement that the pilot fly a constant heading, and that the storm "fixes" are at right angles to the ground track are severe limitations on the use of sferic DF. While there is evidence that thunderstorm intensity is not directly related to sferic activity (see Section 2.8), the sferic indication does give positive evidence of lightning strokes in a storm. Lightning can damage aircraft<sup>8</sup> and geographic areas where lightning is present should be avoided even though there is no severe turbulence or hail.

Though it would be desirable to modify a conventional GA ADF, such as the ones listed in Table 5.13, this does not appear feasible. The instantaneous ADF requires two IF amplifier channels, whereas the conventional ADF has one IF amplifier which is time-shared. Further, there are two types of instantaneous ADF, one with a 180 degree ambiguity and the other with a sense antenna and phase detector to resolve the 180 degree ambiguity. A block diagram of the ambiguity resolving type is shown in Figure 5.17. The cost estimate, Table 5.15, is based upon adding a CRT indicator and Polaroid

**TABLE 5.13**  
**GENERAL AVIATION ADF EQUIPMENT**  
(From April 1970 Business and Commercial Aviation Magazine)

MANUFACTURER	MODEL	FREQ (kc) BANDS	VOLTS INPUT	TYPE LOOP ANT	BFO	UNITS/ WT (lb)	PRICE (uninstalled)	REMARKS
Aircraft Radio, Boonton, N.J. 07005	324	190-1750 3-bands	14 or 28 V DC	fixed with goniometer indicator (semi-flush -protrudes 1 in.)	std	3/10.3	\$2590	panel mtd; fully transistor ized, full repeat capability, RMI compatible, tape read- out of freq TSO -C-41b class A cat BAFBAAX
	521B	190-1750 3-bands	14 or 28 V DC	fixed, with goniometer- indicator (semi-flush -protrudes 1 in.)	option	2/7	\$1295	fully transistorized; panel mtd; includes tuning meter and loop test sw
	21B	190-1750 3-bands	14 or 28 V DC	fixed with goniometer- indicator (semi-flush)	std	5/19.4	\$3230	has "loop" function in addition to "comp" and "ant," fully transistorized TSO -C41b; cat AAAAAAE
Bendix Avionics Div P.O. Box 9414 Ft. Lauderdale, Fla 33310	ADF T-12C	190-1750 3-bands	14 or 28 V DC	fixed with goniometer- indicator (semi-flush)	option	3/10.4	\$895	3 units: rcvr, ind & loop, installation kit supplied fully transistorized; panel mtd; loop test
	DFA-73	190-1750 3-bands	28 V DC, 26 V, 400 cps, 6.5 VA	fixed with goniometer- indicator (semi-flush)	std	5/22.2 (control & ind (RMI), both panel mtd; rec, loop, shock- mount)	\$4072 (less RMI)	fully transistorized; solid- state band and function switching; zero beat tuning, 4 function: "ADF" "ant", "loop", "test" digital tuning opt TSO -C-41b; cat AAAAAAX, class I Arinc 550
	DFA-74	190-1749.5 digital tuning	28 V DC 26 V 400 cps	fixed with goniometer- indicator (semi-flush)	std	3/(rcvr weighs 10 lb)	\$3687	solid-state design, digital tuning, automatic BFO switching TSO DO-138-cat AG/A/KM/JN AAZXXXXXX Arinc 570
Collins Radio, Cedar Rapids, Iowa 52406	DF-206	190-1750 (1/2 kc steps) no manual band switch- ing	28 V DC	fixed with goniometer- indicator (semi-flush)	std	4/19.7	\$4724	fully transistorized, digital tuning, phase detec tor for stable bearing in high noise areas, self-test TSO pending - will be C-41b DO-138 cat AD/A J/G/AZZXXXXXX class A, Arinc 570
Kett Avionics, 920 Santa Monica Blvd Santa Monica, Calif 90403	Polaris S-70	185-1750 2-bands	14 or 28 V DC	fixed loop with goniometer- indicator (semi-flush)	std	2/9.25 (panel mtd rcvr loop & all cabling)	\$795 (complete w/installation kit, less sense ant)	fully transistorized push-to-test, self contained indicator with rotatable azimuth 5-W speaker output
	Polaris X	185-1750 2-bands	14 or 28 V DC	fixed loop with goniometer indicator (semi-flush)	std	3/12 (panel mtd rcvr & ind, loop & all cabling)	\$895 (complete w/installation kit, less sense ant, less indicator)	for use w/remote ind or RMI, gyro or manual cntrl (e.g. Kett Kourse Pointer, Allen, Garmi); panel mtd; solid state, opt solid-state 400 cps in verter for operation of up to 3 indicators for A/C not equip ped w/400 cps; opt audio outpt (5 W for speaker or 0.5 W for phones)
King Radio Olathe, Kans. 66061	KR-80	190-1600 2-bands	14 or 28 V DC	fixed loop with goniometer indicator (semi-flush)	option	2/6.3 (rcvr & loop)	\$1050	fully transistorized panel mtd in 3-in instrument hole, loop test, tuning meter optional

TABLE 5. 13 (Cont'd.)

MANUFACTURER	MODEL	FREQ (kc) BANDS	VOLTS INPUT	TYPE LOOP ANT	BFO	UNITS/ WT (lb)	PRICE (uninstalled)	REMARKS
King Radio (cont'd)	KR-85	200-1699 digital tuning (no band switching)	14 or 28 V DC	fixed loop (semi-flush) with goniometer indicator	std	2/5.5 (rcvr & KI 225 indicator)	\$1295 (includes indicator, sense & loop antennas & cables)	panel-mtd solid-state design crystal controlled, digital electronic tuning, TSO C-41b cat B/DACAAAX class A
	KDF-800	200-1699 digital tuning (no band switching)	28 V DC	fixed loop (semi-flush) ADF has internal goniometer which drives any conventional indicator	std	3/14.4 (control, rcvr & indicator)	\$3090 (includes freq selector loop & sense antennas & cables) KNI 580 or KNI 585 indicators additional at \$375 or \$495	solid-state design, crystal controlled electronic tuning; loop test, TSO C41b cat BABAAAX class A
	KDF 8000	190-1749 digital tuning (no band switching)	28 V DC 26 V, 400 cps, 3 VA	fixed loop (semi-flush) ADF has internal goniometer which drives any conventional indicator	std	2/11.5 (rcvr & KFS 5800 dual freq selector)	\$3130 plus freq sel at \$910	solid-state design, crystal controlled, digitally tuned, TSO C41b cat BABAAAX class A, Arinc 570
Marconi Co., Ltd., Essex, England	AD-370	190-1799.5 ( $\frac{1}{2}$ kc steps) 1-band	28 V DC 1.6 amp	fixed with goniometer indicator (flush & semi-flush loops available)	std	3/16.7 (cntrl, rcvr, loop)	\$4500	solid-state design, fully crystal controlled; electronic tuning; loop test; digital freq readout TSO C-41b, cat AABAAAX, class I Arinc 550 British ARB-WR 679
Narco Avionics, Ft. Washington, Pa. 19034	ADF-31 ADF-31AB ADF-31AM	190-1750 3-bands	14 or 28 V DC, 0.8 amp	fixed with goniometer indicator (semi-flush)	option	2/7.35 (panel mtd unit & re- motely mtd sensor unit)	\$1050 (14 V) \$1080 (28 V)	2 units, rcvr & sensor, fully transistorized, loop test; built-in aural mkr bcn rcvr or BFO; tuning meter, rotatable azimuth scale



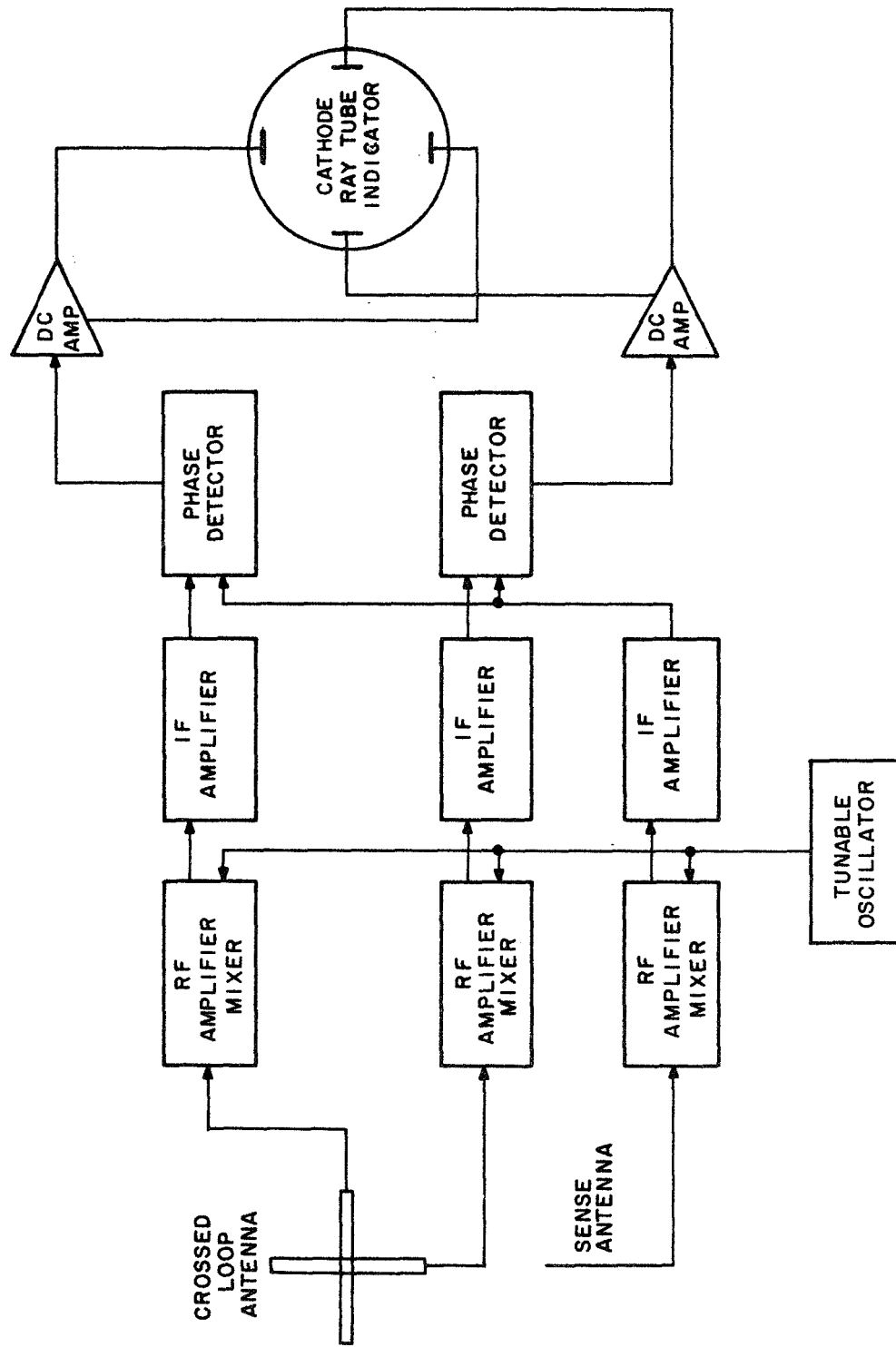


FIGURE 5.17 BLOCK DIAGRAM OF INSTANTANEOUS ADF FOR SFERIC DETECTION AND USE AS CONVENTIONAL ADF

TABLE 5.14  
COMPARATIVE OPERATIONAL CHARACTERISTICS  
AND ADF/SFERIC DETECTOR PARAMETERS

Characteristics	Desirable	Sferic Detection
Display	PPI	Radial Line PPI
Scan Sector	$\pm 90$ degrees	$\pm 180$ degrees
Tilt	$\pm 20$ degrees	Not Necessary
Scan Rate	$> 30$ frames/second	Instantaneous Indications
Altitude	Surface to 20,000 feet	Surface to 20,000 feet
Range		
Detection	100 NM	$> 100$ NM
Analysis	30 NM	$> 30$ NM (Cross Bearing)
Resolution	1/4 NM 6 degrees Az.	$\approx 5$ NM to side $\pm 5$ degrees
Target	Light to Heavy Rain	Sferics
Display Dynamic Range	40 dB	40 dB
False Targets		
Angle	-50 dB sidelobes	N/A
Range	$> 100$ NM	N/A

PARAMETERS

Loop Antenna	1 inch Effective Height
Sense Antenna	6 inch Effective Height
Sensitivity	1 microvolt Sense Receiver
Bandwidth	10 KHz or Greater
Frequency Range	190 KHz to 1.75 MHz

TABLE 5.15  
ESTIMATED COST OF ADF/SFERIC DETECTOR

I. <u>Estimated Cost</u> (Present, Per ADF)		
<u>In 1000 Units</u> (Transistorized)		
Conventional ADF Receiver Plus Second IF and Phase Detector		\$ 1,200
CRT Display		1,500
Scope Camera		<u>250</u>
	<u>Total</u>	\$ 2,950
II. <u>Estimated Cost</u> (Future)		
<u>In 1000 Units</u> (Integrated Circuits)		
Conventional ADF Plus Second IF and Phase Detector		\$ 600
CRT Display		1,000
Scope Camera		<u>250</u>
	<u>Total</u>	\$ 1,850
III. <u>Development Cost</u>		
Two-Year Feasibility Study		\$250,000
Construction of Flyable Model and Flight Test Comparison With Airborne Radar.		

film camera to a conventional ADF with a small allowance for the cost of the second IF and phase detectors. Since there is no need for a conventional ADF pointer indicator when the CRT indicator is present, the cost will be a little more than twice the cost of a conventional ADF. The recording camera can be optional as operational experience may demonstrate the camera to be unnecessary. A long persistence or display storage tube might serve as the graphic display; however, the storage tube cost is high and the dynamic range limited.

## REFERENCES

1. Collis, R. T. H., "Laser Radar Applications," Laser Technology Section of Microwaves, March 1969, pp 94-101. (Contains bibliography on cloud ranging.)
2. Marshall, S. L., Editor, "Laser Technology and Applications," McGraw-Hill Book Company, New York, 1968.
3. Jamieson, J., et al., "Infrared Physics and Engineering," McGraw-Hill Book Company, New York, 1963.
4. Handbook of Geophysics and Space Environments; Air Force Cambridge Research Laboratories, 1965.
5. Petritz, R., "Fundamentals of Infrared Detectors," Proc. of IRE Vol. 47, No. 9, September 1959, p 1458.
6. Roome, G. T., "Thin Ferrites for Integrated Microwave Devices," Final Report AFAL-TR-69-149, Dated 15 July 1969, on Contract AF 33(615)-3332.
7. Ziomek, J. F., et al, "Laser Device Detects Objects in Driver's Rear Blind Spot," SAE Journal, April 1970, pp 62-65.
8. Robb, J. D. and Newman, M. M., "Lightning Strikes to Plastic Components of Light Aircraft," Published by SAE, NBAA Paper 700220, March 18-20, 1970.
9. "Surface Acoustic Waves Curl Into Radar," Electronics, May 25, 1970, p 45.

## 6.0 CONCLUSIONS AND RECOMMENDATIONS

### 6.1 Conclusions

1. The current generation of small aircraft weather radars adequately serve the needs of the light and heavy twin General Aviation aircraft, though additional capabilities to penetrate heavy rain, reduce terrain return and to minimize mutual interference are desirable.

2. No airborne weather sensors (or proven antenna designs) are available for single and dual in-line engine aircraft, though these aircraft often operate in stormy weather.

3. In addition to overcoming the antenna design problem, substantial cost reductions are essential before airborne weather radar use will materially increase in the GA fleet.

4. Simplified or dual function designs; reduced radar range matched to aircraft speed; and increased production as a result of pilot acceptance are likely to be the major factors in lowering radar cost.

5. The engine-driven scanner, with the antenna reflector mounted on the lower engine cowl, is promising for a short-term antenna development for single and dual in-line engine aircraft.

6. Additional study and development are necessary to demonstrate feasibility of the engine-driven scanner concept.

7. Electronic scanned antennas and all solid-state designs are too expensive at present for a low-cost GA radar and this situation will continue until microwave integrated circuits are applied more extensively, particularly to consumer products.

8. Supplementary weather sensor techniques such as pulsed light detection and ranging (LIDAR) for cloud detection during night VFR flight and instantaneous ADF for monitoring lightning activity in storms should be evaluated using state-of-the-art equipments.

9. Improved weather analysis techniques are needed for the longer range (1980 and beyond) general aviation weather sensors. Current weather radar techniques are not adequate to reliably pinpoint hail, tornadoes and other intense phenomena associated with thunderstorms.

## 6.2 Recommendations

1. Study and experimental work should be performed on the engine-driven scanner concept to demonstrate feasibility. If experiments and measurements confirm the usefulness of the basic antenna concept then an operational airborne radar should be designed around modifications to existing marine and/or airborne radar equipments. Also, the cost of the engine-driven scanner should be examined in some detail for large and small quantities after a basic feasibility demonstration is completed.

2. Using modifications to existing equipments; flight tests should be performed with airborne cloud ranging (LIDAR) and instantaneous spheric (lightning) DFing equipments.

3. For a next generation GA airborne radar, techniques for improving 1) penetration (C-Band MODSCAN), 2) reduce terrain return (mono-pulse beam shaping), 3) minimize mutual interference (waveform coding), and 4) improve displays (rapid scan) should be investigated.

4. For the far term weather sensor, techniques are needed for more positive identification of severe weather phenomena such as hail, severe turbulence and tornadoes. Doppler signal analysis and multifrequency radar are useful areas for investigation. Since the improved capabilities for detection of specific severe weather phenomena are also needed by air-transport and military aircraft, a broad program to serve all aspects of aeronautical activity is desirable.

## BIBLIOGRAPHY

1. Baechle, J. R. and McFarland, R. H., "A Flush-Mounted Runway Antenna for Use With the FAA Directional Glide-Path System," IRE Transactions on Aeronautical and Navigational Electronics, June 1960, pp 32-39.
2. Bandy, G. C., et al, "MERA Modules - How Good in an Array?" Microwaves, August 1969, pp 39-49.
3. Barlow, E. J., "Doppler Radar," Proc. of IRE, April 1949, pp 340-355.
4. Barteneva, D. D., Bulletin of Academy of Sciences, USSR, No. 12, 1960, p 852.
5. Bean, B. R., and Dutton, E. J., "Radio Meteorology," Dover Publications, Inc., New York, 1968.
6. Biermann, C. and Herrenstein, W. H., Jr., NACA Report No. 468, "The Interference Between Struts in Various Combinations," Describes interference drag effects, but the results are not directly applicable here.
7. Blackband, W. T. (Editor), "Radar Techniques for Detection, Tracking and Navigation," AGARDograph 100, Gordon and Breach, New York, 1966, pp 428-431.
8. Blake, N. A., "NAS Design Concepts and System Configuration," A presentation at the Third International Aviation R&D Symposium, Automation in Air Traffic Control, Session II, p 6.
9. Boronski, S., "A Multi-Channel Waveguide Rotating Joint," The Microwave Journal, June 1965, pp 102-105.
10. Burns, R. W. and Stark, L., "PIN Diodes Advance High-Power Phase Shifting," Microwaves, November 1965, pp 38-48.
11. Cady, W. M., et al (Editors), "Radar Scanners and Radomes," Vol. 26, MIT Radiation Laboratory Series, McGraw-Hill Book Company, New York, 1948.
12. Collis, R. T. H., "Laser Radar Applications," Laser Technology Section of Microwaves, March 1969, pp 94-101. (Contains bibliography on cloud ranging.)
13. Cooke, H. F. and Stover, H., "Development of a Solid-State X-Band Power Source," Contract F33(615)-67-C-1909, Technical Report AFAL-TR-68-325, by Texas Instruments, Inc., PO Box 5012, Dallas, Texas, 75222.



14. Cosgriff, R. L., et al, "Terrain Scattering Properties for Sensor System Design (Terrain Handbook II)," Bulletin 181, Engineering Experiment Station Bulletin, The Ohio State University, May 1960, 118 pages.
15. Dickey, R. F. and Santa, M. M., "Report on Anti-Clutter Techniques," Final Report on Contract DA 36-039-sc-5446, 1 March 1953, pp 50-56.
16. Dickson, E., "Analysis of Sferics and its Relation to Severe Thunderstorm Phenomena," Proc. of 5th Weather Radar Conference, 1955, SCEL, Fort Monmouth, New Jersey.
17. Fenn, R. W., "Correlation Between Atmospheric Backscattering and Meteorological Visual Range," Applied Optics, Vol. 5, No. 2, February 1966, pp 293-295.
18. Frank, J., Kuck, J. H. and Shipley, C. A., "Latching Ferrite Phase Shifter for Phased Arrays," The Microwave Journal, March 1967, pp 97-102.
19. Grisetti, R. S., Santa, M. M. and Kirkpatrick, G. M., "Effect of Internal Fluctuations and Scanning on Clutter Attenuation in MTI Radar," IRE Transactions on Aeronautical and Navigational Electronics, March 1955, pp 37-41.
20. Hall, J. S. (Editor), "Radar Aids to Navigation," McGraw-Hill Book Company, New York, 1946, pp 171-185.
21. Hamilton, P. M., and Marshall, J. S., "Weather-Radar Attenuation Estimates From Raingauge Statistics," Scientific Report MW-32, Under Contract AF19(604)-2065, January 1961, McGill University.
22. Hanratty, R. J. and Wheeler, H. A., "An End-Fire X-Band Flush Antenna Based on the Branch-Waveguide Directional Coupler," IEEE Transactions on Antennas and Propagation, July 1963, pp 433-438.
23. Hansen, R. C. (Editor), "Microwave Scanning Antennas," Vol. III, Array Systems, Academic Press, 1966.
24. Hardeman, L. J., "Phased Arrays Scan Rapidly Towards Growth in the 70's," Microwaves Magazine, A Hayden Publication, June 1970, pp 38-54.
25. Hovis, W. A., Jr., and Tobin, M., "Spectral Measurements From 1.6 Microns to 5.4 Microns of Natural Surfaces and Clouds," Applied Optics, Vol. 6, No. 8, August 1967, pp 1399-1402.

26. Hyltin, T. M., et al, "Molecular Electronics for Radar Applications (MERA)," Reports on Contract AF33(615)-2525 by Texas Instruments, Inc., PO Box 5012, Dallas, Texas, 75222.
27. Hyltin, T. M. and Pfeifer, L. R., "Annual Report on Molecular Electronics for Radar Applications," Contract AF33(615)-2525, Texas Instruments, Inc., December 1966, and subsequent reports.
28. Jamieson, J., et al, "Infrared Physics and Engineering," McGraw-Hill Book Company, New York, 1963.
29. Jones, H. L., "Recent Advances in Atmospheric Electricity," Pergamon Press, New York, 1958, pp 543-556.
30. Jones, R. R. and Whicker, L. R., "Now - Ferrite Microstrip Devices," Microwaves, January 1969, pp 32-38.
31. Kirkpatrick, G. M., "Angular Accuracy Improvement," Final Engineering Report on Contract DA 36-039-sc-194, 1 August 1952, AD 46,849.
32. Kirkpatrick, G. M., "Clutter Attenuation Radar," U. S. Patent 3,392,387, Filed 4 January 1967, Issued 9 July 1968.
33. Klass, P. J., "Rotor Blade Radar Array to Undergo Test," Aviation Week and Space Technology, 4 July 1966, pp 67-69.
34. Levine, D., "Radargrammetry," McGraw-Hill Book Company, New York, 1960.
35. Marshall, J. S., et al, "Parameters for Airborne Weather Radar," Scientific Report MW-48 (ANTC Report No. 109), May 1965, McGill University.
36. Marshall, S. L., (Editor), "Laser Technology and Applications," McGraw-Hill Book Company, New York, 1968.
37. McFann, H. L., "Outlining Radar Weather Clutter in Digital Processing Systems," Federal Aviation Agency Paper Presented at Aviation Electronics Symposium, U. S. Army Electronics Command, Fort Monmouth, New Jersey, 5-7 March 1968.
38. Miller, B., "Multi-Mode Helicopter Radar Developed," Aviation Week and Space Technology, 26 October 1964, pp 88-91.
39. Miller, B., "Army Plans Rotor Blade Radar Test," Aviation Week and Space Technology, 17 June 1968, pp 66-73.
40. Miller, B., "Moving Target Radar Test Planned," Subtitle, "Army to Evaluate Device Using Solid-State Display in Helicopter; Array Incorporates 2,500 Gallium Arsenide Light Emitting Diodes," Aviation Week and Space Technology, 11 August 1969.

41. Napoli, L. and Hughes, J., "Low-Noise Integrated X-Band Receiver," The Microwave Journal, July 1968, pp 37-42.
42. Odlum, W. J., et al, "Selection of a Phased Array Antenna for Radar Applications," Supplement to IEEE Transactions on Aerospace and Electronic Systems, Vol. AES-3, No. 6, November 1967, pp 226-235.
43. Oetzel, G. N., and Pierce, E. T., "VHF Technique for Locating Lightning," Radio Science, Vol. 4, No. 3, March 1969, pp 199-202.
44. Petritz, R., "Fundamentals of Infrared Detectors," Proc. of IRE, Vol. 47, No. 9, September 1959, p 1458.
45. Plummer, ., "Surface-Wave Beacon Antennas," IRE Transactions on Antennas and Propagation, January 1958, pp 108-112.
46. Poirier, J. L., "Quasi-Monochromatic Scattering and Some Possible Radar Applications," Radio Science, September 1968, pp 881-886.
47. Rhodes, D. R., "Introduction to Monopulse," McGraw-Hill Book Company, Inc., New York, 1959.
48. Robb, J. D. and Newman, N. M., "Lightning Strikes to Plastic Components of Light Aircraft," Society of Automotive Engineers, March 1970, Paper No. 700220.
49. Roome, G. T., "Thin Ferrites for Integrated Microwave Devices," Final Report AFAL-TR-69-149, Dated 15 July 1969, on Contract AF33(615)-3332.
50. Rosenblatt, A., "Potential of Phased-Array Radar Spurs Increasing R&D Activity," Electronics, 2 September 1969, pp 94-103.
51. Ruck, G. E. (Editor), "Radar Cross-Section Handbook," Plenum Press, New York, 1970, Vol. II, Chapter 9.
52. Rudolph, J. F., "Thunderstorms," FAA Advisory Circular, AC No. 100-24, 12 June 1968.
53. Schell, A. C., Sletten, C. J., Blacksmith, P. and Pankiewicz, C. J., "Electronic Scanning," Electro-Technology, November 1968, pp 29-41.
54. Shackford, C. R., "The Relation Between Precipitation and Electrical Activity in New England Thunderstorms," 1958 Proc. 7th Weather Conference, Miami Beach, Florida, pp C-9 and C-15.

55. Siao, T. T., Comments on Paper by Baines, W. D. and Peterson, E. G., "An Investigation of Flow-Through Screens," July 1951, Transactions of the ASME, pp 467-480.
56. Silver, S. (Editor), "Microwave Antenna Theory and Design," Vol. 12, MIT Radiation Laboratory Series, McGraw-Hill Book Company, New York, 1947.
57. Skolnik, M. I., "Introduction to Radar Systems," McGraw-Hill Book Company, New York, 1962.
58. Skolnik, M. I. (Editor), "Radar Handbook," McGraw-Hill Book Company, New York, 1970. (Chapter on Phased Array Antennas.)
59. Stern, E., "Microsound Components, Circuits and Applications," MIT Lincoln Laboratory, Technical Note 1968-36, 30 October 1968.
60. Towmey, S. and Howell, H. B., Applied Optics, Vol. 4, 1965, p 501.
61. Trammell, A., "Night Single-Engine, Yes or No," Flying, Ziff-Davis Publishing Company, September 1969, pp 40-44.
62. Turner, E. M., "Antenna in Perspective," The Microwave Journal, December 1968, pp 32-38.
63. Ward, N. B., et al, "Sferics Reception at 500 KHz, Radar Echoes and Severe Weather," National Severe Storms Laboratory, Norman, Oklahoma, Report RD-65-24, March 1965.
64. Wilk, K. E., et al, "Weather Detection by ARSR-1D, ASR-4, and WSR-57 Radars: A Comparative Study," Technical Memo No. 1, National Severe Storms Laboratory (NSSL), Norman, Oklahoma, March 1965.
65. Wilk, K. E., et al, "Detection and Presentation of Severe Thunderstorms by Airborne and Ground-Based Radars: A Comparative Study," Technical Memorandum ERLTM-NSSL 43, National Severe Storms Laboratory, Norman, Oklahoma, February 1969.
66. Whicker, L. R. and Jones, R. R., "Design Guide to Latching Phase Shifters," (Part I), Microwaves, November 1969, pp 31-39.
67. Whicker, L. R. and Jones, R. R., "Design Guide to Latching Phase Shifters," (Part II), Microwaves, December 1966, pp 43-47.
68. Ziomek, J. F., et al, "Laser Device Detects Objects in Driver's Rear Blind Spot," SAE Journal, April 1970, pp 62-65.

### Miscellaneous Publications

69. "Flight Test Evaluation of Flush-Mounted, Luneberg Lens Antenna for PWI/CAS System," FAA Contract BRD-190, Sperry Report No. CA-4283-0196, December 1961, or see Lorenzo, J. J., et al, "An Airborne Flush-Mounted Scanning Antenna," Sperry Engineering Review, Winter 1963, pp 22-27.
70. Handbook of Geophysics and Space Environments; Air Force Cambridge Research Laboratories, 1965.
71. Air Traffic Training Proficiency Series, "Airborne Weather Radar," Publication S-10, FAA Aeronautical Center, Oklahoma City, Oklahoma, 1 March 1968.
72. "Random Radar," Electronics, McGraw-Hill Publication, 22 July 1968, pp 41-42.
73. "Flat Display Has Inherent Memory," Electronics, 31 March 1969, pp 133-136.
74. "Surface Acoustic Waves Curl Into Radar," Electronics, 25 May 1970, p 45.
75. ARINC Weather Radar Characteristic, No. 564.
76. "1970 Phased-Array Antenna Symposium," Digest and Proceedings Available From Polytechnic Institute of Brooklyn, Long Island Graduate Center, Route 110, Farmingdale, New York 11735.

## APPENDIX A

### RADAR STORM RETURN

Derivations of the radar equation can be found in many reference books (or can be derived from basic considerations); however, Battan's book on "Radar Meteorology" will be followed here. Readers having ready access to Battan's book may prefer to use his more detailed development.

#### The Radar Equation

The power from the transmitter is considered to radiate isotropically. If a sphere of radius,  $r$ , is assumed to enclose the radiating isotropic antenna there is a power flow per unit area through the surface of the sphere equal to the transmitted power divided by the area of the sphere. Directional beams are used to concentrate the power at desired angles where the increase in power flow in a particular direction over isotropic is the antenna gain. If a target is intercepted by the directional antenna beam the intercepted power will be scattered. If the target does not absorb any power but scatters it isotropically, the received power intercepted by the radar antenna is given by Equation (A. 1).

$$P_r = \left( \frac{P_t}{4\pi r^2} \right) G \left( \frac{\sigma}{4\pi r^2} \right) A_e \quad (\text{A. 1})$$

where  $P_r$  = received power, watts

$P_t$  = transmitted power, watts

$r$  = range to target, meters (NM)

$G$  = antenna gain in direction of target

$\sigma$  = target echo area or backscattering cross-section, meters<sup>2</sup>

$A_e$  = effective receiving area of antenna, meters<sup>2</sup>

The antenna gain and effective area are related as shown in Equation (A. 2).

$$G = \frac{4\pi A_e f_e}{\lambda^2} \quad (\text{A. 2})$$

where  $G$  = antenna gain

$A$  = actual area of antenna, meters<sup>2</sup>

$f_e$  = efficiency factor with maximum value one

$\lambda$  = transmitter wavelength, meters

The effective receiving area is the product of the actual area by the efficiency factor, Equations (A.3) and (A.4).

$$A_e = Af_e \quad (\text{A. 3})$$

also

$$A_e = \frac{G\lambda^2}{4\pi} \quad (\text{A. 4})$$

Using Equations (A.2) and (A.3) in Equation (A.1), the expression for received power can be rearranged for a particular problem. For example, for a single scatterer the received power with the actual antenna area as a parameter is:

$$(P_r)_i = \frac{P_t A^2 f^2}{4\pi r^4 \lambda^2} \sigma_i \quad (\text{A. 5})$$

In Equation (A.5),  $\sigma_i$  is the backscattering cross-section of a single scatterer. A weather radar will illuminate a large number of scatterers, e.g., rain drops, at the same time. The number of scatterers is determined by the volume within the product of the beam height, width and pulse length of the radar set. Since the instantaneous received power changes from pulse to pulse because of the random addition of return power from the individual scatterers, the average power is given by Equation (A.6), where the summation is carried out over the scattering volume at each instant.

$$\overline{P_r} = \frac{C_1 P_t A^2}{r^4} \sum_{i=0}^m \sigma_i \quad (\text{A. 6})$$

where  $C_1$  = a constant determined by the unidentified parameters from Equation (A.5).

Equation (A.6) for the average power can be replaced by one in which the reflectivity per unit volume is multiplied by the intercepted volume. Since the beam is not square, the volume must be approximated and, according to Battan, a suitable expression for the volume is given in Equation (A.7).

$$V = \pi \left( r \frac{\theta}{2} \right) \left( r \frac{\phi}{2} \right) \frac{c\tau}{2} \quad (\text{A. 7})$$

where  $V$  = equivalent volume illuminated by radar beam, meters<sup>3</sup>  
 $r$  = range to volume cell, meters (NM)  
 $\theta_{BW}$  = azimuth beamwidth, radians  
 $\phi_{BW}$  = elevation beamwidth, radians  
 $\tau$  = pulse length, seconds  
 $c$  = velocity of propagation,  $3 \cdot 10^8$  meters/second

Assuming the volume of the cell, Equation (A.7), is uniformly filled with precipitation, the expression for average received power can be re-written as in Equation (A.8) using Equations (A.6) and (A.7).

$$\overline{P_r} = \frac{C_2 P_t A c \tau}{r^2} \sum_{\text{vol}} \sigma_i \quad (\text{A. 8})$$

where  $C_2$  = a modified constant  
 $\sum_{\text{vol}} \sigma_i$  = radar reflectivity per unit volume, meters<sup>2</sup>/meter<sup>3</sup>

The significant differences between Equations (A.6) and (A.8) are in the inverse fourth power relation for range in (A.6) and the inverse second power in (A.8); also, the right side of Equation (A.6) varies as the square of the aperture area and Equation (A.8) directly as the area. Since storm cells usually have a limited extent, Equation (A.6) applies when determining the storm detection range (maximum range) of a radar, and Equation (A.8) when the beam is filled and the radar is used to analyze the intensity of a particular storm cell.

#### Scattering by Spherical Water or Ice Particles

Following Battan, when a plane polarized wave passes over a spherical drop, it induces oscillating electric and magnetic dipoles within the drop. Energy is taken from the incident field. Part of the energy is absorbed as heat by the drop, and part is reradiated as a scattered electromagnetic field having the same wavelength as the incident energy. A general treatment of the problem of scattering of a plane wave by a sphere was made by Mie and has also been studied by Stratton, Kerr and others. For the case where the



drop radius,  $a$ , is much less than the wavelength and where the ratio  $2\pi a/\lambda$  is much less than one, the backscattering by a single spherical droplet is given by Equation (A.9a) or (A.9b).

$$\sigma_i = 64 \frac{\pi^5}{\lambda^4} |K_r|^2 a_i^6 \quad (\text{A.9a})$$

or

$$\sigma_i = \frac{\pi^5}{\lambda^4} |K_r|^2 D_i^6 \quad (\text{A.9b})$$

where  $a_i$  = radius of  $i$ th drop, meters

$D_i$  = diameter of  $i$ th drop, meters

$K_r$  = factor describing the complex index of refraction

For water drops at centimeter wavelengths,  $|K_r|^2$  is equal to approximately 0.93 and for ice particles 0.19. The strong dependence upon particle size and wavelength should be noted in Equations (A.9). Again, two cases can be considered paralleling Equations (A.6) and A.8). First, when the beam is not filled, from Equations (A.6) and (A.9) obtain Equation (A.10).

$$\overline{P_r} = \frac{P_t A^2 f^2 \pi^4}{r^4 4 \lambda^4} |K_r|^2 V \sum_{\text{vol}} D_i^6 \quad (\text{A.10})$$

and second, for the beam filling case obtain Equation (A.11)

$$\overline{P_r} = \frac{C_3 P_t A \tau}{r^2} \sum D_i^6 \quad (\text{A.11})$$

According to Battan, it has become common practice to specify particle sizes in terms of their diameters and to use the symbol  $Z$  to replace  $\sum_{\text{vol}} D_i^6$  with the approximate value of  $Z$  as a function of liquid water con-

tent for various types of precipitation given by the following three equations, Equations (A.12), (A.13), and (A.14).

$$\text{Clouds:} \quad Z = 4.8 \cdot 10^{-8} M_w^{2.0} \quad (\text{A.12})$$

$$\text{Snow Aggregates:} \quad Z = 9.6 \cdot 10^{-3} M_w^{2.2} \quad (\text{A.13})$$

$$\text{Rain:} \quad Z = 8.3 \cdot 10^{-2} M_w^{1.82} \quad (\text{A.14})$$

where  $M_w$  = liquid water content milligrams per meter<sup>3</sup>

$Z$  = generally given as millimeters to the sixth power per meter<sup>3</sup>  
but must be converted to meters<sup>6</sup>/meter<sup>3</sup> for Equation (A.10)  
and Equation (A.11).

A more familiar form of expressing the precipitation rate is the rainfall rate,  $R$ , in millimeters (or inches) per hour and after revising Equation (A.14) from  $M_w$  to  $R$  obtain Equation (A.15) for rain.

$$Z = 200 R^{1.6} \quad (\text{A.15})$$

where  $R$  = rainfall rate in millimeters per hour.

The calculated values of precipitation intensity from radar measurements, using the filled beam Equation (A.11), do not compare favorably with measured precipitation rates determined by rain gauges. According to Battan, the observed radar signal is about 5 to 10 dB below the theoretical signal level even after careful examination and correction for all approximations. At the present time, the reason for this discrepancy is unknown and a correction factor of 5 dB is recommended for X-Band. Marshall has suggested that a factor  $F$ , less than one, be used for this correction in Equations (A.10) and (A.11). ( $F = 0.3$  at X-Band corresponds to the 5 dB recommended correction.)

### Attenuation of Microwaves

Following Battan, the attenuation of microwaves is the reduction of intensity of the wave along its path and is defined as:

$$d\overline{P}_r = 2 k_1 \overline{P}_r dr \quad (\text{A.16})$$

where  $\overline{P}_r$  = received power, watts

$d\overline{P}_r$  = incremental reduction of  $\overline{P}_r$ , watts

$r$  = range, meters (NM)

$k_1$  = attenuation coefficient, meters<sup>-1</sup>, generally dB/meter

and the factor, 2, is necessary to account for the radar power traversing the same path twice. When Equation (A.16) is integrated over the range 0 to  $r$ , the result is given by Equation (A.17).

$$\overline{P}_r = \overline{P}_{r0} \exp \left( -2 \int_0^r k_1 dr \right) \quad (\text{A.17})$$

where  $\overline{P}_{r0}$  = power received at range  $r$  without attenuation.

It is customary to use decibels to express power loss or gain, so in terms of dB, the attenuation of microwaves by atmospheric gases, clouds, and precipitation is given by Equation (A.18)

$$\text{dB} = 10 \log_{10} \frac{\overline{P}_r}{\overline{P}_{r0}} = -2 \int_0^r (k_g + k_c + k_p) dr \quad (\text{A.18})$$

where  $k_g$ ,  $k_c$ , and  $k_p$  represent the attenuation (in decibels per unit of range one way) by gases, cloud and precipitation, respectively.

In general, gases act only as absorbers, but cloud and raindrops, as pointed out earlier, both scatter and absorb. At wavelengths greater than a few centimeters, attenuation by atmospheric gas is very small and can be neglected. On the other hand, cloud and rain attenuation is significant at wavelengths shorter than S-Band and can have serious effects in X- and K-Bands. Values for the attenuation coefficient for clouds,  $k_c$ , can be found in Battan, page 47. The factors,  $K_2$  and  $\gamma$ , which determine the more significant attenuation associated with rain, are repeated here in Table A.1 from Battan, page 49, for use in Equation (A.19).

TABLE A.1  
TWO-WAY ATTENUATION FACTORS  $K_2$  AND  $\gamma$

$\lambda$ Parameter	Wavelength (cm) and Band				
	$K_a$ $\lambda - 0.9 \text{ cm}$	$K_u$ $\lambda - 1.8 \text{ cm}$	X $\lambda - 3.2 \text{ cm}$	C $\lambda - 5.6 \text{ cm}$	S $\lambda - 10.0 \text{ cm}$
$2K_2$	0.82	0.168	0.026	0.0082	0.0011
$\gamma$	1.00	1.14	1.31	1.17	1.00

$$2k_p = 2K_2 R^\gamma \quad (\text{A.19})$$

where  $R$  is the rainfall rate in millimeters per hour.

Since the shorter wavelengths, such as 1.8 cm (K<sub>u</sub>-Band) and 3.2 cm (X-Band) are desirable to obtain narrow beams with small apertures, a warning on the use of short wavelengths given by Battan will be repeated here. "Quantitative radar studies made with 3 cm radar have frequently given disappointing results. It is evident that, for quantitative rainfall measurements, radar sets operating at non-attenuating wavelengths should be used whenever possible." While a GA pilot is not interested in making exact measurements on storms, he must estimate the storm severity from reasonably accurate quantitative radar observations.

## APPENDIX B

### RADAR RANGE CALCULATIONS

Starting with the radar equation from Appendix A, the power signal-to-noise ratio (S/N) in the radar receiver is given by Equation (B.1):

$$\frac{S}{N} = \frac{P_t G_t G_r \lambda^2 L V}{(4\pi)^3 r^4 k T \beta NF} \sum_{\text{vol}} \sigma_i \quad (\text{B.1})$$

where the symbols are as defined in Appendix A except

$k$  = Boltzman s constant,  $1.38 \cdot 10^{-23}$  j/degree Kelvin

$T$  = absolute temperature, 290 degrees Kelvin

$\beta$  = receiver bandwidth, Hz

$NF$  = receiver noise figure

$L$  = loss factor

$V$  = volume of precipitation, meters<sup>3</sup>

$\sum_{\text{vol}} \sigma_i$  = cross-section area per unit volume, meters<sup>2</sup>/meter<sup>3</sup>

The target cross-section per unit volume, Equation (B.2), is derived from Equation (A.9b).

$$\sum_{\text{vol}} \sigma_i = \frac{\pi^5 |K_r|^2}{\lambda^4} \sum_{\text{vol}} D_i^6 \quad (\text{B.2})$$

The summation over the droplet diameters,  $D_i$ , can be replaced by the expression Equation (B.3), the empirically determined  $Z$ , as in Equation (A.15).

$$Z = 200 R^{1.6} \quad (\text{B.3})$$

where  $R$  = rainfall rate in mm/hour

$Z$  = proportional to radar cross-section, mm<sup>6</sup>/m<sup>3</sup>

Combining Equations (B.1), (B.2), and (B.3), including an integration factor,  $M$ , and solving for  $r$ , the radar range is given by Equation (B.4).

$$r = \left[ \left( \frac{\pi^2 |K_r|^2 200}{64 kT \cdot 10^{11}} \right) \frac{P_t G_t G_r L M^{\frac{1}{2}} V R^{1.6}}{(S/N) \beta (NF) \lambda^2} \right]^{\frac{1}{4}} \quad (B.4)$$

The numerical terms in the brackets in Equation (B.4) are designated as C with the value  $3.08 \cdot 10^{-10}$  and the units for the other symbols are:

$P_t$	= transmitter power, kilowatts
$G_t$	= antenna gain on transmit, dimensionless
$G_r$	= antenna gain on receive, dimensionless
$L$	= loss factor
$M$	= number of pulses integrated (the square root corresponds to non-coherent integration)
$V$	= intercepted volume with precipitation, meters <sup>3</sup> , from Eq. (A-7)
$R$	= rainfall rate, mm/hour
$k$	= Boltzman's constant, $1.38 \cdot 10^{-23}$ joule/degree Kelvin
$T$	= absolute temperature, 290 degrees Kelvin
$S/N$	= power signal-to-noise ratio required for single pulse detection (10 dB)
$\beta$	= receiver bandwidth, Hz
$NF$	= noise figure, dimensionless
$\lambda$	= wavelength, centimeters

For convenience in computing the value of Equation (B.4) for various combinations of parameter values a range estimation form has been prepared. The form has been used to estimate the detection range of a conventional weather radar and two proposed radars. Additional blank forms are included in this appendix for range estimation for other parameter value combinations.

The integration term,  $M$ , is based upon the non-coherent integration of the available pulses in either one scan (for mechanical scanning) or one second for electronic scanning. Experiments have shown that observers can effectively use integration periods as long as 10 seconds; however, it is not considered feasible to concentrate on a weather display for longer than one or two seconds because of the need to maintain a watch for other traffic. The single pulse signal-to-noise ( $S/N$ ) ratio of 10 dB for detection is used as the  $S/N$  before integration. This  $S/N$  of 10 dB for single pulse detection has been determined empirically by Lawson and others for the case where the

TABLE B. 1  
CONVENTIONAL WEATHER RADAR WITH 12 INCH DISH

$C = 3.08 \cdot 10^{-10} \quad r = \left[ \frac{C P_t G_t G_r L M^{\frac{1}{2}} V R^{1.6}}{(S/N) \beta (NF) \lambda^3} \right]^{\frac{1}{4}}$					
Transmitter Peak Power	$P_t$	10 KW	Transmitter Vertical Beamwidth	BW	7 deg.
Transmitter Antenna Gain	$G_t$	26.5 dB	Transmitter Horizontal Beamwidth	BW	7 deg.
Receiver Antenna Gain	$G_r$	26.5 dB	Receiver Vertical Beamwidth	BW	7 deg.
Transmitter Wave Length	$\lambda$	3.2 cm	Receiver Horizontal Beamwidth	BW	7 deg.
Noise Figure	NF	10 dB	Scan Sector		90 deg.
Signal-to-Noise (Power)	S/N	10 dB	Scan Rate		70 min <sup>-1</sup>
Loss Factor	L	3 dB	Pulse Repetition Frequency	PRF	400 sec <sup>-1</sup>
Pulses Integrated	M	27	Pulse Length	$\tau$	2.5 $\mu$ sec
Volume Intercepted*	V	3.54 · 10 <sup>9</sup> m <sup>3</sup>	Losses a) Radome (2-Way) b) Phase Shifter c) Duplexer Total Losses		1 dB dB 2 dB 3 dB
Receiver Bandwidth	$\beta$	1 MHz			
Remarks: No scan-to-scan integration (27 pulses/scan). * ARINC Specifications 564 Target; 3 NM Sphere; 1 $\mu$ s Pulse; $r \times BW \geq NM$ ; No Attenuation. ** $r \times BW$ less than 3 NM.					

Range Enhancement Factors REF	dB (10 log <sub>10</sub> X)	Range Degradation Factors RDF	dB (10 log <sub>10</sub> X)
Constant Factors	108.6		
$P_t$	10.0	NF	10.0
$G_t$	26.5	L	3.0
$G_r$	26.5	S/N	10.0
S/N		$\lambda^3$	10.1
$M^{\frac{1}{2}}$	7.2	F (Marshall)	5.0
V	95.5	$\beta$	60.0
$R^{1.6}$ (R = 1 mm/hour)	0.0		
$\Sigma$ REF	274.3	$\Sigma$ RDF	98.1
$(\Sigma$ REF - $\Sigma$ RDF) = 176.2 $(\Sigma$ REF - $\Sigma$ RDF)/40 = 4.405 = Meters ( $\times 5.4 \cdot 10^{-4}$ ) = 86.5 NM			
R = 100 mm/hour	r = 6.31 x		66.6
R = 50 mm/hour	r = 4.86 x		34.4
R = 10 mm/hour	r = 2.51 x		26.0
R = 5 mm/hour	r = 1.9 x		(13.7)**
R = 1 mm/hour	r = log <sub>10</sub> <sup>-1</sup> 4.405 = 2.54 · 10 <sup>4</sup>		

TABLE B.2  
WEATHER RADAR WITH ELECTRONIC SCANNING AND GRATING REFLECTOR  
(Figure 3.20)

RANGE ESTIMATION FORM					
$C = 3.08 \cdot 10^{-10}$ $r = \left[ \frac{C P_t G_t G_r L M^{\frac{1}{2}} V R^{1.6}}{(S/N) \beta (NF) \lambda^2} \right]^{\frac{1}{4}}$					
Transmitter Peak Power	$P_t$	10 KW	Transmitter Vertical Beamwidth	BW	7 deg.
Transmitter Antenna Gain	$G_t$	26 dB	Transmitter Horizontal Beamwidth	BW	7 deg.
Receiver Antenna Gain	$G_r$	26 dB	Receiver Vertical Beamwidth	BW	7 deg.
Transmitter Wave Length	$\lambda$	3.2 cm	Receiver Horizontal Beamwidth	BW	7 deg.
Noise Figure	NF	10 dB	Scan Sector		90 deg.
Signal-to-Noise (Power)	S/N	10 dB	Scan Rate		20 sec <sup>-1</sup>
Loss Factor	L	7 dB	Pulse Repetition Frequency	PRF	1000 sec <sup>-1</sup>
Pulses In' grated	M	80	Pulse Length	$\tau$	1 $\mu$ sec.
Volume Intercepted*	V	3.54 · 10 <sup>9</sup> m <sup>3</sup>	Losses		
			a) Radome (2-Way)		0 dB
			b) Phase Shifter		5 dB
			c) Duplexer		2 dB
			Total Losses		7 dB
Receiver Bandwidth	$\beta$	1 MHz			
Remarks: Assumes scan-to-scan integration of one second duration (80 pulses). * ARINC Specifications 564 Target; 3 NM Sphere; 1 $\mu$ s Pulse; $r \times BW \geq 3$ NM; No Attenuation. ** $r \times BW$ less than 3 NM.					

Range Enhancement Factors REF	dB (10 log <sub>10</sub> X)	Range Degradation Factors RDF	dB (10 log <sub>10</sub> X)
Constant Factors	108.6		
P <sub>t</sub>	10.0	NF	10.0
G <sub>t</sub>	26.0	L	7.0
G <sub>r</sub>	26.0	S/N	10.0
S/N		λ <sup>2</sup>	10.1
M <sup>1/2</sup>	9.5	F (Marshall)	5.0
V	95.5	β	60.0
R <sup>1.6</sup> (R = 1 mm/hour)			
ΣREF	275.6	ΣRDF	102.1
(ΣREF - ΣRDF) = 173.5                      (ΣRef - ΣRDF)/40 = 4.34 R = 100 mm/hour    r = 6.31 x 3.10 <sup>4</sup> = Meters (x 5.4 · 10 <sup>-4</sup> ) = 74.5 NM R = 50 mm/hour    r = 4.86 x    57.4 R = 10 mm/hour    r = 2.51 x    29.6 R = 5 mm/hour    r = 1.9 x    (22.4)** R = 1 mm/hour    r = log <sub>10</sub> <sup>-1</sup> 4.34 = 2.18 · 10 <sup>4</sup> (11.8)**			



TABLE B. 3  
WEATHER RADAR WITH INTRA-PULSE SCANNING AND CROSSED-BEAM ANTENNA  
(Sections 3.13 and 5.4)

RANGE ESTIMATION FORM					
$C = 3.08 \cdot 10^{-10} \quad r = \left[ \frac{C P_t G_t G_r L M^{\frac{1}{2}} V R^{1.6}}{(S/N) \beta (NF) \lambda^2} \right]^{\frac{1}{4}}$					
Transmitter Peak Power	$P_t$	10 KW	Transmitter Vertical Beamwidth	BW	7 deg.
Transmitter Antenna Gain	$G_t$	15.4 dB	Transmitter Horizontal Beamwidth	BW	90 deg.
Receiver Antenna Gain	$G_r$	23 dB	Receiver Vertical Beamwidth	BW	15 deg.
Transmitter Wave Length	$\lambda$	3.2 cm	Receiver Horizontal Beamwidth	BW	7 deg.
Noise Figure	NF	10 dB	Scan Sector		90 deg.
Signal-to-Noise (Power)	S/N	10 dB	Scan Rate		1000 sec <sup>-1</sup>
Loss Factor	L	1 dB	Pulse Repetition Frequency	PRF	1000 sec <sup>-1</sup>
Pulses Integrated	M	10 <sup>4</sup>	Pulse Length	$\tau$	1 $\mu$ sec.
Volume Intercepted	V	3.54 · 10 <sup>9</sup> m <sup>3</sup>	Losses		
			a) Radome (2-Way)		1 dB
			b) Phase Shifter		dB
			c) Duplexer		dB
			Total Losses		1 dB
Receiver Bandwidth	$\beta$	1 MHz			
Remarks: Assumes integration period of one second with 10 <sup>3</sup> pulses integrated. * ARINC Specifications 564 Target; 3 NM Sphere; 1 $\mu$ s Pulse; $r \times BW \geq 3$ NM; No Attenuation. ** $r \times BW$ less than 3 NM.					

Range Enhancement Factors REF	dB (10 log <sub>10</sub> X)	Range Degradation Factors RDF	dB (10 log <sub>10</sub> X)
Constant Factors	108.6		
$P_t$	10.0	NF	10.0
$G_t$	15.4	L	1.0
$G_r$	23.0	S/N	10.0
S/N		$\lambda^2$	10.1
$M^{\frac{1}{2}}$	15.0	F (Marshall)	5.0
V	95.5	$\beta$	60.0
$R^{1.6}$ (R = 1 mm/hour)			
$\Sigma$ REF	267.5	$\Sigma$ RDF	96.1
$(\Sigma$ REF - $\Sigma$ RDF) = 171.4		$(\Sigma$ REF - $\Sigma$ RDF)/40 = 4.29	
R = 100 mm/hour	r = 6.31 x	= Meters (x 5.4 · 10 <sup>-4</sup> ) = 66.5 NM	
R = 50 mm/hour	r = 4.86 x	51.0	
R = 10 mm/hour	r = 2.51 x	26.4	
R = 5 mm/hour	r = 1.9 x	(20.0)**	
R = 1 mm/hour	r = log <sub>10</sub> <sup>-1</sup> 4.29 = 1.95 × 10 <sup>4</sup> x 5.4 · 10 <sup>-4</sup>	(10.5)**	

TABLE B.4

RANGE ESTIMATION FORM					
$C = 3.08 \cdot 10^{-10}$ $r = \left[ \frac{P_t G_t G_r L M^{\frac{1}{2}} V R^{1.6}}{(S/N) \beta (NF) \lambda^2} \right]^{\frac{1}{2}}$					
Transmitter Peak Power	$P_t$	KW	Transmitter Vertical Beamwidth	BW	deg.
Transmitter Antenna Gain	$G_t$	dB	Transmitter Horizontal Beamwidth	BW	deg.
Receiver Antenna Gain	$G_r$	dB	Receiver Vertical Beamwidth	BW	deg.
Transmitter Wave Length	$\lambda$	cm	Receiver Horizontal Beamwidth	BW	deg.
Noise Figure	NF	dB	Scan Sector		deg.
Signal-to-Noise (Power)	S/N	dB	Scan Rate		sec <sup>-1</sup>
Loss Factor	L	dB	Pulse Repetition Frequency	PRF	sec <sup>-1</sup>
Pulses Integrated	M		Pulse Length	$\tau$	$\mu$ sec.
Volume Intercepted	V	m <sup>3</sup>	Losses	a) Radome (2-Way) b) Phase Shifter c) Duplexer Total Losses	dB dB dB dB
Receiver Bandwidth	$\beta$	MHz			
Remarks					

Range Enhancement Factors REF	dB (10 log <sub>10</sub> X)	Range Degradation Factors RDF	dB (10 log <sub>10</sub> X)
Constant Factors	148.6		
$P_t$		NF	
$G_t$		L	
$G_r$		S/N	
S/N		$\lambda^2$	
$M^{\frac{1}{2}}$		F (Marshall)	
V	95.5	$\beta$	
$R^{1.6}$ (R = 1 mm/hour)	0.0		
$\Sigma$ REF		$\Sigma$ RDF	
$(\Sigma$ REF - $\Sigma$ RDF) =		$(\Sigma$ REF - $\Sigma$ RDF)/40 =	
R = 100 mm/hour    r =		= (x 5.4 · 10 <sup>-4</sup> ) =    NM	
R = 50 mm/hour    r =			
R = 10 mm/hour    r =			
R = 5 mm/hour    r =			
R = 1 mm/hour    r = log <sub>10</sub> <sup>-1</sup> ( $\Sigma$ REF - $\Sigma$ RDF)/40 = log <sup>-1</sup>			

TABLE B.5

RANGE ESTIMATION FORM					
$C = 3.08 \cdot 10^{-10}$ $r = \left[ \frac{P_t G_t G_r L M^{\frac{1}{2}} V R^{1.6}}{(S/N) \beta (NF) \lambda^2} \right]^{\frac{1}{4}}$					
Transmitter Peak Power	$P_t$	KW	Transmitter Vertical Beamwidth	BW	deg.
Transmitter Antenna Gain	$G_t$	dB	Transmitter Horizontal Beamwidth	BW	deg.
Receiver Antenna Gain	$G_r$	dB	Receiver Vertical Beamwidth	BW	deg.
Transmitter Wave Length	$\lambda$	cm	Receiver Horizontal Beamwidth	BW	deg.
Noise Figure	NF	dB	Scan Sector		deg.
Signal-to-Noise (Power)	S/N	dB	Scan Rate		sec <sup>-1</sup>
Loss Factor	L	dB	Pulse Repetition Frequency	PRF	sec <sup>-1</sup>
Pulses Integrated	M		Pulse Length	$\tau$	μsec.
Volume Intercepted	V	m <sup>3</sup>	Losses a) Radome (2-Way) b) Phase Shifter c) Duplexer Total Losses		dB dB dB dB
Receiver Bandwidth	$\beta$	MHz			
Remarks:					

Range Enhancement Factors REF	dB (10 log <sub>10</sub> X)	Range Degradation Factors RDF	dB (10 log <sub>10</sub> X)
Constant Factors	148.6		
$P_t$		NF	
$G_t$		L	
$G_r$		S/N	
S/N		$\lambda^2$	
$M^{\frac{1}{2}}$		F (Marshall)	
V	95.5	$\beta$	
$R^{1.6}$ (R = 1 mm/hour)	0.0		
$\Sigma$ REF		$\Sigma$ RDF	
$(\Sigma$ REF - $\Sigma$ RDF) =		$(\Sigma$ REF - $\Sigma$ RDF)/40 =	
R = 100 mm/hour	r =	= (x 5.4 · 10 <sup>-4</sup> ) = NM	
R = 50 mm/hour	r =		
R = 10 mm/hour	r =		
R = 5 mm/hour	r =		
R = 1 mm/hour	r = log <sub>10</sub> <sup>-1</sup> (ΣREF - ΣRDF)/40 = log <sup>-1</sup>		

observer knows the signal is present. When the observer does not know whether the signal is present, then false alarms must also be considered. A single pulse S/N of 15 dB may be more realistic in order to reduce the possibility of false alarm to a negligible level. This will reduce the ranges calculated in Tables B-1 through B-3 by about 25%.

## APPENDIX C

### DERIVATION OF ANGLES FOR SPHERICAL EARTH MODEL

The angles of interest are shown in a sketch, Figure C.1, where the earth curvature and the size of the storm are not to scale. For the a, b, and c triangle in Figure C.1 the angle  $\alpha$  opposite the side a can be determined from the relation, Equation (C.1), between an angle and the sides of a plane triangle.

$$\cos\left(\frac{\alpha}{2}\right) = \left[\frac{s(s-a)}{bc}\right]^{\frac{1}{2}} \quad (C.1)$$

$$\text{where } s = 1/2 [a + b + c] \quad (C.2)$$

$$\text{and } a = p + h_2 \quad (C.3)$$

$$b = p + h_1 \quad (C.4)$$

$$c = r \quad (C.5)$$

$p$  = earth radius (4/3 actual earth radius, or (4/3 x 3440 = 4580 NM)

$h_1$  = height of aircraft over earth

$h_2$  = height of storm (zero for terrain) over the earth

$r$  = range from aircraft to terrain or storm

From the triangle property, Equation (C.1), the angle  $\theta$  is

$$\theta = \sin^{-1} \left[ \frac{2p(h_1 - h_2) + (h_1 + h_2)(h_1 - h_2) + r^2}{2r(h_1 + p)} \right]; \text{ where } \theta = \alpha - \frac{\pi}{2} \quad (C.6)$$

For the storm, the approximate value of  $\theta$  is (designated as  $\theta_s$ )

$$\theta_s = \sin^{-1} \left[ \frac{h_1 - h_2}{r} + \frac{r}{2p} \right] \quad \text{for } p \gg h_1 \text{ or } h_2 \quad (C.7)$$

or small angles.

$$\theta_s = \left[ \frac{h_1 - h_2}{r} + \frac{r}{2p} \right] \quad \text{for } \theta < 1; h_1 \text{ and } h_2 \ll p \quad (C.8)$$

For the terrain,  $h_2$  is assumed zero and Equation (C.6) for  $\theta$  becomes (designated  $\theta_t$ )

$$\theta_t = \sin^{-1} \left[ \frac{h_1}{r} + \frac{r}{2p} \right] \quad \text{for } p \gg h_1 \quad (C.9)$$

$$\theta_t = \frac{h_1}{r} + \frac{r}{2p} \quad \text{for } \theta < 1; p \gg h_1 \quad (\text{C.10})$$

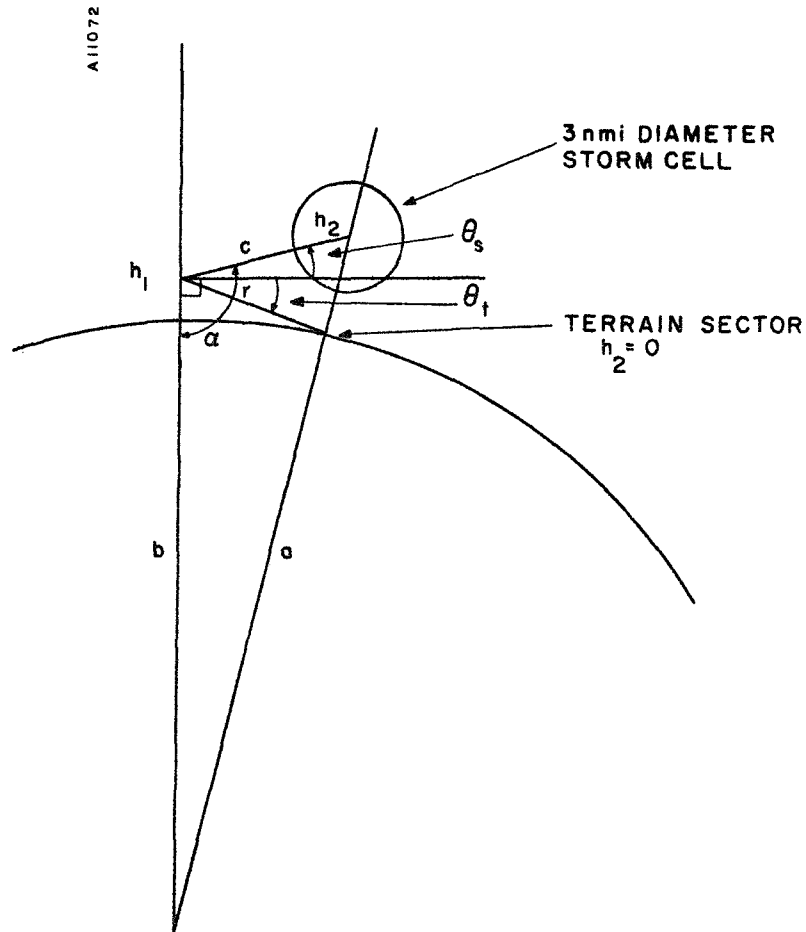


FIGURE C.1 GEOMETRIC RELATIONSHIPS FOR DETERMINING DEPRESSION ANGLE TO TERRAIN AND STORM, AND ANGLE OF INCIDENCE ON TERRAIN

For a flat earth the grazing angle between the radar line-of-sight and the terrain sector is equal to the angle of depression. For a spherical earth this relationship no longer holds, and from the triangle relation, Equation (C.1), the grazing angle opposite side  $b$  is given by Equation (C.11).

$$\theta_g = \sin^{-1} \left[ \frac{h_1}{r} + \frac{h_1^2}{2pr} - \frac{r}{2p} \right] \quad (\text{C.11})$$

For  $p \gg h_1$  the above becomes

$$\theta_g = \sin^{-1} \frac{h_1}{r} - \frac{r}{2p} \quad (\text{C.12})$$

and for  $\theta_g \ll 1$

$$\theta_g = \frac{h_1}{r} - \frac{r}{2p} . \quad (\text{C.13})$$

The difference between the expressions for the grazing angle, Equation (C.13), and the terrain angle, Equation (C.9), is the sign of the second term, plus in one and negative for the other. If the relationship  $r_{\text{LOS}} = (2ph_1)^{\frac{1}{2}}$ , for the line-of-sight distance, is substituted into Equations (C.9) and (C.13), then the terrain angle, doubles over the value for a flat earth approximation and the grazing angle is zero indicating the LOS is tangent to the terrain.

The total angle between the storm center and the terrain sector, at the same range, is nearly constant over a considerable extent of aircraft altitudes,  $h_1$ , for a fixed storm height,  $h_2$ . This is demonstrated by subtracting Equation (C.8) from Equation (C.10).

$$\theta_t - \theta_s = h_2/r \quad \text{for } \theta_t \text{ and } \theta_s \ll 1 \quad (\text{C.14})$$

# APPENDIX D ANALYSIS OF CLUTTER ATTENUATION

The clutter packet has a finite extent in both azimuth and in range, whereas the beam crossover (null) is a line so the cancellation of ground clutter will not be complete. The width of the clutter packet in elevation angle,  $\delta\theta$ , is derived first and, using this angle, the cancellation ratio is computed assuming perfect tracking of the center of the instantaneous clutter packet in elevation. The pulse packet will be  $c\tau/2$  long in radial dimension, where  $\tau$  is the pulse length and  $c$  the velocity of propagation (velocity of light). The width of the packet in azimuth is  $r\phi_{BW}$ , where  $r$  is the slant range to the packet and  $\phi_{BW}$  is the azimuth beamwidth.

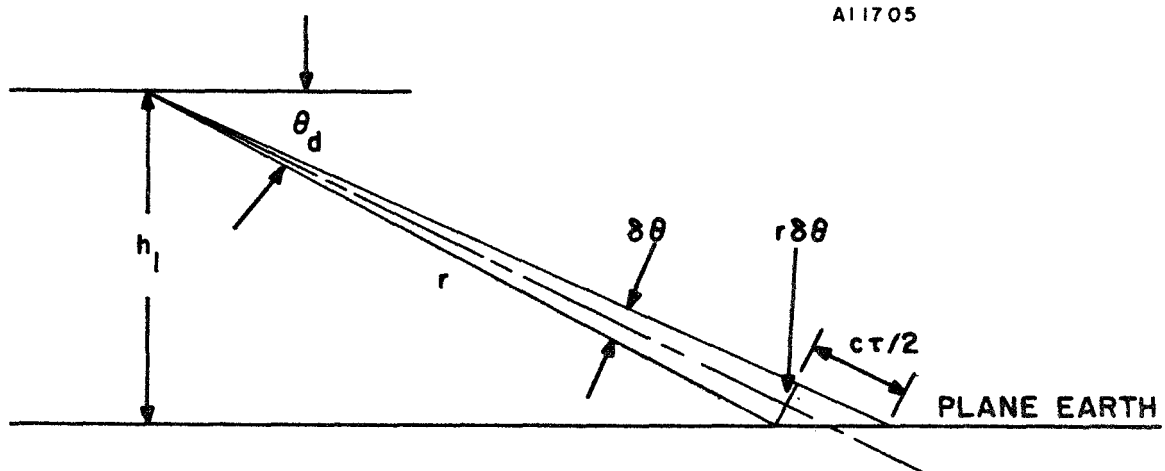


FIGURE D.1 SKETCH USED TO DERIVE  $\delta\theta$



Referring to Figure D.1, the following relations hold for the right triangles:

$$\frac{r\delta\theta}{c\tau/2} = \tan \theta_d \text{ and } r = \frac{h_1}{\sin \theta_d} \quad (\text{D.1})$$

where  $\theta_d$  = depression angle

$r$  = slant range to clutter element

$c$  = velocity of light, 986 feet/ microsecond

$\tau$  = pulse length

$h_1$  = height of the radar

Solving for  $\delta\theta$  as a function of  $\theta_d$ , and eliminating  $r$ , using the two relations in (D.1), the result is:

$$\delta\theta = \frac{c\tau}{2h_1} \frac{\sin^2 \theta_d}{\cos \theta_d} \quad (\text{D.2})$$

The functional dependence of  $\delta\theta$  on  $\theta_d$  for two selected values of the parameter  $c\tau/2h_1$  is shown on Figure D.2. Under the assumption that the null is pointed at the center of the clutter patch at a particular instant the elevation beams are positioned as sketched in Figure D.3. In addition, the clutter is assumed to consist of many individual elements more or less independent of each other and sufficiently numerous that any given target area usually contains a large number of clutter elements. Targets at the crossover are received on the sum pattern with a gain  $G_0$  and the voltage gain of the difference pattern varies in a linear manner near the crossover.

$$G^{\frac{1}{2}} \sim K\alpha \quad \text{for } \alpha < 1 \quad (\text{D.1})$$

where  $G = 4\pi a_d f / \lambda^2$

$G_0$  = maximum value of  $G$ , ( $f = 1$ )

$$K = \frac{\partial G^{\frac{1}{2}}}{\partial \alpha} \quad (\text{D.2})$$

$$K_0 = \text{maximum value of } K = G_0^{\frac{1}{2}} / \sqrt{12} \quad (\text{D.3})$$

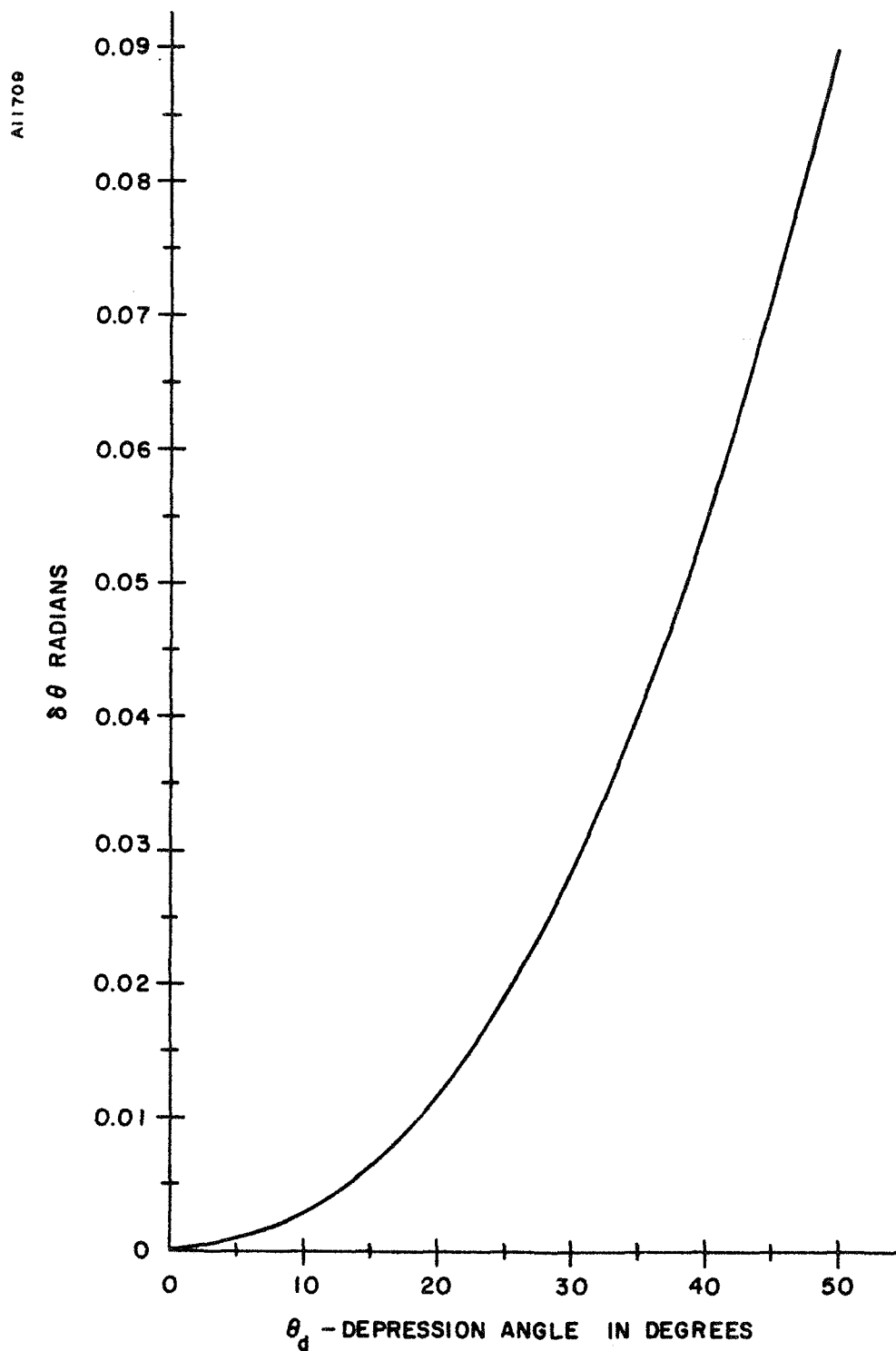


FIGURE D.2  $\delta\theta$  AS A FUNCTION OF DEPRESSION ANGLE  
 FROM EQUATION (D.2) FOR  $(c\tau/2h_1) = 0.1$   
 (e.g.,  $\tau = 0.1$  microseconds;  $h_1 = 500$  feet)

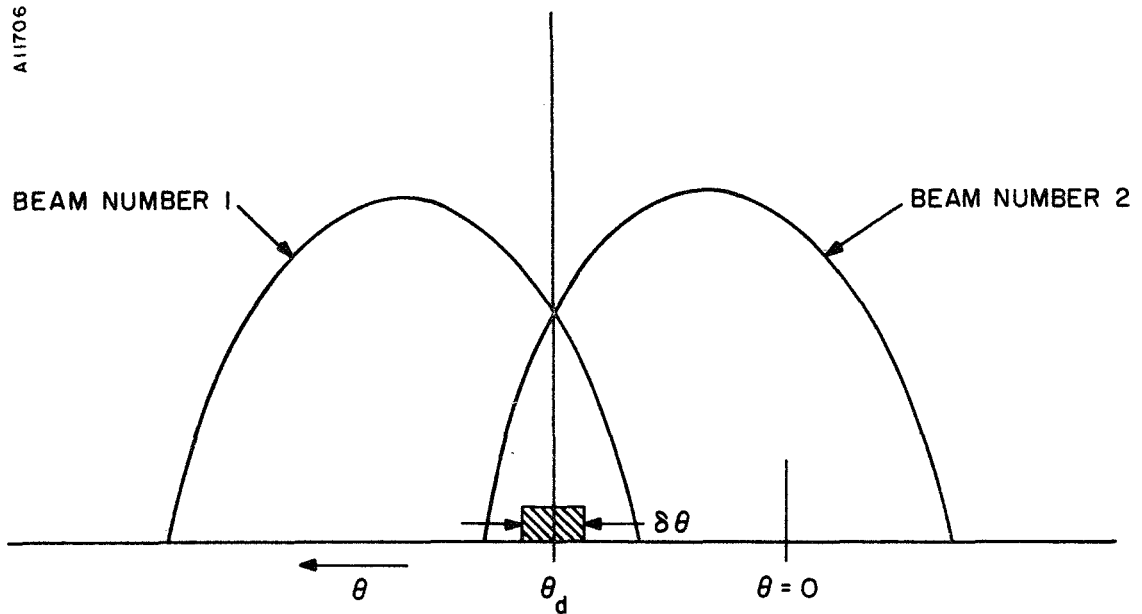


FIGURE D.3 CLUTTER PACKET AT CROSSOVER OF ELEVATION BEAMS

and  $G$  = antenna power gain

$a$  = antenna aperture dimension in  $\theta$  direction

$d$  = antenna aperture dimension in the  $\phi$  direction

$f$  = antenna efficiency factor

$\lambda$  = wavelength

$\alpha$  = electrical angle  $[2\pi a_1 \sin \theta]/\lambda$  (D.4)

Referring to Figure D.3 at a particular instant of time, the clutter subtends a vertical angle of plus and minus  $\delta\theta/2$  about a depression angle of  $\theta_d$ . If a new figure is constructed with signal amplitude (either clutter or antenna pattern response) as the ordinate and centered at the angle  $\theta_d$ , Figure D.4 results

Under the given assumptions, the ratio by which the clutter is attenuated is  $R_c$ .

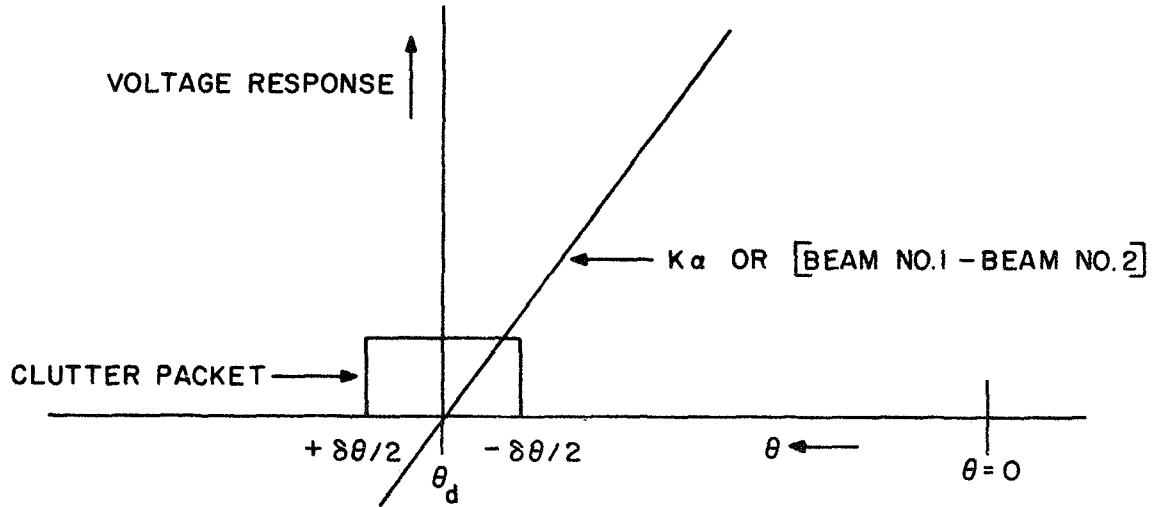


FIGURE D.4 SKETCH FOR CLUTTER ATTENUATION CALCULATION

$$R_c = \frac{\int_{-\delta\theta'/2}^{\delta\theta'/2} G_0 \sigma^0 \sin \theta_d r^2 \phi_{BW} d\theta'}{\int_{-\delta\theta'/2}^{\delta\theta'/2} [K 2\pi a_1 \theta'/\lambda]^2 \sigma^0 \sin \theta_d r^2 \phi_{BW} d\theta'} \quad (D.5)$$

- where  $\sigma^0$  = radar cross-section per unit of intercepted area  
 $\phi_{BW}$  = antenna beamwidth in  $\phi$  (azimuth) direction  
 $\theta_d$  = depression angle-to-clutter patch  
 $r$  = range-to-clutter patch  
 $\delta\theta$  = elevation angle subtended by clutter patch in radians

$$R_c = 144 \lambda^2 / (2\pi a_1)^2 (\delta\theta)^2 \quad (D.6)$$

The above result (D.6) indicates that a small vertical aperture  $a_1/\lambda$  gives more clutter rejection than a large aperture. This is to be expected since increasing  $a_1/\lambda$  increases the slope of the null pattern and permits more clutter to pass. Using the following values:

$$a_1/\lambda = 10$$

$$\delta\theta = 1.25 \times 10^{-4} \text{ radians for } \theta_d = 3 \text{ degrees}$$

$$\tau = 0.1 \text{ microsecond, } h_1 = 10^3 \text{ feet}$$

then

$$10 \log_{10} R_c = 63.8 \text{ dB.}$$

If the expression for  $\delta\theta$  from (D.2) is substituted into Equation (D.6), the clutter reduction becomes:

$$R_c = 3.65 \left( \frac{\lambda}{a_1} \right)^2 \left( \frac{2h_1}{c\tau} \right)^2 \frac{\cos^2 \theta_d}{\sin^4 \theta_d} \quad (\text{D.7})$$

The clutter reduction in dB is plotted on Figure D.5 for selected values of the ratios  $(\lambda/a_1)$  and  $(2h_1/c\tau)$ .

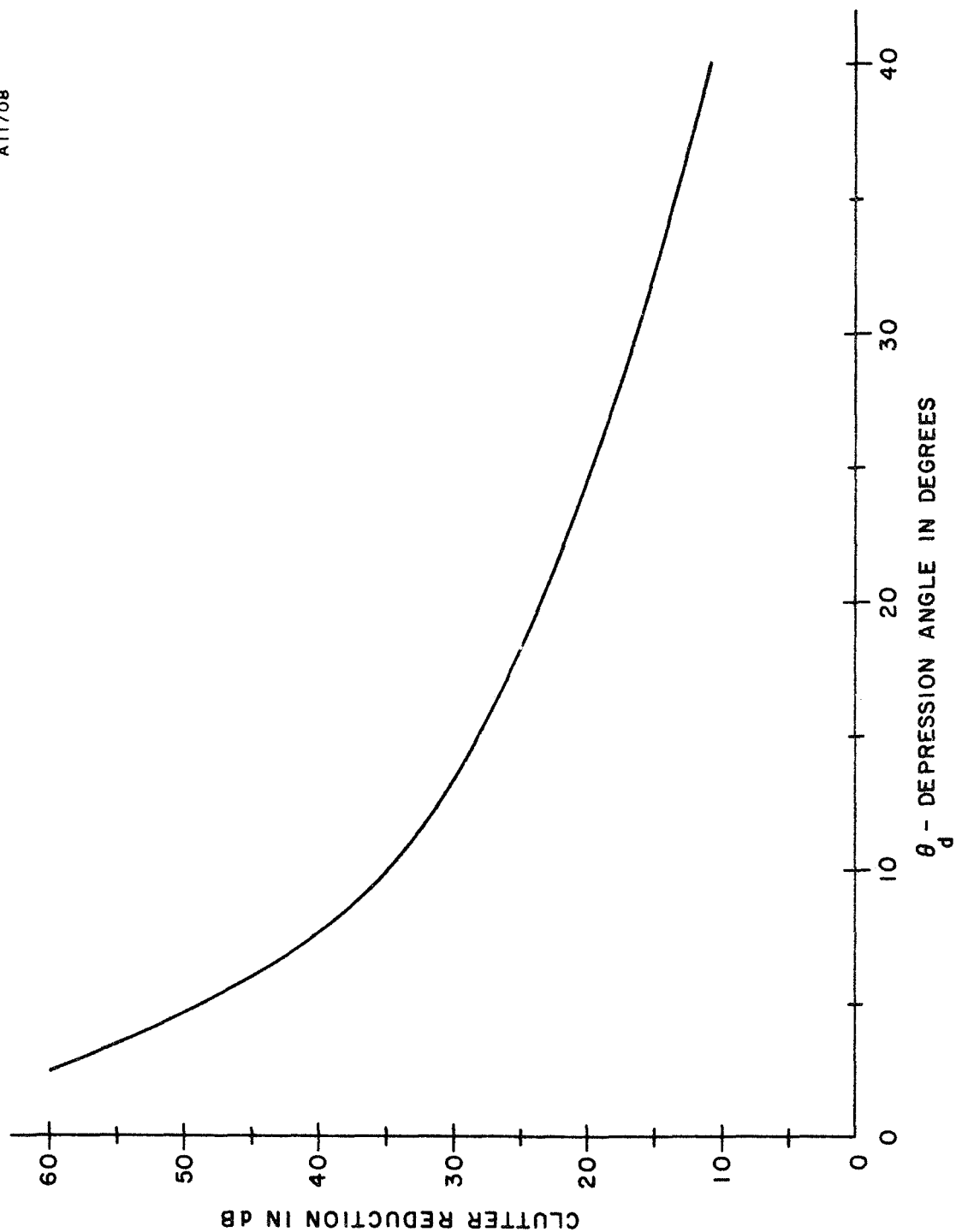


FIGURE D.5 CLUTTER REDUCTION AS A FUNCTION OF DEPRESSION ANGLE  
 FROM EQUATION (D.7) FOR  $(\lambda^2 h_1 / a_c \tau) = 1$   
 (e.g.,  $\lambda / a_1 = 0.1$ ;  $h_1 = 500$  feet;  $\tau = 0.1$  microsecond)

## APPENDIX E

### MONOPULSE BEAM TILT

The monopulse technique of tilting the antenna beam can be explained by the use of a Taylor Series Expansion of the antenna pattern  $f(\alpha)$  about any unsteered point  $\alpha$ .

$$f(\alpha + \delta\alpha) = f(\alpha) + \frac{\alpha}{1!} f'(\alpha) + \frac{(\delta\alpha)^2}{2!} f''(\alpha) ++ \quad (\text{E.1})$$

where the primed terms are derivatives with respect to  $\alpha$ . For the monopulse analogy, the first term of the series,  $f(\alpha)$ , corresponds to the  $\Sigma$  pattern and the second term to the  $\Delta$  pattern of the antenna, Figure 3.42 in the text. The remainder, after  $n$  terms, is

$$R_n = \frac{(\delta\alpha)^n}{n!} f^n(\xi), \quad \xi = \alpha + k(\delta\alpha) \quad 0 < k < 1 \quad (\text{E.2})$$

so to keep the error small then  $\delta\alpha < 1$ . The derivatives of the one dimensional far-field pattern can be readily determined in terms of the initial aperture distribution  $A(x)$ . The Fourier transform relation for the aperture function  $A(x)$  and the approximate far-field  $f(\alpha)$  is, for one axis

$$f(\alpha) = \int_{-a_1/2}^{a_1/2} A(x) \exp(j\alpha x/a_1) dx \quad (\text{E.3})$$

where  $\alpha = \frac{2\pi a_1 \sin \theta}{\lambda}$

$a_1$  = aperture height

$\theta$  = far-field angle

$\lambda$  = wavelength

The first derivative of  $f(\alpha)$  with respect to  $\alpha$  is

$$f'(\alpha) = \int_{-a_1/2}^{a_1/2} A(x) (jx/a_1) \exp(j\alpha x/a_1) dx \quad (\text{E.4})$$

With repeated differentiation of the right side of Equation (E.3) it is apparent that the  $n$ (th) aperture illumination is the original aperture function multiplied by  $(jx/a_1)^n$  or

$$f^n(\alpha) = F[(jx/a_1)^n A(x)]. \quad (E.5)$$

Returning to Equation (E.1) and substituting the far-field derivatives in terms of the aperture distribution from relation (E.5), the steered beam obtained by summing the F transforms of the individual terms is

$$f(\alpha) = \int_{-a_1/2}^{a_1/2} A(x) \left[ 1 + \frac{\delta\alpha}{1!} \frac{jx}{a_1} + \frac{(\delta\alpha)^2}{2!} \left( \frac{jx}{a_1} \right)^2 + \dots \right] \cdot \exp(j\alpha x/a_1) dx \quad (E.6)$$

If  $(\delta\alpha x/a_1) = y$  and with the bracketed terms separated into even and odd series, then the right side of (E.6) becomes:

$$= \int A(x) \left[ \left( 1 - \frac{y^2}{2!} + \frac{y^4}{4!} - \dots \right) + j \left( \frac{y}{1!} - \frac{y^3}{3!} + \dots \right) \right] \cdot \exp(j\alpha x/a_1) dx \quad (E.7)$$

The two series in the parenthesis within the brackets of (E.7) are recognized as  $\cos y$  and  $\sin y$ , therefore,

$$= \int A(x) [\cos y + j \sin y] \exp(j\alpha x/a_1) dx \quad (E.8)$$

and using Eulers relation and  $y = (\delta\alpha x/a_1)$

$$f(\alpha + \delta\alpha) = \int A(x) \exp[j(\delta\alpha + \alpha)(x/a_1)] dx \quad (E.9)$$

The integral expression on the right of Equation (E.9) has been derived by retaining all the terms of the original Taylor Series expansion from Equation (E.1). This expression indicates that by using a phase shift in the aperture of  $\delta\alpha x/a_1$ , a linear phase shift, the beam can be tilted through a desired angle  $\delta\alpha$ , which is recognized as phase scanning. The intermediate form, expression (E.8), corresponds to scanning by adjusting the amplitudes of sine and cosine aperture functions and is designated amplitude scanning. The basis for monopulse beam tilt, an approximate scanning technique for small angles,  $\delta\alpha < 1$ , could be derived by starting with the right side of Equation (E.9) and proceeding in the reverse direction to arrive at Equation (E.1). The phase and amplitude techniques for scanning require complex and generally expensive amplitude and/or phase adjustments of the aperture currents. The monopulse method of beam tilt is limited to  $\delta\alpha < 1$ , but requires only a single amplitude adjustment.



## APPENDIX F

### LASER CLOUD RANGING

Detection and ranging of clouds can be accomplished in daylight or at night using an infrared laser pulsed light source. Because of the much shorter wavelength compared to microwave, there is considerable back-scattering by clouds. The clouds may be considered as a perfectly diffused reflector with reflectivity ranging from one to sixty percent, Section 2.3. For the best signal-to-noise ratio, a wavelength of about 3 microns\* should be used, although a shorter wavelength such as the 0.92 microns of gallium arsenide diodes is also possible. The reason that a wavelength of 3 microns is preferred is that the operation will be primarily background noise limited. Since the solar spectrum and the spectral radiance of the clear sky are lower at 3 microns, the maximum signal-to-noise ratio for daylight operation may be obtained in this spectral region.

Since the 0.92 micron wavelength gallium arsenide diode is commercially available, the laser power requirement for ranging of clouds is estimated for a maximum distance of 5 miles. Typical characteristics of a diode laser are:

Wavelength $\lambda$	= 0.92 microns
Half-power spectral width $\Delta\lambda$	= 50 Å <sup>0</sup>
Pulse rate	= 1000 pps
Pulse width $\tau$	= 0.1 μs
Beam size $\Omega$	= 0.001 sr

A pulse width of 0.1 microsecond will provide a range resolution of about 50 feet, which will be sufficient for this type of application. The radiant power received from a cloud by a collector is given by Equation (F.1) assuming the cloud fills the beam.

$$P_r = \frac{P_{i_{180}} D_a^2 \eta e^{-2\sigma_a r}}{16 r^2} \quad (F.1)$$

where  $P_r$  = received radiant power, watts  
 $P$  = transmitter radiant power output, watts  
 $i_{180}$  = backscattering coefficient

---

\*A micron is  $10^{-4}$  cm, an angstrom unit is  $10^{-8}$  cm.

$D_a$  = diameter of receiver optics aperture, feet  
 $\eta$  = efficiency of lenses, filters, etc., assumed 1  
 $\sigma_a$  = the extinction coefficient, assumed 0.122/kilometer  
 $r$  = range to cloud, feet

For a 0.5 foot receiver optics and a backscatter coefficient of 0.1, the radiant power received from a range of 5 NM per unit of transmitter power is given by Equation (F.2).

$$\frac{P_r}{P} = 1.73 \cdot 10^{-12} \quad (F.2)$$

The background noise level will limit the sensitivity of the receiver. Assuming a 2 degree field (corresponding to 0.001 steradian) of view for the single element detector in the receiver the noise equivalent flux (NEF) due to the background radiation may be calculated from Equation (F.3).

$$NEF = (\pi \beta I_b D_a^2)^{\frac{1}{2}} \quad (F.3)$$

where  $\beta$  = receiver bandwidth, Hz

$I_b$  = background flux density in photons/second/cm<sup>2</sup>

$D_a$  = diameter of receiver optics

The background spectral radiance at 1 micron (the approximate wavelength of the semi-conductor diode laser) is about  $2 \cdot 10^{16}$  photons/cm<sup>2</sup>/steradian/micron. The spectral width of the laser radiation is about 50 Å so a 200 Å filter will be adequate to pass the light pulse. The background flux density, using these parameter values is  $4 \cdot 10^{11}$  photons/second/cm<sup>2</sup>. Using this value for the background flux density, the NEF, as calculated by Equation (F.3) with an assumed receiver bandwidth of 10 MHz, is  $5 \cdot 10^{10}$  photons/second which is a noise equivalent power (NEP) of  $10^{-8}$  watt. If a power signal-to-noise ratio of 6 is specified, then from Equation (F.2) the transmitter power at a wavelength of 1 micron is 35,000 watts. If a different type of laser operating at 3 microns is used, to take advantage of the lower background level, the power requirement would be reduced by a factor of 20.

The above calculations indicate that the peak power required for daylight ranging to 5 NM is far beyond the capability (less than 50 watts peak power) of semi-conductor, single diode lasers. A neodymium Nd laser, operating at a wavelength of 1.06 microns, should give the desired performance. Nd lasers have power outputs in excess of  $10^6$  watts, use pulse

repetition rates of approximately 1 per second, the beam divergence is approximately  $3 \cdot 10^{-6}$  steradian, and the spectral width is less than one angstrom so that an interference filter with a passband of  $20 \text{ \AA}$  may be used with the receiver. Because of the smaller beam divergence and spectral width, the peak power required can be reduced by a factor of 3,000, thus a laser with a peak power of one kilowatt will be sufficient even assuming that a cloud only partially fills the beam. With the lower laser power the repetition rate can be increased considerably beyond one pulse per second.

A cloud ranger for operation only at night can be appreciably lower power and consequently lower cost. If the detector is assumed to have a night background level of  $10^{-11}$  watt instead of the daytime level of  $10^{-8}$  watt then the power level is compatible with a diode laser. Assuming a diode laser with a beam of 0.1 steradian, a 10 microsecond pulse, a receiver bandwidth of 100 KHz, and a signal-to-noise ratio of 5, the range is 3.5 NM with a peak radiant power of 13.5 watts.

Tabulations of commercially available lasers can be found in various trade journals, for example, see the Laser Technology Section of Microwaves for November 1968, pages 120-137.

## APPENDIX G

### NEW TECHNOLOGY

A diligent review of the work performed under this contract indicates that the following items are innovations.

1. Engine -Driven Scanner for Airborne Radar. In Sections 3.2 and 5.2, a low-cost antenna scanner, particularly useful on single and in-line engine aircraft, is described.
2. Monopulse Beam Control for Terrain Return Suppression. A method of achieving near-optimum tilt control simultaneously at near and far ranges is described in Section 3.17 and Appendix E.

# REPORT DISTRIBUTION LIST

CONTRACT NO. 12-2032

1. NASA/ERC  
55 Broadway Street  
Cambridge, Massachusetts 02139  

Attn: Robert W. Wedan	Code: P	1
Dr. Gene G. Mannella	Code: T	1
William J. Rhine	Code: PH	1
Leo M. Keane	Code: PS	1
Ronald J. Madigan	Code: PHD	1
Joseph LoVecchio	Code: PHD	1
Dr. Robert J. Mailloux	Code: ROI	1
Janis Vilcans	Code: PHD	10
Thomas F. McDonough	Code: AN	10 + 1
		Reproducible
  
2. NASA, Ames Research Center  
Moffett Field  
California 94035  

Attn: John Dimeff	Code: FI	1
-------------------	----------	---
  
3. NASA, Headquarters  
OART  
Washington, D. C. 20546  

Attn: Albert J. Evans	Code: RA	1
-----------------------	----------	---
  
4. NASA, Headquarters  
OART  
Washington, D. C. 20546  

Attn: Frank J. Sullivan	Code: RE	1
-------------------------	----------	---
  
5. NASA, Goddard Space Flight Center  
Greenbelt  
Maryland 20771  

Attn: Dr. Robert J. Coates	Code: 520	1
----------------------------	-----------	---
  
6. NASA, Langley Research Center  
Langley Station  
Hampton, Virginia 23365  

Attn: W. M. Moore	Code: MS 590 FID-TRB	1
-------------------	----------------------	---

7. NASA, Marshall Space Flight Center  
Alabama  
Attn: D. O. Lowrey                      Code: S&E E-ASTR-IA                      1
8. FAA  
800 Independence Avenue  
Washington, D. C. 20590  
Attn: James H. Muncy                      Code: RD 241                      1
9. AFSC STLO  
Massachusetts Institute of Technology  
68 Albany Street  
Cambridge, Massachusetts 02139  
Attn: Captain Mark R. Jansen                      1
10. United States Air Force (AFSC)  
Systems Engineering Group (RTD)  
Wright-Patterson Air Force Base  
Dayton, Ohio 45433  
Attn: R. J. Harnett, SEKRA                      1
11. NASA, Langley Research Center  
Langley Station  
Hampton, Virginia 23365  
Attn: G. B. Graves, Jr.                      1  
Chief, Flight Instrumentations Division
12. Wright-Patterson Air Force Base  
USAF Flight Dynamics Laboratory  
Dayton, Ohio 45433  
Attn: George Yingling                      1
13. AOPA  
P. O. Box 5800  
Washington, D. C. 20014  
Attn: M. Huck                      1
14. Beech Aircraft  
Wichita  
Kansas 67201  
Attn: Mr. Thomas Harvey                      1

15. Piper Aircraft  
Lock Haven  
Pennsylvania 17745  
Attn: Mr. Howard Piper 1
16. Cessna Commercial Aircraft  
Box 1521  
Wichita, Kansas 67201  
Attn: Mr. William Thompson 1
17. Narco Corporation  
Fort Washington Industrial Park  
Fort Washington, Pennsylvania 19034  
Attn: Mr. Lewis Wells 1
18. Gates Lear Jet  
Municipal Airport  
Wichita, Kansas 67201  
Attn: Mr. E. D. Wiggins 1
19. Mooney Aircraft  
Louis Schreuer Field  
Kerrville, Texas 78028  
Attn: Mr. R. M. Harmon 1
20. King Radio  
P. O. Box 106  
Olathe, Kansas 66061  
Attn: Mr. Paul Wulfsberg 1
21. National Pilots Association  
806 Fifteenth Street, N. W.  
Washington, D. C. 20005  
Attn: Mr. W. Ottley 1
22. National Business Aircraft Association  
401 Pennsylvania Building  
Washington, D. C. 20004  
Attn: Mr. F. B. McIntoch 1

23. Bendix Corporation  
2100 Northwest 62nd Street  
Fort Lauderdale, Florida 33310  
Attn: Mr. E. A. Post 1
24. RCA Aviation Equipment Department  
11819 West Olympic Boulevard  
Los Angeles, California 90064  
Attn: Mr. A. Vose 1
25. Collins Radio  
Cedar Rapids,  
Iowa 52406  
Attn: Dr. G. Marner 1
26. Westinghouse Electric Corporation  
Aerospace Division  
Friendship International Airport  
Baltimore, Maryland 21203  
Attn: Mr. W. Fegely 1
27. Texas Instruments, Inc.  
13500 North Central Expressway  
Dallas, Texas 75222  
Attn: Mr. Floyd Simmonds, Mail Stop 257 1
28. North American-Rockwell Corporation  
Autonetics Division  
3370 Miraloma Avenue  
Anaheim, California 92803  
Attn: Dr. L. O. Krause, DC13 1